JSCSEN 76(3)317–478(2011)

International Year of CHEMISTRY 2011

Journal of the Serbian Chemical Society

Electronic Version

VOLUME 76

No 3

BELGRADE 2011

Available on line at

www.shd.org.rs/JSCS/

The full search of JSCS is available through

DOAJ DIRECTORY OF OPEN ACCESS JOURNALS

www.doaj.org

Journal of the Serbian Chemical Society
JSCS-info@shd.org.rs • www.shd.org.rs/JSCS

J. Serb. Chem. Soc. Vol. 76, No. 3 (2011)

CONTENTS

Published by the Serbian Chemical Society
Karnegijeva 4/III, 11000 Belgrade, Serbia
Printed by the Faculty of Technology and Metallurgy
Karnegijeva 4, P.O. Box 35-03, 11120 Belgrade, Serbia

Journal of the Serbian Chemical Society
JSCS-info@shd.org.rs • www.shd.org.rs/JSCS
J. Serb. Chem. Soc. 76 (3) 317–328 (2011) UDC 547.78/.79+547.313:66.095.21:543.422.25
JSCS–4120 *Original scientific paper*

Thermal solid-state *Z*/*E* isomerization of 2-alkylidene-4--oxothiazolidines: effects of non-covalent interactions

ZDRAVKO DŽAMBASKI[1#], MILOVAN STOJANOVIĆ[1#], MARIJA BARANAC-STOJANOVIĆ[1,2#], DRAGICA M. MINIĆ[1,3#] and RADE MARKOVIĆ[1,2*#]

[1]*Centre for Chemistry, ICTM, P. O. Box 473, 11001 Belgrade,* [2]*Faculty of Chemistry, University of Belgrade, Studentski trg 16 P. O. Box 158, 11001 Belgrade and* [3]*Faculty of Physical Chemistry, University of Belgrade, Studentski trg 16, 11000 Belgrade, Serbia*

(Received 7 July 2010)

Abstract: Configurational isomerization of stereo-defined 5-substituted and unsubstituted 2-alkylidene-4-oxothiazolidines (**1**) in the solid state, giving the *Z*/*E* mixtures in various ratios, was investigated by ^{1}H-NMR spectroscopy, X-ray powder crystallography and differential scanning calorimetry (DSC). The *Z*/*E* composition can be rationalized in terms of non-covalent interactions, involving intermolecular and intramolecular hydrogen bonding and directional non-bonded 1,5-type S···O interactions. X-Ray powder crystallography, using selected crystalline (*Z*)-4-oxothiazolidine substrate, revealed transformation to the amorphous state during the irreversible *Z*→*E* process. A correlation between previous results on the *Z*/*E* isomerization in solution and now in the solid state was established.

Keywords: 4-thiazolidinones; solid-state isomerisation; non-covalent interactions; dynamic ^{1}H-NMR spectroscopy.

INTRODUCTION

Over the last decade, the chemistry of an extensive series of 5-substituted and unsubstituted 4-oxothiazolidines (**1**, Fig. 1), bearing a trisubstituted exocyclic C–C double bond at position C-2 was investigated.[1]

They undergo a number of useful transformations into diverse heterocyclic systems, including 1,2-dithioles,[2a] 1,3-thiazines,[2b] pyridinium salts containing a 4-oxothiazolidinyl moiety,[2c] tetrahydrofuro[2,3-*d*]thiazolo derivatives[2d] and other thiazolidine-condensed 5-, 6- and 7-membered heterocycles.[2e,f] The thiazolidine derivatives **1** belong to a class of push-pull compounds,[3] usually represented by the general formula D-π-A, where D and A denote electron donor(s) and electron acceptor(s), respectively, bonded to a C–C double bond or a π-conjugating spacer.[4]

* Corresponding author. E-mail: markovic@chem.bg.ac.rs
# Serbian Chemical Society member.
doi: 10.2298/JSC100607038D

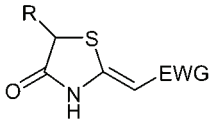

1

R = H, Me, CH_2CO_2Et
EWG = CO_2Et, COPh, CONHPh, $CONH(CH_2)Ph$, CN

Fig. 1. 2-Alkylidene-4-oxothiazolidinones.

The strong D–A interactions *via* C=C bond(s) in various push-pull derivatives, for example in D–A-substituted tetraethynylethenes **2**,[4a] or benzodithiole polyenes **3**,[4b] (Fig. 2) are associated with their interesting electrochemical and non-linear optical properties.[5]

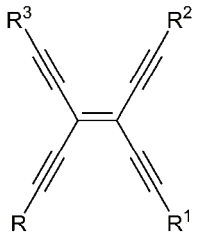

2

R, R^1 = *p*-$C_6H_4NO_2$; R^2, R^3 = *p*-$C_6H_4NMe_2$
R = *p*-$C_6H_4NMe_2$; R^1, R^2, R^3 = $SiMe_3$
R = *p*-$C_6H_4NMe_2$; R^1 = *p*-$C_6H_4NO_2$; R^2, R^3 = Si(*i*Pr)$_3$

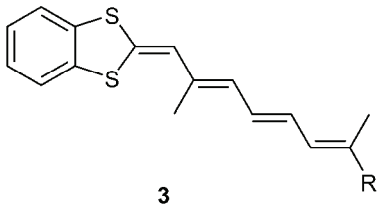

3

R =

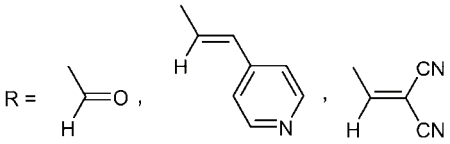

Fig. 2. D–A-Substituted tetraethynylethenes and benzodithiole polyenes.

It was previously shown that electronic interactions in the (*Z*)-4-oxothiazolidine derivatives **1** in solution, between the two electron-releasing substituents –NH and –S–, and an electron-withdrawing substituent (COPh, CO_2Et, CONHPh, *etc*.) through the π-conjugated bond, have a decisive influence on lowering the rotational barrier of the exocyclic C=C bond at position C-2.[6] As a result of the partial single bond character of the C=C bond, configurational isomerization of these highly dipolar compounds, controlled by an appropriate choice of solvent, occurs in solution. On the other hand, the literature contains only a few examples describing the *Z*/*E* isomerization of organic compounds in the solid state.[7]

It is the intent of this paper to report herein *i*) a ^{1}H-NMR investigation of the stereodynamic behaviour of the stereo-defined 2-alkylidene-4-oxothiazolidines **1** in the solid state, proving that a rare type of thermally induced configurational isomerization occurs to form *Z*/*E* mixtures in different ratios. This is combined with *ii*) X-ray powder analysis and DSC measurements in terms of an evaluation of the crystallinity change occurring during the heating process of a representta-

tive of the push-pull alkenes **1**, *i.e.*, (*Z*)-ethyl 4-oxo-2-[2-oxo-2-[(2-phenylethyl)amino]ethylidene]-5-thiazolidineacetate (**1d**) (Fig. 3).

(*Z*)-**1a** (R = CH_2CO_2Et; EWG = CO_2Et)
(*Z*)-**1b** (R = CH_2CO_2Et; EWG = CONHPh)
(*Z*)-**1c** (R = CH_3; EWG = CONHPh)
(*Z*)-**1d** (R = CH_2CO_2Et; EWG = $CONHCH_2CH_2Ph$)
(*Z*)-**1e** (R = CH_2CO_2Et; EWG = COPh)
(*Z*)-**1f** (R = H; EWG = COPh)

(2*E*,5*Z*)-**1g**

Fig. 3. Structures of 2-alkylidene-4-oxothiazolidines.

RESULTS AND DISCUSSION

Several structural features of compounds **1**, that is, their polyfunctional nature, the stereogenic centre at the C-5 position of the thiazolidine ring, the *Z*- or *E*-geometry of the exocyclic donor–acceptor substituted C=C bond, and, importantly, the *cis*-configured –S–C=C–C=O unit of the *Z*-isomers, make them interesting substrates for investigating their properties and reactivity. To probe the impact of inter- and intramolecular interactions on the solid state thermal *Z*/*E*-isomerization of the structurally related (*Z*)-5-substituted and unsubstituted 2-alkylidene-4-oxothiazolidines **1a**–**f** (Fig. 3), the behaviour of ethyl (*Z*)-ethyl 2-[2--(ethoxycarbonyl)ethylidene]-4-oxo-5-thiazolidineacetate (**1a**) was examined first.

The *Z*-configuration of the thiazolidines **1a**–**f**, obtained from the corresponding β-oxonitriles and α-mercaptoesters,[1a,b] was previously elucidated from ^{1}H--NMR spectroscopic data, including 1D nuclear Overhauser effect measurements in the case of the enaminoketone **1e**. X-ray structural analysis confirmed the configuration of the trisubstituted C=C bond in **1a**, having the lactam hydrogen involved in intermolecular hydrogen bonding to the C-4 carbonyl oxygen of an adjacent molecule. Upon slow heating of the solid crystalline compound **1a** (1–2 °C min^{-1}), from room temperature to 120 °C, which is slightly above its melting point, followed by fast cooling of the melt to 0 °C, the extent of the *Z*/*E* process was determined by ^{1}H-NMR spectroscopy, employing DMSO-d_6 or $CDCl_3$ as solvents. As Fig. 4 depicts, the spectrum of **1a** in DMSO-d_6 contained two sets of signals, including typical resonances of the olefinic protons at δ 5.44 ppm for the original *Z*-isomer and δ 5.21 ppm assigned to the newly formed *E*-isomer (the characteristic δ values of the olefinic protons are given in Experimental). The *Z*/*E* ratio, determined by integration of the corresponding chemical shifts, was 83/17.

Likewise, the composition of the *Z*/*E* mixtures of all thiazolidines **1a**–**g**, based on assignments of the characteristic signals for the vinylic protons in the corresponding ^{1}H-NMR spectra, recorded in DMSO-d_6 and/or $CDCl_3$, is compiled in Table I.

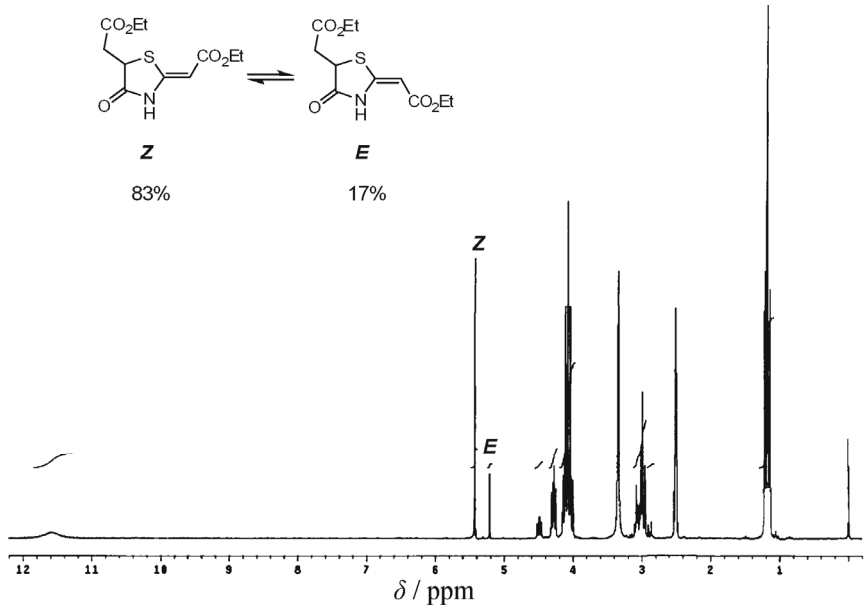

Fig. 4. ^{1}H-NMR spectrum of the *Z*/*E* mixture of thiazolidine derivative **1a**, recorded in DMSO-d_6 after thermal solid-state isomerization.

TABLE I. Configurational isomerization of compounds **1a**–**g** in the solid state

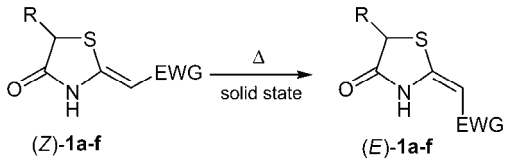

Entry	Substrate	R	EWG	Temperature range, °C[a]	Z/*E* ratio (DMSO-d_6)[b]	Z/*E* ratio ($CDCl_3$)[b]
	Z-**1a**	CH_2CO_2Et	CO_2Et	rt[c]–120	83/17	78/22
1				rt–120		49/51[e]
				rt–110[d]		90/10
2	*Z*-**1b**	CH_2CO_2Et	CONHPh	rt–195	41/59	–[e,f]
3	*Z*-**1c**	CH_3	CONHPh	rt–203	48/52	–
4	*Z*-**1d**	CH_2CO_2Et	$CONH(CH_2)_2Ph$	rt–166	58/42	–
5	*Z*-**1e**	CH_2CO_2Et	COPh	rt–90	100/0	57/43
6	*Z*-**1f**	H	COPh	rt–245	100/0	69/31
7	2*E*,5*Z*-**1g**	$=CHCO_2Et$	CO_2Et	rt–180	70/30 (2*E*,5*Z*/2*Z*,5*Z*)	–

[a]From room temperature to ≈5–10 °C above the melting point; [b]0 time (1–2 min after dissolution of a sample); [c]room temperature; [d]precursor heated below the melting point; [e]2nd heating; [f]insoluble in $CDCl_3$

It is interesting to note that in the case of substrates **1e** or **1f** of the thiazolidine series **1a**–**f** with one exocyclic C=C bond, the corresponding *Z*-isomers were the only species at the end of the heating process, as detected by ^{1}H-NMR

in DMSO-d_6 (Table I, entries 5 and 6). Apparently, the precursors *Z*-**1e** and *Z*-**1f** are either unable to undergo thermally induced solid state *Z*/*E* isomerization (*vide infra*) or, more likely, the *E*-isomer of the *Z*/*E* mixture formed during the isomerization, as found for 4-oxothiazolidines **1a**–**d** (Table I, entries 1–4), transforms in a rapid DMSO-induced $E \rightarrow Z$ interconversion back to original *Z*-form. Indeed, the observation of two ^{1}H-NMR vinylic signals at δ 6.83 and 6.32 ppm in non-polar $CDCl_3$ for substrate **1e**, ascribed to the *Z*- and *E*-isomer, respectively, in a 57/43 ratio (Table I, entry 5), verifies that the solid state isomerization does occur. This is consistent with the finding that the ^{1}H-NMR spectrum of the second enaminoketone **1f**, similarly to **1e**, displayed a pair of =CH signals in $CDCl_3$ at δ 6.78 ppm for *Z*-**1f** and at δ 6.33 ppm for *E*-**1f**, whereas the ^{1}H-NMR spectrum in DMSO-d_6 of the same sample **1f** after heating, showed only the vinylic proton of the *Z*-isomer at δ 6.82 ppm. This is in line with the fact that the ^{1}H-NMR spectra of the highly dipolar compounds **1a**–**f**, or, in principle, related push-pull compounds,[8] are solvent-dependent. The ^{13}C values of C-2 at rather low field for a vinylic carbon (151–163 ppm) of compounds **1a**–**f**, together with a high field position for vinylic C-2' atom (89–95 ppm) reflect their dipolar character[1,3] and hydrogen bonding ability. In some cases, depending on the relative rate of the configurational isomerization pertinent to dipolar compounds of the type **1**, the *Z*/*E* ratio can be appreciably affected in accordance to the general Scheme 1, even during the shortest NMR recording time possible.

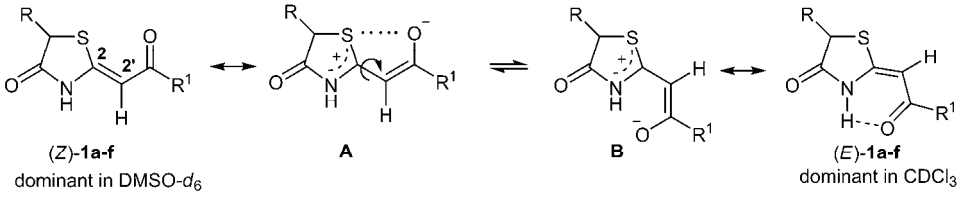

Scheme 1. Configurational isomerization of compounds **1a**–**g** in solvents of different polarity.

In accordance to earlier generalization, the *E*-isomers **1a**–**f** are the preferred species for equilibrated *Z*/*E* mixtures in non-polar $CDCl_3$, as the NH···O=C non-covalent interaction leads to favourable six-membered H-bonding.[6a,b] Upon increasing the ground-state polarization of thiazolidines **1a**–**f** in polar DMSO, the neutral, intramolecularly H-bonded structure of *E*-**1a**–**f** is no longer the dominant one. The strong 1,5-type electrostatic S···O interaction due to the maximum charge stabilization in DMSO, as depicted in Scheme 1, enhances the contribution of the resonance form **A**.[9] Thus, the intramolecular H-bonding in the original *E*-isomer is suppressed at the expense of its *Z*-counterpart. The formation of competitive intermolecular H-bonding between the solvent and corresponding *Z*-**1**,

acting in the same direction, favouring the *Z*-form, further attenuates the fast process of C=C bond isomerization. This is obviously a draw-back of using DMSO-d_6 for ^{1}H-NMR determination of the *Z*/*E* composition for **1e** and **1f** after heating, due to the rapid *E*→*Z* isomerization. Fortunately, in contrast to the counter-effect of DMSO on reliable determination of the *Z*/*E* ratio, the kinetic data obtained for the configurational isomerization at room temperature of (*Z*)-ethyl 4-oxo-2-(2-oxo-2-phenylethylidene)-5-thiazolidineacetate (**1e**), and a series of related compounds, in $CDCl_3$ show that the configurational change at room temperature is rather slow. More precisely, starting from the pure (*Z*)-**1e** isomer, the $t_{1/2}$, *i.e.*, the time needed to obtain a 50:50 mixture of the isomers during the *Z*/*E* process in $CDCl_3$ at 25 °C, monitored at regular time intervals (1 h) by dynamic ^{1}H-NMR, was 5 h. The variable-temperature ^{1}H-NMR data for the isomerization of **1e** in $CDCl_3$ indicated that the rotational barrier $\Delta G^{\#}$, separating the (*Z*)-**1e** and (*E*)-**1e** isomers, is 98.5 kJ mol^{-1} (at 298 K).[6a,b] The use of $CDCl_3$ can actually circumvent the problem of rapid *E*→*Z* isomerization, or specifically that of the enaminoketones (*E*)-**1e** or (*E*)-**1f** (EWG = COPh) in DMSO. Thus, an accurate estimate of the relative amounts of each isomer and, consequently, an evaluation of the extent of the thermally induced configurational isomerization of **1a**–**f** in the solid state is possible.

An interesting point concerning the different percentages of the *Z*-isomers in the *Z*/*E* mixtures **1a**–**f**, as determined by ^{1}H-NMR in DMSO-d_6, revealed clearly the influence of the EWGs on an extent of the dictated *E*→*Z* isomerization in polar solvents, as illustrated in Scheme 1. Namely, an increase of the Z-isomers in the order **1e**, **1f** > **1a** > **1b** (Table I, entries 5, 6, 1 and 2, respectively) parallels the order COPh > CO_2Et > CONHR in terms of the stronger electron withdrawing effect of the keto group present in **1e** and **1f**, *vs*. the ester group in **1a**, with the amido group in **1b** being somewhat weaker. Consequently, the better electron withdrawing ability of the keto group to decrease the double bond character at C-2 enhances the contribution of the resonance forms **A** and **B**, enabling faster *E*→*Z* isomerization. This is indicated by the fact that the ^{1}H-NMR spectrum of **1e** (EWG = COPh) after the thermal process showed the presence of only the *Z*-isomer, whereas a *Z*/*E* ratio of 57/43 was determined for the same compound in $CDCl_3$. In contrast, the corresponding *Z*/*E* ratio was 78/22 for **1a** (EWG = CO_2Et) in $CDCl_3$ and only slightly higher (83/17) in DMSO-d_6, which convincingly suggest a slower *E*/*Z* interconversion on the NMR scale. On a second heating of the melt **1a** under identical conditions (Experimental), the *Z*/*E* composition, as determined by ^{1}H-NMR in $CDCl_3$, as for the other substrates **1b**–**f**, amounted to 49/51 (Table I, entry 1). Obviously, the greater percentage of the *E*-isomer in the second melt *vs*. that of the first melt proves the progressive extent of the *Z*→*E* process. When the thermal process, employing **1a** was performed from rt to 110 °C, which is below its melting point, the *Z*/*E* ratio was 90/10.

For stereodefined ethyl (2*E*,5*Z*)-ethyl 2-[2-[2-(ethoxycarbonyl)ethylidene)-4--oxo-5-thiazolidinylilidene]acetate (**1g**), possessing two exocyclic C=C bonds at positions C-2 and C-5, a 2*E*,5*Z*/2*Z*,5*Z* ratio of 70/30 was observed in DMSO-d_6 after thermal isomerization (Table I, entry 7). The *Z*-configuration at the C-5 position stayed intact due to the unfavourable steric interactions in the respective *E*-configuration.[10] By analysis of variable-temperature ^{1}H-NMR data for the solvent-initiated isomerization of 2*E*,5*Z*-**1g** into 2*Z*,5*Z*-**1g** in DMSO-d_6 from room temperature (Fig. 5) to 55 °C, the reliability of the extent of this isomerization occurring in the solid state was assessed.

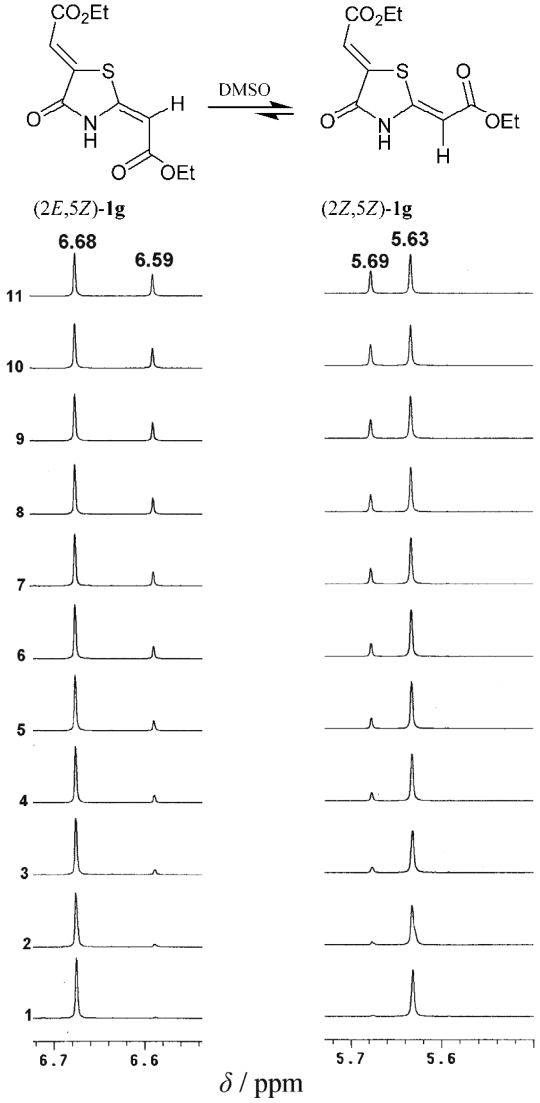

Fig. 5. Spectral evidence for the presence of the 2*E*,5*Z*-**1g** isomer (olefinic signals at δ 5.63 and 6.68 ppm, and 2*Z*,5*Z*-**1g** isomer (olefinic signals at δ 5.69 and 6.59 ppm) in DMSO-d_6 at rt; 30 min ^{1}H-NMR recording interval; partial ^{1}H-NMR spectrum **1** at initial recording time indicates the presence of the starting 2*E*,5*Z*-**1g** isomer, based on the observation of the olefinic signals at δ 5.63 and 6.68 ppm; partial ^{1}H-NMR spectrum **11**, recorded after 5 h, indicates the presence of both isomers, 2*E*,5*Z*-**1g** and 2*Z*,5*Z*-**1g**, in the 72/28 ratio; partial ^{1}H-NMR spectrum **21** (not given), recorded after 10 h, indicates that the signals of 2*E*,5*Z*-**1g** at δ 5.63 and 6.68 ppm, and these of 2*Z*,5*Z*-**1g** at δ 5.69 and 6.59 ppm, have almost the same intensities.

Thus, Fig. 5, displaying the partial ^{1}H-NMR spectra of 2*E*,5*Z*-**1g** and 2*Z*,5*Z*--**1g** isomers recorded during a 5-h period at 30-min intervals at room temperature, indicates only the characteristic signals of the olefinic protons. As seen from Fig. 5, the 2*E*,5*Z*/2*Z*,5*Z* ratio reached a value of 72/28 after 5 h (spectrum 11). By monitoring the kinetics of the configurational isomerization during an extended period (20 h), a relatively long isomerization half-life ($t_{1/2}$) of around 10 h was observed. An equilibrated 2*E*,5*Z*/2*Z*,5*Z* ratio of 10/90 was established after 20 h. These data clearly suggest that the 2*E*,5*Z*→2*Z*,5*Z* process in DMSO-d_6 is rather slow at room temperature. Accordingly, it was concluded that the overall estimate of the thermally induced isomerization of isomer 2*E*,5*Z*-**1g** (Table I, entry 7), based on the determination of the 2*E*,5*Z*/2*Z*,5*Z* ratio in this polar solvent, is quite accurate. The same conclusion applies to the 4-oxothiazolidine **1a**, differing from 2*E*,5*Z*-**1g** only at the C-5 atom that is not sp^2 but sp^3 hybridized.

The solid-state *Z*→*E* process of (*Z*)-ethyl 4-oxo-2-[2-oxo-2-[(2-phenylethyl)-amino]ethylidene]-5-thiazolidineacetate (**1d**) was also studied by powder X-ray diffraction and DSC in the temperature interval from rt to m.p.[11] The crystalline structure of *Z*-**1d** was stable up to approximately 136 °C when a breakdown of the ordered crystal structure and melting occurred (t_p = 145 °C at a heating rate β = 5 °C min^{-1}). The diffractogram of the melted structure, characterized by ^{1}H-NMR as the expected *E*-isomer, indicated the formation of an amorphous compound. The observation of a sharp peak of very low intensity was evidence for the presence of a small quantity of the crystalline *E*-isomer in a matrix of amorphous material. An analysis of the X-ray diffraction data obtained for a melt stored under inert conditions for four months showed an increase in the intensity of this peak. This fact suggested a slow and progressive conversion of the amorphous *E*-isomer into the crystalline form.

DSC measurements of the *E*-isomer **1d** demonstrated that, in comparison to the *Z*-isomer, the *E*-isomer melts at a significantly lower temperature (t_p = 130.9 °C for β = 5 °C min^{-1}). The volume fraction, α, *i.e.*, the fractional conversion of the *Z*→*E* process from the starting *Z*-isomer, was determined from the DSC curves as a function of the temperature (Fig. 6a). A consistent shifting of the DSC curves towards higher temperatures with increasing heating rate indicates that the well-defined endothermic peak on each DSC curve involves, in addition to the melting of the compound and the *Z*→*E* process, other thermally activated steps, such as cleavage of the crystal lattice, disruption of the stabilizing non-bonded 1,5-type S···O interaction and inter-molecular hydrogen bonds, as integral parts of the phase transformation.

As depicted in Figs. 6a and 6b, all curves, depending on the heating rate, exhibit a slow initial period ranging from 7–27 min, which corresponded to the dominant transformation step, followed by the faster steps of the transformation.

The well-shaped sigmoid pattern of the fractional conversion curves (Fig. 6a) indicates that the overall transformation occurs in the bulk of material.

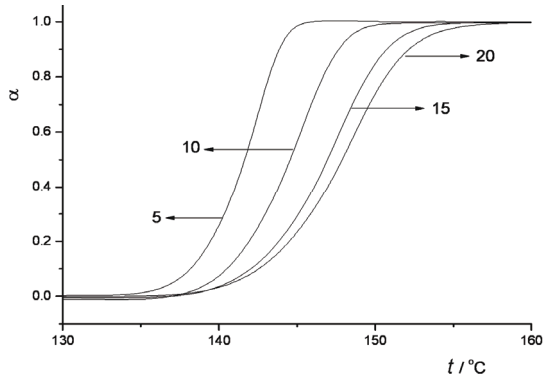

(a)

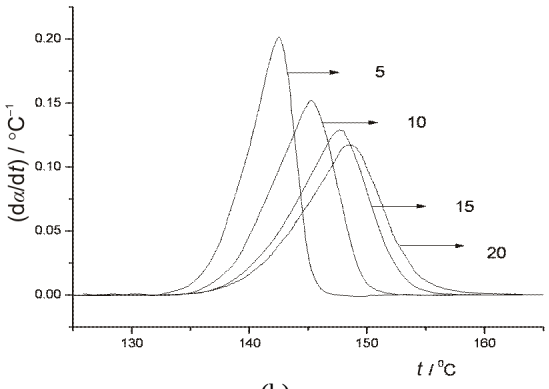

(b)

Fig. 6 a) Fractional conversion, α, as a function of temperature for the $Z \rightarrow E$ process of (*Z*)-**1d** and b) differential rate curves at different heating rates: 5, 10, 15 and 20 °C/min.

For a preliminary determination of the kinetic model of the phase transformation, the Dollimore method was applied.[12] The procedure was applied to the conversion and differential rate curves for the thiazolidine derivative **1d** (Figs. 6a and 6b), the asymmetry of which was observed between the initial temperature (t_i) and final temperature (t_f) for the differential rate curves. The other parameters, such as the conversion at the rate of maximum crystallization, α_{max}, peak temperature, t_p, at $(d\alpha/dt)_{max}$, and asymmetry (shape factor), which is the ratio between the low and high temperature at the half-width of the differential rate curve peak, are presented in Table II.

Fig. 6b depicts that the position of the broad endotherms, which are pertinent to the phase transformation, involving the $Z \rightarrow E$ isomerization, are shifted towards higher temperatures with increasing heating rate (Table II, column 4). Simultaneously, the symmetry of curves decreased (column 3). These features suggest that the investigated process should not be characterized by a definite critical

temperature independent of the heating rate. The determined values of α_{max} for all heating rates were 0.58 and the values of the half-width of peaks were in the range of 5.4–8.0 °C. Thus, the sharpness of the initial and final part of differential curve, together with other parameters presented in Table II, indicate that the investigated process corresponds to the Avrami–Erofe'ev Equation, $f(\alpha) = n(1-\alpha)(-\ln(1-\alpha))^{1/n}$, where n = 2, 3 or 4, describes the random nucleation and growth of the nuclei. In the case of continuous heating, the generalization of the Avrami–Erofe'ev Equation, by applying the Kissinger equation,[13] gives the relations:

$$\beta\left(\frac{E_a}{k_p R T_p^2}\right) = 1 \text{ and } \left(\frac{d\alpha}{dt}\right)_p = 0.37 n k_p$$

where n is the Avrami exponent, T_p is the peak temperature and k_p is the rate constant at the peak temperature.

TABLE II. Parameters describing the asymmetry of the differential curves

β / °C min^{-1}	$(d\alpha/dt)_{max}$ °C^{-1}	Asymmetry	Half-width °C	Shape of initial part	Shape of final part	α_{max}
5	0.20	0.78	5.4	Sharp	Sharp	0.58
10	0.15	0.75	5.5	Sharp	Sharp	0.58
15	0.13	0.67	6.5	Sharp	Sharp	0.58
20	0.12	0.64	8.0	Sharp	Sharp	0.58

The average value of n = 1.83 obtained by applying these relations is very close to the value n = 2, suggesting the validity of the Avrami–Erofe'ev equation, $f(\alpha) = n(1-\alpha)(-\ln(1-\alpha))^{1/n}$ (n = 2), for a description of the whole phase transformation occurring in the bulk of the material. Based on previously reported kinetic parameters,[8] the overall structural transformation, including the $Z \rightarrow E$ isomerization of (*Z*)-ethyl 4-oxo-2-(2-oxo-2-[(2-phenylethyl)amino]ethylidene]-5-thiazolidineacetate (**1d**), can be described by the kinetic triplet, *i.e.*, E_a = 317.7 kJ mol^{-1}, ln A = 93.4 min^{-1} and $f(\alpha) = 2(1-\alpha)(-\ln(1-\alpha))^{1/2}$.

In summary, it has been shown that an irreversible configurational isomerization of a series of stereo-defined 2-alkylidene-4-oxothiazolidines occurs in the solid state.

EXPERIMENTAL

General Procedures

The configurational isomerization of the stereo-defined 5-substituted and unsubstituted 2-alkylidene-4-oxothiazolidines **1a–g** was investigated by the slow heating (1–2 °C min^{-1}) of the corresponding solid crystalline compounds from room temperature to a temperature which is 5––10 °C above the melting point, followed by fast cooling to 0 °C. The extent of the isomerization process was determined by ^{1}H-NMR spectroscopy, employing DMSO-d_6 or $CDCl_3$ as solvents. The structural assignments of all configurational isomers of 4-oxothiazolidines **1a–g** were

made based on reported spectroscopic data (IR, ^{1}H- and ^{13}C-NMR, MS and UV) and elemental analysis.[1a,6b] The ^{1}H-NMR data for the characteristic olefinic hydrogens of the configurational isomers **1a**–**g**, employed for monitoring the extent of the solid state isomerization, are listed in Table III.

TABLE III. Diagnostic ^{1}H-NMR chemical shifts (the ^{1}H-NMR spectra were recorded on a Varian Gemini 2000 instrument (^{1}H at 200 MHz); the chemical shifts are given in ppm downfield from TMS as the internal standard) of the olefinic hydrogens in the configurational isomers **1a–g**

Substrate	R	EWG	DMSO-d_6	$CDCl_3$
Z-**1a**	CH_2CO_2Et	CO_2Et	5.44	5.59
E-**1a**	CH_2CO_2Et	CO_2Et	5.21	5.12
Z-**1b**	CH_2CO_2Et	CONHPh	5.79	–
E-**1b**	CH_2CO_2Et	CONHPh	5.36	–
Z-**1c**	CH_3	CONHPh	5.80	–
E-**1c**	CH_3	CONHPh	5.36	–
Z-**1d**	CH_2CO_2Et	$CONH(CH_2)_2Ph$	5.55	5.44
E-**1d**	CH_2CO_2Et	$CONH(CH_2)_2Ph$	5.15	4.88
Z-**1e**	CH_2CO_2Et	COPh	6.78	6.83
E-**1e**	CH_2CO_2Et	COPh	–[a]	6.32
Z-**1f**	H	COPh	6.82	6.78
E-**1f**	H	COPh	–[a]	6.33
2*Z*,5*Z*-**1g**	$=CHCO_2Et$	CO_2Et	5.68	5.83
2*E*,5*Z*-**1g**	$=CHCO_2Et$	CO_2Et	5.64	5.35

[a]Due to the instantaneous *E*→*Z* isomerisation, there were no signals for the olefinic *E*-**1e** and *E*-**1f** isomers in DMSO-d_6

The overall thermally induced process of the structural transformation of (*Z*)-ethyl 4--oxo-2-(2-oxo-2-[(2-phenylethyl)amino]ethylidene]-5-thiazolidineacetate (**1d**) was also investigated non-isothermally by differential scanning calorimetry (DSC) using a DuPont Thermal analyzer (model 1090). Samples weighing several milligrams (3–7 mg) were heated in the DSC cell from room temperature to 170 °C, at heating rates in the range 5–20 °C min^{-1}, in a stream of nitrogen at normal pressure. The temperature peaks (t_p) were determined from the DSC curves using the program Interactive DSC V1.1. Then X-ray powder diffraction patterns of the *Z*- and *E*-isomer **1d** were investigated.

Acknowledgements. This research was partially supported by the Ministry of Science and Technological Development of the Republic of Serbia, Grant No. 142007 (to R. M.).

И З В О Д

ТЕРМАЛНА *Z*/*E* ИЗОМЕРИЗАЦИЈА 2-АЛКИЛИДЕН-4-ОКСОТИАЗОЛИДИНА У ЧВРСТОМ СТАЊУ: УТИЦАЈ НЕКОВАЛЕНТНИХ ИНТЕРАКЦИЈА

ЗДРАВКО ЏАМБАСКИ[1], МИЛОВАН СТОЈАНОВИЋ[1], МАРИЈА БАРАНАЦ-СТОЈАНОВИЋ[1,2], ДРАГИЦА М. МИНИЋ[1,3] и РАДЕ МАРКОВИЋ[1,2]

[1]Центар за хемију, ИХТМ, п. пр. 473, 11001 Београд, [2]Хемијски факултет, Универзитет у Београду, Студентски трг 16, п. пр. 158, 11001 Београд и [3]Факултет за физичку хемију, Универзитет у Београду, Студентски трг 12, 11000 Београд

Конфигурациона изомеризација стереодефинисаних 5-супституисаних и несупституисаних 2-алкилиден-4-оксотиазолидина **1** у чврстом стању, при чему се ствара *Z*/*E* смеса у различитим односима, проучавана је помоћу ^{1}H-NMR спектроскопије, рендгенске кристало-

графије праха и диференцијалне скенирајуће калориметрије (ДСК). Однос *Z*/*E* изомера може се објаснити у контексту нековалентних интеракција, које обухватају интермолекулско и интрамолекулско водонично везивање и усмерене невезивне S···O интеракције 1,5-типа. Рендгенска кристалографија праха одабраног кристалног (*Z*)-4-оксотиазолидинског супстрата, потврдила је трансформацију у аморфно стање у току иреверзибилног *Z*→*E* процеса. Постављена је корелација између претходних резултата који се односе на *Z*/*E* изомеризацију у раствору, и сада, у чврстом стању.

(Примљено 7. јула 2010)

REFERENCES

1. a) R. Marković, M. Baranac, Z. Džambaski, M. Stojanović, P. J. Steel, *Tetrahedron* **59** (2003) 7803; b) R. Marković, M. M. Pergal, M. Baranac, D. Stanisavljev, M. Stojanović, *Arkivoc* (2006) 1; c) G. Satzinger, *Liebigs Ann. Chem.* (1978) 473
2. a) R. Marković, M. Baranac, S. Jovetić, *Tetrahedron Lett.* **44** (2003) 7087; b) A. Rašović, P. J. Steel, E. Kleinpeter, R. Marković, *Tetrahedron* **63** (2007) 1937; c) M. Baranac-Stojanović, J. Tatar, E. Kleinpeter, R. Marković, *Synthesis* (2008) 2117; d) R. Marković, M. Baranac, P. J. Steel, E. Kleinpeter, M. Stojanović, *Heterocycles* **65** (2005) 2635; e) R. Marković, M. Stojanović, *Synlett* (2009) 1997; f) A. V. Tverdokhlebov, A. P. Andrushko, A. A. Tolmachev, *Synthesis* (2006) 1433
3. a) E. Kleinpeter, S. Klod, W.-D. Rudorf, *J. Org. Chem.* **69** (2004) 4317; b) E. Kleinpeter, *J. Serb. Chem. Soc.* **71** (2006) 1; c) J. Sandström, *Top. Stereochem.* **14** (1983) 83
4. a) M. Kivala, F. Diederich, *Acc. Chem. Res.* **42** (2009) 235; b) J.-M. Lehn, *Angew. Chem. Int. Ed. Engl.* **29** (1990) 1304 (and references therein)
5. a) J. L. Brédas, G. B. Street, *Acc. Chem. Res.* **48** (1985) 309; b) A. O. Patil, A. J. Heeger, F. Wudl, *Chem. Rev.* **88** (1988) 183
6. a) R. Marković, A. Shirazi, Z. Džambaski, M. Baranac, D. Minić, *J. Phys. Chem.* **17** (2004) 118; b) R. Marković, M. Baranac, N. Juranić, S. Macura, I. Cekić, D. Minić, *J. Mol. Struct.* **800** (2006) 85
7. G. Kaupp, *Top. Stereochem.* **25** (2006) 303 (and references therein)
8. a) E. Kleinpeter, B. A. Stamboliyska, *J. Org. Chem.* **73** (2008) 8250; b) A. Basheer, Z. Rappoport, *Org. Biomol. Chem.* **6** (2008) 1071
9. a) J. G. Ángyán, R. A. Poirier, Á. Kucsman, I. G. Csizmadia, *J. Am. Chem. Soc.* **109** (1987) 2237; b) S. Wu, A. Greer, *J. Org. Chem.* **65** (2000) 4883
10. S. F. Tan, K. P. Ang, G. F. How, *J. Chem. Soc. Perkin Trans. 2* (1988) 2045
11. D. M. Minić, Z. Nedić, R. Marković, *J. Therm. Anal. Cal.* **95** (2009) 167
12. Y. F. Lee, D. Dollimore, *Thermochim. Acta* **323** (1998) 75
13. D. S. dos Santos, R.S. de Biasi, *J. Alloy Compd.* **335** (2002) 266.

Journal of the Serbian Chemical Society
JSCS-info@shd.org.rs • www.shd.org.rs/JSCS
J. Serb. Chem. Soc. *76* (3) 329–339 (2011)
JSCS–4121
UDC 547.852.7+542.913:547.571:547.7:615.281–188
Original scientific paper

Design, synthesis and antibacterial activity of new phthalazinedione derivatives

ABD EL-GALIL M. KHALIL, MOGED A. BERGHOT and MOSTAFA A. GOUDA*

Department of Chemistry, Faculty of Science, Mansoura University, Mansoura, 35516, Egypt

(Received 22 November 2009, revised 16 July 2010)

Abstract: Dibenzobarallene (**1**) was utilized as the key intermediate for the synthesis of some new 2-substituted 1,4-dioxo-3,4,4a,5,10,10a-hexahydro-1*H*--5,10-[1',2']-benzenobenzo[*g*]phthalazine: **2**, **5a**–**d**, **8a**–**c** and **10**. Condensation of **2** with benzaldehyde or anisaldehyde gave the corresponding acrylonitrile derivatives **3a** and **b**, respectively. Thiophene derivatives **4a** and **b** were obtained *via* the Gewald reaction of **2** with cyclohexanone or cyclopentanone, respectively. Treatment of **5d** with acetyl chloride or *p*-toluenesulfonyl chloride afforded the corresponding esters **6** and **7**, respectively. Cyclization of **8a**–**c** with formalin afforded the corresponding triazine derivatives **9a**–**c**. Ring opening of **10** with sodium hydroxide gave the corresponding triazole derivative **11**, which when alkylated with pentyl bromide afforded the pentylthio derivative **12**. Representative compounds of the synthesized products were established and evaluated as antibacterial agents.

Keywords: dibenzobarallene; phthalazine; thiophene; triazine; triazole; antibacterial agents.

INTRODUCTION

In the past decades, the synthesis of heterocyclic compounds was a subject of great interest due to their wide applicability. Heterocyclic compounds occur very widely in nature and are essential to life. Among a large variety of heterocyclic compounds, heterocycles containing the phthalazine moiety are of interest due to their pharmacological and biological activities (Fig. 1).[1–3]

The phthalazine nucleus has pronounced pharmacological applications due to its anticonvulsant,[4] cardiotonic,[5] and vasorelaxant,[6] activities. In continuation of efforts[7,8] to identify new candidates that may be of value in designing new, potent, selective and less toxic antimicrobial agent, herein the syntheses of some new heterocycles incorporating the phthalazine moiety starting from dibenzobarallene are reported.[9]

* Corresponding author. E-mail: dr_mostafa_chem@yahoo.com
doi: 10.2298/JSC091122028K

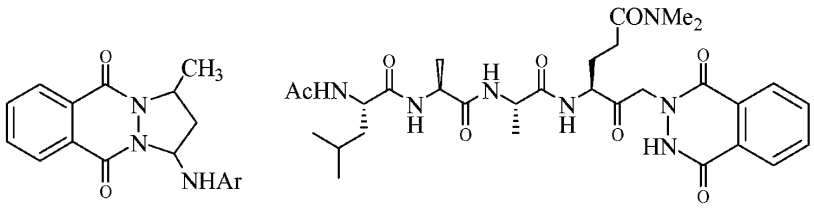

(a) (b)

Fig. 1. Antihypoxic, antipyretic agent (a),[1] and HAV 3C inhibitor (b).[2]

RESULTS AND DISCUSSION

Analytical and spectral data of the synthesized compounds are given in the Supplementary material.

Chemistry

The synthetic procedures adopted to obtain the target compounds are depicted in Schemes 1–3. Dibenzobarallene,[1] and 3-(1,4-dioxo-3,4,4a,5,10,10a-hexahydro-1*H*-5,10-[1',2']-benzenobenzo[*g*]phthalazin-2-yl)-3-oxopropiononitrile (**2**) were prepared according to previously reported methods.[9,10]

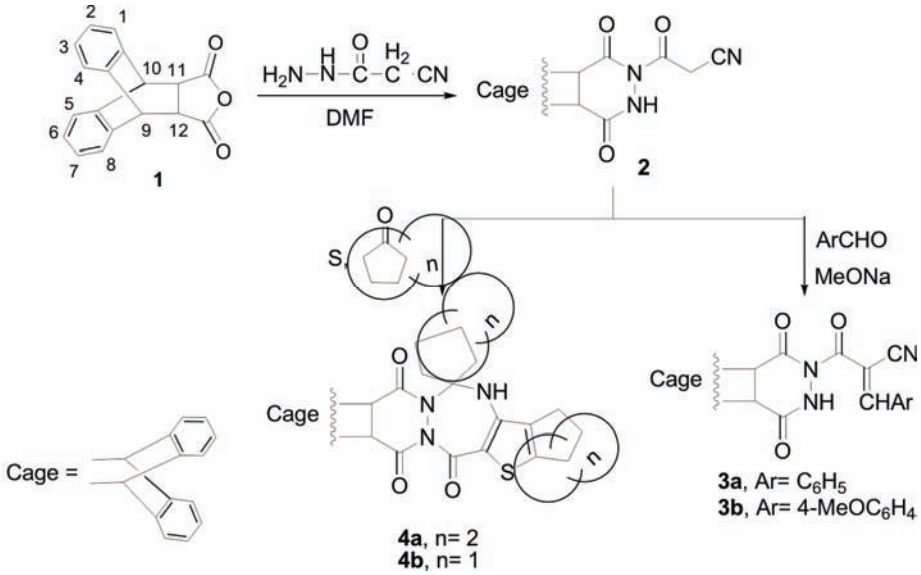

Scheme 1. Gewald and Knoevenagel reactions of propiononitrile derivative **2**.

Reaction of the propiononitrile derivative **2** with benzaldehyde or *p*-anisaldehyde, in the presence of sodium methoxide afforded the corresponding acrylonitrile derivatives **3a** and **b**, respectively. The structures of **3a** and **b** were supported by both their analytical and spectral data. The ^{1}H-NMR spectrum of **3a**

displayed a singlet signal at δ 7.8 ppm due to the methine proton of benzylidene. In addition, compound **3b** displayed two singlet signals at δ 3.8 and 7.7 ppm due to OCH_3 and methine protons, respectively. The ^{13}C-NMR spectrum of **3a** exhibited signals at 118.3 and 112.4 ppm due to ethylenic carbons; in addition, **3b** exhibited, among others, signals at δ 114, 109 and 55.3 ppm due to ethylenic and OCH_3 carbons, respectively. Furthermore, the reaction of the propiononitrile derivative **2** with cyclohexanone or cyclopentanone in a 1:2 molar ratio under Gewald reaction condition[11–13] afforded the products **4a** and **b**, respectively, in low yields (Scheme 1).

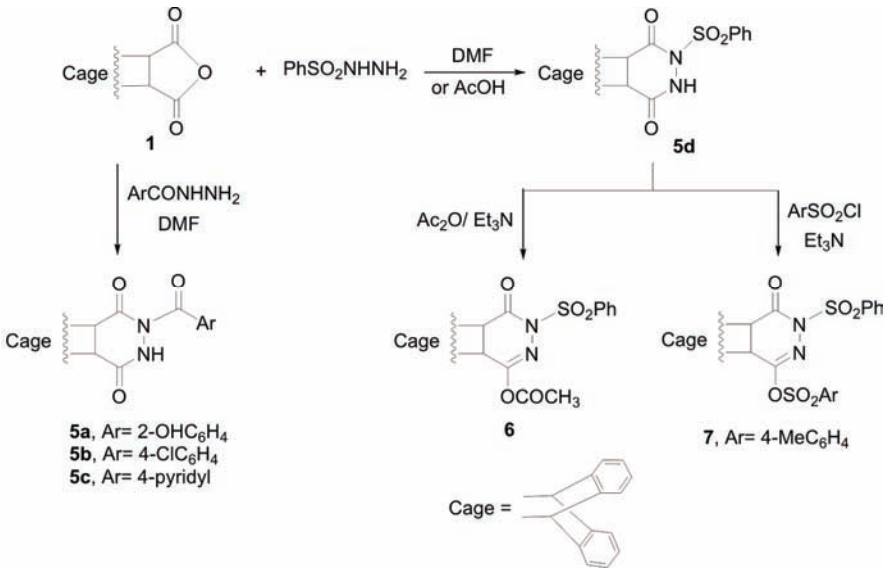

Scheme 2. Reaction of dibenzobarallene (**1**) with some acid hydrazide derivatives.

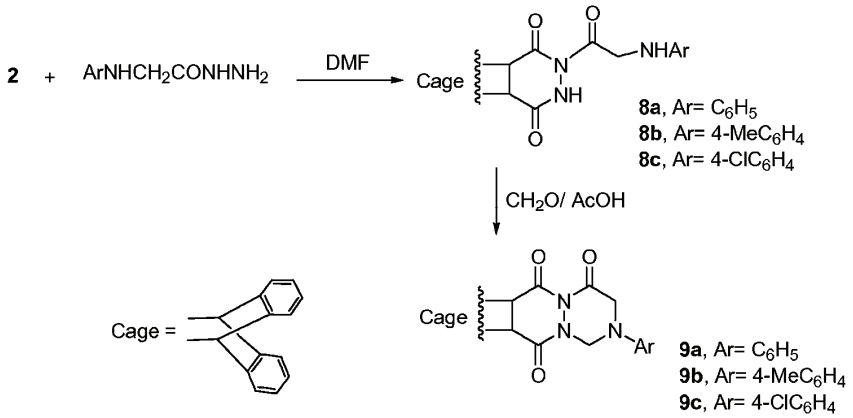

Scheme 3. Synthesis of 1,2,4-triazine derivatives **9a**–**c**.

The formulation of **4a** and **b** were based on their mass, IR, ^{1}H- and ^{13}C-NMR spectra. The ^{1}H-NMR spectra of **4a** and **b** displayed multiplet signals at δ 1.4–2.9 ppm and 1.4–3.0 ppm due to methylene and NH protons, respectively. The ^{13}C--NMR spectrum of **4a** displayed signals at δ 21.8, 22.1, 23.1, 23.8, 24.5, 24.9, 25.3, 25.7 and 26.9 ppm due to CH_2 carbons; signals at δ 78.5 due to spiro-, 139.5, 128.2, 126.6 and 125.0 due to thiophene- and 194.8, 177.3 and 174.6 ppm, due to carbonyl carbons. The mass spectrum of **4a** exhibited the molecular ion peak at *m*/*z* 549, which is in agreement with its molecular formula $C_{33}H_{31}N_3O_3S$, in addition to other fragment ion peaks at *m*/*z* 506 and 493, 451, 371, 328, 275 and 259, which are illustrated in the fragmentation pattern shown in Fig. 2.

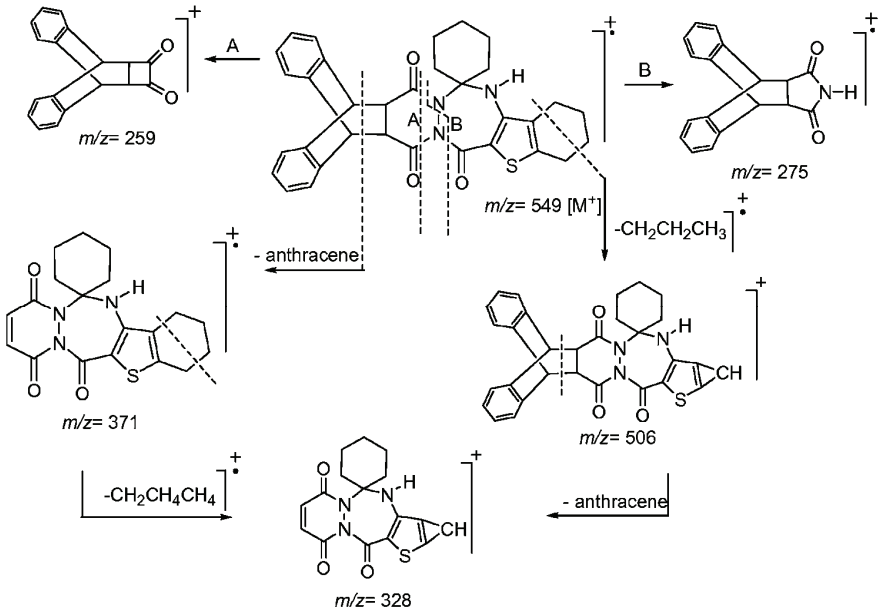

Fig. 2. Fragmentation pattern of compound **4a**.

Additionally, reaction of adduct **1** with the appropriate acid hydrazide,[14] in acetic acid or DMF afforded the interesting phthalazinedione derivatives **5a**–**d**; an analogous reaction behavior has already been reported.[15–18] The structures of **5a**–**d** were confirmed based on their spectral data. The IR spectra of **5a**–**d** showed NH bands at 3374–3163 cm^{-1} and three carbonyl bands at around 1729 and 1660 cm^{-1}. Moreover, the IR spectra of **5a** and **d** showed additional bands at 3387 and 1357 cm^{-1}, due to –OH and –SO_2N groups, respectively. Furthermore, the ^{1}H-NMR spectrum of **5a** displayed singlet signals at δ 10.8 and 11.4 ppm due to OH and NH protons, respectively; also, **5d** displayed a singlet signal at δ 10.8 ppm due to the NH proton of the phthalazine ring. The ^{13}C-NMR spectrum of **5a** revealed signals at 173.9 and 177.4 ppm due to three carbonyl carbons. The mass

spectrum of **5b** gave the molecular ion peak at *m/z* 428 and 430 corresponding to M^+ and M^++2, which are in agreement with its molecular formula $C_{25}H_{17}ClN_2O_3$. In addition to the base, a peak at *m*/*z* 178 corresponding to anthracene was also observed.

Treatment of **5d** with acetic anhydride and *p*-toluenesulfonyl chloride in the presence of a few drops of TEA yielded the phthalazine derivatives **6** and **7**, respectively. The ^{1}H-NMR spectrum of **7** revealed a singlet signal at δ 2.4 ppm due to the CH_3 group; analogous behaviors were recorded in the literature (Scheme 2).[15,17–20]

Furthermore, condensation of compound **1** with the appropriate 2-(arylamino) acetic acid hydrazide[21] in DMF yielded the corresponding phthalazinedione derivatives **8a**–**c**. The structures of **8a**–**c** were based on spectral data. Thus, the IR spectra of **8a**–**c** showed 2NH bands at 3386–3365 cm^{-1} and 3210–3197 cm^{-1} in addition to carbonyl bands at 1725–1717 cm^{-1} and 1660–1658 cm^{-1}. The mass spectrum of **8b** exhibited a molecular ion peak at *m*/*z* 437, which is in agreement with its molecular formula $C_{27}H_{23}N_3O_3$, the base peak at *m*/*z* 178 corresponding to anthracene and a fragment ion peak at *m*/*z* 259 due to M^+–anthracene. The ^{1}H--NMR spectrum of **8b** displayed singlet signals at δ 2.4, 4.8, 5.4 and 9.4 ppm due to CH_3, NHAr, CH_2 and NHCO protons, respectively.

Cyclization of the phthalazinediones **8a**–**c** by reaction with 37 % formaldehyde in glacial acetic acid was studied with the aim of preparing the 1,2,4-triazine derivatives **9a**–**c** with potential biological activities (Scheme 3).[22,23] The structures of **9a**–**c** were based on analytical and spectral data. The IR spectra of **9a**–**c** showed the absence of NH bands. The ^{1}H-NMR spectrum of **9c** revealed, beside the disappearance of NH signal, the appearance of signals at δ 5.4 and 6.2 ppm due to CH_2CO and NCH_2N protons, respectively. The mass spectrum of **9c** exhibited a molecular ion peak at *m*/*z* 469 and 471 corresponding to M^+ and M^++2, which is in agreement with its molecular formula $C_{27}H_{20}ClN_3O_3$. The major fragment ion peaks at *m*/*z* 291 and 178 were attributed to M^+–anthracene and anthracene, respectively (Scheme 3).

The remarkable biological importance of 1,2,4-triazole derivatives,[24–26] prompted an investigation of the synthesis of some new triazole derivatives of expected antimicrobial activity. Thus, the adduct **1** was reacted with thiosemicarbazide in acetic acid or in THF to give **10**. The structure of **10** was ascertained through spectral data. Its mass spectrum exhibited the molecular ion peak M^+ at *m*/*z* 348, which is consistent with the molecular formula $C_{19}H_{15}N_3O_2S$, in addition to other fragment ion peaks at *m*/*z* 275 and 178 due to M^+–$NCSNH_2$ and anthracene, respectively. The derivative **10** was then heated with dilute aqueous sodium hydroxide to yield the corresponding 5-thioxo-2,5-dihydro-1*H*-1,2,4--triazole derivative **11**, the structure of which was confirmed by analytical and spectral data (Scheme 4).

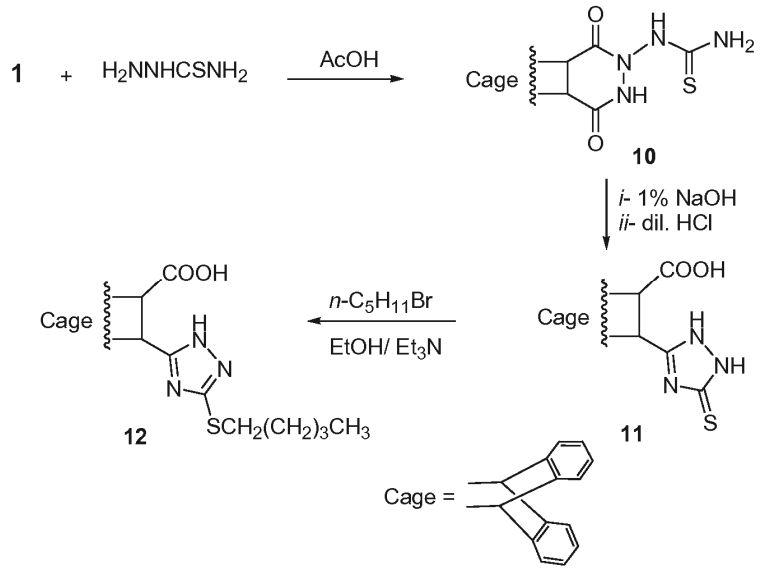

Scheme 4. Synthesis of triazole derivative **12**.

The IR spectrum of **11** showed bands at 3136, 3111 (2NH), 2937–2866 (*br*, OH), 1709 (*br*, 3CO) and 1461, 1256 cm^{-1} (C=S). Moreover, the mass spectrum of **11** exhibited the molecular ion peak at *m*/*z* 203, corresponding to M^+–(CO_2, triazole moiety). Subsequent alkylation of **11** using *n*-pentyl bromide and a few drops of TEA furnished the 5-(pentylthio)-2*H*-1,2,4-triazole derivative **12**. The spectral data of **12** are fully in accordance with the proposed structure, particularly the ^{1}H-NMR spectrum that displayed signals at δ 0.8, 1.2–1.7, 3.6, 11.5 and 12.3 ppm due to CH_3, $3CH_2$, CH_2S, NH and OH protons, respectively. The mass spectrum of **12** added further support to the assigned structure. The molecular ion peak appeared at *m*/*z* 420, the fragmentation pattern proceeded by two different routes. In one pathway, the consecutive expulsion of CO_2 and N_2 from M^+ gave peaks at *m*/*z* 375 and 347, respectively. In the other route, the molecular ion peak underwent fragmentation with the cleavage anthracene (*m*/*z* 178) and another fragment ion at *m*/*z* 241. The synchronous loss of CO_2 from the latter species gave a fragment ion peak at *m*/*z* 197. The characteristic fragment ions are shown in the fragmentation pattern given in Fig. 3.

Pharmacology

Twenty compounds were screened by the agar diffusion technique[27] for their *in vitro* antibacterial activities against two strains of bacteria *Bacillus thuringiensis* and *Escherichia coli*. The bacteria were maintained on nutrient agar. DMSO showed no inhibition zones. The agar media were incubated with different cultures of the tested microorganism. After 24 h of incubation at 30 °C, the

diameter of inhibition zone (mm) was measured (Table I). Ampicillin and chloramphenicol were purchased from the Egyptian market and used in a concentration of 2 mg ml^{-1} as references.

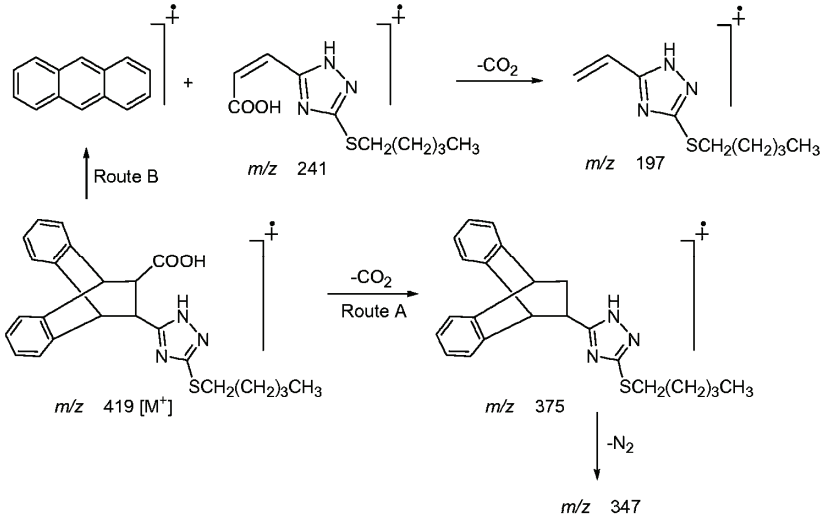

Fig. 3. Fragmentation pattern of triazole derivative **12**.

TABLE I. Inhibition zone (mean diameter of the disc in mm) as a criterion of the antibacterial activities of the newly synthesized compounds

Compound	*B. thuringiensis*	*E. coli*
2	22	16
3a	27	20
3b	28	19
4a	21	20
4b	18	17
5a	17	15
5b	32	25
5c	16	17
5d	27	22
6	26	21
7	40	22
8a	18	16
8b	16	18
8c	20	17
9a	17	16
9b	18	16
9c	17	16
10	15	14
11	16	13
12	24	22
Ampicillin	18	19
Chloramphenicol	23	20

The results depicted in Table I revealed that compounds **3a**, **3b**, **4a**, **5b**, **5d**, **6**, **7** and **12** exhibited interestingly high antibacterial activities against the reference drugs.

Thus, it would appear that the introduction of arylidene, benzothiophene, sulfonyl, sulfonate or triazole moieties enhances the antibacterial properties of 3--(1,4-dioxo-3,4,4a,5,10,10a-hexahydro-1*H*-5,10-[1',2']-benzenobenzo[*g*]phthalazin-2-yl)-3-oxopropiononitrile (**2**) (Fig. 2). By comparing the results obtained for the antibacterial activity of the compounds reported in this study with their structures, the following structure activity relationships (SARs) were postulated: *i*) compounds **3a** and **3b** were more potent than compound **2**, which may be attributed to the introduction of the arylidene moiety; *ii*) compound **4a** was more potent than compound **2** due to presence of the benzothiophenetriazaepine moiety; *iii*) compounds **5d**, **6** and **7** were more potent than compound **2** due to the replacement of the propiononitrile moiety by an arylsulfonyl moiety; *iv*) compound **7** was more potent than **5d** and **6**, which may be due to the presence of two arylsulfonate groups; *v*) compound **12** was more potent than compound **2** which may be attributed to the replacement of the pyridazinedione moiety with a triazole moiety.

EXPERIMENTAL

All melting points are in degree centigrade and were measured on a Gallenkamp electric melting point apparatus. Thin layer chromatography, TLC, analysis was performed on silica gel 60 F254 pre-coated aluminum sheets. The IR spectra were recorded using the KBr wafer technique on a Matson 5000 FTIR spectrometer, at the Faculty of Science, Mansoura University, India. The ^{1}H-NMR spectra were determined on either a Varian XL 200 MHz instrument at the Faculty of Science, Cairo University, Egypt, a Bruker WP 300 instrument at the Georg-August University Göttingen, Germany, or a Brucker AC 300 instrument at the Eberhard-Karls University, Tubingen, Germany, in $CDCl_3$ or DMSO solvent using TMS as the internal standard. The ^{13}C-NMR spectra were determined on a Brucker AC 300 instrument at the Eberhard-Karls University, Tubingen, Germany, in $CDCl_3$ or DMSO solvent using TMS as the internal standard. The mass spectra were recorded on a Finnigan MAT 212 instrument and the elemental analyses (C, H, and N) were performed in the Microanalytical Center of Cairo University, Egypt.

*2-[1,4-Dioxo-3,4,4a,5,10,10a-hexahydro-1*H*-5,10-[1',2']-benzenobenzo[g]-phthalazine-2--carbonyl]-3-(phenyl or* p*-methoxyphenyl)-acrylonitriles **3a**,**b***

General procedure. A mixture of **2** (3.57 g; 0.01 mol) and benzaldehyde or *p*-anisaldehyde (0.011 mol) was added to a solution of sodium methoxide (0.34 g; 0.015 mol) in methanol (20 ml). The reaction mixture was heated until a clear solution was obtained. The reaction mixture was left overnight. The products were separated and crystallized from ethanol–benzene to give **3a** and **3b**, respectively.

*Synthesis of (4*H*)-1,2,4-triazepin-7-one derivatives (**4a**,**b**)*

General procedure. To a mixture of **2** (1.07 g; 0.003 mol), cyclohexanone or cyclopentanone (0.006 mol) and sulfur (0.11 g; 0.0035 mol) in ethanol (30 ml) was added morpholine (0.45 ml). The reaction mixture was heated on a water bath at 80–90 °C with stirring for 1 h. Another portion of morpholine (0.15 ml) was added to the reaction mixture and stirred

for another 3.5 h. The separated products were crystallized from ethanol–benzene to give **4a** and **4b** as colorless crystals and a white powder, respectively.

*Synthesis of 2-[(2-hydroxybenzoyl) or (4-chlorobenzoyl) or (pyridine-4-carbonyl) or (benzenesulfonyl)]-2,3,4a,5,10,10a-hexahydro-5,10[1',2']-benzenobenzo[g]phthalazine-1,4-dione (**5a**–**d**)*

General procedure. A solution of **1** (2.76 g; 0.01 mol) and the corresponding acid hydrazide derivatives (0.01 mol) in DMF (20 ml) were refluxed for 3–4 h. The reaction mixture was poured into a beaker containing ice and then the separated product was crystallized from a suitable solvent to afford the phthalazine-1,4-diones **5a**–**d**. **5a**: white powder, **5b**: crystallization from DMF and separated as colorless needless crystals, **5c**: crystallization from benzene–ethanol and separated as colorless needless crystal, **5d**: crystallization from DMF–methanol.

*Synthesis of acetic acid 3-(benzenesulfonyl)-4-oxo-3,4,4a,5,10,10a-hexahydro-5,10-[1',2']--benzenobenzo[g]phthalazin-1-yl ester (**6**)*

A mixture of **5d** (0.75 g; 0.0017 mol) and a few drops of TEA in (10 ml) acetic anhydride was warmed for 2 h. The separated product was crystallized from benzene–ethanol to give **6**.

*Synthesis of toluene-4-sulfonic acid 3-(benzenesulfonyl)-4-oxo-3,4,4a,5,10,10a-hexahydro-5,10-[1',2']-benzenobenzo[g]phthalazin-1-yl ester (**7**)*

A mixture of **5d** (1.3 g; 0.003 mol) *p*-toluenesulfonyl chloride (0.66 g; 0.0035 mol) and few drops of TEA in dichloromethane (20 ml) was heated under reflux for 3 h. The solvent was distilled off and the residue was washed with water and crystallized from methanol–benzene to give **7**.

*Synthesis of 2-[1-oxo-2-[[(phenyl)/(*p*-tolyl)/(*p*-chlorophenyl)]-amino]-ethyl]-2,3,4a,5,10,10a-hexahydro-5,10-[1',2']-benzenobenzo[g]-phthalazine-1,4-dione (**8a**–**c**)*

General procedure. A solution of **1** (2.76 g; 0.01 mol) and the appropriate arylaminoacetohydrazide, namely anilinoacetohydrazide, *p*-toluidinoacetohydrazide or *p*-chloroanilinoacetohydrazide (0.01 mol) in DMF (20 ml) were heated under reflux for 3–4 h. The reaction mixture was diluted with water. The separated products were filtered and crystallized from a suitable solvent to give **8a**–**c**. **8a**: crystallized from methanol–benzene; white powder, **8b**: crystallized from methanol–benzene; **8c**: crystallized from benzene–ethanol.

*Synthesis of {2-(phenyl)/ (*p*-tolyl)/(*p*-chlorophenyl)}-2,3,5a,6,11,11a-hexahydro-6,11-[1',2']--benzenobenzo[g]-1H-[1,2,4]triazino[1,2-b]phthalayine-4,5,12-trione (**9a**–**c**)*

General procedure. A solution of **8a**–**c** (0.0017 mol), formalin 37 % (0.3 ml, 0.0035 mol) and a few drops of glacial acetic acid in DMF (10 ml) were warmed on a water bath for 2–3 h. The reaction mixture was diluted with water. The separated product was filtered and crystallized from a suitable solvent to give **9a**–**c**. **9a**: crystallized from benzene; **9b**: crystallized from benzene; colorless crystals; **9c**: crystallized from benzene–ethanol; white powder.

Synthesis of N-*[1,4-dioxo-3,4,4a,5,10,10a-hexahydro-1*H-*5,10-[1',2']-benzenobenzo[g]--phthalazin-2-yl]-thiourea (**10**)*

A mixture of **1** (1.38 g; 0.005 mol) and thiosemicarbazide (0.53 g; 0.005 mol) in glacial acetic acid (20 ml) was heated on a water path at 90 °C for 8 h. The separated product was crystallized from benzene–ethanol to give **10**. The above procedure was carried out in THF (20 ml) instead of glacial acetic acid. The reaction mixture was heated under reflux for 2.5 h. The separated product was crystallized to give **10**.

*Synthesis of 12-(5-thioxo-2,5-dihydro-1*H*-1,2,4-triazol-3-yl)-9,10-dihydro-9,10-ethanoanthracene-11-carboxylic acid (**11**)*

A solution of **10** (0.6 g; 0.0017 mol) in 1 % sodium hydroxide (100 ml) was heated on water bath at 95 °C for 2 h. The solution was left to cool and acidified with dilute hydrochloric acid. The separated product was crystallized from benzene–ethanol to give **11**.

*Synthesis of 12-[5-(pentylthio)-2*H*-1,2,4-triazol-3-yl]-9,10-dihydro-9,10-ethanoanthracene--11-carboxylic acid (**12**)*

A solution of **11** (1.0 g; 0.0028 mol), 1-bromopentane (0.5 g; 0.0032 mol) and a few drops of TEA in ethane (25 ml) was heated under reflux for 1 h. The reaction mixture was diluted with water. The separated product was crystallized from ethanol–benzene to give **12**.

In vitro *antimicrobial activity*

The tested compounds were evaluated by the agar diffusion technique,[27] using a 2 mg ml^{-1} solution in DMSO. The test organisms were *B. thuringiensis* as gram-positive bacteria and *E. coli* as gram-negative bacteria. A control using DMSO without the test compound was included for each organism. Ampicillin and chloramphenicol in DMSO were used as the reference drugs.

CONCLUSION

In conclusion, we reported herein a simple and convenient route for the synthesis of some new heterocycles based on the phthalazinedione moiety, which were tested for their antibacterial activity.

SUPPLEMENTARY MATERIAL

Analytical and spectral data of the synthesized compounds are available electronically at http://www.shd.org.rs/JSCS/, or from the corresponding author on request.

Acknowledgements. Dr. S. Bondock and Dr. E. Abd El-Latif, Chemistry Department, Faculty of Science, Mansoura University, for performing the spectral measurements, and Dr. A. Mohamadin and Dr. A. El-Morsey, Botany Department, Faculty of Science, Mansoura University, for the microbiological screening, are greatly acknowledged.

ИЗВОД

СИНТЕЗА И АНТИБАКТЕРИЈСКА АКТИВНОСТ НОВИХ ДЕРИВАТА ФТАЛАЗИНДИОНА

ABD EL-GALIL M. KHALIL, MOGED A. BERGHOT и MOSTAFA A. GOUDA

Department of Chemistry, Faculty of Science, Mansoura University, Mansoura, 35516, Egypt

Дибензобарелен (**1**) је коришћен као главни интермедијер у синтези нових 2-супституисаних (1,4-диоксо-3,4,4a,5,10,10a-хексахидро-1*H*-5,10-бензено-[1',2']-бензо[*g*]фталазина: **2**, **5a**–**d**, **8a**–**c** и **10**. Кондензацијом **2** са бензалдехидом или анизалдехидом добијени су нови деривати акрилонитрила **3a и 3b**. Деривати тиофена **4a** и **4b** добијени су Гевалдовом (*Gewald*) реакцијом **2** са циклохексаноном или циклопентаноном. Реакцијом **5d** са ацетил-хлоридом или *para*-толуенсулфонил-хлоридом добијени су одговарајући деривати триазина **6** и **7**. Циклизацијом деривата **8a**–**c** са формалдехидом добијени су одговарајући деривати триазина **9a**–**c**. Отварањем прстена деривата **10** натријум-хидроксидом добијен је одговарајући дериват **11** који алкиловањем са пентил-бромидом даје пентилтио дериват **12**. Одабрана једињења су испитана као антибактеријски агенси.

(Примљено 22. новембра 2009, ревидирано 16. јула 2010)

REFERENCES

1. F. Al'-Assar, K. N. Zelenin, E. E. Lesiovskaya, I. P. Bezhan, B. A. Chakchir, *Pharm. Chem. J.* **36** (2002) 598
2. R. P. Jain, J. C. Vederas, *Bioorg. Med. Chem. Lett.* **14** (2004) 3655
3. R. W. Carling, K. W. Moore, L. J. Street, D. Wild, C. Isted, P. D. Leeson, S. Thomas, D. O'Connor, R. M. McKernan, K. Quirk, S. M. Cook, J. R. Atack,; K. A. Wafford, S. A. Thompson, G. R. Dawson, P. Ferris, J. L. Castro, *J. Med. Chem.* **47** (2004) 1807
4. S. Grasso, G. De Sarro, A. De Sarro, N. Micale, M. Zappalà, G. Puja, M. Baraldi, C. De Micheli, *J. Med. Chem.* **43** (2000) 2851
5. Y. Nomoto, H. Obase, H. Takai, T. Hirata, M. Teranishi, J. Nakamura, T. Ohno, K. Kubo, *Chem. Pharm. Bull.* **38** (1990) 2467
6. N. Watanabe, Y. Kabasawa, Y. Takase, M. Matsukura, K. Miyazaki, H. Ishihara, K. Kodama, H. Adachi, *J. Med. Chem.* **41** (1998) 3367
7. M. A. Berghot, *Arch. Pharm.* **325** (1992) 285
8. M. A. Berghot, *Arch. Pharmacal. Res.* **24** (2001) 263
9. O. Diels, K. Alder, *Chem. Ber*. **64(B)** (1931) 2194
10. A. M. Khalil, M. A. Berghot, M. A. Gouda, *Eur. J. Med. Chem.* **44** (2009) 4434
11. B. P. McKibben, C. H. Cartwright, A. L. Castelhano, *Tetrahedron Lett*. **40** (1999) 5471
12. H. Zhang, G. Yang, J. Chen, Z. Chen, *Synlett* (2004) 3055
13. K. Gewald, E. Schinke, H. Boettcher, *Chem. Ber*. **99** (1966) 94
14. H. H. Fox, J. T. Gibas, *J. Org. Chem.* **17** (1952) 1653
15. A. Srivastava, V. Srivastava, S. A. Verma, *Pol. J. Chem*. **68** (1994) 29; *C.A.* **121** (1994) 157621t
16. H. Satoh, M. Tonegawa, K. Kitahara, R. Aoyagi, *Tokyo Ika Daigaku Kiyo* **5** (1979) 71; *C.A.* **93** (1981) 84045v
17. E. Dunkels, S. Hillers, *Latvijas PSR Zinatnu Akad. Vestis* **2** (1954) 105; *C.A.* **49** (1955) 9659h
18. E. Domagalina, I. Kurpiel, J. Mojejko, *Roczniki Chem*. 38 (1964) 571; *C.A.* 58 (1964) 10678b
19. D. Stefanye, W. L. Howard, *J. Org. Chem.* 19 (1954) 115
20. H. Śladowska, J. Potoczek, M. Sokowska, G. Rajtar, M. Sieklucka-Dziuba, T. Kocki, Z. Kleinrok, *Farmaco* **53** (1998) 468
21. S. Passeron, G. A. Brieux, *Bull. Soc. Chim. France* (1963) 35; *C.A.* **58** (1963) 13305e
22. L. C. March, G. S. Bajwa, J. Lee, J. K. Wasti, *J. Med. Chem*. **19** (1976) 845
23. I. M. Labouta, F. S. G. Soliman, M. G. Kassem, *Pharmazie* **41** (1986) 812
24. F. H. Havaldar, A. R. Patil, *Eur. J. Chem.* **5** (2008) 347
25. G. I. Chipen, D. E. Duka, V. Ya. Grinshtein, *Chem. Heterocycl. Compd.* **2** (1966) 84
26. O. M. Aboul Wafa, F. A. Berto, *Arch. Pharm. (Weinheim)* **325** (1992) 123
27. R. Cruickshank, J. P. Duguid, B. P. Marion, R. H. A. Swain, *Medicinal Microbiology*, Vol. II, 12th ed., Churchill Livingstone, London, 1975, p. 196.

Journal of the Serbian Chemical Society
JSCS@tmf.bg.ac.rs • www.shd.org.rs/JSCS
J. Serb. Chem. Soc. 76 (3) S1–S4 (2011) *Supplementary material*

SUPPLEMENTARY MATERIAL TO

Design, synthesis and antibacterial activity of new phthalazinedione derivatives

ABD EL-GALIL M. KHALIL, MOGED A. BERGHOT and MOSTAFA A. GOUDA*

Department of Chemistry, Faculty of Science, Mansoura University, Mansoura, 35516, Egypt

J. Serb. Chem. Soc. **76** (3) (2011) 329–339

Analytical and spectral data of the synthesized compounds

*Compound **3a***. Yellow crystals; yield: 65 %, 2.89 g; m.p. 330 °C. Calcd. for $C_{28}H_{19}N_3O_3$ (445.47): C, 75.49, H; 4.30; N, 9.43 %. Found: C, 75.57; H, 4.38; N, 9.50 %. IR (KBr, cm^{-1}): 3345 (NH), 2856 (aliphatic C–H), 2214 (CN), 1718 (2CO), 1662 (CO). ^{1}H-NMR (300 MHz, $CDCl_3$, δ / ppm): 3.2 (2H, *s*, C_{11}–H, C_{12}–H), 4.7 (2H, *s*, C_9–H, C_{10}–H), 7.5–7.7 (13H, *m*, Ar-H), 7.8 (1H, *s*, C=CH–Ar), 10.5 (1H, *s*, NH). ^{13}C-NMR (75 MHz, $CDCl_3$, δ / ppm): 173.8, 163.6, 145.1, 142.3, 139.4, 133.3, 129.9, 129.0, 128.5, 126.1, 125.8, 124.5, 123.7, 118.3, 112.4, 44.6, 44.4. MS (*m*/*z*, (relative abundance, %)): 445 (M^+, 0.6), 378 (0.15), 347 (0.1), 275 (5.3), 204 (0.9), 202 (3.5), 178 (100), 101 (3.5), 89 (11.5), 76 (6.2), 44 (2.0).

*Compound **3b***. Pale yellow powder; yield: 60 %, 2.85 g; m.p. 324 °C. Calcd. for $C_{29}H_{21}N_3O_4$ (475.49): C, 73.25; H, 4.45; N, 8.84 %. Found: C, 73.20; H, 4.39; N, 8.97 %. IR (KBr, cm^{-1}): 3330 (NH), 2863 (aliphatic C–H), 2220 (CN), 1721 (2CO), 1658 (CO). ^{1}H-NMR (300 MHz, $CDCl_3$, δ / ppm): 3.2 (2H, *s*, C_{11}–H, C_{12}–H), 3.8 (*s*, 3H, OCH_3), 4.7 (2H, *s*, C_9–H, C_{10}–H), 7.0–7.5 (12H, *m*, Ar–H), 7.7(1H, *s*, C=CH–Ar), 10.5 (1H, *s*, NH). ^{13}C-NMR (75 MHz, $CDCl_3$ δ / ppm): 174.0, 163.8, 160.8, 144.6, 142.2, 139.2, 131.1, 126.3, 126.0, 123.2, 124.7, 124.0, 119.1, 114.3, 109.7, 55.3, 44.6, 44.5.

*Compound **4a***. Yield: 61 %, 1.01 g; m.p. 303 °C. Calcd. for $C_{33}H_{31}N_3O_3S$ (549.68): C, 72.11; H, 5.68; N, 7.64 %. Found: C, 72.28; H, 5.74; N, 7.76 %. IR (KBr, cm^{-1}): 3270 (NH), 2939 (aliphatic C–H), 1718 (2CO), 1652 (CO). ^{1}H-NMR (300 MHz, $CDCl_3$, δ / ppm): 1.4–2.9 (19H, *m*, $9CH_2$, NH), 3.2–3.3 (2H, *s*, C_{11}–H, C_{12}–H), 4.8 (2H, *s*, C_9–H, C_{10}–H), 7.1–7.8 (8H, *m*, Ar-H). ^{13}C-NMR (75 MHz, $CDCl_3$, δ / ppm): 194.8, 174.6, 173.7, 141.3, 139.5, 138.3, 128.2, 127.1, 126.9,

* Corresponding author. E-mail: dr_mostafa_chem@yahoo.com

126.6, 125.2, 125.0, 124.2, 78.5, 45.3, 45.0, 41.8, 38.3, 32.0, 26.9, 25.7, 25.3, 24.9, 24.5, 23.8, 23.1, 22.1, 21.8. MS (*m*/*z*, (relative abundance, %)): 549 (M^+, 27.0), 506 (9.8), 493 (3.5), 451 (0.1), 371 (7.9), 328 (8.8), 275 (1.7), 259 (9.7), 193 (5.3), 178 (100), 151 (26.5), 123 (2.6), 78 (15.0), 44 (6.6).

Compound ***4b***. Yield: 67 %, 1.05 g; m.p. 274 °C. Calcd. for $C_{31}H_{27}N_3O_3S$ (521.63): C, 71.38; H, 5.22; N, 8.06 %. Found: C, 71.45; H, 5.31; N, 8.17 %. IR (KBr, cm^{-1}): 3266 (NH), 2945 (aliphatic C–H), 1725 (2CO), 1660 (CO). ^{1}H-NMR (300 MHz, $CDCl_3$, δ / ppm): 1.4–3.0 (15H, *m*, $7CH_2$, NH), 3.4 (2H, *s*, C_{11}–H, C_{12}–H), 4.9 (2H, *s*, C_9–H, C_{10}–H), 7.1–7.7 (8H, *m*, Ar–H).

Compound ***5a***. Yield: 75 %, 3.07 g; m.p. 306 °C. Calcd. for $C_{25}H_{18}N_2O_4$ (410.42): C, 73.16; H, 4.42; N, 6.83 %. Found: C, 73.21; H, 4.53; N, 6.92 %. IR (KBr, cm^{-1}): 3387 (OH), 3260 (NH), 1724 (2CO), 1659 (CO). ^{1}H-NMR (300 MHz, DMSO-d_6, δ / ppm): 3.2 (2H, *s*, C_{11}–H and C_{12}–H), 4.9 (2H, *s*, C_9–H and C_{10}–H), 7.0–7.8 (12H, *m*, Ar–H), 10.8 (1H, *s*, OH), 11.4 (1H, *s*, NH). ^{13}C-NMR (75 MHz, DMSO-d_6, δ / ppm): 177.4, 173.8, 159.1, 142.3, 139.4, 135.2, 129.4, 127.2, 126.8, 125.3, 124.7, 119.6, 117.7, 114.3, 44.9, 44.7.

Compound ***5b***. Yield: 77 %, 3.3 g; m.p. 328 °C. Calcd. for $C_{25}H_{17}ClN_2O_3$ (428.87): C, 70.01; H, 4.00; N, 6.53 %. Found: C, 70.08; H, 4.06; N, 6.61 %. IR (KBr, cm^{-1}): 3374 (NH), 2964, 2927 (aliphatic C–H), 1727 (2CO), 1661 (CO). MS (*m*/*z*, (relative abundance, %)): 430 (M^++2, 2.6), 428 (M^+, 8.0), 383 (0.7), 319 (2.7), 277 (1.8), 253 (1.1), 204 (1.2), 202 (6.2), 178 (100), 139 (40.7), 105 (17.6), 77 (8.0), 55 (1.7).

Compound ***5c***. Yield: 86 %, 3.4 g; m.p. 322 °C. Calcd. for $C_{24}H_{17}N_3O_3$ (395.41): C, 72.90; H, 4.33; N, 10.63 %. Found: C, 72.96; H, 4.38; N, 10.74 %. IR (KBr, cm^{-1}): 3163 (NH), 2996 (aliphatic C–H), 1729 (2CO), 1660 (CO). MS (*m*/*z*, (relative abundance, %)): 395 (M^+, 10.6), 370 (0.2), 316 (0.4), 275 (0.3), 231 (0.1), 202 (3.5), 178 (100), 152 (1.7), 106 (3.5), 78 (1.7).

Compound ***5d***. Yield: 72 %, 3.1 g; m.p. 250 °C. Calcd. for $C_{24}H_{18}N_2O_4S$ (430.48): C, 66.96; H, 4.21; N, 6.51 %. Found: C, 67.04; H, 4.33; N, 6.68 %. IR (KBr, cm^{-1}): 3166 (NH), 2959 (aliphatic C–H), 1718, 1662 (2CO), 1357 (SO_2N). ^{1}H-NMR (200 MHz, DMSO-d_6, δ / ppm): 3.1 (2H, *s*, C_{11}–H, C_{12}–H), 4.8 (2H, *s*, C_9–H, C_{10}–H), 7.1–7.8 (13H, *m*, Ar-H), 10.8 (1H, *s*, NH).

Compound ***6***. Yield: 93 %, 0.75 g; m.p. 282 °C. Calcd. for $C_{26}H_{20}N_2O_5S$ (472.51): C, 66.09; H, 4.27; N, 5.93 %. Found: C, 66.12; H, 4.30; N, 5.98 %. IR (KBr, cm^{-1}): 2880 (aliphatic C–H), 1707, 1673 (2CO), 1380 (SO_2N).

Compound ***7***. Yield: 82 %, 1.4 g; m.p. 269 °C. Calcd. for $C_{31}H_{24}N_2O_6S_2$ (584.66): C, 63.68; H, 4.14; N, 4.79 %. Found: C, 63.76; H, 4.26; N, 4.89 %. IR (KBr, cm^{-1}): 2910 (aliphatic C–H), 1732 (CO), 1387 (SO_2N). ^{1}H-NMR (200 MHz, DMSO-d_6, δ / ppm): 2.4 (3H, *s*, CH_3), 3.2 (2H, *s*, C_{11}–H, C_{12}–H), 4.7 (2H, *s*, C_9–H, C_{10}–H), 6.8–7.6 (17H, *m*, Ar–H).

Compound ***8a***. Yield: 80 %, 3.48 g; m.p. 257 °C. Calcd. for $C_{26}H_{21}N_3O_3$ (423.46): C, 73.74; H, 5.00; N, 9.92 %. Found: C, 73.64; H, 4.92; N, 9.85 %. IR (KBr, cm^{-1}): 3369, 3200 (2NH), 1727 (2CO), 1660 (CO).

Compound ***8b***. Yield: 62 %, 2.71 g; m.p. 248 °C. Calcd. for $C_{27}H_{23}N_3O_3$ (437.49): C, 74.12; H, 5.30; N, 9.60 %. Found: C, 74.23; H, 5.43; N, 9.74 %. IR (KBr, cm^{-1}): 3386, 3197 (NH), 2939 (aliphatic C–H), 1717 (2CO), 1658 cm^{-1} (CO). ^{1}H-NMR (200 MHz, DMSO-d_6, δ / ppm): 2.4 (3H, *s*, CH_3), 3.2 (2H, *s*, C_{11}–H, C_{12}–H), 4.7 (2H, *s*, C_9–H, C_{10}–H), 4.8 (1H, *s*, NH), 5.4 (2H, *s*, CH_2), 6.8–7.4 (12H, *m*, Ar–H), 9.4 (1H, *s*, NH). MS (*m*/*z*, (relative abundance, %)): 437 (M^+, 3.2), 259 (1.1), 202 (11.3), 178 (100), 120 (9.5), 91 (33).

Compound ***8c***. Yield: 75 %, 3.4 g; m.p. 260 °C. Calcd. for $C_{26}H_{20}ClN_3O_3$ (457.91): C, 68.20; H, 4.40; N, 9.18 %. Found: C, 68.27; H, 4.48; N, 9.27 %. IR (KBr, cm^{-1}): 3365, 3210 (2NH), 1725 (2CO), 1658 (CO).

Compound ***9a***. Yield: 78 %, 0.6 g; m.p. 274 °C. Calcd. for $C_{28}H_{22}N_2O_3$ (434.49): C, 77.40; H, 5.10; N, 6.45 %. Found: C, 77.48; H, 5.23; N, 6.53 %. IR (KBr, cm^{-1}): 2963 (aliphatic C–H), 1737 (2CO), 1732 (CO). MS (*m*/*z*, (relative abundance, %)): 435 (M^+, 14.0), 391 (0.9), 347 (2.2), 288 (0.8), 257 (5.3), 243 (2.2), 203 (7.0), 178 (100), 161 (5.3), 105 (22.6), 91 (9.7), 77 (1.3).

Compound ***9b***. Yield: 70 %, 0.52 g; m.p. 275 °C. Calcd. for $C_{29}H_{24}N_2O_3$ (448.51): C, 77.66; H, 5.39; N, 6.25 %. Found: C, 77.72; H, 5.46; N, 6.33 %. IR (KBr, cm^{-1}): 2867 (aliphatic C–H), 1727 (2CO), 1718 (CO).

Compound ***9c***. Yield: 80 %, 0.64 g; m.p. 292 °C. Calcd. for $C_{28}H_{21}ClN_2O_3$ (468.93): C, 71.72; H, 4.51; N, 5.97 %. Found: C, 71.69; H, 4.47; N, 5.95 %. IR (KBr, cm^{-1}): 2851 (aliphatic C–H), 1742 (2CO), 1730 (CO). ^{1}H-NMR (200 MHz, DMSO-d_6, δ / ppm): 3.2 (2H, *s*, C_{11}–H, C_{12}–H), 4.7 (2H, *s*, C_9–H, C_{10}–H), 5.4 (2H, *s*, NCH_2CO), 6.2 (2H, *s*, NCH_2N), 6.8–7.6 (12H, *m*, Ar–H). MS (*m*/*z*, (relative abundance, %)): 471 (M^++2, 0.12), 469 (M^+, 0.4), 291 (0.1), 178 (100), 138 (18.8), 75 (7.1).

Compound ***10***. Yield: 70 %, 1.22 g; m.p. 267–268 °C (glacial acetic); yield: 80 %, 1.4 g; m.p. 269 °C (THF). Calcd. for $C_{19}H_{16}N_4O_2S$ (364.42): C, 62.62; H, 4.43; N, 15.37 %. Found: C, 62.70; H, 4.46; N, 15.42 %. IR (KBr, cm^{-1}): 3409, 3248, 3142 (NH, NH_2), 1775, 1736 (2CO), 1461, 1111 (CSNH). MS (*m*/*z*, (relative abundance, %)): 348 (M^+, 1.0), 275 (0.7), 202 (3.2), 178 (100), 101 (9.7), 84 (6.4).

Compound ***11***. Yield: 84.7 %, 0.503 g; m.p. 197 °C. Calcd. for $C_{19}H_{15}N_3O_2S$ (349.41): C, 65.31; H, 4.33; N, 12.03 %. Found: C, 65.38; H, 4.39; N, 12.07 %. IR (KBr, cm^{-1}): 3136, 3111 (2NH), 2937–2866 (OH), 1709 (CO), 1461, 1256 (CSNH). MS (*m*/*z*, (relative abundance, %)): 203 (ethenoanthracene, 3.0), 178 (100), 152 (13.0), 81 (11.7), 59 (13.0).

Compound ***12***. Yield: 85 %, 0.7 g; m.p. 229 °C. Calcd. for $C_{24}H_{25}N_3O_2S$ (419.54): C, 68.71; H, 6.01; N, 10.02 %. Found: C, 68.80; H, 6.07; N, 10.06 %.

IR (KBr, cm^{-1}): 3172 (NH), 2949–2851 (OH), 1703 (CO). ^{1}H-NMR (200 MHz, DMSO-d_6, δ / ppm): 0.8 (3H, *t*, CH_3), 1.2–1.7 (6H, *m*, $3CH_2$), 3.2 (2H, *br*, *s*, C_{11}–H, C_{12}–H), 3.6 (2H, *t*, SCH_2), 4.7 (2H, *br*, *s*, C_9–H, C_{10}–H), 7.1–7.3 (8H, *m*, Ar-H), 11.5 (1H, *s*, NH), 12.3 (1H, *s*, OH). MS (*m*/*z*, (relative abundance, %)): 420 (M^+, 0.6), 375 (1.1), 347 (0.5), 330 (0.6), 241 (1.3), 197 (1.4), 194 (4.7), 178 (100), 97 (3.3), 51 (3.0).

Journal of the Serbian Chemical Society
JSCS-info@shd.org.rs • www.shd.org.rs/JSCS
J. Serb. Chem. Soc. 76 (3) 341–352 (2011)
JSCS–4122
UDC 542.913+57–188:547.79+547.53
Original scientific paper

Synthesis and biological activity of some triazole-bearing benzimidazole derivatives

K. F. ANSARI, C. LAL* and R. K. KHITOLIYA

Department of Chemistry, Harcourt Butler Technological Institute, Kanpur-208002, India

(Received 1 March 2010)

Abstract: A number of *N*'-(arylmethylidene)-2-(2-methyl-1*H*-benzimidazol--1-yl)acetohydrazide and 4-aryl-5-[(2-methyl-1*H*-benzimidazol-1-yl)methyl]--4*H*-1,2,4-triazole-3-thiol derivatives were synthesized by incorporating various aromatic and heterocyclic substituents on 2-methyl-1*H*-benzimidazole. The structures of all the synthesized compounds were elucidated based on their elemental analyses and spectral data. The *in vitro* activities of these compounds against bacteria and fungi were evaluated by the disc diffusion and the minimum inhibitory concentration (MIC) methods. Some of the synthesized derivatives were found to be as active as kanamycin (standard drug).

Keywords: benzimidazole; triazole; antimicrobial activity; ampicillin; kanamycin; amphotericin B.

INTRODUCTION

The benzimidazole nucleus, which is a useful structure for research and development of new pharmaceutical molecules, has received much attention in the last decade. Due to their antimicrobial activities, new benzimidazoles have been synthesized and investigated for medical applications. As resistance to antimicrobial drugs is widespread; there is an increase necessity for the identification of novel structures which could lead to the design of new, potent and less toxic antimicrobial agents. Numerous attempts have been made to develop new structural prototypes to search for more effective antimicrobials. The benzimidazoles still remain one of the most versatile classes of compounds against microbes and, therefore, are useful substructures for further molecular exploration. They exhibit a range of biological activities. Specifically, this ring system is present in numerous antioxidants,[1,2] antiparasitic,[3,4] antimicrobial,[5–8] anthelmintic,[9,10] antiproliferative,[11] anti-inflammatory,[12,13] anticonvulsant,[14] antineoplastic,[15,16] antihypertensive[17] anti HIV[18] agents. Owing to the immense importance and varied biological activities exhibited by the benzimidazoles, efforts

* Corresponding author. E-mail: c_lal12@rediffmail.com
doi: 10.2298/JSC100301029A

have been made periodically to generate libraries of these compounds and screen them for their potential biological activities. In addition, it is well documented that the triazole nucleus is associated with a variety of pharmacological activities. It displays pronounced antimicrobial,[19,20] anti-inflammatory[21] and analgesic[22] activities. The effectiveness of the benzimidazole and triazole moieties towards various microbes prompted the synthesis of some new benzimidazole derivatives bearing the triazole nucleus and the screening of their potential biological activities. In continuation of studies on biologically active benzimidazole derivatives,[23–25] the results of the synthesis of some new benzimidazole derivatives having a triazole nucleus are reported herein.

RESULTS AND DISCUSSION

Chemistry

The physical, analytical and spectral data are given in Supplementary material.

The key intermediate used for the synthesis of both series of the final compounds was 2-(2-methyl-1*H*-benzimidazol-1-yl)acetohydrazide (**3**), which in turn was prepared by the reaction of 2-methyl-1*H*-benzimidazole (**1**) with ethyl chloroacetate in the presence of anhydrous potassium carbonate as a base,[23] followed by the reaction with hydrazine hydrate (Scheme 1).[24] The reaction of compound **3** with different arylaldehyde and acetophenones in absolute ethanol gave the desired *N*'-[(aryl)methylidene]-2-(2-methyl-1*H*-benzimidazol-1-yl)acetohydrazides **4a**–**v**. The *N*-(aryl)-2-[(2-methyl-1*H*-benzimidazol-1-yl)acetyl]hydrazinecarbothioamides **5a**–**k** were prepared by condensing compound **3** with appropriate phenyl isothiocyanates. Cyclization of compounds **5a**–**i** in 2 M NaOH solution under reflux finally gave the 4-(aryl)-5-[(2-methyl-1*H*-benzimidazol-1-yl)methyl]-4*H*-1,2,4-triazole-3-thiols **6a**–**k**. The purity of the synthesized compounds was monitored by TLC and the structures of all the derivatives were supported by spectral data. The IR, ^{1}H-NMR, ^{13}C-NMR and mass spectra are in agreement with the proposed structures. The structures of all the compounds were established based on analysis of the spectral data. The compounds **4a**–**v** showed the –CONH group band between 1657–1679 cm^{-1} in their IR spectra. The ^{1}H-NMR spectra of these compounds showed the signal of the –CONH proton between δ 9.00–9.27. In compounds **5a**–**k**, the appearance of a new band between 1220––1246 cm^{-1} showed the formation of thiosemicarbazide and the ^{1}H-NMR signal for the –NH– proton peak appeared between δ 7.04–9.03, depending on the type of substitution at the benzene ring. Compounds **6a**–**k** showed the –N–N– group band between 1253–1275 cm^{-1} and S–H group band between 2545–2562 cm^{-1}, which indicate the formation of the triazole ring. In the ^{1}H-NMR spectra of compounds **6a**–**k**, a sharp peak between δ 12.90–12.92 showed the presence of the C–SH proton and the –N–CH_2 proton signal appeared between δ 6.00–6.18. The

mass spectra of compounds **6a**–**k** exhibited molecular ion peaks at *m*/*z* 321, 351, 337, 355, 444 and 336 together with their fragmentation peaks, which indicated the formation of triazole derivatives.

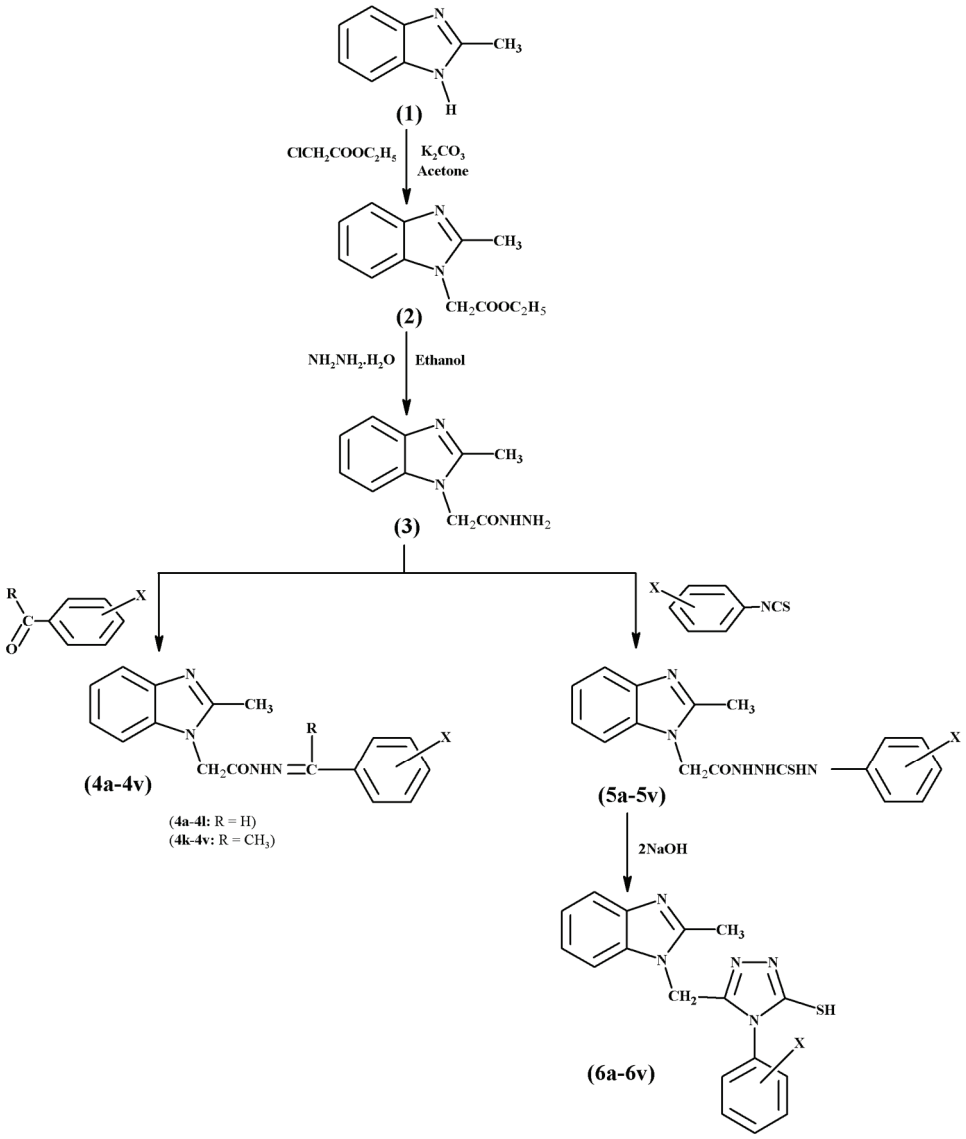

Scheme 1. Reagents and conditions: *i*) $ClCH_2COOC_2H_5$/dry acetone, K_2CO_3; RT: 10 h, *ii*) $NH_2NH_2.H_2O$/dry methanol; RT: 4–5 h, *iii*) substituted arylaldehyde or actophenone/absolute ethanol; RT: 5 h, *iv*) substituted phenyl isothiocyanate/absolute ethanol; RT: 1 h and *v*) 2NaOH; RT: 4 h.

Antimicrobial evaluation

The *in vitro* antimicrobial activity against different strains of bacteria and fungi was screened using the disc diffusion and the minimum inhibitory concentration (MIC) methods. Ampicillin, nalidixic acid and kanamycin were used as the positive controls for the bacteria and amphotericin B for the fungi.

By comparing the antimicrobial activity of the synthesized compounds, it was found that the tested compounds were more effective against the Gram positive bacteria. It is believed that the strong lipophilic character of a molecule plays an essential role in producing antimicrobial effects. These properties are seen as an important parameters related to membrane permeation in biological systems. Many of the processes of drug disposition depend on the capability of a drug to cross membranes and hence there is a high correlation with measures of lipophilicity. Hydrophobic drugs with high partition coefficients are preferentially distributed to hydrophobic compartments, such as lipid bilayers of cells, while hydrophilic drugs (low partition coefficients) are found preferentially in hydrophilic compartments, such as blood serum. Hydrophobicity/lipophilicity play a major role in determining where drugs are distributed within the body after adsorption and as a consequence in how rapidly they are metabolized and excreted. In this context, the presence of a hydrophobic moiety would be important for such activity. Moreover, many of the proteins involved in drug disposition have hydrophobic binding sites, further adding to the importance of lipophilicity.

The lipophilicity of compounds, expressed as log *P*, represents the main predictor for activity. The octanol/water partition coefficient, *C*log *P*, being a measure of hydrophobicity/ lipophilicity was calculated using ChemDraw Ultra 11.0 software integrated with Cambridgesoft Software (Cambridgesoft Corporation).[26] The results obtained are given in Table I. The calculated values of log *P* for the *N*'-(arylmethylidene)-2-(2-methyl-1*H*-benzimidazol-1-yl)acetohydrazides **4a**–**v** were lower than for the corresponding 4-aryl-5-[(2-methyl-1*H*-benzimidazol-1-yl)methyl]-4*H*-1,2,4-triazole-3-thiols **6a**–**k**. The lipophilic power of the compounds increased with increasing log *P*. The activity observed for compounds **6a**–**k**, having higher values of log *P* was slightly higher than that of the corresponding compounds **4a**–**v**, which shows that incorporation of triazole nucleus on benzimidazole derivatives did not favor antimicrobial activity.

Regarding the correlation of the antimicrobial activity of substituted benzimidazoles with the planarity of their molecules, the *ortho*-substitution in the benzene nucleus of the *N*'-(arylmethylidene)-2-(2-methyl-1*H*-benzimidazol-1--yl)acetohydrazides **4a**–**v**, *N*-aryl-2-[(2-methyl-1*H*-benzimidazol-1-yl)acetyl]-hydrazinecarbothioamides **5a**–**k** and 4-aryl-5-[(2-methyl-1*H*-benzimidazol-1--yl)methyl]-4*H*-1,2,4-triazole-3-thiols **6a**–**k** generates steric hindrance, hence they were less active than the corresponding *para*-substituted derivatives, thereby showing a marginal steric effect. The molar refractivity (*MR*), which represents

the size and polarizability of a molecule describing steric effects, was calculated (using ChemDraw Ultra 11.0 software) to explain the activity behavior of the synthesized compounds. From Table I, it can be inferred that a slightly lower value of the molar refractivity favored the activity ratio.

TABLE I. Calculated log *P* and molar refractivity of compounds **4a**–**4v**, **5a**–**5k** and **6a**–**6k** (calculated from ACD/Labs software, v.12.0 (Advanced Chemistry Development, Inc.))

Compound	X	*C* log *P*	*MR*
4a	–	2.626	85.62
4b	2-CH_3	2.858	91.58
4c	2-CH_2CH_3	2.754	96.12
4d	2-$CH_2CH_2CH_3$	3.283	100.72
4e	2-OH	3.225	87.44
4f	4-OH	2.595	87.44
4g	2-OCH_3	2.415	92.87
4h	4-OCH_3	2.845	92.87
4i	2-Cl	2.739	90.23
4j	4-Cl	3.339	90.23
4k	4-NH_2	1.999	90.45
4l	–	3.485	89.72
4m	2-CH_3	3.984	95.62
4n	2-CH_2CH_3	4.513	100.21
4o	2-$CH_2CH_2CH_3$	5.042	104.81
4p	2-OH	2.818	91.53
4q	4-OH	2.818	91.53
4r	2-OCH_3	3.404	96.97
4s	4-OCH_3	3.404	96.97
4t	2-Cl	4.198	94.32
4u	4-Cl	4.198	94.32
4v	4-NH_2	2.258	94.54
5a	–	1.978	96.49
5b	2-CH_3	2.477	102.39
5c	2-CH_2CH_3	3.006	106.99
5d	2-$CH_2CH_2CH_3$	3.535	111.59
5e	2-OH	1.311	98.31
5f	4-OH	1.311	98.31
5g	2-OCH_3	1.897	103.74
5h	4-OCH_3	1.897	103.74
5i	2-Cl	2.691	101.10
5j	4-Cl	2.691	101.10
5k	4-NH_2	0.751	101.32
6a	–	3.455	93.15
6b	2-CH_3	3.954	99.05
6c	2-CH_2CH_3	4.483	103.65
6d	2-$CH_2CH_2CH_3$	5.012	108.25
6e	2-OH	3.160	94.97
6f	4-OH	3.160	94.97

TABLE I. Continued

Compound	X	*C* log *P*	*MR*
6g	2-OCH_3	3.434	100.4
6h	4-OCH_3	3.434	100.4
6i	2-Cl	4.171	97.76
6j	4-Cl	4.171	97.76
6k	4-NH_2	2.576	97.98

Considering the structure of the compounds that exhibit antimicrobial activity, substituted methylidene and triazole may play a role for the antimicrobial activity. From the results, which indicated that tested compounds were more active against Gram-positive bacteria than Gram-negative bacteria, it may be concluded that the antimicrobial activity of the compounds is related to cell wall structure of the bacteria. This is possible because the cell wall is essential for the survival of many bacteria and some antibiotics are able to kill bacteria by inhibiting a step in the synthesis of peptidoglycan. Gram positive bacteria possess a thick cell wall containing many layers of peptidoglycan and teichoic acids, but in contrast, Gram negative bacteria have a relatively thin cell wall consisting of a few layers of peptidoglycan surrounded by a second lipid membrane containing lipopolysachharides and lipoproteins. These differences in cell wall structure can produce differences in the antibacterial susceptibility and some antibiotics that can kill only Gram-positive bacteria are ineffective against Gram negative bacteria.[27]

Antibacterial activity

The results of the preliminary testing of the antibacterial activity of the final compounds are given in Table II. The results revealed that the majority of the synthesized compounds show varying degrees of inhibition against the tested microorganisms. In general, the inhibitory activity against the Gram-positive bacteria was higher than against the Gram-negative bacteria. The triazole derivatives **6a**–**k** displayed the lowest activity. Compounds **4a**, **4b**, **4e**, **4f**, **4k** and **4l** showed excellent activity against the Gram-positive bacteria. None of the compounds tested in this study displayed any effect against *Escherichia coli* and *Salmonella typhi* and only an insignificant effect against *Pseudomonas aeruginosa* (except compound **4a**, which showed the same activity as the standard drug against *P. aeruginosa*).

The values of the minimum inhibitory concentration (*MIC*) against the microorganism susceptible in the preliminary test are reported in Table III. The results showed significant inhibitory effects, with the majority of the compounds tested having *MIC* values of 2–16 μg mL^{-1}. This class of compounds presented high activity against *Staphylococcus aureus* and *Bacillus subtilis*, especially compounds **4a**, **4b**, **4f**, **4h**, **4j**, **4l**, **4s**, **4u**, **5f** and **5j** showed good antibacterial activity against these two microorganisms. For *Streptococcus mutans*, these compounds

were as active as the standard kanamycin (*MIC* = 4 μg mL^{-1}), but less active than ampicillin. Activity compared to ampicillin was also encountered for **4a**, **4f**, **4k**, and **4v** against *B.subtilis* and for **4a**, **4b**, **4f**, **4l**, **4s**, **4v** and **5j** against *P. aeruginosa*.

TABLE II. Inhibitory zone diameter of compounds against bacterial strains using the disc diffusion method (Sa – *S. aureus*, Bs – *B. subtilis*, Sm – *S. mutans*, Ec – *E. coli*, Pa – *P. aeruginosa* and St – *S. typhi*)

Compd.	Mean zone inhibition, mm[a]					
	Gram-positive bacteria			Gram-negative bacteria		
	Sa	Bs	Sm	Ec	Pa	St
4a	35	25	20	–[b]	18	–
4b	33	24	19	–	16	–
4d	28	23	18	–	17	–
4e	24	23	16	–	14	–
4f	35	25	19	–	17	–
4g	24	19	15	–	13	–
4h	33	28	18	–	16	–
4i	27	18	14	–	12	–
4j	30	25	20	–	16	–
4k	35	–	16	–	16	–
4l	33	23	19	–	16	–
4m	29	20	17	–	16	–
4p	22	20	16	–	15	–
4r	21	–	16	–	14	–
4s	28	24	18	–	17	–
4t	24	18	15	–	–	–
4u	28	22	18	–	17	–
4v	29	24	20	–	17	–
5a	24	18	–	–	10	–
5b	28	24	17	–	16	–
5d	25	21	17	–	14	–
5f	29	24	19	–	17	–
5g	18	20	–	–	–	–
5j	24	18	20	–	15	–
6b	20	18	12	–	10	–
6f	24	19	18	–	12	–
6h	21	18	18	–	16	–
Ampicillin[c]	38	28	22	20	NT[d]	NT
Nalidixic acid[c]	NT	NT	NT	28	18	20

[a]*n* = 3; [b]indicates no sensitivity or mean inhibition zone diameter less than 7 mm; [c]ampicillin (10 μg/disc) and nalidixic acid (30 μg/disc) used as positive reference, synthesized compounds, 300 μg/disc; [d]not tested

Antifungal activity

The *in vitro* antifungal activities of the derivatives of *N*'-(arylmethylidene)--2-(2-methyl-1*H*-benzimidazol-1-yl)acetohydrazide (**4a**–**v**), *N*-aryl-2-[(2-methyl-1*H*-benzimidazol-1-yl)acetyl]hydrazinecarbothioamide (**5a**–**k**) and 4-aryl-5-[(2-

-methyl-1*H*-benzimidazol-1-yl)methyl]-4*H*-1,2,4-triazole-3-thiol (**6a**–**k**) and of amphotericin B as a reference drug on three fungi species are given in Table IV. Some of the compounds tested were endowed with a good activity against *Candida albicans*. Of these, 2-(2-methyl-1*H*-benzimidazol-1-yl)-*N*'-(phenylmethylidene)acetohydrazide **4a** and *N*'-[1-(4-aminophenyl)ethylidene]-2-(2-methyl-1*H*--benzimidazol-1-yl)acetohydrazide (**4v**) were found to be the most potent, showing an *MIC* value 4 μg mL^{-1}, whereas the *MIC* value for compounds **4b**, **4f**, **4i**, **4k**, **4v** and **5a** was 8 μg mL^{-1} (Table III). Compounds with a *para*-substitution in the benzene ring (**4a**, **4b**, **4d**, **4f**, **4j**, **4k**, **4s**, **4u**, **5d** and **5j**) were also found to be potent against *Aspergillus flavus* (inhibition zone 18–22 mm) with medium activity. All the other tested compounds exhibited insignificant chemotherapeutical activity against the tested microorganism.

TABLE III. Antimicrobial activity of tested compounds expressed as *MIC* in μg mL^{-1} (Sa – *S. aureus*, Bs – *B. subtilis*, Sm – *S. mutans*, Pa – *P. aeruginosa* and Ca – *C. albicans*)

Compd.	Sa	Bs	Sm	Pa	Ca
4a	4	4	4	8	4
4b	8	8	4	8	8
4d	16	16	16	NT[a]	32
4e	16	16	16	16	NT
4f	4	4	4	8	8
4g	16	NT	32	16	32
4h	16	8	4	4	16
4i	8	8	16	16	8
4j	16	32	4	16	16
4k	4	4	8	16	8
4l	4	8	4	8	16
4m	8	16	8	NT	16
4p	NT	16	16	32	32
4r	16	32	16	16	16
4s	8	8	4	8	16
4t	16	NT	32	16	NT
4u	8	8	4	16	8
4v	8	4	4	8	4
5a	8	16	8	16	8
5b	8	16	8	32	16
5d	16	16	8	16	16
5f	4	8	4	NT	16
5g	32	32	64	32	16
5j	4	8	4	8	NT
6b	NT	NT	16	16	32
6f	8	16	16	16	NT
6h	8	16	32	32	32
Ampicillin	2	2	≤1	4	NT
Kanamycin	2	≤1	4	2	NT
Amphotericin B	NT	NT	NT	NT	2

[a]Not tested

TABLE IV. Inhibitory zone of compounds against fungal strains using the disc diffusion method (Ca – *C. albicans*, An – *A. niger* and Af – *A. flavus*)

Compd.	Mean zone of inhibition, mm (n = 3)		
	Ca	An	Af
4a	28	24	18
4b	24	23	20
4d	22	22	22
4e	20	20	–[a]
4f	24	22	22
4g	–	–	10
4h	25	10	12
4i	16	14	–
4j	18	23	20
4k	26	22	22
4l	24	20	17
4m	–	13	15
4p	18	17	10
4r	12	14	13
4s	18	24	18
4t	12	14	–
4u	18	18	18
4v	28	20	–
5a	18	–	12
5b	17	10	12
5d	15	22	20
5f	16	18	12
5g	12	12	10
5j	16	20	22
6b	17	14	10
6f	18	14	10
6h	18	16	15
Amphotericin B[b]	28	32	28

[a]No sensitivity or mean inhibition zone diameter lower than 7 mm; [b]amphotericin B (30μg/disc) used as positive reference; synthesized compounds: 300μg/disc

EXPERIMENTAL

All melting points were determined in an open capillary tube and are uncorrected. Infrared spectra were recorded in KBr on Perkin-Elmer RX1 spectrophotometer. The ^{1}H-NMR and ^{13}C-NMR spectra were measured in $CDCl_3$ solutions on a Bruker DRX-300 MHz spectrometer using TMS as an internal reference (chemical shift in δ / ppm). The mass spectra were recorded on a Jeol SX-102 instrument. Elemental analyses were realized using an Elementar Vario EL III elemental analyzer. Thin layer chromatography was performed on silica plates pre-coated with Merck Silica Gel 60 F254 and column chromatography with silica gel.

Synthesis of N'*-(arylmethylidene)-2-(2-methyl-1*H*-benzimidazol-1-yl)acetohydrazides* ***4a–v***

General procedure. An equimolar (0.001 mol) mixture of compound **3** and substituted arylaldehyde or substituted acetophenone in absolute ethanol (50 ml) containing 2–3 drops of

glacial acetic acid was refluxed for 5 h and the solvent removed. The separated solid was filtered and recrystallized from a suitable solvent to give compounds **4a**–**v**.

Synthesis of N-*aryl-2-[(2-methyl-1*H-*benzimidazol-1-yl)acetyl]hydrazinecarbothioamides* ***5a–k***

General procedure. To a boiling solution of compound **3** (0.001 mol) in absolute ethanol (30 ml) was added an appropriate substituted phenyl isothiocyanate (0.001 mol) and the reaction mixture was refluxed for 1 h, concentrated and cooled. The separated solid was filtered and recrystallized from an appropriate solvent to give **5a**–**k**.

*Synthesis of 4-aryl-5-[(2-methyl-1*H-*benzimidazol-1-yl)methyl]-4*H-*1,2,4-triazole-3-thiols* ***6a–k***

General procedure. A solution of compound **5** (0.001 mol) in 2 M NaOH (20 ml) was refluxed for 4 h, cooled, poured into ice cold water (50 ml) and neutralized with acetic acid. The precipitate was filtered, washed with water and recrystallized from an appropriate solvent to afford compounds **6a**–**k**.

Antimicrobial activity test

All the synthesized compounds **4a**–**v** and **6a**–**k** were screened for their *in vitro* antimicrobial activity against the standard strains: *Staphylococcus aureus* (ATCC 29213), *Bacillus subtilis* (MTCC 121), *Streptococcus mutans* (MTCC 890), *Escherichia coli* (ATCC 25922), *Pseudomonas aeruginosa* (MTCC 741) and *Salmonella typhi* (MTCC 733) and the fungi *Candida albicans* (MTCC 1637), *Aspergillus flavus* (AIIMS) and *Aspergillus niger* (AIIMS).

The preliminary antimicrobial activity was reported using the disc diffusion method.[28] In this method, paper discs (6 mm) containing specific amounts of an antimicrobial agent (300 μg for the synthesized compounds) were placed on the surface of an agar plate inoculated with a standardized suspension of the tested microorganisms. The plates were incubated at 35 °C for 24 and 48 h, respectively, for the bacteria and fungi. Amphotericin B (30 μg) for the fungi, ampicillin (10 μg) for the Gram-positive bacteria and nalidixic acid (30 μg) for the Gram-negative bacteria were used as standard drugs. Paper discs with only dimethyl sulfoxide (DMSO) were utilized as the negative control.

The twofold serial dilution technique[29,30] was followed to determine the *MIC* of the compounds against the microorganisms susceptible in the preliminary tests (Gram positive bacteria and fungi). The test compounds were dissolved in DMSO and then diluted with culture medium (Mueller–Hinton agar medium for the bacteria and Sabouraud liquid medium for the fungi), at the required final concentration, within the range 128–1.0 μg mL^{-1}. A plate for the bacteria and a tube for the fungi containing only culture medium and DMSO, in the same dilution as in the experiments, were used as negative controls.

The final amount applied was of 10^4 CFU/plate for the bacteria and 10^3 CFU/tube for the fungi. The *MIC* values were read after incubation at 35 °C for a period of 20 (bacteria) and 48 h (fungi). The lowest concentration of the test substance that completely inhibited growth of the microorganism was recorded as the *MIC*, expressed in μg mL^{-1}. Ampicillin and kanamycin for the bacteria and amphotericin B for the fungi were used as standard drugs. All experiments were performed in triplicate.

CONCLUSIONS

In conclusion, several benzimidazole derivatives were synthesized starting with 2-methylbenzimidazole. A microbiological study was undertaken to evaluate the effect of the synthesized compounds on different bacteria and fungal strains. With regards to the structure–activity relationship of the derivatives of

N'-(arylmethylidene)-2-(2-methyl-1*H*-benzimidazol-1-yl)acetohydrazide **4a**–**v**, *N*-aryl-2-[(2-methyl-1*H*-benzimidazol-1-yl)acetyl]hydrazinecarbothioamide **5a**–**k** and 4-aryl-5-[(2-methyl-1*H*-benzimidazol-1-yl)methyl]-4*H*-1,2,4-triazole-3-thiol **6a**–**k**, the group with a substituent on *para*-position exhibited enhanced antimicrobial activity in comparison to *ortho*-substitution on the same ring. Moreover, *para* substituted hydroxy and chloro derivatives produced activity equal to that of ampicillin for *S. aureus*. Similarly, in the case of the antifungal activity, *para* hydroxy and *para* chloro substituted derivatives were proved to be the most active compounds and their activity was equal to that of amphotericin B. These differences in activity depended on the substitution of different reactive group on the benzimidazole moiety. Based on the observations, it may be concluded that the order of inhibitory effect against S. *aureus* was influenced by the type of substitution present at *para* position, *i.e.*, the derivatives with chloro and hydroxyl groups showed maximum activity in comparison to those with a methyl group, which in turn were more reactive than the methoxy derivatives.

More extensive studies are required to confirm these preliminary results and studies involving the mechanism of action are necessary for a complete understanding of their antimicrobial activity, as well as structural modifications on the final investigated compounds to improve their biological activity.

SUPPLEMENTARY MATERIAL

The physical, analytical and spectral data of synthesized compounds are available electronically from http://www.shd.org.rs/JSCS/, or from the corresponding author on request.

Acknowledgement. The authors are thankful to the Head, RSIC, Central Drug Research Institute, Lucknow, India, for providing the spectral and analytical data of the compounds. Authors are thankful to the University Grants Commission, New Delhi, India, for providing financial grant vide F. No. 37-494/2009 (SR).

И З В О Д

СИНТЕЗА И БИОЛОШКА АКТИВНОСТ НЕКИХ ТРИАЗОЛСКИХ ДЕРИВАТА КОЈИ САДРЖЕ БЕНЗИМИДАЗОЛНИ СТРУКТУРНИ СЕГМЕНТ

K. F. ANSARI, C. LAL и R. K. KHITOLIYA

Department of Chemistry, Harcourt Butler Technological Institute, Kanpur – 208002, India

Синтетисани су бројни деривати *N*'-(супституисани фенилметилиден)-2-(2-метил-1*H*-бензимидазол-1-ил)ацетохидразида и 4-(супституисани фенил)-5-[(2-метил-1*H*-бензимидазол-1-ил)метил]-4*H*-1,2,4-триазол-3-тиола који садрже различите ароматичне и хетероароматичне супституенте на 2-метил-1*H*-бензимидазолу. Структуре синтетисаних једињења утврђене су на основу елементалне анализе и спектралних података. Испитане су *in vitro* активности једињења према бактеријама и гљивама диск-дифузионом методом и методом минималних инхибиторних концентрација. Нека од испитиваних једињења активна су у истој мери као и стандардни лек канамицин.

(Примљено 1. марта 2010)

REFERENCES

1. G. Ayhan-Kilcigil, C. Kus, E. D. Ozdamar, B. Can-Eke, M. Iscan, *Arch. Pharm.* **34** (2007) 607
2. Z. Ates-Alagoz, C. Kus, T. Coban, *J. Enzyme Inhibit. Med. Chem.* **20** (2005) 325
3. G. Navarrete-Vázquez, R. Cedillo, A. Hernández-Campos, L. Yépez, F. Hernädez-Luis, J. Valdez, R. Morales, R. Cortés, M. Hernández, R. Castillo, *Bioorg. Med. Chem.* **11** *(*2001) 187
4. F. Hernández-Luis, A. Hernández-Campos, R. Castillo, G. Navarrete-Vázquez, O. Soria-Arteche, M. Hernández-Hernández, L. Yépez-Muli, *Eur. J. Med. Chem.* **45** (2010) 3135
5. Y. Özkay, Y. Tunalı, H. Karaca, İ. Işıkdağ, *Eur. J. Med. Chem.* **45** (2010) 3293
6. N. S. Pawar, D. S. Dalal, S. R. Shimpi, P. P. Mahulikar, *Eur. J. Pharm. Sci.* **21** (2004) 115
7. K. G. Desai, K. R. Desai, *Bioorg. Med. Chem.* **14** (2006) 8271
8. O. O. Guven, T. Erdogan, H. Goker, S. Yildiz, *Bioorg. Med. Chem. Lett.* **17** (2007) 2233
9. A. T. Mavrova, P. S. Denkova, Y. A. Tsenov, K. K. Anichina, D. I. Vutchev, *Bioorg. Med. Chem.* **15** (2007) 6291
10. A. Ts. Mavrova, D. Vuchev, K. Anichina, N. Vassilev, *Eur. J. Med. Chem.* **45** (2010) 5856
11. L. Garuti, M. Roberti, M. Malagoli, T. Rossi, M. Castelli, *Bioorg. Med. Chem. Lett.* **10** (2000) 2193
12. H. T. Le, I. B. Lemaire, A. K. Gilbert, F. Jolicoeur, N. Leduc, S. Lemaire, *J. Pharmacol. Exp. Ther.* **309** (2004) 146
13. P. A. Thakurdesai, S. G. Wadodkar, C. T. Chopade, *Pharmacol. Online* **1** (2007) 314
14. A. Chimirri, A. De Sarro, G. De Sarro, R. Gitto, M. Zappala, *Farmaco* **56** (2001) 821
15. S. Ram, D. S. Wise, L. L. Wotring, J. W. McCall, L. B. Townsend, *J. Med. Chem.* **35** (1992) 539
16. A. A. M. Abdel-Hafez, *Arch. Pharm. Res.* **30** (2007) 678
17. K. Kubo, Y. Inada, Y. Kohara, Y. Sugiura, M. Ojima, K. Itoh, Y. Furukawa, Y. K. Nishikawa, T. Naka, *J. Med. Chem.* **36** (1993) 1772
18. A. Rao, A. Chimirri, E. De Clercq, A. M. Monforte, P. Monforte, C. Pannecouque, M. Zappala, *Farmaco* **57** (2002) 819
19. B. G. Mohammed, M. A. Hussein, A. M. Abdel-Alim, M. Hashem, *Arch. Pharm. Res.* **29** (2006) 26
20. N. N. Güllerman, H. N. Dogan, S. Rollas, C. Johansson, C. Celik, *Farmaco* **56** (2001) 953
21. J. R. Maxwell, D. A. Wasdahl, A. C. Wolfson, *J. Med. Chem.* **27** (1984) 1565
22. G. T-Zitouni, Z. A. Kaplancikli, K. Erol, F. S. Kilic, *Farmaco* **54** (1999) 218
23. K. F. Ansari, C. Lal, *Eur. J. Med. Chem.***44** (2009) 2294
24. K. F. Ansari, C. Lal, *Eur. J. Med. Chem.* **44** (2009) 4028
25. K. F. Ansari, C. Lal, *J. Chem. Sci*. **121** (2009) 1017
26. ChemDraw Ultra 11.0.1, CambridgeSoft Corporation, Cambridge.
27. A. L. Koch, *Clin. Microbiol. Rev.* **16** (2003) 573
28. National Committee for Clinical Laboratory Standards, *Performance Standards for Antimicrobial Disk Susceptibility tests; Approved Standard M2-A8*, Clinical and Laboratory Standards Institute, Wayne, PA, USA, 2003.
29. National Committee for Clinical Laboratory Standards, *Methods for Dilution Antimicrobial Susceptibility Tests for Bacteria that Grow Aerobically, Approved Standard M7--A6*, Clinical and Laboratory Standards Institute, Wayne, PA, USA, 2003.
30. National Committee for Clinical Laboratory Standards, *Reference Method for Broth Dilution Antifungal Susceptibility Testing of Yeast; Approved Standard M27-A2*, Clinical and Laboratory Standards Institute, Wayne, PA, USA, 2002.

Journal of the Serbian Chemical Society
JSCS@tmf.bg.ac.rs • www.shd.org.rs/JSCS
J. Serb. Chem. Soc. 76 (3) S5–S17 (2011) *Supplementary material*

SUPPLEMENTARY MATERIAL TO

Synthesis and biological activity of some triazole-bearing benzimidazole derivatives

K. F. ANSARI, C. LAL* and R. K. KHITOLIYA

Department of Chemistry, Harcourt Butler Technological Institute, Kanpur-208002, India

J. Serb. Chem. Soc. 76 (3) (2011) 341–352

TABLE I-S. Physical and analytical properties of compounds **4a**–**k**

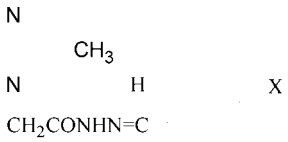

Compd.	X	Yield %	M.p. °C	Formula	MW g mol^{-1}	Recrystalization solvent	Calcd.; Found, % C	H	N
4a	–	78	170–72	$C_{17}H_{16}N_4O$	292.33	Methanol	69.85; 69.83	5.52; 5.50	19.17; 19.15
4b	4-CH_3	75	188–90	$C_{18}H_{18}N_4O$	306.36	Methanol	70.57; 70.54	5.92; 5.90	18.29; 18.27
4c	4-CH_2CH_3	69	195–97	$C_{19}H_{20}N_4O$	320.38	Methanol	71.23; 71.23	6.29; 6.27	17.49; 17.48
4d	4-$CH_2CH_2CH_3$	72	196–98	$C_{20}H_{22}N_4O$	334.41	Methanol	71.83; 71.80	6.63; 6.60	16.75; 16.74
4e	2-OH	82	182–84	$C_{17}H_{16}N_4O_2$	308.33	Methanol–water	66.22; 66.20	5.23; 5.21	18.17; 18.15
4f	4-OH	74	185–87	$C_{17}H_{16}N_4O_2$	308.33	Methanol–water	66.22; 66.21	5.23; 5.20	18.17; 18.15
4g	2-OCH_3	75	160–62	$C_{18}H_{18}N_4O_2$	322.36	Acetone	67.07; 67.05	5.63; 5.60	17.38; 17.36
4h	4-OCH_3	70	169–71	$C_{18}H_{18}N_4O_2$	322.36	Acetone	67.07; 67.04	5.63; 5.60	17.38; 17.36
4i	2-Cl	81	196–98	$C_{17}H_{15}N_4OCl$	326.78	Methanol	62.48; 62.46	4.63; 4.61	17.15; 17.14
4j	4-Cl	80	178–80	$C_{17}H_{15}N_4OCl$	326.78	Methanol–water	62.48; 62.46	4.63; 4.60	17.15; 17.14
4k	4-NH_2	73	150–52	$C_{17}H_{17}N_5O$	307.35	Acetone	66.43; 66.41	5.58; 5.56	22.79; 22.77

* Corresponding author. E-mail: c_lal12@rediffmail.com

TABLE II-S. Physical and analytical properties of compounds **4l–v**

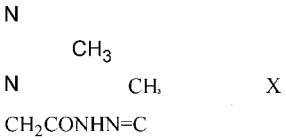

Compd.	X	Yield %	M.p. °C	Formula	MW g mol^{-1}	Recrystalization solvent	Calcd.; Found, % C	H	N
4l	–	80	160–62	$C_{18}H_{18}N_4O$	306.36	Glacial acetic acid	70.57; 70.55	5.92; 5.90	18.29; 18.27
4m	4-CH_3	79	180–82	$C_{19}H_{20}N_4O$	320.38	Ethanol	71.23; 71.20	6.29; 6.27	17.49; 17.46
4n	4-CH_2CH_3	78	188–90	$C_{20}H_{22}N_4O$	334.41	Ethanol	71.83; 71.81	6.63; 6.60	16.75; 16.73
4o	4-$CH_2CH_2CH_3$	75	195–97	$C_{21}H_{24}N_4O$	348.44	Ethanol	72.39; 72.36	6.94; 6.92	16.08; 16.06
4p	2-OH	82	178–80	$C_{18}H_{18}N_4O_2$	322.36	Glacial acetic acid	67.07; 60.05	5.63; 5.61	17.38; 17.33
4q	4-OH	74	184–86	$C_{18}H_{18}N_4O_2$	322.36	Glacial acetic acid	67.07; 60.05	5.63; 5.60	17.38; 17.38
4r	2-OCH_3	75	145–47	$C_{19}H_{20}N_4O_2$	336.38	Chloroform–water	67.84; 67.82	5.99; 5.97	16.66; 16.64
4s	4-OCH_3	72	153–55	$C_{19}H_{20}N_4O_2$	336.38	Chloroform–water	67.84; 67.82	5.99; 5.97	16.66; 16.63
4t	2-Cl	81	178–80	$C_{18}H_{17}N_4OCl$	340.80	Chloroform–water	63.44; 63.41	5.03; 5.01	16.44; 16.42
4u	4-Cl	80	171–73	$C_{18}H_{17}N_4OCl$	340.80	Chloroform–water	63.44; 63.42	5.03; 5.01	16.44; 16.41
4v	4-NH_2	73	180–82	$C_{18}H_{19}N_5O$	321.34	Acetic acid	67.27; 67.25	5.96; 5.94	21.79; 21.76

TABLE III-S. Physical and analytical properties of compounds **5a–k**

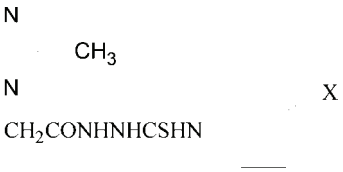

Compd.	X	Yield %	M.p. °C	Formula	MW g mol^{-1}	Recrystalization solvent	Calcd.; Found, % C	H	N
5a	–	76	170–72	$C_{17}H_{17}N_5OS$	339.4g1	Methanol	60.16; 60.14	5.05; 5.03	20.63; 20.61
5b	4-CH_3	79	189–91	$C_{18}H_{19}N_5OS$	353.44	Methanol	61.17; 61.15	5.42; 5.40	19.81; 19.80
5c	4-CH_2CH_3	76	200–02	$C_{19}H_{21}N_5OS$	367.46	Methanol	62.10; 62.08	5.76; 5.74	19.06; 19.03

TABLE III-S. Continued

Compd.	X	Yield %	M.p. °C	Formula	MW g mol^{-1}	Recrystalization solvent	Calcd.; Found, % C	H	N
5d	4-$CH_2CH_2CH_3$	71	197–99	$C_{20}H_{23}N_5OS$	381.49	Methanol	62.97; 62.95	6.08; 6.06	18.36; 18.33
5e	2-OH	71	182–84	$C_{17}H_{17}N_5O_2S$	355.41	Methanol–water	57.45; 57.42	4.82; 4.80	19.70; 19.68
5f	4-OH	80	185–87	$C_{17}H_{17}N_5O_2S$	355.41	Methanol–water	57.45; 57.43	4.82; 4.80	19.70; 19.65
5g	2-OCH_3	78	160–62	$C_{18}H_{19}N_5O_2S$	369.44	Acetone	58.52; 58.50	5.18; 5.16	18.96; 18.94
5h	4-OCH_3	82	169–71	$C_{18}H_{19}N_5O_2S$	369.44	Acetone	58.52; 58.50	5.18; 5.15	18.96; 18.93
5i	2-Cl	85	196–98	$C_{17}H_{16}N_5OSCl$	373.85	Methanol	54.61; 54.59	4.31; 4.29	18.73; 18.70
5j	4-Cl	74	178–80	$C_{17}H_{16}N_5OSCl$	373.85	Methanol–water	54.61; 54.60	4.31; 4.28	18.73; 18.70
5k	4-NH_2	82	150–52	$C_{17}H_{18}N_6OS$	354.42	Acetone	57.61; 57.59	5.12; 5.10	23.71; 23.70

TABLE IV-S. Physical and analytical properties of compounds **6a–k**

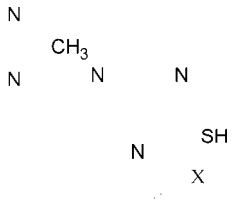

Compd.	X	Yield %	M.p. °C	Formula	MW g mol^{-1}	Recrystalization solvent	Calcd.; Found, % C	H	N
6a	–	78	184–86	$C_{17}H_{15}N_5S$	321.39	Ethanol	63.53; 63.51	4.70; 4.68	21.79; 21.76
6b	4-CH_3	74	192–94	$C_{18}H_{17}N_5S$	335.42	Ethanol	64.45; 64.43	5.11; 5.10	20.88; 20.86
6c	4-CH_2CH_3	72	198–00	$C_{19}H_{19}N_5S$	349.45	Ethanol	65.30; 65.27	5.48; 4.47	20.04; 20.02
6d	4-$CH_2CH_2CH_3$	70	196–98	$C_{20}H_{21}N_5S$	363.46	Ethanol	66.09; 66.06	5.82; 5.79	19.27; 19.25
6e	2-OH	79	197–99	$C_{17}H_{15}N_5OS$	337.39	Ethanol	60.52; 60.50	4.48; 4.46	20.76; 20.74
6f	4-OH	70	181–83	$C_{17}H_{15}N_5OS$	337.39	Ethanol	60.52; 60.50	4.48; 4.45	20.76; 20.73
6g	2-OCH_3	65	165–67	$C_{18}H_{17}N_5OS$	351.42	Ethanol–water	61.52; 61.51	4.88; 4.85	19.93; 19.90

TABLE IV-S. Continued

Compd.	X	Yield %	M.p. °C	Formula	MW g mol^{-1}	Recrystalization solvent	Calcd.; Found, % C	H	N
6h	4-OCH_3	67	178–80	$C_{18}H_{17}N_5OS$	351.42	Ethanol–water	61.52; 61.50	4.88; 4.85	19.93; 19.90
6i	2-Cl	77	181–83	$C_{17}H_{14}N_5SCl$	355.84	Acetone–water	57.38; 57.36	3.97; 3.95	19.68; 19.65
6j	4-Cl	82	177–79	$C_{17}H_{14}N_5SCl$	355.84	Acetone–water	57.38; 57.36	3.97; 3.95	19.68; 19.65
6k	4-NH_2	75	148–50	$C_{17}H_{18}N_6S$	336.41	Ethanol	60.69; 60.67	4.79; 4.77	24.98; 24.96

SPECTRAL DATA OF THE SYNTHESIZED COMPOUNDS

*2-(2-Methyl-1*H*-benzimidazol-1-yl)-N'-(phenylmethylidene)acetohydrazide* ***(4a)***. IR (KBr, cm^{-1}): 1659 (–C=O amide). ^{1}H-NMR (300 MHz, $CDCl_3$, δ / ppm): 2.60 (*s*, 3H, $–CH_3$ at C-2 of Bz), 3.77 (*s*, 2H, $–N–CH_2$), 6.39-7.61 (*m*, 9H, *J* = 4.2 Hz, 5.5 Hz, Ar–H), 9.08 (*s*, 1H, –CONH). ^{13}C-NMR (300 MHz, $CDCl_3$, δ / ppm): 12.35 ($–CH_3$ at C-2 of benzimidazole), 50.80 ($–CH_2$), 175.42 (amide carbon), 145.50 (–N=CH), 135.19, 130.52, 111.31, 107.79, 122.24, 122.10, 137.43, 130.46, 114.35, 146.52, 125.47 (aromatic carbons). MS (*m*/*z*): 292 (M^+), 277, 266, 264, 250.

*2-(2-Methyl-1*H*-benzimidazol-1-yl)-*N*'-[(*E*)-(2-methylphenyl)methylidene]-acetohydrazide* ***(4b)***. IR (KBr, cm^{-1}): (–C=O amide). ^{1}H-NMR (300 MHz, $CDCl_3$, δ / ppm): 2.32 (*s*, 3H, $–CH_3$), 2.51 (*s*, 3H, $–CH_3$ at C-2 of Bz), 4.62 (*s*, 2H, $–N–CH_2$), 7.0 (*s*, 1H, –CONH), 7.22-7.79 (*m*, 8H, *J* = 4.5, 5.1, 3.9 Hz, Ar–H). ^{13}C-NMR (300 MHz, $CDCl_3$, δ / ppm): 14.4 ($–CH_3$ at C-2 of benzimidazole), 39.7 ($–CH_2$), 171.0 (amide carbon), 147.7 (–N=CH), 16.7 ($–CH_3$), 149.3, 142.2, 134.2, 137.5, 131.0, 128.8. 128.2, 123.0, 119.8, 110.0 (aromatic carbons). MS (*m*/*z*): 306 (M^+).

*N'-[(*E*)-(2-Ethylphenyl)methylidene]-2-(2-methyl-1*H*-benzimidazol-1-yl)ace-tohydrazide* ***(4c)***. IR (KBr, cm^{-1}): 1665 (–C=O amide). ^{1}H-NMR (300 MHz, $CDCl_3$, δ / ppm): 1.25 (*t*, 3H, *J* = 3.5, 1.2 Hz, $–CH_2CH_3$), 2.51 (*s*, 3H, $–CH_3$ at C-2 Bz), 2.60 (*q*, 2H, *J* = 4.7 and 1.2 Hz, $–CH_2CH_3$), 4.62 (*s*,2H, $–N–CH_2$), 7.0 (*s*, 1H, –CONH), 7.22–7.72 (*m*, 8H, *J* = 6.2, 4.9 Hz, Ar-H). ^{13}C-NMR (300 MHz, $CDCl_3$, δ / ppm): 14.4 ($–CH_3$ at C-2 of benzimidazole), 39.7 ($–CH_2$), 171.0 (amide carbon), 168.8 (–N=C), 17.0 ($–CH_3$), 27.9 ($–CH_2$), 14.5 ($–CH_3$), 149.3, 142.2, 134.2, 130.9, 128.3, 124.4, 126.0, 123.0, 119.8, 110.0 (aromatic carbons). MS (*m*/*z*): 320 (M^+).

*2-(2-Methyl-1*H*-benzimidazol-1-yl)-*N*'-[(*E*)-(2-propylphenyl)methylidene]-acetohydrazide* ***(4d)***. IR (KBr, cm^{-1}): 1670 (–C=O amide); ^{1}H-NMR (300 MHz, $CDCl_3$, δ / ppm): 2.32 (*s*, 3H, $–CH_3$), 2.51 (*s*, 3H, $–CH_3$ at C-2 of Bz), 4.62 (*s*, 2H, $–N–CH_2$), 7.0 (*s*, 1H, –CONH), 7.22–7.52 (*m*, 8H, *J* = 6.2 and 4.7 Hz, Ar–H). ^{13}C-NMR (300 MHz, $CDCl_3$, δ / ppm): 14.4 ($–CH_3$ at C-2 of benzimida-

zole), 39.7 (–CH_2), 171.0 (amide carbon), 147.7 (–N=CH), 16.7 (–CH_3), 149.3, 142.2, 134.2, 137.5, 131.0, 128.8. 128.2, 123.0, 119.8, 110.0 (aromatic carbons). MS (*m*/*z*):334 (M^+).

N'-*[(2-Hydroxyphenyl)methylidene]-2-(2-methyl-1*H*-benzimidazol-1-yl)acetohydrazide (**4e**)*. IR (KBr, cm^{-1}): 1672 (–C=O amide), 907 (Ar–OH) cm^{-1}. ^{1}H--NMR (300 MHz, $CDCl_3$, *δ* / ppm): δ 2.61 (*s*, 3H, –CH_3 at C-2 Bz), 3.81 (*s*, 2H, –N–CH_2), 6.53–7.68 (*m*, 8H, *J* = 6.2 and 4.7 Hz, Ar–H), 9.12 (*s*, 1H, –CONH), 12.25 (*s*, 1H, Ar–OH). ^{13}C-NMR (300 MHz, $CDCl_3$, *δ* / ppm): 12.31 (–CH_3 at C-2 of benzimidazole), 50.82 (–CH_2), 175.73 (amide carbon), 147.79 (–N=CH), 135.19, 130.52, 111.31, 107.79, 122.24, 122.10, 137.43, 131.23, 115.32, 141.65, 124.23 (aromatic carbons). MS (*m*/*z*): 308 (M^+), 293, 282, 280, 266.

N'-*[(4-Hydroxyphenyl)methylidene]-2-(2-methyl-1*H*-benzimidazol-1yl)acetohydrazide (**4f**)*. IR (KBr, cm^{-1}): 1677 (–C=O amide), 890 (Ar–OH). ^{1}H-NMR (300 MHz, $CDCl_3$, *δ* / ppm): 2.65 (*s*, 3H, –CH_3 at C-2 Bz), 3.75 (*s*, 2H, –N–CH_2), 6.48–8.10 (*m*, 8H, *J* = 6.2 and 4.7 Hz, Ar–H), 9.10 (*s*, 1H, –CONH), 9.68 (*s*, 1H, Ar–OH). ^{13}C-NMR (300 MHz, $CDCl_3$, *δ* / ppm): 12.30 (–CH_3 at C-2 of benzimidazole), 50.83 (–CH_2), 172.60 (amide carbon), 145.87 (–N=CH), 141.90, 135.98, 118.45, 102.45, 123.14, 123.30, 146.41, 160.65, 131.88, 128.56, 117.97, 116.23 (aromatic carbons). MS (*m*/*z*): 308 (M^+), 293, 282, 280, 266.

N'-*[(2-Methoxyphenyl)methylidene]-2-(2-methyl-1*H*-benzimidazol-1-yl)acetohydrazide (**4g**)*. IR (KBr, cm^{-1}): 1679 (–C=O amide), 2810 (O–CH_3). ^{1}H-NMR (300 MHz, $CDCl_3$, *δ* / ppm): δ 2.60 (s, 3H, –CH_3 at C-2 Bz), 3.78 (s, 2H, –N–CH_2), 4.80 (*s*, 3H, O–CH_3), 6.49–7.65 (*m*, 8H, *J* = 7.8 and 5.1 Hz, Ar–H), 9.08 (*s*, 1H, –CONH). ^{13}C-NMR (300 MHz, $CDCl_3$, *δ* / ppm): 12.34 (–CH_3 at C-2 of benzimidazole), 50.81 (–CH_2), 175.65 (amide carbon), 145.83 (–N=CH), 57.32 (O–CH_3), 141.90, 135.98, 118.45, 102.45, 123.14, 123.30, 146.41, 160.85, 131.45, 128.99, 117.34, 116.55 (aromatic carbons). MS (*m*/*z*): 322 (M^+), 307, 296, 294, 291.

N'-*[(4-Methoxyphenyl)methylidene]-2-(2-methyl-1*H*-benzimidazol-1-yl)acetohydrazide (**4h**)*. IR (KBr, cm^{-1}): 1660 (–C=O amide), 2808 (O–CH_3). ^{1}H-NMR (300 MHz, $CDCl_3$, *δ* / ppm): δ 2.59 (*s*, 3H, –CH_3 at C-2 Bz), 3.69 (*s*, 3H, O–CH_3), 3.72 (*s*, 2H, –N–CH_2), 5.52–7.70 (*m*, 8H, *J* = 7.8, 5.2 Hz, Ar–H), 9.00 (*s*, 1H, –CONH). ^{13}C-NMR (300 MHz, $CDCl_3$, *δ* / ppm): 12.35 (–CH_3 at C-2 of benzimidazole), 50.79 (–CH_2), 174.11 (amide carbon), 145.85 (–N=CH), 56.68 (O–CH_3), 143.10, 136.38, 116.15, 103.35, 124.14, 124.90, 144.81, 162.35, 132.15, 128.29, 113.14, 116.65 (aromatic carbons). MS (*m*/*z*): 322 (M^+), 307, 296, 294, 291.

N'-*[(2-Chlorophenyl)methylidene]-2-(2-methyl-1*H*-benzimidazol-1-yl)acetohydrazide (**4i**)*. IR (KBr, cm^{-1}): 1668 (–C=O amide), 709 (C–Cl) cm^{-1}. ^{1}H-NMR (300 MHz, $CDCl_3$, *δ* / ppm): 2.63 (*s*, 3H, –CH_3 at C-2 Bz), 3.70 (*s*, 2H, –N–CH_2), 6.34–7.51 (*m*, 8H, *J* = 8.0 and 7.3 Hz, Ar–H), 9.27 (*s*, 1H, -CONH). ^{13}C-NMR (300 MHz, $CDCl_3$, *δ* / ppm): 12.36 (–CH_3 at C-2 of benzimidazole), 50.81 (–CH_2),

175.65 (amide carbon), 145.76 (–N=CH), 142.46, 132.50, 118.13, 108.12, 124.21, 123.78, 146.98, 118.24, 118.11, 161.72, 126.22, 121.56, 126.23, 121.77 (aromatic carbons). MS (*m*/*z*): 326 (M^+), 311, 300, 298, 290, 284.

N'-*[(4-Chlorophenyl)methylidene]-2-(2-methyl-1*H*-benzimidazol-1-yl)acetohydrazide* (***4j***). IR (KBr, cm^{-1}): 1674 (–C=O amide), 745 (C–Cl). ^{1}H-NMR (300 MHz, $CDCl_3$, δ / ppm): 2.62 (*s*, 3H, $–CH_3$ at C-2 Bz), 3.74 (*s*, 2H, $–N–CH_2$), 6.53–7.68 (*m*, 8H, *J* = 8.0 and 7.3 Hz, Ar–H), 9.18 (*s*, 1H, –CONH). ^{13}C-NMR (300 MHz, $CDCl_3$, δ / ppm): 12.30 ($–CH_3$ at C-2 of benzimidazole), 50.82 ($–CH_2$), 175.62 (amide carbon), 145.12 (–N=CH), 142.22, 132.12, 117.87, 107.64, 124.23, 123.87, 146.56, 118.34, 118.25, 161.82, 126.44, 121.57, 126.55, 121.29 (aromatic carbons). MS (*m*/*z*): 326 (M^+), 311, 300, 298, 290, 284.

N'-*[(4-Aminophenyl)methylidene]-2-(2-methyl-1*H*-benzimidazol-1-yl)acetohydrazide* (***4k***). IR (KBr, cm^{-1}): 1672 (–C=O amide), 3348 ($–NH_2$). ^{1}H-NMR (300 MHz, $CDCl_3$, δ / ppm): 2.50 (*s*, 3H, $–CH_3$ at C-2 Bz), 3.69 (*s*, 2H, $–N–CH_2$), 5.58 ($–C–NH_2$), 6.55 (*s*, 1H, –CONH), 6.50–7.88 (*m*, 8H, *J* = 5.4, 3.7 Hz, Ar–H). ^{13}C--NMR (300 MHz, $CDCl_3$, δ / ppm): 12.30 ($–CH_3$ at C-2 of benzimidazole), 50.82 ($–CH_2$), 175.62 (amide carbon), 145.71 (–N=CH), 14.35 ($–CH_3$), 135.19, 130.52, 111.31, 107.79, 122.24, 122.10, 137.43, 130.09, 114.12, 146.32, 125.37 (aromatic carbons); MS (*m*/*z*): 307 (M^+), 292, 281, 279, 263, 256.

*2-(2-Methyl-1*H*-benzimidazol-1-yl)*-N'-*[1-phenylethylidene]acetohydrazide* (***4l***). IR (KBr, cm^{-1}): 1685 (–C=O amide). ^{1}H-NMR (300 MHz, $CDCl_3$, δ / ppm): 2.17 (*s*, 3H, $–CH_3$), 2.43 (*s*, 3H, $–CH_3$ at C-2 of Bz), 3.73 (*s*, 2H, $–N–CH_2$), 7.10––7.80 (*m*, 9H, *J* = 6.4 and 6.9 Hz, Ar–H), 9.04 (*s*, 1H, –CONH). ^{13}C-NMR (300 MHz, $CDCl_3$, δ / ppm): 12.64 ($–CH_3$ at C-2 of benzimidazole), 51.07 ($–CH_2$), 176.88 (amide carbon), 148.96 (–N=CH), 15.14 ($–CH_3$), 140.29, 135.52, 118.97, 108.85, 123.24, 123.44, 145.41, 136.97, 127.69, 127.79, 125.23, 127.69 (aromatic carbons); MS (*m*/*z*). 306 (M^+), 291, 280, 278, 264, 262, 230.

*2-(2-Methyl-1*H*-benzimidazol-1-yl)*-N'-*[(1*E*)-1-(2-methylphenyl)ethylidene]-acetohydrazide* (***4m***). IR (KBr, cm^{-1}): 1689 (–C=O amide); ^{1}H-NMR (300 MHz, $CDCl_3$, δ / ppm): 1.81 (*s*, 3H, $–CH_3$), 2.48 (*s*, 3H, $–CH_3$ at benzene ring), 2.54 (*s*, 3H, $–CH_3$ at C-2 of Bz), 4.65 (*s*, 2H, $–N–CH_2$), 7.00 (*s*, 1H, –CONH), 7.28–7.95 (*m*, 9H, *J* = 6.9, 6.3 and 6.3 Hz, Ar–H). ^{13}C-NMR (300 MHz, $CDCl_3$, δ / ppm): 14.4 ($–CH_3$ at C-2 of benzimidazole), 39.7 ($–CH_2$), 171.0 (amide carbon), 168.8 (–N=C), 19.2 ($–CH_3$), 149.3, 142.2, 135.1, 134.2, 130.9, 129.6, 128.0, 125.8, 123.0, 119.8, 110.0 (aromatic carbons). MS (*m*/*z*): 320 (M^+).

N'-*[(1*E*)-1-(2-Ethylphenyl)ethylidene]-2-(2-methyl-1*H*-benzimidazol-1-yl)-acetohydrazide* (***4n***). IR (KBr, cm^{-1}): 1687 (–C=O amide); ^{1}H-NMR (300 MHz, $CDCl_3$, δ / ppm): 2.02 (*q*, 2H, *J* = 4.7, 3.2, 0.9 Hz, CH_2CH_3), 2.48 (*s*, 3H, $–CH_3$ at benzene ring), 2.54 (*s*, 3H, $–CH_3$ at C-2 of Bz), 2.95 (*t*, 3H, *J* = 4.5 and 3.9 Hz, $–CH_2CH_3$), 4.65 (*s*, 2H, $–N–CH_2$), 7.02 (*s*, 1H, –CONH), 7.28–7.95 (*m*, 9H, *J* = 6.7 and 3.8 Hz, Ar–H). ^{13}C-NMR (300 MHz, $CDCl_3$, δ / ppm): 14.4

(–CH_3 at C-2 of benzimidazole), 39.7 (–CH_2), 171.0 (amide carbon), 168.8 (–N=C), 19.2 (–CH_3), 149.3, 142.2, 135.1, 134.2, 130.9, 129.6, 128.0, 124.9, 123.2, 119.7, 110.3 (aromatic carbons). MS (*m*/*z*): 334 (M^+).

*2-(2-Methyl-1*H*-benzimidazol-1-yl)-*N*'-[(1*E*)-1-(2-propylphenyl)ethylidene]-acetohydrazide (**4o**)*. IR (KBr, cm^{-1}): 1686 (–C=O amide). ^{1}H-NMR (300 MHz, $CDCl_3$, δ / ppm): 0.90 (*t*, 3H, *J* = 6.5 Hz, –$CH_2CH_2CH_3$), 1.65 (*m*, 2H, *J* = = 6.8 and 7.5 Hz, –$CH_2CH_2CH_3$), 2.48 (*s*, 3H, –CH_3), 2.62 (*m*, 2H, *J* = 6.5 and 1.2 Hz, –$CH_2CH_2CH_3$), 2.54 (*s*, 3H, –CH_3 at C-2 of Bz), 4.65 (*s*, 2H, N–CH_2), 7.02 (*s*, 1H, CONH), 7.28–7.95(*m*, 9H, *J* = 6.7 and 3.8 Hz, Ar–H). ^{13}C-NMR (300 MHz, $CDCl_3$, δ / ppm): 14.4 (–CH_3 at C-2 of benzimidazole), 39.7 (–CH_2), 171.0 (amide carbon), 168.8 (–N=C), 19.2 (–CH_3), 148.2, 142.0, 134.1, 134.2, 130.9, 127.6, 128.4, 124.5, 123.0, 119.1, 109.5 (aromatic carbons). MS (*m*/*z*): 348 (M^+).

N'-*[1-(2-Hydroxyphenyl)ethylidene]-2-(2-methyl-1*H*-benzimidazol-1-yl)acetohydrazide (**4p**)*. IR (KBr, cm^{-1}): 1682 (–C=O amide), 982 (Ar–OH). ^{1}H-NMR (300 MHz, $CDCl_3$, δ / ppm): 2.21 (*s*, 3H, –CH_3), 2.40 (*s*, 3H, CH_3 at C-2 of Bz), 3.71 (*s*, 2H, NCH_2), 6.67–7.98 (*m*, 8H, *J* = 8.1 and 7.5 Hz, Ar–H), 9.12 (*s*, 1H, CONH), 12.03 (*s*, 1H, Ar–OH). ^{13}C-NMR (300 MHz, $CDCl_3$, δ / ppm): 12.68 (–CH_3 at C-2 of benzimidazole), 51.05 (–CH_2), 176.73 (amide carbon), 152.69 (–N=CH), 15.72 (–CH_3), 140.24, 135.50, 118.91, 108.79, 123.14, 123.30, 146.41, 118.45, 118.89, 132.52, 159.13, 119.79, 127.33 (aromatic carbons). MS (*m*/*z*): 322 (M^+), 307, 296, 294, 278, 271.

N'-*[1-(4-Hydroxyphenyl)ethylidene]-2-(2-methyl-1*H*-benzimidazol-1-yl)acetohydrazide (**4q**)*. IR (KBr, cm^{-1}): 1687 (–C=O amide), 982 (Ar-OH). ^{1}H-NMR (300 MHz, $CDCl_3$, δ / ppm): 2.18 (*s*, 3H, –CH_3), 2.41 (*s*, 3H, –CH_3 at C-2 of Bz), 3.75 (*s*, 2H, –N–CH_2), 6.86–8.00 (*m*, 8H, *J* = 8.1 and 7.2 Hz, Ar–H), 9.10 (*s*, 1H, CONH), 9.49 (*s*, 1H, Ar–OH). ^{13}C-NMR (300 MHz, $CDCl_3$, δ / ppm): 12.62 (–CH_3 at C-2 of benzimidazole), 51.03 (–CH_2), 176.76 (amide carbon), 150.49 (–N=CH), 15.21 (–CH_3), 140.24, 135.50, 118.91, 108.79, 123.14, 123.30, 146.41, 160.35, 130.88, 127.46, 118.97, 117.34 (aromatic carbons). MS (*m*/*z*): 322 (M^+), 307, 296, 294, 280, 278, 271.

N'-*[1-(2-Methoxyphenyl)ethylidene]-2-(2-methyl-1*H*-benzimidazol-1-yl)acetohydrazide (**4r**)*. IR (KBr, cm^{-1}): 1689 (–C=O amide), 2815 (O–CH_3). ^{1}H-NMR (300 MHz, $CDCl_3$, δ / ppm): 2.19 (*s*, 3H, –CH_3), 2.45 (*s*, 3H, –CH_3 at C-2 of Bz), 3.75 (*s*, 2H, –N–CH_2), 3.89 (*s*, 3H, O–CH_3), 6.58–7.78 (*m*, 8H, *J* = 7.8 and 6.2 Hz, Ar–H), 9.08 (*s*, 1H, –CONH). ^{13}C-NMR (300 MHz, $CDCl_3$, δ / ppm): 12.60 (–CH_3 at C-2 of benzimidazole), 51.09 (–CH_2), 176.49 (amide carbon), 147.73 (–N=CH), 15.94 (–CH_3), 56.16 (O–CH_3), 140.29, 135.52, 118.97, 108.85, 123.24, 123.44, 146.41, 118.19, 118.88, 132.87, 159.76, 121.08, 129.24 (aromatic carbons). MS (*m*/*z*): 336 (M^+), 321, 310, 308.

N'-*[1-(4-Methoxyphenyl)ethylidene]-2-(2-methyl-1*H-*benzimidazol-1-yl)acetohydrazide (**4s**)*. IR (KBr, cm^{-1}): 1680 (–C=O amide), 2811 (O–CH_3). ^{1}H-NMR (300 MHz, $CDCl_3$, δ / ppm): 2.12 (*s*, 3H, –CH_3), 2.48 (*s*, 3H, CH_3 at C-2 Bz), 3.78 (*s*, 2H, –NCH_2), 3.84 (*s*, 3H, OCH_3), 6.61–7.88 (*m*, 8H, *J* = 7.8 and 6.2 Hz, Ar–H), 9.00 (*s*, 1H, –CONH). ^{13}C-NMR (300 MHz, $CDCl_3$, δ / ppm): 12.62 (–CH_3 at C-2 of benzimidazole), 51.11 (–CH_2), 176.40 (amide carbon), 147.78 (–N=CH), 15.91 (–CH_3), 55.33 (O–CH_3), 140.29, 135.52, 118.97, 108.85, 123.24, 123.44, 146.41, 118.19, 118.88, 160.75, 126.97, 121.08, 126.97, 121.08 (aromatic carbons). MS (*m*/*z*): 336 (M^+), 321, 310, 308, 294, 260.

N'-*[1-(2-Chlorophenyl)ethylidene]-2-(2-methyl-1*H-*benzimidazol-1-yl)acetohydrazide (**4t**)*. IR (KBr, cm^{-1}): 1668 (–C=O amide), 775 (C–Cl). ^{1}H-NMR (300 MHz, $CDCl_3$, δ / ppm): 2.10 (*s*, 3H, –CH_3), 2.37 (*s*, 3H, –CH_3 at C-2 of Bz), 3.61 (*s*, 2H, –N–CH_2), 6.54–7.63 (*m*, 8H, *J* = 7.1 and 5.5 Hz, Ar–H), 8.97 (*s*, 1H, –CONH). ^{13}C-NMR (300 MHz, $CDCl_3$, δ / ppm): 12.59 (–CH_3 at C-2 of benzimidazole), 51.08 (–CH_2), 176.38 (amide carbon), 147.75 (–N=CH), 15.85 (–CH_3), 140.26, 135.50, 118.93, 108.82, 123.21, 123.42, 146.38, 118.14, 118.85, 160.72, 126.97, 121.06, 126.94, 121.07 (aromatic carbons). MS (*m*/*z*): 340 (M^+), 325, 314, 312, 304, 296.

N'-*[-1-(4-Chlorophenyl)ethylidene]-2-(2-methyl-1*H-*benzimidazol-1-yl)acetohydrazide (**4u**)*. IR (KBr, cm^{-1}): 1674 (–C=O amide), 780 (C–Cl). ^{1}H-NMR (300 MHz, $CDCl_3$, δ / ppm): 2.15 (*s*, 3H, –CH_3), 2.39 (*s*, 3H, –CH_3 at C-2 of Bz), 3.64 (*s*, 2H, –N–CH_2), 6.66–7.79 (*m*, 8H, *J* = 7.1, 5.4 Hz, Ar–H), 9.00 (*s*, 1H, –CONH). ^{13}C-NMR (300 MHz, $CDCl_3$, δ / ppm): 12.52 (–CH_3 at C-2 of benzimidazole), 51.04 (–CH_2), 176.36 (amide carbon), 147.71 (–N=CH), 15.80 (–CH_3), 140.23, 135.45, 118.89, 108.80, 123.15, 123.34, 146.36, 118.10, 118.81, 160.71, 126.94, 121.02, 126.90, 121.03 (aromatic carbons). MS (*m*/*z*): 340 (M^+), 325, 314, 312, 304, 296.

N'-*[1-(4-Aminophenyl)ethylidene]-2-(2-methyl-1*H-*benzimidazol-1-yl)acetohydrazide (**4v**)*. IR (KBr, cm^{-1}): 1672 (–C=O amide), 3348 (–NH_2). ^{1}H-NMR (300 MHz, $CDCl_3$, δ / ppm): 2.11 (*s*, 3H, –CH_3), 2.50 (*s*, 3H, –CH_3 at C-2 of Bz), 3.69 (*s*, 2H, –N–CH_2), 5.58 (*s*, 2H, C–NH_2), 6.55 (*s*, 1H, –CONH), 6.50–7.88 (*m*, 8H, *J* = 6.2 and 4.4 Hz, Ar–H). ^{13}C-NMR (300 MHz, $CDCl_3$, δ / ppm): 12.64 (–CH_3 at C-2 of benzimidazole), 51.07 (–CH_2), 176.88 (amide carbon), 146.84 (–N=CH), 14.97 (–CH_3), 55.26 (O–CH_3), 140.29, 135.52, 118.97, 108.85, 123.24, 123.44, 146.41, 131.13, 115.32, 147.93, 126.66 (aromatic carbons). MS (*m*/*z*): 321 (M^+), 306, 295, 293, 279, 245.

*2-[(2-Methyl-1*H-*benzimidazol-1-yl)acetyl]-*N-*phenylhydrazinecarbothioamide (**5a**)*. IR (KBr, cm^{-1}): 1650 (–C=O amide), 1220 (–C=S). ^{1}H-NMR (300 MHz, $CDCl_3$, δ / ppm): 2.38 (*s*, 3H, –CH_3 at C-2 of Bz), 3.68 (*s*, 2H, –N–CH_2), 7.08–7.68 (*m*, 9H, *J* = 6.6 and 6.3 Hz, Ar–H), 7.42 (*s*, 1H, CONH). ^{13}C-NMR (300 MHz, $CDCl_3$, δ / ppm): 12.83 (–CH_3 at C-2 of benzimidazole), 50.16 (–CH_2),

171.43 (amide carbon), 178.04 (–C=S), 142.98, 137.27, 118.97, 108.26, 123.24, 123.44, 148.16, 13.00, 125.80, 128.25, 125.85 (aromatic carbons). MS (*m*/*z*): 339 [M^+], 324, 313, 311, 297, 263.

*2-[(2-Methyl-1*H*-benzimidazol-1-yl)acetyl]*-N-*(2-methylphenyl)hydrazine-carbothioamide (**5b**)*. IR (KBr, cm^{-1}): 1658 (–C=O amide), 1225 (–C=S). ^{1}H--NMR (300 MHz, $CDCl_3$, δ / ppm): 1.25 (*t*, 3H, *J* = 3.6 Hz, $–CH_3$), 2.00 (*s*, 1H, –NH), 2.51 (*s*, 3H, $–CH_3$ at C-2 of Bz), 2.60 (*q*, 2H, *J* = 3.3 Hz, $–CH_2$), 4.62 (*s*, 2H, $–N–CH_2$), 6.02–7.59 (*m*, 8H, *J* = 6.3, 6.6 Hz, Ar–H), 8.20 (*s*, 1H, –CONH), 10.08 (*s*, 1H, –NH). ^{13}C-NMR (300 MHz, $CDCl_3$, δ / ppm): 14.4 ($–CH_3$ at C-2 of benzimidazole), 40.0 ($–CH_2$), 164.4 (amide carbon), 181.1 (–C=S), 17.9 ($–CH_3$ at benzene) 142.20, 136.217, 135.02, 134.12, 130.24, 129.24, 127.16, 126.12, 125.80, 119.8, 110.02 (aromatic carbons). MS (*m*/*z*): 353 [M^+].

N-*(2-Ethylphenyl)-2-[(2-methyl-1*H*-benzimidazol-1-yl)acetyl]hydrazinecar-bothioamide (**5c**)*. IR (KBr, cm^{-1}): 1654 (–C=O amide), 1222 (–C=S). ^{1}H-NMR (300 MHz, $CDCl_3$, δ / ppm): 1.25 (*t*, 3H, *J* = 3.9 Hz, $–CH_3$), 2.51 (*s*, 3H, $–CH_3$ at C-2 of Bz), 2.60 (*q*, 2H, *J* = 3.2 Hz, $–CH_2$), 4.62 (*s*, 2H, $–N–CH_2$), 6.04–7.65 (*m*, 8H, *J* = 6.3, 6.5 Hz, ArH), 8.0 (s, 1H, –CONH). ^{13}C-NMR (300 MHz, $CDCl_3$, δ / / ppm): 14.4 ($–CH_3$ at C-2 of benzimidazole), 40.0 ($–CH_2$), 164.4 (amide carbon), 181.1 (–C=S), 17.9, 14.4 ($–CH_2CH_3$ at benzene)142.20, 136.217, 135.02, 134.12, 130.24, 129.24, 127.16, 126.12, 125.80, 119.8, 110.02 (aromatic carbons). MS (*m*/*z*): 367 [M^+].

*2-[(2-Methyl-1*H*-benzimidazol-1-yl)acetyl]*-N-*(2-propylphenyl)hydrazine-carbothioamide (**5d**)*. IR (KBr, cm^{-1}): 1654 (–C=O amide), 1222 (–C=S). ^{1}H-NMR (300 MHz, $CDCl_3$, δ / ppm): 0.91 (*t*, 3H, *J* = 4.5 Hz, $–CH_2CH_2CH_3$), 1.62 (*m*, 2H, *J* = 6.5, 1.2 Hz, $–CH_2CH_2CH_3$), 2.51 (*s*, 3H, $–CH_3$ at C-2 of Bz), 2.60 (*t*, 2H, *J* = 6.5, 1.5 Hz, $–CH_2CH_2CH_3$), 4.62 (*s*, 2H, $–N–CH_2$), 6.04–7.65 (*m*, 8H, *J* = = 8.1 and 4.5 Hz, ArH), 8.0 (*s*, 1H, –CONH). ^{13}C-NMR (300 MHz, $CDCl_3$, δ / / ppm): 14.4 ($–CH_3$ at C-2 of benzimidazole), 40.0 ($–CH_2$), 164.4 (amide carbon), 181.1 (–C=S), 17.9, 14.4, 10.6 ($–CH_2CH_2CH_3$ at benzene) 142.20, 136.217, 135.02, 134.12, 130.24, 129.24, 127.16, 126.12, 125.80, 119.8, 110.02 (aromatic carbons). MS (*m*/*z*): 381 [M^+].

N-*(2-Hydroxyphenyl)-2-[(2-methyl-1*H*-benzimidazol-1-yl)acetyl]hydrazine-carbothioamide (**5e**)*. IR (KBr, cm^{-1}): 1654 (–C=O amide), 1225 (–C=S) 990 (Ar–OH). ^{1}H-NMR (300 MHz, $CDCl_3$, δ / ppm): 2.35 (*s*, 3H, $–CH_3$ at C-2 of Bz), 3.67 (*s*, 2H, $–N–CH_2$), 7.42–7.85 (*m*, 8H, *J* = 7.8 and 4.5 Hz, Ar–H), 7.47 (*s*, 1H, –CONH), 12.03 (*s*,1H, Ar–OH). ^{13}C-NMR (300 MHz, $CDCl_3$, δ / ppm): 12.64 ($–CH_3$ at C-2 of benzimidazole), 50.25 ($–CH_2$), 171.54 (amide carbon), 178.18 (–C=S), 143.12, 137.45, 119.23, 108.41, 123.24, 123.44, 148.15, 13.25, 126.14, 128.47, 125.91 (aromatic carbons). MS (*m*/*z*): 355 [M^+], 340, 329, 327, 313, 311, 304.

N-*(4-Hydroxyphenyl)-2-[(2-methyl-1*H-*benzimidazol-1-yl)acetyl]hydrazine-carbothioamide (**5f**)*. IR (KBr, cm^{-1}): 1649 (–C=O amide), 1220 (–C=S) 1022 (Ar–OH). ^{1}H-NMR (300 MHz, $CDCl_3$, δ / ppm): 2.31 (*s*, 3H, $–CH_3$ at C-2 of Bz), 3.62 (*s*, 2H, $–N–CH_2$), 7.40–7.81 (*m*, 8H, *J* = 7.8 and 4.5 Hz, Ar–H), 7.44 (*s*, 1H, –CONH), 9.48 (*s*, 1H, Ar–OH). ^{13}C-NMR (300 MHz, $CDCl_3$, δ / ppm): 12.60 ($–CH_3$ at C-2 of benzimidazole), 50.14 ($–CH_2$), 171.54 (amide carbon), 178.18 (–C=S), 143.12, 137.45, 119.23, 108.41, 123.24, 123.44, 148.27, 13.32, 126.29, 128.54, 125.98 (aromatic carbons). MS (*m*/*z*): 355 [M^+], 340, 329, 327, 313, 311, 304.

N-*(2-Methoxyphenyl)-2-[(2-methyl-1*H-*benzimidazol-1-yl)acetyl]hydrazine-carbothioamide (**5g**)*:IR (KBr, cm^{-1}): 1653 (–C=O amide), 1232 (–C=S) 2829 ($O–CH_3$). ^{1}H-NMR (300 MHz, $CDCl_3$, δ / ppm): 2.35 (*s*, 3H, $–CH_3$ at C-2 of Bz), 3.69 (*s*, 2H, $–N–CH_2$), 7.49 (*s*, 1H, –CONH), 7.54–8.35 (*m*, 8H, *J* = 7.7 and 5.0 Hz, Ar–H), 9.48 (*s*, 3H, $O-CH_3$). ^{13}C-NMR (300 MHz, $CDCl_3$, δ / ppm): 12.88 ($–CH_3$ at C-2 of benzimidazole), 50.18 ($–CH_2$), 171.45 (amide carbon), 178.14 (–C=S), 55.53 ($O–CH_3$), 143.21, 137.49, 119.28, 108.47, 123.26, 123.25, 148.45, 127.87, 126.08, 123.54, 111.44, 123.27, 151.67 (aromatic carbons). MS (*m*/*z*): 369 [M^+], 354, 343, 338, 326.

N-*(4-Methoxyphenyl)-2-[(2-methyl-1*H-*benzimidazol-1-yl)acetyl]hydrazine-carbothioamide (**5h**)*. IR (KBr, cm^{-1}): 1653 (–C=O amide), 1232 (–C=S) 2835 ($O-CH_3$). ^{1}H-NMR (300 MHz, $CDCl_3$, δ / ppm): 2.31 (*s*, 3H, $–CH_3$ at C-2 of Bz), 3.65 (*s*, 2H, $–N–CH_2$), 3.80 (*s*, 3H, $O–CH_3$), 7.30–8.25 (*m*, 8H, *J* = 7.7 and 5.1 Hz, Ar–H), 7.44 (s, 1H, –CONH). ^{13}C-NMR (300 MHz, $CDCl_3$, δ / ppm): 12.82 ($–CH_3$ at C-2 of benzimidazole), 50.13 ($–CH_2$), 171.41 (amide carbon), 178.28 (–C=S), 55.50 ($O–CH_3$), 143.15, 137.32, 119.21, 108.44, 123.21, 123.24, 148.43, 132.58, 158.38, 113.84, 125.49 (aromatic carbons). MS (*m*/*z*): 369 [M^+], 354, 343, 338, 326.

N-*(2-Chlorophenyl)-2-[(2-methyl-1*H-*benzimidazol-1-yl)acetyl]hydrazinecar-bothioamide (**5i**)*. IR (KBr, cm^{-1}): 1665 (–C=O amide), 1245 (–C=S) 775 (C–Cl). ^{1}H-NMR (300 MHz, $CDCl_3$, δ / ppm): 2.37 (*s*, 3H, $–CH_3$ at C-2 of benzimida-zole), 3.69 (*s*, 2H, $–N–CH_2$), 7.48 (*s*, 1H, –CONH), 7.11–8.28 (*m*, 8H, Ar–H) 2.37 (*s*, 3H, $–CH_3$ at C-2 of Bz), 3.69 (*s*, 2H, $–N–CH_2$), 7.48 (*s*, 1H, –CONH), 7.11–8.28 (*m*, 8H, *J* = 8.5 and 5.9 Hz, Ar–H). ^{13}C-NMR (300 MHz, $CDCl_3$, δ / / ppm): 12.96 ($–CH_3$ at C-2 of benzimidazole), 50.24 ($–CH_2$), 171.55 (amide carbon), 178.36 (–C=S), 143.11, 137.25, 119.24, 108.40, 123.20, 123.21, 148.47, 137.14, 130.19, 128.93, 124.48 (aromatic carbons). MS (*m*/*z*): 373 [M^+], 358, 347, 345, 331.

N-*(4-Chlorophenyl)-2-[(2-methyl-1*H-*benzimidazol-1-yl)acetyl]hydrazinecar-bothioamide (**5j**)*. IR (KBr, cm^{-1}): 1660 (–C=O amide), 1240 (–C=S) 782 (C–Cl). ^{1}H-NMR (300 MHz, $CDCl_3$, δ / ppm): 2.34 (*s*, 3H, $–CH_3$ at C-2 of Bz), 3.62 (*s*, 2H, $–N–CH_2$), 7.04–8.12 (*m*, 8H, *J* = 8.5 and 5.8 Hz, Ar–H), 7.42 (*s*, 1H,

–CONH). ^{13}C-NMR (300 MHz, $CDCl_3$, δ / ppm): 12.96 (–CH_3 at C-2 of benzimidazole), 50.24 (–CH_2), 171.55 (amide carbon), 178.36 (–C=S), 143.02, 137.27, 119.20, 108.47, 123.19, 123.32, 148.48, 137.25, 130.14, 128.18, 124.58 (aromatic carbons). MS (*m*/*z*): 373 [M^+], 358, 347, 345, 331.

N-*(4-Aminophenyl)-2-[(2-methyl-1*H*-benzimidazol-1-yl)acetyl]hydrazinecarbothioamide (**5k**)*. IR (KBr, cm^{-1}): 1658 (–C=O amide), 1232 (–C=S), 3340 (–C–NH_2). ^{1}H-NMR (300 MHz, $CDCl_3$, δ / ppm): 2.45 (*s*, 3H, –CH_3 at C-2 of benzimidazole), 3.54 (*s*, 2H, –N–CH_2), 8.31 (*s*, 1H, –CONH), 6.42 (*s*, 2H, –C–NH_2) 7.40–8.59 (*m*, 8H, Ar–H) 2.45 (*s*, 3H, –CH_3 at C-2 of Bz), 3.54 (*s*, 2H, –N–CH_2), 6.42 (*s*, 2H, –C–NH_2), 7.40–8.59 (*m*, 8H, *J* = 6.2, 4.8 Hz, Ar–H), 8.31 (*s*, 1H, –CONH). ^{13}C-NMR (300 MHz, $CDCl_3$, δ / ppm): 12.90 (–CH_3 at C-2 of benzimidazole), 50.11 (–CH_2), 171.53 (amide carbon), 178.41 (–C=S), 143.45, 137.40, 119.27, 108.60, 123.21, 123.44, 132.56, 145.96, 113.77, 125.09 (aromatic carbons). MS (*m*/*z*): 354 [M^+], 339, 328, 326, 312, 310, 278.

*5-[(2-Methyl-1*H*-benzimidazol-1-yl)methyl]-4-phenyl-4*H*-1,2,4-triazole-3--thiol (**6a**)*. IR (KBr, cm^{-1}): 2550 (SH).^{1}H-NMR (300 MHz, $CDCl_3$, δ / ppm): 2.56 (s, 3H, -CH_3 at C-2 of Bz), 6.00 (*s*, 2H, –N–CH_2), 6.61–7.57 (*m*, 9H, *J* = 7.5 and 6.6 Hz, Ar–H), 12.90 (*s*, 1H, –C–SH). ^{13}C-NMR (300 MHz, $CDCl_3$, δ / / ppm): 13.12 (–CH_3 at C-2 of benzimidazole), 41.73 (–CH_2), 141.84, 133.22, 119.55, 106.84, 122.30, 126.56, 147.72, 161.16, 172.51, 146.11, 127.08, 129.35, 132.60, 127.08, 129.35 (aromatic carbons). MS (*m*/*z*): 321 [M^+], 306, 295, 245, 270.

*5-[(2-Methyl-1H-benzimidazol-1-yl)methyl]-4-(2-methylphenyl)-4H-1,2,4--triazole-3-thiol (**6b**)*. IR (KBr, cm^{-1}): 2538 (SH). ^{1}H-NMR (300 MHz, $CDCl_3$, δ / / ppm): 2.25 (*s*, 3H, –CH_3), 2.51 (*s*, 3H, –CH_3 at C-2 of Bz), 4.99 (*s*, 2H, –N–CH_2), 7.22–7.68 (*m*, 8H, *J* = 7.2, 6.6 Hz, Ar–H), 11.15 (*s*, 1H, –C–SH). ^{13}C-NMR (300 MHz, $CDCl_3$, δ / ppm): 14.7 (–CH_3 at C-2 of benzimidazole), 49.1 (–CH_2), 149.2, 142.2, 164.2, 128.3, 119.8, 110.0, 131.9, 129.5, 128.7, 123.0, 125.9, (aromatic carbons). MS (*m*/*z*): 321 [M^+], 335.

*4-2-Ethylphenyl-5-[(2-methyl-1H-benzimidazol-1-yl)methyl]-4H-1,2,4-triazole-3-thiol (**6c**)*. IR (KBr, cm^{-1}): 2536 (SH). ^{1}H-NMR (300 MHz, $CDCl_3$, δ / / ppm): 1.25 (*t*, 3H, *J* = 6.2 Hz, –CH_2CH_3), 2.51 (*s*, 3H, –CH_3 at C-2 of Bz), 2.60 (*q*, 2H, *J* = 6.5 and 4.2 Hz, –CH_2CH_3),4.99 (*s*, 2H, –N–CH_2), 7.22–7.62 (*m*, 8H, *J* = 7.2 and 4.9 Hz, Ar–H), 11.15 (*s*, 1H, –C–SH). ^{13}C-NMR (300 MHz, $CDCl_3$, δ / ppm): 14.7 (–CH_3 at C-2 of benzimidazole), 49.1 (–CH_2), 29.1 and 14.6 (–CH_2CH_3) 168.9, 149.3, 145.7, 142.2, 134.2, 128.3, 119.8, 110.0, 131.9, 129.5, 128.7, 123.0, 125.9, (aromatic carbons). MS (*m*/*z*): 321 [M^+], 349.

*5-[(2-methyl-1H-benzimidazol-1-yl)methyl]-4-(2-propylphenyl)-4H-1,2,4-triazole-3-thiol (**6d**)*. IR (KBr, cm^{-1}): 2538 (SH). ^{1}H-NMR (300 MHz, $CDCl_3$, δ / / ppm): 0.90 (*t*, 3H, *J* = 4.5 Hz, –$CH_2CH_2CH_3$), 1.65 (*m*, 2H, *J* = 6.5, 1.8 Hz, –$CH_2CH_2CH_3$), 2.51 (*s*, 3H, –CH_3 at C-2 of Bz), 2.62 (*t*, 2H, *J* = 6.5 Hz,

–$CH_2CH_2CH_3$), 4.99 (*s*, 2H, –N–CH_2), 7.22–7.68 (*m*, 8H, *J* = 7.7, 4.9 Hz, Ar–H), 11.15 (*s*, 1H, –C–SH). ^{13}C-NMR (300 MHz, $CDCl_3$, δ / ppm): 14.7 (–CH_3 at C-2 of benzimidazole), 49.1 (–CH_2), 32.8, 24.1 and 13.7 (–$CH_2CH_2CH_3$) 168.9, 149.3, 145.7, 142.2, 134.2, 128.3, 119.8, 110.0, 131.9, 129.5, 128.7, 123.0, 125.9 (aromatic carbons). MS (*m*/*z*): 321 [M^+], 363.

*2-{3-[(2-Methyl-1*H*-benzimidazol-1-yl)methyl]-5-sulfanyl-4*H*-1,2,4-triazol--4-yl}phenol (**6e**)*. IR (KBr, cm^{-1}): 2548 (SH), 997 (Ar-OH). ^{1}H-NMR (300 MHz, $CDCl_3$, δ / ppm): 2.58 (*s*, 3H, –CH_3 at C-2 of Bz), 6.02 (*s*, 2H, –N–CH_2), 6.60––7.69 (*m*, 8H, *J* = 7.9 and 5.1 Hz, Ar–H), 10.01 (*s*, 1H, Ar–OH), 11.15 (*s*, 1H, –C-SH). ^{13}C-NMR (300 MHz, $CDCl_3$, δ / ppm): 13.13 (–CH_3 at C-2 of benzimidazole), 41.58 (–CH_2), 141.84, 133.22, 119.55, 106.84, 122.30, 126.56, 147.72, 160.05, 171.40, 125.16, 148.63, 116.65, 126.71, 117.31, 120.03 (aromatic carbons). MS (*m*/*z*): 337 [M^+], 322, 311, 295, 261, 286.

*4-{3-[(2-Methyl-1*H*-benzimidazol-1-yl)methyl]-5-sulfanyl-4*H*-1,2,4-triazol-4-yl}phenol (**6f**)*. IR (KBr, cm^{-1}): 2545 (SH), 982 (Ar–OH). ^{1}H-NMR (300 MHz, $CDCl_3$, δ / ppm): 2.60 (*s*, 3H, –CH_3 at C-2 of Bz), 6.08 (*s*, 2H, –N–CH_2), 6.78––7.89 (*m*, 8H, *J* = 7.9 and 8.5 Hz, Ar–H), 9.40 (*s*, 1H, Ar–OH), 11.15 (*s*, 1H, –C–SH). ^{13}C-NMR (300 MHz, $CDCl_3$, δ / ppm): 13.11 (–CH_3 at C-2 of benzimidazole), 41.52 (–CH_2), 141.84, 133.22, 119.55, 106.84, 122.30, 126.56, 147.72, 160.05, 171.62, 137.13, 124.26, 115.34, 158.34, (aromatic carbons). MS (*m*/*z*): 337 [M^+], 322, 311, 295, 261, 286.

*4-(2-Methoxyphenyl)-5-[(2-methyl-1*H*-benzimidazol-1-yl)methyl]-4*H*-1,2,4--triazole-3-thiol (**6g**)*. IR (KBr, cm^{-1}): 2548 (SH), 2817 (OCH_3). ^{1}H-NMR (300 MHz, $CDCl_3$, δ / ppm): 2.52 (*s*, 3H, –CH_3 at C-2 of Bz), 3.88 (*s*, 3H, –OCH_3), 6.06 (*s*, 2H, –N–CH_2), 6.59–7.70 (*m*, 8H, *J* = 9.0 and 6.1 Hz, Ar–H), 11.15 (*s*, 1H, –C–SH). ^{13}C-NMR (300 MHz, $CDCl_3$, δ / ppm): 13.10 (–CH_3 at C-2 of benzimidazole), 41.66 (–CH_2), 55.87 (OCH_3), 159.24, 170.59, 125.85, 138.40, 112.50, 129.55, 117.27, 120.86 (aromatic carbons). MS (*m*/*z*): 351 [M^+], 336, 325, 320, 300.

*4-(4-Methoxyphenyl)-5-[(2-methyl-1*H*-benzimidazol-1-yl)methyl]-4*H*-1,2,4--triazole-3-thiol (**6h**)*. IR (KBr, cm^{-1}): 2549 (SH), 2810 (OCH_3). ^{1}H-NMR (300 MHz, $CDCl_3$, δ / ppm): 2.50 (*s*, 3H, –CH_3 at C-2 of Bz), 3.82 (*s*, 3H, –OCH_3), 6.08 (*s*, 2H, –N–CH_2), 6.66–7.65 (*m*, 8H, *J* = 8.9 and 6.2 Hz, Ar–H), 11.15 (*s*, 1H, –C–SH). ^{13}C-NMR (300 MHz, $CDCl_3$, δ / ppm): 13.15 (–CH_3 at C-2 of benzimidazole), 41.71 (–CH_2), 55.66 (OCH_3), 161.15, 172.50, 167.96, 124.22, 114.18, 163.03, 124.22, 114.18 (aromatic carbons). MS (*m*/*z*): 351 [M^+], 336, 325, 320, 308, 375, 300.

*4-(2-chlorophenyl)-5-[(2-methyl-1H-benzimidazol-1-yl)methyl]-4H-1,2,4--triazole-3-thiol (**6i**)*. IR (KBr, cm^{-1}): 2550 (SH), 750 (C-Cl). ^{1}H-NMR (300 MHz, $CDCl_3$, δ / ppm): 2.62 (*s*, 3H, –CH_3 at C-2 of Bz), 6.07 (*s*, 2H, –N–CH_2), 6.56–7.72 (*m*, 8H, *J* = 8.9 and 7.2 Hz, Ar–H), 11.15 (*s*, 1H, –C–SH). ^{13}C-NMR

(300 MHz, $CDCl_3$, δ / ppm): 13.18 ($–CH_3$ at C-2 of benzimidazole), 41.75 ($–CH_2$), 154.14, 172.12, 167.87, 124.11, 114.24, 163.54, 124.78, 114.77 (aromatic carbons). MS (*m*/*z*): 355 [M^+], 340, 329, 319, 279, 304.

*4-(4-chlorophenyl)-5-[(2-methyl-1H-benzimidazol-1-yl)methyl]-4H-1,2,4--triazole-3-thiol (**6j**)*. IR (KBr, cm^{-1}): 2552 (SH), 742 (C-Cl). ^{1}H-NMR (300 MHz, $CDCl_3$, δ / ppm): 2.61 (*s*, 3H, $–CH_3$ at C-2 of Bz), 6.07 (*s*, 2H, $–N–CH_2$), 6.50–7.70 (*m*, 8H, *J* = 8.9 and 7.2 Hz, Ar–H), 11.15 (*s*, 1H, –C–SH). ^{13}C-NMR (300 MHz, $CDCl_3$, δ / ppm): 13.12 ($–CH_3$ at C-2 of benzimidazole), 41.72 ($–CH_2$), 160.71, 172.06, 142.58, 120.24, 126.97, 135.38, 120.24, 126.97 (aromatic carbons). MS (*m*/*z*): 355 [M^+], 340, 329, 319, 279, 304.

*4-(4-aminophenyl)-5-[(2-methyl-1H-benzimidazol-1-yl)methyl]-4H-1,2,4--triazole-3-thiol (**6k**)*. IR (KBr, cm^{-1}): 2560 (SH). ^{1}H-NMR (300 MHz, $CDCl_3$, δ / / ppm): 2.61 (*s*, 3H, $–CH_3$ at C-2 of Bz), 6.07 (*s*, 2H, $–N–CH_2$), 6.50–7.70 (*m*, 8H, *J* = 8.9 and 7.2 Hz, Ar–H), 11.15 (*s*, 1H, –C–SH). ^{13}C-NMR (300 MHz, $CDCl_3$, δ / ppm): 13.11 ($–CH_3$ at C-2 of benzimidazole), 41.71 ($–CH_2$), 141.84, 133.22, 119.55, 106.84, 122.30, 126.56, 147.72, 162.66, 174.01, 138.00, 105.48, 148.27, 105.48, 116.19 (aromatic carbons). MS (*m*/*z*): 336 [M^+], 321, 310, 260, 285, 309.

Journal of the Serbian Chemical Society
JSCS-info@shd.org.rs • www.shd.org.rs/JSCS
J. Serb. Chem. Soc. *76* (3) 353–362 (2011) UDC 637.12:637.146.3+542.92+632.95+546.18
JSCS–4123 *Original scientific paper*

Degradation kinetics of seven organophosphorus pesticides in milk during yoghurt processing

LI-YING BO[1], YING-HUA ZHANG[1,2] and XIN-HUAI ZHAO[1,2]*

[1]*Key Laboratory of Dairy Science, Ministry of Education, Northeast Agricultural University, Harbin 150030 and* [2]*Department of Food Science, Northeast Agricultural University, Harbin 150030, P. R. China*

(Received 15 June, revised 3 September 2010)

Abstract: Bovine milk spiked with seven organophosphorus pesticides, *i.e.*, dimethoate, fenthion, malathion, methyl parathion, monocrotophos, phorate and trichlorphon, was fermented at 42 °C with commercial directed vat set (DVS) starters to investigate the degradation kinetics of the pesticides during yoghurt processing. The spiked pesticides were extracted from the prepared samples with an organic solvent and analyzed by gas chromatography after purification. Based on published results that the degradation kinetics of pesticides is first order, the rate constant of degradation and the half live period of the pesticides were calculated. The results indicated that degradation of the pesticides in milk during yoghurt processing were enhanced by one or both starters, except for malathion, and the two commercial DVS starters had different influences on the degradation kinetics of the pesticides.

Keywords: bovine milk; organophosphorus pesticide; degradation kinetics; yoghurt; starter.

INTRODUCTION

Organophosphorus pesticides are widely used in agriculture to protect plants from insects. When dairy cows are fed with organophosphorus pesticide polluted forages or drinking water, bovine milk and dairy products might be tainted with pesticide residues,[1,2] which could lead to health risks.[3] Mallatou *et al.* investigated organophosphorus pesticide residues in thirty-eight samples of bovine milk and twenty-eight samples of cheese and found that eleven milk samples contained residues, and the contents of methyl parathion in two samples were 43 and 280 μg kg^{-1}.[4] Pagliuca *et al.* analyzed organophosphorus pesticide contamination in one hundred and thirty-five raw milk samples and found that thirty-seven samples tested positive for traces and ten samples contained residues ranging

* Corresponding author. E-mail: zhaoxh@mail.neau.edu.cn
doi: 10.2298/JSC100615035B

from 5 to 18 μg kg^{-1}.[5] These studies illustrated the existence of organophosphorus pesticides in milk and dairy products.

The residue levels of pesticides in foods are affected by food processing, including fermentation, heat treatment and drying. In addition, the chemical nature of the pesticides and some factors, such as pH, light, metal ions and ozone, also impact the degradation of pesticide residues.[6,7] Uygun and Senoz studied the degradation of five organophosphorus pesticides in wheat during storage.[8] More interesting, the results of Abou-Arab showed that some starters could enhance the degradation of dichlorodiphenyl-trichloroethane and lindane.[9,10] The degradation of organophosphorus pesticides in bovine milk during yoghurt processing has not hitherto been reported. In the present study, seven organophosphorus pesticides, which were or are used in China, were added to bovine milk and the spiked milk was subjected to yoghurt processing with two commercial directed vat set (DVS) starters, in an attempt to study the impacts of the starters on the degradation of the pesticides. A gas chromatography-based method was used to analyze the amount of pesticide residues in the prepared yoghurt samples, and the degradation kinetics of the pesticides were calculated, treating the degradation of organophosphorus pesticides as a first order reaction.

EXPERIMENTAL

Reagents and materials

Seven organophosphorus pesticide standards, dimethoate, fenthion, malathion, methyl parathion, monocrotophos, phorate and trichlorphon, were purchased from Dr. Ehrenstorfer (Augsburg, Germany) with declared purity from 94.5 to 99.5 %, and stored at −18 °C. Initial stock solutions (500 mg L^{-1}) of each pesticide individually were prepared by dissolving the pesticides in acetone. Working stock solutions of the individual pesticides were prepared by diluting the initial stock solutions with acetone to give concentrations ranging from 20 to 40 mg L^{-1}. Working solutions of mixed pesticides were prepared by combining the working stock solutions of the individual pesticides in different ratios and diluting to a fixed volume with acetone. These solutions were used to determine the standard curve or to spike bovine milk. Two commercial DVS starters applied in yoghurt preparation were purchased from Rhodia (Melle, France) and Danisco (Copenhagen, Denmark), and stored at −18 °C before use. The chemicals and solvents used were of analytic and chromatographic grade and procured from Sigma-Aldrich (Schnelldorf, Germany). The water used to prepare all solutions was highly purified using a Milli-Q PLUS unit (Millipore Corporation, New York, NY, USA). Bovine milk used was collected daily from a dairy farm in Harbin, Heilongjiang Province, China, and stored at 4 °C before use.

Preparation of yoghurt

Seven organophosphorus pesticides were added to bovine milk at a level of about 1.5 mg kg^{-1}. The spiked milk was shaken vigorously and stood at ambient temperature for 30 min. The procedure of yoghurt preparation followed the method reported by Isleten and Karagul--Yuceer.[11] A stainless steel vessel containing the spiked milk was placed in a water bath and heated to 95 °C for 15 min with continuous gentle stirring, and then cooled in a water bath to 42 °C. A commercial DVS starter was added to the milk at 0.6 g kg^{-1} milk, recommended by

the producer. The inoculated milk was poured into glass cups (each had a capacity of 200 mL) with lids, and incubated at 42 °C in an incubator for 8 h. At regular time intervals, three cups were selected at random from the bulk samples, rapidly cooled in an ice water bath and subjected to pesticide extraction and purification. A control was also prepared by the same procedure but without starter addition.

Extraction and purification of organophosphorus pesticides

The extraction and purification of organophosphorus pesticides from the yoghurt samples followed the methods of Pagliuca *et al.*[12] The sample (10.0 g) was extracted with 20 mL of a 1:4, v/v acetone–acetonitrile mixture, shaken vigorously for 2 min and centrifuged at 400× *g* for 6 min. The liquid phase was transferred to a separation funnel, and the residue of the sample was collected and re-extracted with 15 mL of the acetone–acetonitrile mixture as above. The obtained liquid phases were combined and vigorously shaken with 50 mL dichloromethane for 10 min, and left for 20 min for phase separation. The dichloromethane phase was separated, filtered through anhydrous sodium sulfate (2.0 g) and collected as a purified pesticide extract. A sample of the purified extract (15.0 mL) was measured and evaporated to dryness at 30 °C with nitrogen gas in an evaporation station. The residue was reconstituted to a volume of 1.0 mL with acetone and filtered through a 0.45 μm microporous membrane filter before GC analysis.

GC analysis of organophosphorus pesticides

The GC analysis of organophosphorus pesticides for the standard solutions or the samples was performed using an Agilent 7890 gas chromatography (Agilent Technologies, Inc., Santa Clara, USA), equipped with a flame photometric detector and a capillary column (DB--1701, 30 m×0.250 mm×0.25 μm), and nitrogen as the carrier gas at a flow rate of 3 mL min^{-1}. The method described by Pagliuca *et al.* was employed.[12] The temperature profile was set as follows: initial temperature 100 °C for 1 min, heating from 100 to 195 °C at 30 °C min^{-1}, holding for 8 min at 195 °C, heating from 195 to 202 °C at 10 °C min^{-1}, holding for 1 min at 202 °C, heating from 202 to 205 °C at 1 °C min^{-1} and heating from 205 to 240 °C at 15 °C min^{-1}. The temperatures of the injector and detector were set at 200 and 250 °C, respectively. Quantification of the pesticides was performed by comparing the peak areas of the pesticides to a calibration curve of the standards. A multitude-point calibration was used.

Statistical analysis

All data are expressed as means ±*SD* (standard deviation) from at least three independent trials. The rate constant of pesticide degradation was calculated by linear regression analysis. SPSS 13.0 software (SPSS Inc., Chicago, IL, USA) was used to analyze the data.

RESULTS AND DISCUSSION

Analysis of organophosphorus pesticides by GC

With the selected analysis procedure, seven organophosphorus pesticides, the chemical structures of which are shown in Fig. 1, could be extracted efficiently from the prepared yoghurt or milk samples and measured accurately. Typical GC profiles of the seven pesticides for standard solutions and the samples are given in Fig. 2, which shows that seven pesticides were well-separated by the column. Practical GC analysis found that the linear range of detection for the pesticides was from 0.1 to 8 mg kg^{-1} ($R^2 \geq 0.995$). The data listed in Table I

demonstrate that the detection limits for the pesticides ranged from 0.01 to 0.02 mg kg^{-1}, and the recovery of the pesticides at two addition levels ranged from 80.26 (fenthion, at 0.1 mg kg^{-1}) to 125.9 % (dimethoate, at 1.0 mg kg^{-1}). The relative standard deviation of the recovery of monocrotophos at an addition level of 0.1 mg kg^{-1} was the largest, but less than 7.0 %. This means that the applied extraction and purification procedure appeared to be efficient and the GC analysis procedure was suitable for the detection of the pesticide residues in the prepared samples.

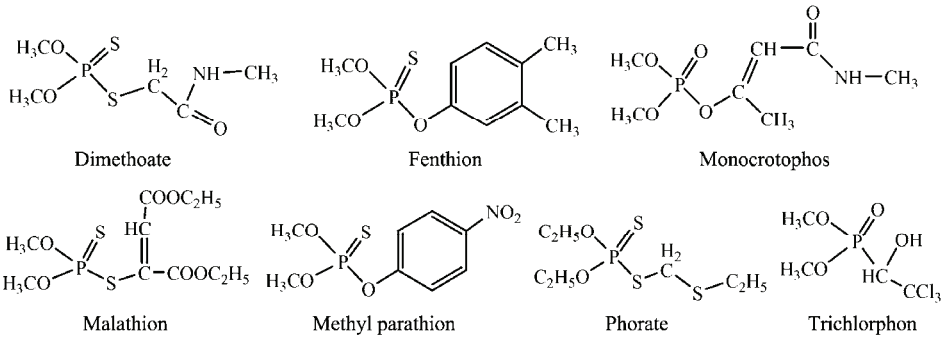

Fig. 1. Chemical structures of the seven studied organophosphorus pesticides.

Degradation parameters of organophosphorus pesticides in bovine milk during yoghurt processing

There was no effect of presence of organophosphorus pesticides on yoghurt formation from bovine milk. This indicated that the microbial cultures of both commercial starters were tolerant to the added pesticides. To insure more pesticides remained in the milk after heat treatment at 95 °C and to obtain higher extraction efficiencies of the pesticides, the seven pesticides were added at a higher level of 1.5 mg kg^{-1}. The pesticides residues remaining in the milk at different treatment times were analyzed. The results are given in Table II. The contents of the pesticides in the milk subjected to fermentation or heat treatment showed a decreasing trend with progressing treatment time, indicating degradation of the pesticides.

The degradation of organophosphorus pesticides was reported to be a first order reaction.[13,14] This means that the content of each pesticide in the milk at different times would follow Eq. (1):

$$\frac{dc}{dt} = kt \quad (1)$$

where c is the content of the studied pesticide, t is the treatment time and k is rate constant of degradation of the pesticide.

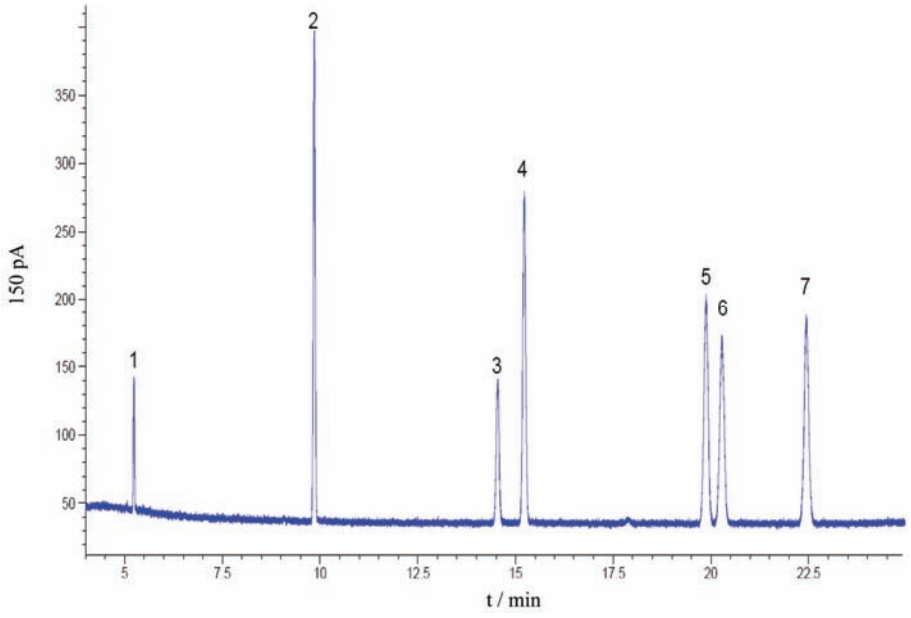

(a)

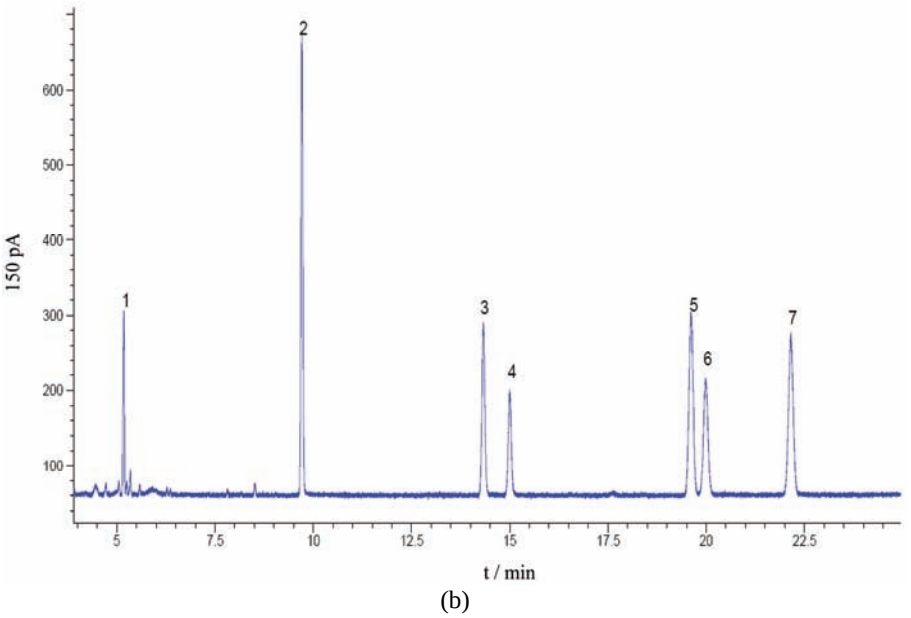

(b)

Fig. 2. Typical GC profiles of the seven studied organophosphorus pesticides for the standard solution (a) and the spiked milk sample heated at 42 °C (b). Peaks 1–7 represent trichlorphon, phorate, monocrotophos, dimethoate, fenthion, malathion and methyl parathion, respectively. The concentration of the pesticides standard solution was 0.6 mg kg^{-1}. The control or yoghurt samples were spiked with pesticides at 1.5 mg kg^{-1} and heated or fermented for 2 h.

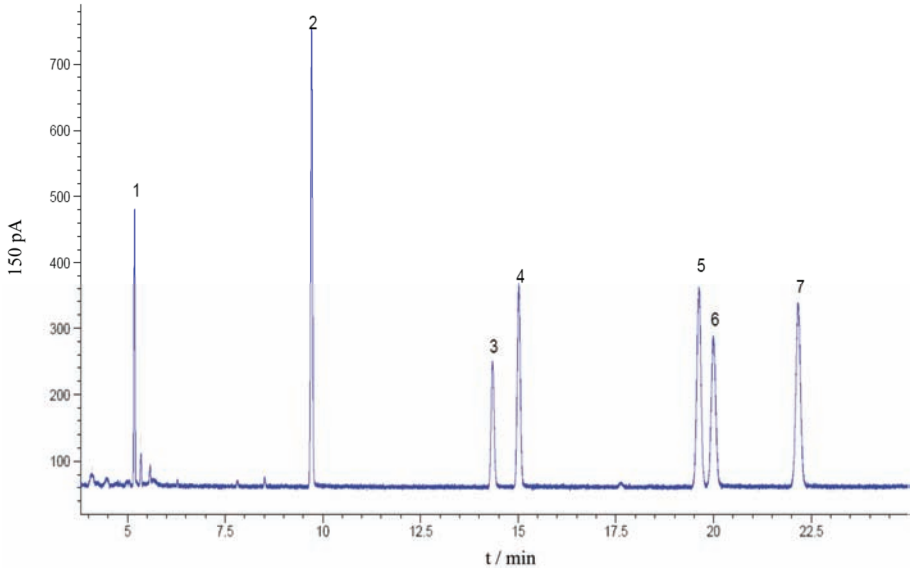

(c)

Fig. 2 (continued). Typical GC profiles of the seven studied organophosphorus pesticides for the prepared yoghurt sample (c). Peaks 1–7 represent trichlorphon, phorate, monocrotophos, dimethoate, fenthion, malathion and methyl parathion, respectively. The concentration of the pesticides standard solution was 0.6 mg kg^{-1}. The control or yoghurt samples were spiked with pesticides at 1.5 mg kg^{-1} and heated or fermented for 2 h.

TABLE I. Recovery and limits of detection (*LOD*) of the seven studied organophosphorus pesticides during the preparation of yoghurt in GC analysis (the number of trials was nine)

Pesticide	Spiking levels and recovery (mean±*SD*, %)		*LOD* / mg kg^{-1}
	0.1 mg kg^{-1}	1.0 mg kg^{-1}	
Dimethoate	114.0±3.7	125.9±2.3	0.01
Fenthion	80.26±4.6	118.7±3.3	0.01
Malathion	87.24±3.6	98.90±5.0	0.01
Methyl parathion	89.85±5.2	94.40±4.1	0.01
Monocrotophos	108.7±7.5	115.7±2.8	0.02
Phorate	81.47±3.5	95.87±3.8	0.01
Trichlorphon	80.75±4.3	96.53±4.3	0.01

The rate constant of degradation and half-life period of the seven pesticides in the milk during yoghurt processing or heat treatment are thus calculated from the data listed in Table II using, respectively, Eqs. (2) and (3):

$$\ln c = -kt + A \quad (2)$$

$$t_{1/2} = \frac{0.693}{k} \quad (3)$$

where A is a constant and $t_{1/2}$ is half-life period of the pesticide. The obtained values are listed in Table III.

TABLE II. Contents of seven organophosphorus pesticides in the control and yoghurt samples after different treatment times (mean±*SD*, mg·kg^{-1}; the number of trials was three)

Pesticide	Sample[a]	*t* / h				
		0	2	4	6	8
Dimethoate	Control	1.073±0.045	0.964±0.046	0.938±0.036	0.874±0.031	0.831±0.030
	Yoghurt 1	1.163±0.040	1.042±0.047	0.987±0.023	0.943±0.046	0.892±0.044
	Yoghurt 2	1.171±0.013	1.034±0.027	0.972±0.018	0.923±0.011	0.881±0.035
Fenthion	Control	1.121±0.036	0.994±0.028	0.942±0.045	0.901±0.025	0.852±0.020
	Yoghurt 1	1.152±0.040	1.023±0.035	0.974±0.042	0.921±0.038	0.842±0.025
	Yoghurt 2	1.133±0.027	1.024±0.031	0.954±0.032	0.932±0.026	0.853±0.019
Malathion	Control	1.023±0.030	0.931±0.051	0.863±0.050	0.832±0.042	0.814±0.045
	Yoghurt 1	1.134±0.025	1.043±0.031	0.992±0.032	0.953±0.025	0.942±0.031
	Yoghurt 2	1.231±0.020	1.142±0.036	1.094±0.027	1.062±0.033	1.053±0.029
Methyl	Control	1.051±0.030	0.983±0.035	0.934±0.035	0.873±0.045	0.832±0.051
parathion	Yoghurt 1	1.214±0.030	1.124±0.055	1.042±0.050	0.981±0.045	0.940±0.042
	Yoghurt 2	1.312±0.023	1.251±0.031	1.184±0.024	1.122±0.021	1.081±0.033
Monocrotophos	Control	1.082±0.055	1.033±0.035	0.954±0.031	0.895±0.025	0.872±0.025
	Yoghurt 1	1.031±0.040	0.983±0.040	0.912±0.046	0.833±0.062	0.814±0.063
	Yoghurt 2	1.192±0.017	1.093±0.020	1.042±0.011	0.963±0.013	0.951±0.033
Phorate	Control	1.131±0.026	1.093±0.016	1.031±0.046	0.983±0.020	0.952±0.026
	Yoghurt 1	1.101±0.032	1.052±0.036	0.983±0.035	0.914±0.035	0.890±0.031
	Yoghurt 2	1.215±0.016	1.142±0.013	1.103±0.020	1.054±0.023	1.012±0.019
Trichlorphon	Control	1.036±0.012	0.933±0.016	0.892±0.011	0.871±0.015	0.860±0.015
	Yoghurt 1	1.071±0.015	0.953±0.010	0.914±0.015	0.873±0.025	0.854±0.030
	Yoghurt 2	1.131±0.023	1.022±0.013	0.991±0.017	0.952±0.014	0.921±0.020

[a]Yoghurts 1 and 2 were produced with commercial DVS starter of Rhodia and Danisco, respectively, at 42 °C. The control was bovine milk subjected to heat treatment at 42 °C

Compared to the degradation of seven pesticides in the control, the degradation of the pesticides in the milk during yoghurt processing was impacted by the applied starters. Based on the corresponding rate constants listed in Table III, the degradation of dimethoate, fenthion and trichlorphon in the milk during yoghurt processing increased when either of the two starters was added, leading to a larger rate constant of degradation or a shorter half-live period of these pesticides. The starter from Rhodia also accelerated the degradation of methyl parathion, monocrotophos and phorate but the starter from Danisco had little or no impact on the degradation of these three pesticides. The two starters had different influences on the degradation of the six pesticides in the milk during yoghurt processing. The half-live period of fenthion was the shortest, indicating fenthion was the most unstable pesticide. It was unexpected that the degradation of malathion in the milk was not enhanced by the starters, because its rate constant of degradation in the milk fermented with two starters was lower than that in the control.

The reason for this unusual result remains unclear and needs further study. In addition, studies of the degradation products and of the impact of other microbial starters on the degradation of the pesticide are required.

TABLE III. Kinetic parameters for degradation of seven organophosphorus pesticides in the bovine milk during yoghurt processing or heat treatment

Pesticide	Sample[b]	Kinetic parameters[a]		
		k / h^{-1}	R^2	$t_{1/2}$ / h
Dimethoate	Control	0.0305	0.969	22.7
	Yoghurt 1	0.0315	0.965	22.0
	Yoghurt 2	0.0343	0.951	20.2
Fenthion	Control	0.0324	0.955	21.4
	Yoghurt 1	0.0366	0.976	18.9
	Yoghurt 2	0.0331	0.966	20.9
Malathion	Control	0.0285	0.930	24.3
	Yoghurt 1	0.0231	0.925	30.0
	Yoghurt 2	0.0192	0.905	36.1
Methyl parathion	Control	0.0293	0.997	23.6
	Yoghurt1	0.0324	0.987	21.4
	Yoghurt 2	0.0248	0.996	27.9
Monocrotophos	Control	0.0287	0.978	24.1
	Yoghurt1	0.0319	0.975	21.7
	Yoghurt 2	0.0289	0.958	24.0
Phorate	Control	0.0225	0.991	30.8
	Yoghurt 1	0.0283	0.983	24.5
	Yoghurt 2	0.0223	0.992	31.1
Trichlorphon	Control	0.0221	0.857	31.4
	Yoghurt 1	0.0270	0.910	25.7
	Yoghurt 2	0.0241	0.932	28.8

[a]k – rate constant of degradation, R – coefficient of regression, $t_{1/2}$ – half-life period; [b]yoghurts 1 and 2 were produced with commercial DVS starter of Rhodia and Danisco, respectively, at 42 °C. The control was bovine milk subjected to heat treatment at 42 °C

Uygun and Senoz[8] studied the degradation of methyl chlorpyrifos, fenitrothion, malathion and methyl pirimiphos in wheat stored at ambient temperature for five months and found the levels of malathion, fenitrothion, methyl chlorpyrifos and methyl pirimiphos were decreased by 88, 86, 84 and 76 %, respectively. Unfortunately, the rate constant of degradation of these pesticides was not given. In practical yoghurt processing, the milk is fermented with a starter for about 4 h at 42 °C. According to the present results, the decrease in the level of seven pesticides in yoghurt samples with fermentation time of 4 h would range from 9.2 (phorate) to 17.1 % (dimethoate).

CONCLUSIONS

The degradation of seven organophosphorus pesticides, dimethoate, fenthion, malathion, methyl parathion, monocrotophos, phorate and trichlorphon, in

bovine milk during yoghurt processing was studied in the present work. The bovine milk was spiked with the pesticides and fermented with two commercial DVS starters at 42 °C. The pesticide residues were extracted from the prepared samples and measured by GC. The content of the pesticides in the milk all decreased as the treatment time progressed, indicating degradation of the pesticides. The calculated rate constant of degradation or half-live period of the pesticides revealed that the degradation of the selected pesticides, except for malathion, was enhanced by one or both of the applied starters and the two starters had different impacts on the degradation of the pesticides.

Acknowledgements. The authors gratefully acknowledge the financial support from the National Key Technological Research and Development Program of China during the 11th Five-Year Plan Period (No. 2006BAD04A08). The authors also thank the anonymous reviewers and editors for their constructive comments and valuable suggestions to this paper.

И З В О Д

КИНЕТИКА РАЗГРАДЊЕ СЕДАМ ОРГАНОФОСФОРНИХ ПЕСТИЦИДА У МЛЕКУ ТОКОМ ПРОЦЕСА ПРОИЗВОДЊЕ ЈОГУРТА

LI-YING BO[1], YING-HUA ZHANG и XIN-HUAI ZHAO[1,2]

[1]*Key Laboratory of Dairy Science, Ministry of Education, Northeast Agricultural University, Harbin 150030 и* [2]*Department of Food Science, Northeast Agricultural University, Harbin 150030, P. R. China*

Крављем млеку је додато седам органофосфорних пестицида и ферментисано је на 42 °C у присуству комерцијалних стартера (DVS), у циљу испитивања кинетике разградње пестицида током процеса производње јогурта. Додати су следећи пестициди: диметоат, фентион, малатион, метил-паратион, монокротофос, форат и трихлорфон. Пестициди су изоловани из узорака млека органским растварачем и анализирани гасном хроматографијом након пречишћавања. Узевши у обзир да је кинетика разградње пестицида првог реда, израчунате су константе брзине разлагања и време полуживота пестицида. Резултати су показали да је разлагање пестицида (осим малатиона) у млеку током процеса производње јогурта убрзано стартерима и да комерцијани DVS стартери имају различит утицај на кинетику разлагања.

(Примљено 15. јуна, ревидирано 3. септембра 2010)

REFERENCES

1. R. S. Battu, B. Singh, B. K. Kang, *Ecotox. Environ. Safety* **59** (2004) 324
2. K. Fytianos, G. Vasilikiotis, L. Well, E. Kavlendis, N. Laskaridis, *Bull. Environ. Contam. Toxicol.* **34** (1985) 504
3. M. V. Russo, L. Campanella, P. Avino, *J. Chromatogr. B* **780** (2002) 431
4. H. Mallatou, C. P. Pappas, E. Kondyli, T. A. Albanis, *Sci. Total Environ.* **196** (1997) 111
5. G. Pagliuca, A. Serraino, T. Gazzotti, E. Zironi, A. Borsari, R. Rossmini, *J. Dairy Res.* **73** (2006) 340
6. S. Bogialli, R. Curini, A. Di Corcia, A. Laganà, A. Stabile, E. Sturchio, *J. Chromatogr. A* **1102** (2006) 1
7. A. Ozbey, U. Uygun, *Int. J. Food Sci. Technol.* **42** (2007) 380
8. U. Uygun, B. Senoz, H. Koksel, *Food Chem.* **109** (2008) 355

9. A. A. K. Abou-Arab, *Food Chem.* **64** (1997)115
10. A. A. K. Abou-Arab, *Food Chem. Toxicol.* **40** (2002) 33
11. M. Isleten, Y. Karagul-Yuceer, *J. Dairy Sci.* **89** (2006) 2865
12. G. Pagliuca, T. Gazzotti, E. Zironi, P. Ssicca, *J. Chromatogr. A* **1071** (2005) 67
13. M. Vanclooster, S. Ducheyne, M. Dust, H. Vereecken, *Agr. Water Manage.* **44** (2000) 371
14. N. von Götz, P. Nörtersheuser, O. Richte, *Chemosphere* **38** (1999) 1615.

Journal of the Serbian Chemical Society
JSCS-info@shd.org.rs • www.shd.org.rs/JSCS
J. Serb. Chem. Soc. 76 (3) 363–373 (2011)
JSCS–4124
UDC 582.282.23:663.4:66.081:57+
546.48:541.121+544.4
Original scientific paper

Application of immobilized waste brewery yeast cells for Cd^{2+} removal. Equilibrium and kinetics

SZENDE TONK[1], ANDRADA MĂICĂNEANU[2]*, CERASELLA INDOLEAN[2], SILVIA BURCA[2] and CORNELIA MAJDIK[2]

[1] *Sapientia University, Science and Art Faculty, 4 Matei Corvin St., RO-400112 Cluj-Napoca, Romania and* [2] *"Babeş-Bolyai" University, Faculty of Chemistry and Chemical Engineering, 1 Kogălniceanu St., RO-400028 Cluj-Napoca, Romania*

(Received 27 May, revised 10 September 2010)

Abstract: In this investigation, the removal of Cd^{2+} by a brewery waste biomass in immobilized (Ca alginate beads) form was studied. The removal process was conducted at room temperature under batch conditions (magnetic stirring) using different initial cadmium concentrations. The equilibrium of biosorption was reached in 150 min for all employed initial concentrations. The maximum biosorption capacity was calculated to be 5.96 mg Cd^{2+} g^{-1} yeast for an initial Cd^{2+} concentration of 169 mg L^{-1}. Langmuir and Freundlich adsorption isotherms were used to correlate the equilibrium adsorption data. Based on the correlation coefficients, it was concluded that the Langmuir isotherm is more suitable for describing the equilibrium data of cadmium biosorption. In addition, first and pseudo-second order kinetic models were applied to describe the biosorption process. The kinetic parameters for the pseudo-second order kinetics were determined.

Keywords: *Saccharomyces cerevisiae*; immobilization; cadmium biosorption; Freundlich and Langmuir models; kinetic models.

INTRODUCTION

Heavy metal ions, such as cadmium, lead and mercury, are highly toxic to living organisms. Cadmium is one of the three most toxic heavy metals, its toxicity being attributed in part to its ability to accumulate in living organisms. Cadmium tends to accumulate slowly over time in bones, liver and kidneys, where it can impair normal functions.

Adsorption of metals by microbial biomass and agricultural materials is a relatively recent method for the removal and recovery of metals. This method

* Corresponding author. E-mail: andrada@chem.ubbcluj.ro
doi: 10.2298/JSC100527032T

was used to remove toxic metals from industrial liquid waste products and, due to its high efficiency, it appears to be more attractive in comparison to other processes.[1] Various kinds of microbial biomasses (*e.g.*, yeast, algae and fungi)[2–4] and agricultural by-products (*e.g.*, rice straw, soybean hull, sugarcane bagasse, peanut shells, pecan and walnut shells, almond shells, olive stones and peach stones)[5,6] have been tested for this purpose. For example, Norris and Kelly[7] studied the adsorption of cadmium and cobalt ions by *Saccharomyces cerevisiae* yeast surface. Biosorption is considered a fast physical and/or chemical process depending on the yeast type and treatment. The biosorption rate depends on the type of the process. According to the literature, biosorption can be divided into two main processes: adsorption of the ions on the cell surface and bioaccumulation within the cell.[8]

The uptake capacity of biomasses is always affected by many factors, such as pH, temperature, initial concentrations of biomass and metal ions, culture condition and some others, such as the presence of various ligands and metal ions. If all other culture conditions are the same, the biosorption capacity of a biomass depends mainly on the type of biomass cells. To understand the interaction between metal ions and the biomass, the hard and soft principle of metal ions proposed by Nieboer and Richardson has been widely used.[9–12]

The commercial applications of biomass as biosorbents has been hindered by operational limitations associated with their physical characteristics, such as small particle size, low density, poor mechanical strength, low rigidity and solid/liquid separation problems.[13] These difficulties can be overcome by entrapment of microbial biomass in immobilized preparations. The efficiency of these preparations as potential metal biosorbents can be further enhanced by using plant waste material as the immobilizing matrix.[14] Immobilization techniques are one of the key elements for the practical application of biosorption, especially by dead biomass.[15] The most commonly used matrix materials for the immobilization of microbial cells *via* entrapment are carbohydrate polymers, such as alginate, chitosan, chitin and carboxymethyl-cellulose,[16] polysulphone, polyacrylamide, polyurethane and silica.[17] The selection of immobilization matrix is crucial in the application of immobilized biomass. The polymer matrix determines the mechanical strength, rigidity, and porosity characteristics and chemical resistance of the final biosorbent particles to be utilized for successive sorption–desorption cycles; thus, it is very important to choose the appropriate immobilization matrix in every case.[18] Natural polymers, such as Na alginate, have been used as the matrix for cell immobilization. Chang and co-workers found that the adsorption capacity of Ca alginate immobilized cells was greater than that of polyacrylamide-entrapped cells for the adsorption of Cd^{2+}.[19]

Other authors studied the removal of different heavy metals (Cd^{2+}, Cu^{2+}, Hg^{2+}, Zn^{2+}, *etc.*) onto diverse immobilized bacteria, fungi, algae, yeasts, *etc.*

(*Spirulina platensis*, *Laminaria digitata*, *Aspergillus niger*, *etc*.).[20–24] All proved to be very efficient in the removal of heavy metal ions from aqueous solutions.

Yeast biomass has been successfully used as a biosorbent for the removal of Ag, Au, Cd, Co, Cr, Cu, Ni, Pb, U, Th and Zn. A number of studies showed that *Saccharomyces cerevisiae* could remove toxic metals, recover precious metals and clean radionuclides from aqueous solutions to various extents. The advantages of *S. cerevisiae* for metal biosorption, the forms of *S. cerevisiae* in biosorption research, the biosorptive capacity of *S. cerevisiae*, and the selective and competitive biosorption by *S. cerevisiae* were depicted in detail by Wang and Chang.[25]

The same authors reviewed the metal uptake capacity of *S. cerevisiae*, in different forms (calculated for dry biomass), and found values ranging between 10 and 300 mg M^{n+} g^{-1}.[18] In case of cadmium, the uptake (adsorption) capacity was usually above 10 but less than 100 mg Cd^{2+} g^{-1} dry mass. It should be noted that comparing results from different studies involves standardizing the different ways the adsorption capacity may be expressed. Simultaneously, metal uptake should be compared in almost the same equilibrium concentration of metals in the solution when evaluating the performance of a biomaterial. In particular, there is no standard measurement of dry weight of biomass, *i.e*., no standard drying temperature and time when drying biomass.[18]

Various kinds of immobilized *S. cerevisiae* have been studied with different support materials suitable for use in practical applications.[15,26]

The objective of this work was to investigate the biosorption of Cd^{2+} by immobilized Romanian brewery waste biomass. The cadmium removal efficiency and adsorption capacity were determined. Adsorption equilibrium (Langmuir and Freundlich isotherms) and kinetic models (first and pseudo second order) were used to describe the biosorption process.

EXPERIMENTAL

Biosorbent

The biosorbent, brewery waste biomass, *S. cerevisiae*, was collected from the CIUC brewery (Miercurea-Ciuc, Romania) after use in fermentation processes and transported to the laboratory in plastic containers. The yeast was then washed with bi-distilled water, separated by vacuum filtration and dried in a hot air oven at 80 °C for 24 h.

Biosorbent immobilization

The employed cross-linking procedure with calcium alginate was an adapted version of the method for treatment of fungi biomass outlined by Schiewer and co-workers.[27,28]

For immobilization of yeast, 2 g of biosorbent (brewery waste biomass) was suspended in 50 mL distilled water. This suspension was then blended with a mixture formed from 1 g sodium alginate and 2 mL ethanol. The mixture was then dropped using a peristaltic pump into 200 ml of 0.2 M $CaCl_2$ solution. During this process, the drops of alginate-biomass mixture were gelled into beads of diameter of 4.0±0.2 mm. The Ca alginate immobilized yeast beads were left in the 0.2 M $CaCl_2$ solution at 4 °C for 1 h to cure and form cross-linking

bonds. The beads were rinsed with distilled water to remove the excess of calcium ions and stored at 4 °C prior to use.

Cadmium solution preparation

A stock metal ion solution, 1.0 g L^{-1}, was prepared by dissolving $Cd(NO_3)_2$ $4H_2O$ of analytical grade reagent into an appropriate amount of distilled water. Cadmium solutions of different concentrations (10, 24, 48, 100, 169 mg L^{-1}) were obtained by diluting the stock solution. The concentration of Cd^{2+} in the supernatant fluids was determined using a flame atomic absorption spectrophotometer (SensAA Dual GBS scientific equipment, Australia).

Metal biosorption studies

Experiments were realised under batch conditions with continuously magnetic stirring (875 rpm) at room temperature (20 °C), pH 6.5, for 3 h. The immobilized brewery yeast biomass was contacted with 100 mL of the initial cadmium solutions, as described. The kinetic studies were performed using different concentrations of cadmium solutions. In order to determine the exact concentration of cadmium ions and establish the evolution of the removal process, samples of 100 μL (dilution ratio in each case was 50) from the supernatant were collected at different time intervals (Fig. 1).

The amount of adsorbed cadmium was calculated using the following equation:

$$q_t = \frac{(c_0 - c_t)}{w} \frac{V}{1000} \quad (1)$$

where q_t is the adsorption capacity (mg g^{-1}) at time t, c_0 is the initial cadmium concentration (mg L^{-1}), c_t is the cadmium concentration (mg L^{-1}) at time t, V = 100 mL and w is the quantity of the adsorbent (g).

RESULTS AND DISCUSSION

Cadmium biosorption

The dynamics of cadmium uptake until equilibrium by the waste brewery biomass for various initial cadmium concentrations are represented in Fig. 1.

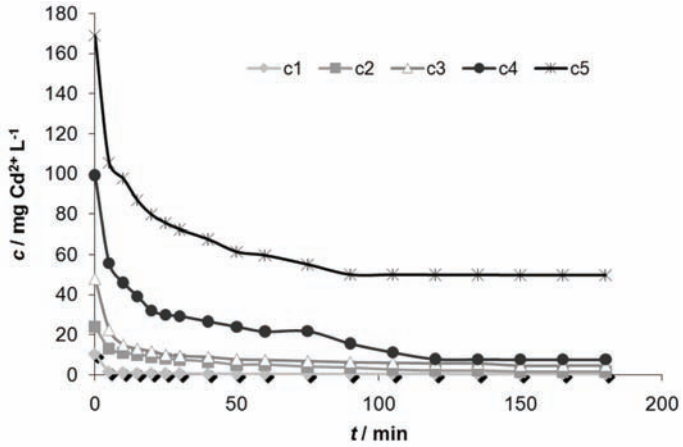

Fig. 1. Dynamics of cadmium uptake by waste brewery biomass for various initial cadmium concentrations; c_1 = 10 mg Cd^{2+} L^{-1}, c_2 = 24 mg Cd^{2+} L^{-1}, c_3 = 48 mg Cd^{2+} L^{-1}, c_4 = 100 mg Cd^{2+} L^{-1}, c_5 = 169 mg Cd^{2+} L^{-1}.

Following the decrease in concentrations with time, three distinct zones can be discerned, which represent:

a) a rapid decrease in the cadmium concentration during the first 5 min, corresponding to cell surface adsorption by interactions between the metal ions and functional groups, such as carboxyl, phosphate, hydroxyl, amino, sulphur, sulphide, thiol, *etc*., present in the cell walls;

b) a slow decrease in the cadmium concentration, corresponding to metal ions that penetrate the cell membrane and enter into the cells; this decrease of the adsorption rate could be associated with a diffusion limitation of the transport of heavy metal ions through the cell wall;

c) the attainment of adsorption equilibrium between metal ions from solution and the immobilized cell surface. Biosorption equilibrium was reached in 150 min for all the investigated initial cadmium concentrations.

The obtained results are in good agreement with those from the literature.[29–32]

Maximum adsorption capacities (Fig. 2) increased from 0.5003 mg Cd^{2+} g^{-1} for an initial cadmium concentration of 10 mg L^{-1} to 5.960 mg Cd^{2+} g^{-1} for an initial concentration of 169.0 mg Cd^{2+} L^{-1}.

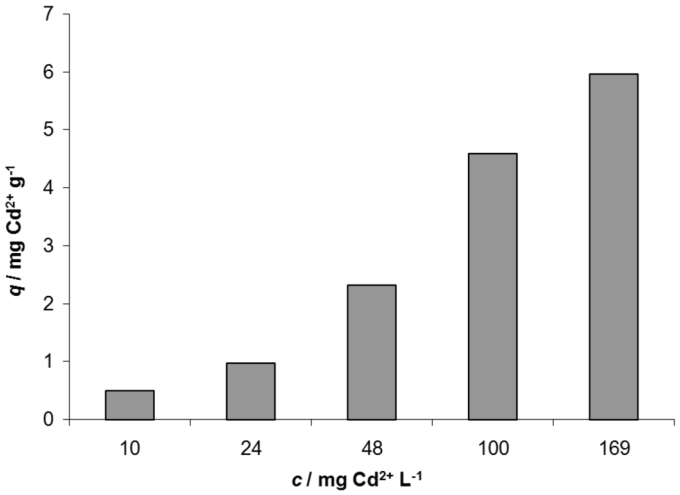

Fig. 2. Maximum adsorption capacities obtained during cadmium adsorption experiments: influence of the initial concentration.

Adsorption equilibrium models

The cadmium biosorption equilibrium was described using the Langmuir and Freundlich models, which are widely used to fit biosorption data.[26,33] The Langmuir model suggests a monolayer adsorption, with no lateral interaction between the adsorbed molecules. The Freundlich model assumes heterogeneous adsorp-

tion due to the diversity of the adsorption sites or diverse nature of the adsorbed metal ions, free or hydrolyzed species.[33]

The Langmuir isotherm can be expressed as follows:

$$q_e = \frac{q_{max} b c_e}{1 + b c_e} \tag{2}$$

where q_e is the solid-phase adsorbate concentration at equilibrium (mg g^{-1}), q_{max} is the maximum adsorption capacity corresponding to a monolayer adsorption capacity (mg g^{-1}), c_e is the concentration Cd^{2+} in solution at equilibrium (mg L^{-1}) and b is related to the strength of the adsorbent–adsorbate affinity.

The linear form of the Langmuir isotherm, Eq. (1), is expressed as:

$$\frac{1}{q_e} = \frac{1}{q_{max} b} \frac{1}{c_e} + \frac{1}{q_{max}} \tag{3}$$

From the linear $1/q_e$ *vs.* $1/c_e$ plot, Fig. 3, the q_{max} and b values were calculated to be 17.4825 mg Cd^{2+} g^{-1} and 0.0660 L mg^{-1}. The experimental values of q_e and c_e, represented in Fig. 4, fitted well on a Langmuir type of isotherm.

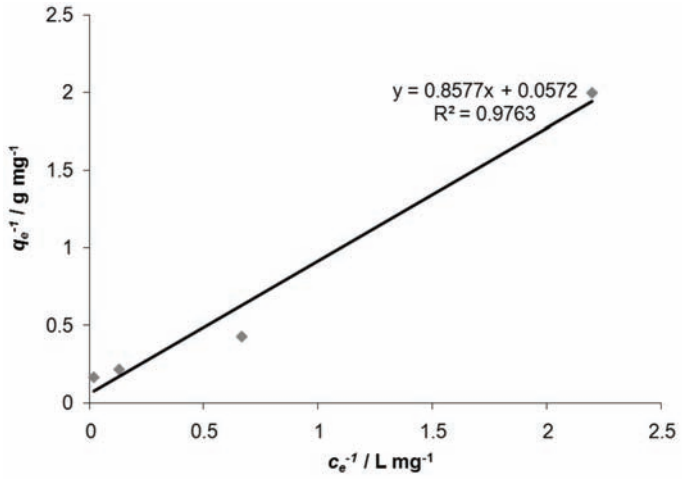

Fig. 3. Langmuir adsorption model of cadmium biosorption on immobilized brewery waste biomass.

The Freundlich isotherm can be expressed as:

$$q_e = k c_e^{1/n} \tag{4}$$

and in the logarithmic (linear) form:

$$\log q_e = \log k + \frac{1}{n} \log c_e \tag{5}$$

where k is related to the adsorption capacity and n to the intensity of the adsorption.

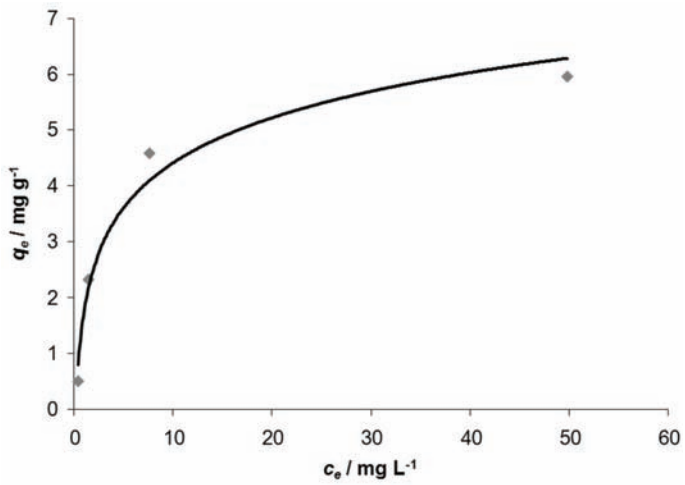

Fig. 4. Adsorption isotherm of cadmium biosorption on immobilized brewery waste biomass.

From the linear log q_e *vs.* log c_e plot, Fig. 5, a correlation coefficient of 0.9183 was determined, which is smaller than that obtained for the Langmuir model, 0.9763. Therefore, it was concluded that cadmium biosorption on immobilized brewery waste biomass followed a Langmuir isotherm.

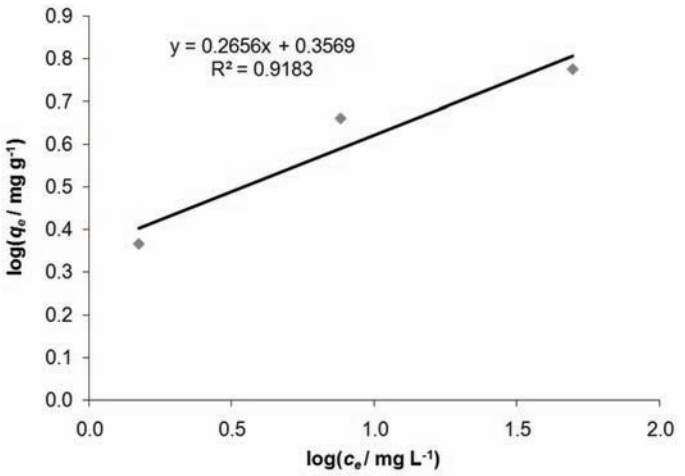

Fig. 5. Freundlich adsorption model of cadmium biosorption on immobilized brewery waste biomass.

Kinetic models

Kinetic data were analyzed using first and pseudo-second order models. Using these models it is possible to investigate the mechanism of adsorption and rate controlling steps.[19,33–35]

The first order equation for adsorption in a liquid/solid system based on capacity of the solid can be expressed as follows:

$$\frac{dq_t}{dt} = k_1(q_e - q_t) \quad (6)$$

Integrating Eq. (2) from the boundary conditions $t = 0$ to t and $q_t = 0$ to q_t gives:

$$\ln (q_e - q_t) = \ln q_e - k_1 t \quad (7)$$

where q_e and q_t are the amounts of cadmium adsorbed (mg g^{-1}) at equilibrium and time t, respectively, and k_1 is the rate constant of the first order adsorption (min^{-1}).

In order to determine the rate constant and equilibrium cadmium uptake, straight line plots of ln ($q_e - q_t$) against t, Eq. (7), were made at five different initial cadmium concentrations. Correlation coefficients between 0.8126 and 0.9513 were obtained (figure not shown).

The pseudo-second order kinetic model is derived based on the adsorption capacity of the solid phase, which assumes that the measured heavy metal ion concentrations are equal to the cell surface concentration, expressed as:

$$\frac{dq_t}{dt} = k_2(q_e - q_t)^2 \quad (8)$$

Integrating Eq. (8) over the boundary conditions $t = 0$ to $t = t$ and $q_t = 0$ to q_t gives:

$$\frac{1}{q_e - q_t} = \frac{1}{q_e} + k_2 t \quad (9)$$

where k_2 is the rate constant of second order adsorption (g mg^{-1} min^{-1}).

Eq. (9) can be rearranged in linear form, as follows:

$$\frac{t}{q_t} = \frac{1}{k_2 q_e^2} + \frac{t}{q_e} \quad (10)$$

In order to determine the rate constant and equilibrium cadmium uptake, the straight line plots of t/q_t against t, Eq. (10), were made at five different initial cadmium concentrations. Correlation coefficients between 0.9966 and 1.0000 were obtained (Fig. 6 and Table I).

Compare the correlation coefficients for the first- and pseudo-second order models, it can be concluded that cadmium biosorption on immobilized brewery waste biomass can be classified as pseudo-second order.

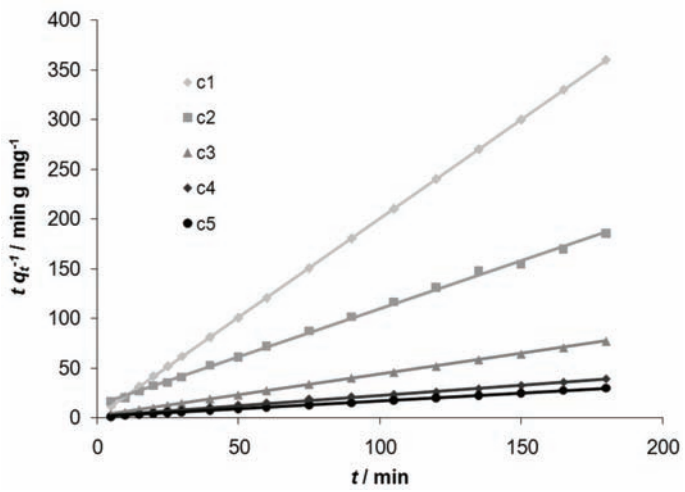

Fig. 6. Correlation of the experimental data using the pseudo-second order model for cadmium biosorption on immobilized brewery waste biomass; c_1 = 10 mg Cd^{2+} L^{-1}, c_2 = 24 mg Cd^{2+} L^{-1}, c_3 = 48 mg Cd^{2+} L^{-1}, c_4 = 100 mg Cd^{2+} L^{-1}, c_5 = 169 mg Cd^{2+} L^{-1}.

Table I. Second order adsorption kinetic parameter

c / mg Cd^{2+} L^{-1}	q_e(exp) / mg Cd^{2+} g^{-1}	q_e(calc) / mg Cd^{2+} g^{-1}	k_2 / g mg^{-1}·min^{-1}	R^2
10	0.5003	0.5033	2.2189	1.0000
24	0.9715	1.0331	0.0727	0.9986
48	2.3250	2.3958	0.0754	0.9998
100	4.5825	4.8614	0.0186	0.9966
169	5.9600	6.2657	0.0211	0.9994

CONCLUSIONS

In this study, an immobilized Ca alginate beads from waste brewery biomass (yeast cells), from Miercurea-Ciuc, Romania, was successfully used as a biosorbent for the removal of Cd^{2+} from aqueous solutions. Calcium alginate proved to be a suitable matrix for the immobilization of bakers' yeast cells.

The maximum biosorption capacity was calculated to be 5.9600 mg Cd^{2+} g^{-1} yeast for an initial concentration of Cd^{2+} of 169 mg L^{-1}.

Langmuir and Freundlich adsorption isotherms were used to correlate the equilibrium adsorption data. Based on the correlation coefficients, it was concluded that the Langmuir isotherm is more suitable to describe the equilibrium data of cadmium biosorption.

In addition, first- and pseudo-second order kinetic models were applied to describe the cadmium biosorption process. Based on the performed mathematical calculations, it was concluded that this process followed pseudo second order kinetics and the parameters for this kinetic model were determined.

The results presented in this paper proved that a biosorbent from the fermentation industry, *i.e.*, waste brewery biomass, which as a by-product of an industrial process is inexpensive and available in large quantities, could be successfully used to remove cadmium ions from aqueous solutions. Further investigations will be conducted in order to explain the adsorption mechanism and to establish the optimum parameters for the biosorption process.

Acknowledgments. The authors would like to thank the Hungarian Academy of Science, "MTA's Hungarians Erudition Scholarship Programme" (MTA HTMTÖ), for the financial support of this study.

И З В О Д

ПРИМЕНА ИМОБИЛИЗОВАНИХ ЋЕЛИЈА ПИВСКОГ КВАСЦА ЗА УКЛАЊАЊЕ Cd^{2+}. РАВНОТЕЖА И КИНЕТИКА

SZENDE TONK[1], ANDRADA MĂICĂNEANU[2], CERASELLA INDOLEAN[2], SILVIA BURCA[2] и CORNELIA MAJDIK[2]

[1]*Sapientia University, Science and Art Faculty, 4 Matei Corvin St., RO-400112 Cluj-Napoca и*
[2]*"Babeş-Bolyai" University, Faculty of Chemistry and Chemical Engineering, 1 Kogălniceanu St., RO-400028 Cluj-Napoca, Romania*

У раду је описан поступак укањања Cd^{2+} имобилисаном отпадном биомасом пивског квасца на честицама калцијум-алгината. Процес уклањања је изведен тзв. "batch" методом, на магнетној мешалици и собној температури, користећи различите почетне концентрације кадмијума. Равнотежа биосорпције је постигнута после 150 min без обзира на почетну концентрацију кадмијума. Максималан капацитет биосорпције је био 5,96 mg Cd^{2+} g^{-1} квасца за 169 mg Cd^{2+} L^{-1} почетне концентрације. Ленгмирове и Фројндлихове адсорпционе изотерме су коришћене за корелацију података. На основу израчунатих коефицијената корелације закључено је да Ленгмирова изотерма боље описује равнотежу биосорпције кадмијума. Тестирани су, такође, кинетички модели првог и псеудо-другог реда за описивање процеса биосорпције. Одређени су кинетички параметри за кинетику псеудо-другог реда.

(Примљено 27. маја, ревидирано 10. септембра 2010)

REFERENCES

1. L. Deng, X. Zhu, Y Su, H. Su, X. Wang, *Chin. J. Oceanol. Limnol.* **26** (2008) 45
2. P. Dostalek, M. Patzak, P. Matejka, *Int. Biodeter. Biodegrad.* **54** (2004) 203
3. A. Saeed, M. Iqbal, *J. Microbiol. Biotechnol.* **22** (2006) 775
4. M. G. Lee, J. H. Lim, S. K. Kam, *Korean J. Chem. Eng.* **19** (2002) 277
5. R. R. Bansode, J. N. Losso, W. E. Marshall, R. M. Rao, R. J. Portier, *Bioresour. Technol.* **89** (2003) 115
6. M. A. Ferro-Garcia. J. Rivera-Utilla, J. Rodriguez-Gordillo, I. Bautista-Toledo, *Carbon* **26** (1988) 363
7. P. R. Norris, D. P. Kelly, *J. General Microbiol.* **99** (1977) 317
8. C. Chen, J. L. Wang, *Appl. Microbiol. Biotechnol.* **74** (1980) 911
9. E. Neiboer, D. H. S. Richardson, *Environ. Pollut. Series B1* **1** (1980) 3
10. C. Chen, J. L. Wang, *J. Hazard. Mater.* **151** (2008) 65
11. J. M. Brady, J. M. Tobin, *Enzyme Microb. Technol.* **17** (1995) 791
12. A. Kogej, A. Parko, *World J. Microbiol. Biotechnol.* **17** (2001) 677

13. J. K. Park, Y. P Jim, H. N. Chang, *Biotechnol. Bioeng.* **63** (1999) 116
14. M. Gopal, K. Pakshirajan, T. Swaminathan, *Appl. Biochem. Biotechnol.* **102**–**103** (2002) 227
15. F. Veglio, F. Beolchini, *Hydrometallurgy* **44** (1997) 301
16. M. Yakup Arica, M. Bayramolu, G. Yılmaz, M. Bekta, G. Genc, *J. Hazard. Mater.* **109** (2004) 191
17. K. Vijayaraghavan, Y. S. Yun, *Biotechnol. Adv.* **26** (2008) 266
18. J. Wang, C. Chen, *Biotechnol. Adv*. **27** (2009) 195
19. J. Wu, H.-Q. Yu, *Bioresour. Technol*. **98** (2007) 253
20. Y. Lu, E. Wilkins, *J. Hazard. Mater.* **49** (1996) 165
21. T. Lebean, D. Bagot, K. Jezequel, B. Fabre, *Sci. Total Environ.* **291** (2002) 78
22. N. Rangsayatorn, P. Pokethitiyook, E. S. Upatham, G. R. Lanza, *Environ. Int.* **33** (2006) 57
23. M. Y Arica, G. Bayramoglu, M. Yilmaz, S. Bekta, Ö. Genc, *J. Hazard. Mater.* **109** (2004) 191
24. Y.-L. Lai, G. Annadurai, F.-C. Huang, J.-F. Lee, *Bioresour. Technol.* **99** (2008) 6480
25. J. L. Wang, C. Chen, *Biotechnol. Adv.* **24** (2006) 427
26. J. Park, S. B. Choi, *Korean J. Chem.* **19** (2002) 68
27. S. Schiewer, E. Fourest, K. H. Chong, B. Volesky, *Biohydrometall. Proc.* **2** (1995) 219
28. M. Zhao, J. R. Duncan, *Biotechnol. Lett.* **19** (1997) 953
29. Y. Göksungur, S. Üren, U. Güvenç, *Bioresour. Technol.* **96** (2005) 103
30. K. K. I. U. Arunakumara, Z. Xuecheng, *J. Ocean Univ. Chin.* **7** (2008) 60
31. P. Vasudevan, V. Padmavathy, S. C. Dhingra, *Bioresour. Technol.* **89** (2003) 281
32. P. Vasudevan, V. Padmavathy, S. C. Dhingra, *J. Sci. Ind. Res.* **65** (2006) 1013
33. C. Namasivayam, D. Sangeetha, *Adsorp. Sci. Technol.* **12** (2006) 103
34. J. Febrianto, A. N. Kosasih, J. Sunarsao, Y. Ja, N. Indraswati, S. Ismadji, *J. Hazard. Mater.* **162** (2009) 616
35. J. L. Wang, C. Chen, *Biotechnol. Adv.* **24** (2006) 427.

Journal of the Serbian Chemical Society
JSCS-info@shd.org.rs • www.shd.org.rs/JSCS
J. Serb. Chem. Soc. *76* (3) 375–384 (2011) UDC 582.752.3+581.45:547.972.2:615.281/.282
JSCS–4125 *Original scientific paper*

Antimicrobial activity screening of isolated flavonoids from *Azadirachta indica* leaves

QUDSIA KANWAL[1], ISHTIAQ HUSSAIN[1,2], HAMID LATIF SIDDIQUI[1] and ARSHAD JAVAID[3]*

[1]*Institute of Chemistry, University of the Punjab, Quaid-e-Azam Campus Lahore-54590,* [2]*University of Sargodha and* [3]*Institute of Mycology and Plant Pathology, University of the Punjab, Quaid-e-Azam Campus Lahore, Pakistan*

(Received 6 April, revised 1 September 2010)

Abstract: The antimicrobial activities of two flavonoids, namely genistein 7-*O*--glucoside (**1**) and (–)-epi-catechin (**2**), isolated from *Azadirachta indica* A. Juss (neem) leaves, were evaluated against five fungal species, *viz*: *Alternaria alternata* (Fr.) Keissler, *Aspergillus fumigatus* Fresenius, *Aspergillus niger* van Tieghem, *Macrophomina phaseolina* (Tassi) Goid. and *Penicillium citrii*, and four bacterial species, *viz*. *Lactobacillus* sp., *Escherichia coli*, *Azospirillium lipoferum* and *Bacillus* sp. Six concentrations, *viz*. 100, 300, 500, 700, 900 and 1000 ppm of each of the two flavonoids were employed using malt extract agar medium. All the concentrations of both the test compounds significantly suppressed fungal as well as bacterial growth. The highest concentration (1000 ppm) of both fractions **1** and **2** reduced the growth of the different test fungal species by 83–99 % and 82–95 %, respectively. Compound **1** was highly effective against *Lactobacillus* sp., against which its various concentrations reduced the bacterial growth by 52–99.8 %. Compound **2** was highly effective against *A. lipoferum* and *Bacillus* sp., resulting in 94–100 % and 73–99% reduction in bacterial growth, respectively.

Keywords: antibacterial; antifungal; *Azadirachta indica*; flavonoids; leaves; neem.

INTRODUCTION

Azadirachta indica, a tree of the family Meliaceae, is known as a versatile source of components with bioactive properties. It has great medicinal importance and its chemical constituents possess anti-inflammatory, anti-oxidant, antipyretic, analgesic, immunostimulant, diuretic, hypoglycaemic, cardiovascular, antimicrobial, antiviral, antimalarial and anthelmintic activities.[1–4] Various types of chemical compounds, such as diterpenoids, triterpenoids, polyphenolics, sul-

* Corresponding author. E-mail: arshadjpk@yahoo.com
doi: 10.2298/JSC100406027K

phurous, and polyacetate derivatives have hitherto been isolated from differrent parts of this tree.[5,6]

Flavonoids are a major class of oxygen-containing heterocyclic natural products that are widespread in green plants.[7] Generally, they are found as plant pigments in a broad range of fruits and vegetables.[8] These are C_{15} compounds composed of two aromatic rings linked through three carbon bridges with a carbonyl function located at one end of the bridge. Flavonoids were recognized to have a protective effect in plants towards microbial invasion by plant pathogens.[9,10] Flavonoid-rich plant extracts have been used for centuries to treat human disease.[11] Isolated flavonoids were shown to possess a host of important biological activities, including antifungal[12,13] and antibacterial activities.[14] The present study was aimed at investigating the antifungal and antibacterial activities of two flavonoids, isolated from *A. indica* leaves.

EXPERIMENTAL

General procedure

All the reagents and the solvents used in the present study were procured from E. Merck Germany, Fluka Switzerland, BDH Chemicals England and Sigma–Aldrich Chemicals Co., USA. All the employed solvents were of analytical grade. For column chromatography, silica gel 60 (Merck 230–400 mesh) and for TLC silica gel 60F254 (Merck,) were used. Melting points were determined by the sealed capillary method with the help of a Gallenkamp melting point apparatus.

The infrared spectra of the flavonoids in the solid state in KBr discs were recorded on FTIR Shimadzu 4200 spectrophotometer. ^{1}H- and ^{13}C-NMR in $CDCl_3$ and D_2O for compounds **1** and **2,** respectively, were recorded on a Bruker 14.1 T NMR spectrometer, operating at a frequency of 600 MHz. DEPT experiments were performed using polarization transfer pulses of 90 and 135°. The EI-MS spectra were measured with a JEOL JMS-AX 505 HAD mass spectrometer at an anionization voltage of 70 eV.

Procurement of microorganisms

Five fungal strains, namely, *Alternaria alternata*, *Aspergillus fumigatus*, *A. niger*, *Macrophomina phaseolina* and *Penicillium citrii*, and four bacterial species, *viz*. *Lactobacillus* sp., *Escherichia coli*, *Azospirillium lipoferum* and *Bacillus* sp. were procured from the Fungal Culture Bank of the Institute of Mycology and Plant Pathology, University of the Punjab, Lahore, Pakistan.

Extraction and isolation

Fresh leaves of *A. indica* (neem) were collected from the University of the Punjab, Quaid-e-Azam Campus, Lahore, Pakistan, washed with distilled water and air-dried. The leaves (500 g) were soaked in CH_3OH (1 L) for 15 min, to remove chlorophyll, and filtered. The leaves were then cut into small pieces, blended with methanol (750 mL), centrifuged at 2000 rpm for 5 min and the supernatant was evaporated under vacuum at 50 °C. The gummy material (50 mL) thus obtained was diluted with water (1:1), whereby precipitation occurred. These precipitates were removed by filtration, purified by preparative TLC (EtOAc:MeOH, 4:1), and recrystallized with $CHCl_3$:MeOH (98:2), to afford compound **1** (175 mg). To the filtrate, *n*-

-butanol was added (1:1) and the butanol extract was purified by silica gel column chromatography using the solvent system MeOH:$CHCl_3$:H_2O (3:1:1) to yield compound **2** (202 mg).

Antifungal bioassay

The antifungal activities of flavonoids **1** and **2** were evaluated by the poisoned medium technique.[15] Two percent malt extract agar medium was prepared by autoclaving at 121 °C for 30 min. Weighed quantities of compounds **1** and **2** (6, 16, 30, 42, 54 and 60 mg) were dissolved in 0.5 mL of sterilized distilled water, and added to flasks containing 59.5 mL of malt extract agar medium, when still molten, to obtain final concentrations of 100, 300, 500, 700, 900 and 1000 ppm, respectively. The control received the same quantity of distilled water. Twenty millilitres of each medium was poured in each 90 mm-diameter sterilized Petri dishes and the medium was allowed to solidify. Mycelia discs of 5 mm-diameter were prepared from the tips of 5–7 day-old cultures of the five test fungal species with the help of a sterilized cork borer and placed in the centre of each Petri plate. Each treatment was replicated three times. The plates were incubated at 25±2 °C for 7 days. Fungal growth was measured by averaging the three diameters taken at right angles for each colony.

Antibacterial bioassay

The antibacterial activities of the isolated flavonoids were assessed following the produced of Kanwal *et al.*[16] LBA broth medium was autoclaved at 121 °C and cooled to room temperature. Ten millilitres of LBA broth was added to 20 mL culture tubes. To achieve final concentrations of 100, 300, 500, 700, 900 and 1000 ppm, 1, 3, 5, 7, 9 and 10 mg, respectively, of the two flavonoids were added to the LBA broth medium in the culture tubes. The control did not receive the flavonoid solutions. One drop of suspension of each bacterial species was added to each culture tubes. Each treatment was replicated three times. The tubes were incubated at 37 °C for 24 h. Subsequently, the optical density of each suspension was recorded at 630 nm using a spectrophotometer. The greater the optical density of the suspension, the lower was the activity of the compound.

Statistical analysis

All the data were analyzed by analysis of the variance followed by the Duncan multiple range test ($P \leq 0.05$) to separate the treatment means.[17]

RESULTS AND DISCUSSION

Identification of the isolated compounds

*Compound **1***. Greenish powder; m.p. 165–167 °C (decomposed, uncorrected); IR (KBr, cm^{-1}): 3310, 2970, 2940, 1670, 1650, 1620, 1600, 1450, 1300, 1270, 880. ^{1}H-NMR (600 MHz, $CDCl_3$, δ / ppm): 8.12, (1H, *s*, H-2), 6.64 (1H, *d*, *J* = 2.2 Hz, H-6), 6.44 (1H, *d*, *J* = 2.2 Hz, H-8), 7.43 (1H, *dd*, *J* = 8.6 Hz, 2.6 Hz, H-2'), 6.91 (1H, *dd*, *J* = 8.3 Hz, 2.6 Hz, H-3', H-5'), 7.37 (1H, *dd*, *J* = 8.3 Hz, 2.6 Hz, H-6'), 5.00 (1H, d, *J* = 7.5 Hz, H-1"), 3.42–3.55 (2H, *m*, H-2", H-5"), 3.93 (1H, *dd*, *J* = 2.2 Hz, 12.0 Hz, H-6a"), 3.73 (1H, *dd*, *J* = 5.0 Hz, 2.2 Hz, H-6b"). ^{13}C-NMR (150 MHz, $CDCl_3$, δ / ppm): 154.8 (C-2), 122.6 (C-3), 180.3 C-4), 161.5 (C-5), 99.4 (C-6), 162.6 (C-7), 94.5 (C-8), 157.1 (C-9), 106.1 (C-10), 132.0 (C-1'), 130.1 (C-2', C-6'), 115.6 (C-3', C-5'), 162.3 (C-4'), 100.3 (C-1"),

73.4 (C-2”), 76.6 (C-3”), 69.4 (C-4”), 77.2 (C-5”), 60.7 (C-6”). EI-MS (*m*/*z*): 352 (M^+), 305, 245, 184, 170, 153, 125, 97, 108, 107. UV(MeOH, λ_{max} / nm): 270, 221.

*Compound **2***. Off-white powder, m.p. 241–245 °C (uncorrected). IR (KBr, cm^{-1}): 3331, 2923, 1650 1240, 1070, 880. ^{1}H-NMR: (600 MHz, CD_3OD, δ / / ppm): 4.87 (1H, *d*, *J* = 2.4 Hz, H-2), 3.98 (1H, *m*, H-3), 2.85 (1H, *dd*, *J* = 5.4 Hz, 16.2 Hz, H-4α), 2.51 (1H, *dd*, *J* = 4.2 Hz, 16.2 Hz, H-4β), 5.88 (1H, *d*, *J* = = 2.1 Hz, H-8), 6.03 (1H, *d*, *J* = 2.1 Hz, H-6), 6.89 (1H, *d*, *J* = 1.7 Hz, H-2’), 6.77 (1H, *d*, *J* = 7.4 Hz, H-5’), 6.73 (1H, *dd*, *J* = 7.4 Hz, 1.7 Hz, H-6’). ^{13}C-NMR (150 Hz, CD_3OD, δ / ppm): 74.8 (C-2), 71.8 (C-3), 31.4 (C-4), 160.1 (C-5), 96.8 (C-6), 156.1 (C-7), 96.5 (C-8), 155.3 (C-9), 104.0 (C-10), 132.1 (C-1’), 110.1 (C--2’), 145.5 (C-3’) 146.4 (C-4’), 116.0 (C-5’) 115.2 (C-6’). EI-MS (*m*/*z*): 290 (M^+), 245, 227, 170, 153, 126. UV (MeOH, λ_{max} / nm): 280, 212. $[\alpha]^{25}$: 14.9°.

The molecular formula of compound **1** was deduced from elemental analysis results and the EI-MS mass spectrum, which exhibited a (M^+) at *m*/*z* 352. Bands at 3310 (OH), 1670 (C=O) and 1650 and 1600 cm^{-1} (phenyl group) were observed in the IR spectrum. The ^{1}H-NMR spectrum showed a singlet at δ 8.12 ppm (H-2) and δ 154.8 ppm (C-2) characteristic for the isoflavone skeleton.[18] This was further supported by the UV spectrum with λ_{max} at 270 nm. The ^{1}H--NMR data indicated doublets of doublets (*J* = 8.6 and 2.6 Hz) at 7.43 (H-2’), 6.91 (H-3’ and H-5’) and 7.37 (H-6’), showing the presence of 4’–OH on ring B of the isoflavonoid. The OH at C-7 was not free as UV with NaOAc failed to produce any bathochromic shift.[19] The proton NMR resonance of an anomeric carbon at 5.00 (1H, *d*, *J* = 7.5 Hz, H-1”) suggests the glucose moiety is in the β-configuration. The ^{13}C-NMR upfield signals of C-8 and C-6 and the downfield resonance of C-7 indicate that the glucose moiety was attached to that of C-7. These data suggested compound **1** was (genistein 7-*O*-glucoside). This compound was previously isolated from *Trifolium subterraneum* with a feeding deterrent activity for red-legged earth mite (*Halotydeus destructor*).[20]

Compound **2** was positive to butanol/HCl and vanillin/HCl reagents. The UV spectrum (MeOH) showed absorbance maxima at 280 and 212 nm. Its EI-MS *m*/*z* of 313 $(Na+M)^+$ indicated a monomeric unit of *m*/*z* of 290. Bands at 3331, 2923 and 1650 cm^{-1} were observed in the IR spectrum. The ^{1}H-NMR data suggested that the compound was epicatechin, which was further supported by ^{13}C-NMR signals, especially at 74.8 (C-2) and 71.8 (C-3).[21] This compound was previously isolated from *Adansonia digitata*.[22]

Antifungal activity

Analysis of the variance showed that there was a highly significant difference ($P \leq 0.001$) in the antifungal activity of the two tested flavonoids (*F*). Similarly, the effect of concentration (*c*) as well as the response of various fungal

species (*S*) was also significant. The interactive effects of *F*×*S*, *F*×*c*, *S*×*c* and *F*×*S*×*c* were also significant (Table I).

TABLE I. Analysis of variance for the effect of different concentrations of two flavonoids isolated from neem, against different fungal species

Sources of variation	*df*	*SS*	*MS*	*F* values[a]
Treatments	69	128318	1860	529
Flavonoids (*F*)	1	203	203	58
Fungal species (*S*)	4	3273	818	233
Conc. (*c*)	6	122594	20432	5816
F×*S*	4	659	165	47
F×*c*	6	107	17.9	5
S×*c*	24	862	35.9	10
F×*S*×*c*	24	621	25.9	7
Error	139	492	3.5	–
Total	209	128809	–	–

[a]Significant at $P \leq 0.001$

In general, at all the tested concentrations, both flavonoids significantly reduced the growth of all the five test fungal species. There was a gradual reduction in fungal colony diameter as the concentration of the compounds was increased from 100 to 1000 ppm. Compound **1** was most effective against *A. fumigatus*, where the highest tested concentration of this compound significantly reduced the fungal colony diameter by 95 %. The highest concentration of this compound also resulted in a 91, 85, 82 and 94 % reduction of the colony diameter of *A. alternata*, *A. niger*, *M. phaseolina* and *P. citrii*, respectively (Fig. 1). Compound **2** was highly effective against *P. citrii*, *A. alternata* and *A. fumigatus*, where its highest concentration resulted in significant reductions of 94, 90 and 95 % in the fungal colony diameters, respectively. *A. niger* and *M. phaseolina* were found comparatively less susceptible to **2**, where the highest tested concentration of this compound resulted in only a 78 and 80 % suppression of the colony diameters, respectively.

Antibacterial activity

Analysis of variance showed that there was a highly significant difference ($P \leq 0.001$) in the antibacterial activities of the two tested flavonoids (*F*). Similarly, the effects of concentration (*c*) as well as the response of the various bacterial species (*B*) were also significant. The interactive effects of *F*×*B*, *F*×*c*, *B*×*c* and *F*×*B*×*c* were also significant (Table II).

In general, all the tested concentrations of both isolated flavonoids significantly suppressed the growth of all the four-targeted bacterial species. However, the activities of the two flavonoids varied with the bacterial species involved (Fig. 2).

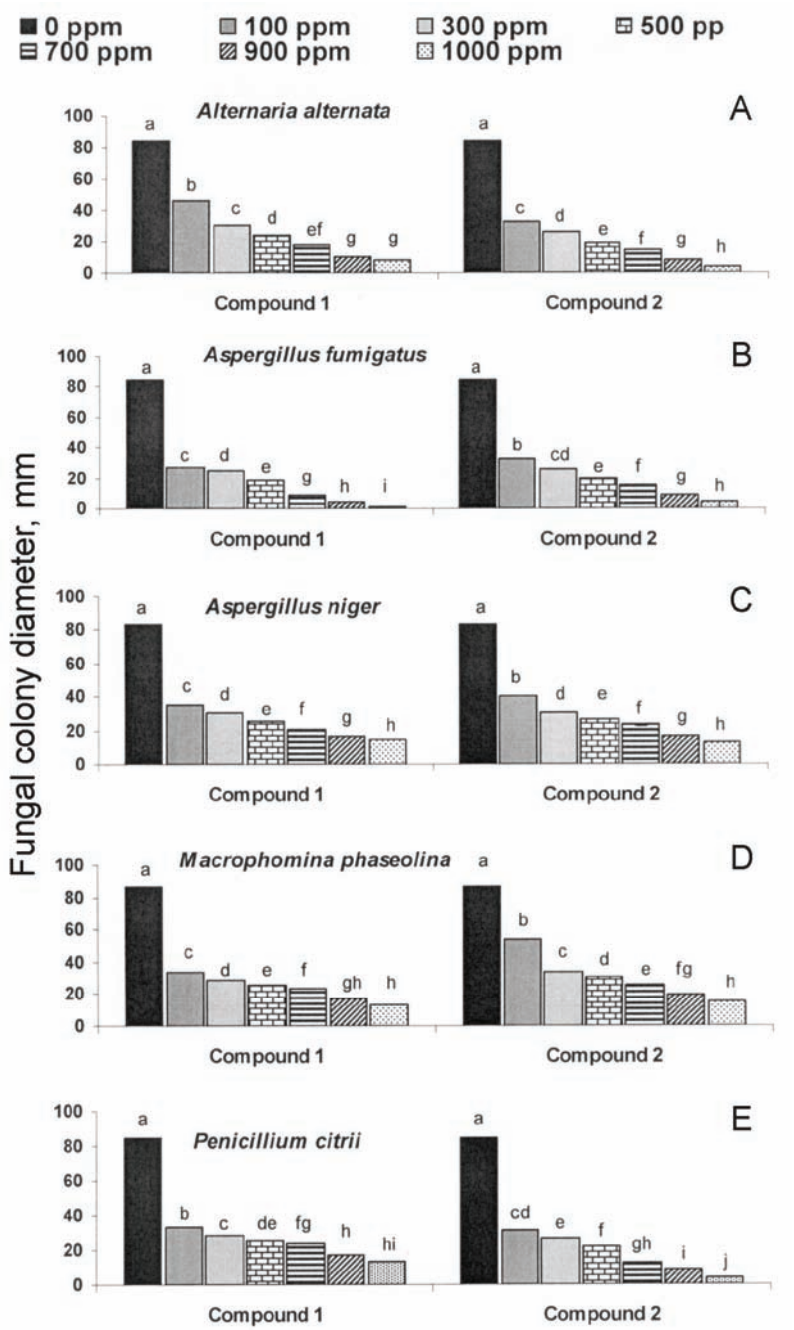

Fig. 1. Effect of different concentrations of the two flavonoids on the *in vitro* growth of fungi. Bars with different letters show significant difference ($P \leq 0.05$), as determined by the Duncan multiple range test. Compound **1**: genistein 7-*O*-glucoside, compound **2**: (–)-epi-catechin.

TABLE II. Analysis of variance for the effect of different concentrations of two flavonoids isolated from neem, against four bacterial species

Sources of variation	*df*	*SS*	*MS*	*F* values[a]
Treatments	55	52	0.93	4627
Flavonoids (*F*)	1	1.88	1.87	9256
Bacterial species (*B*)	3	5.35	1.78	8802
Conc. (*c*)	6	38.43	6.40	31593
F×*B*	3	2.85	0.95	4694
F×*c*	6	1.14	0.19	940
B×*c*	18	0.74	0.04	202
F×*B*×*c*	18	1.21	0.067	330
Error	112	0.023	0.0002	–
Total	167	52	–	–

[a]Significant at $P \leq 0.001$

Compound **1** was highly effective against *Lactobacillus* sp., where its various concentrations (100–1000 ppm) reduced the bacterial growth by 52–99.8 % (Fig. 2A). This compound was comparatively less effective against the other bacterial species, resulting in 40–92 %, 31–95 % and 39–91 % reduction in the growth of *E. coli*, *A. lipoferum* and *Bacillus* sp., respectively (Figs. 2B–2D). Compound **2** exhibited comparatively higher antibacterial activities compared to those of compound **1**. *A. lipoferum* was the bacterial species most susceptible to compound **2**, where 900 and 1000 ppm completely arrested bacterial growth (Fig. 2C). This compound was also highly toxic to *Bacillus* sp., where its different concentrations suppressed bacterial growth by 73–99% (Fig. 2D). Compound **2** was found to be comparatively less effective against *Lactobacillus* sp. and *E. coli*, where it suppressed bacterial growth by 59–96 % and 45–83 %, respectively (Figs. 2A and 2B). Recently, similar antibacterial activities were reported for other flavonoids isolated from different plant species.[14,23,24] Reports of activity in the field of antibacterial flavonoid research are widely conflicting, probably owing to inter- and intra-assay variation in the susceptibility testing.[11] Various antibacterial mechanisms of action of different flavonoids have were proposed, including inhibition of nucleic acid synthesis,[25] inhibition of cytoplasmic membrane function,[26] and inhibition of energy metabolism.[27]

From the results of the present study, it can be concluded that both the tested neem flavonoids possess antifungal as well as antibacterial activities. The antimicrobial activities of these natural compounds may be further enhanced by some structural modifications to use these compounds as commercial pesticides, especially against *M. phaseolina*. This soil-borne phytopathogenic fungal species attacks about 400 plant species, including such crops as soybean, sunflower, maize and sorghum,[28] but there are no registered fungicides to control it.

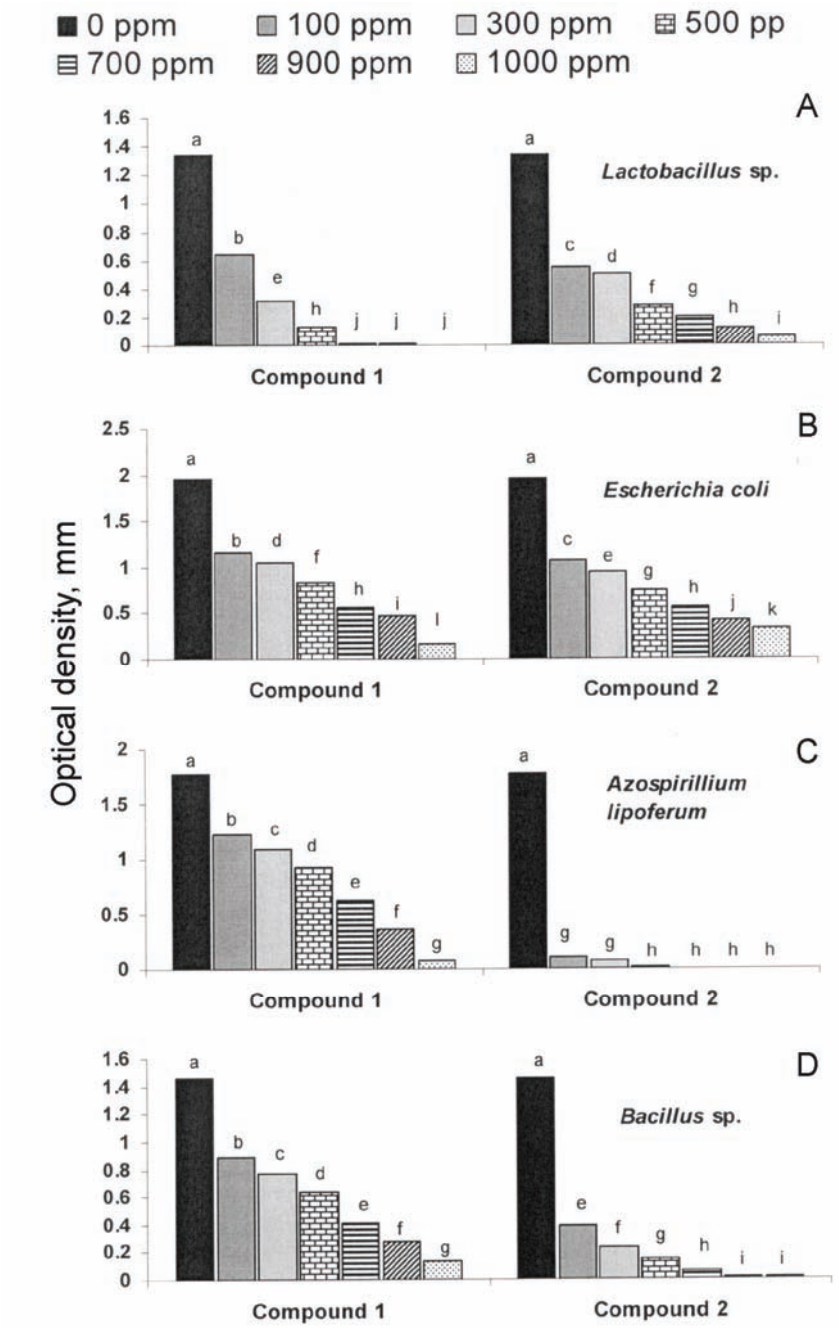

Fig. 2. Effect of different concentrations of two flavonoids on the *in vitro* growth of bacteria. Bars with different letters show significant difference ($P \leq 0.05$) as determined by the Duncan multiple range test. Compound **1**: genistein 7-*O*-glucoside; Compound **2**: (–)-epi-catechin.

ИЗВОД

АНТИМИКРОБНА АКТИВНОСТ ФЛАВОНОИДА ИЗОЛОВАНИХ ИЗ ЛИШЋА *Azadirachta indica*

QUDSIA KANWAL[1], ISHTIAQ HUSSAIN[1,2], HAMID LATIF SIDDIQUI[1] и ARSHAD JAVAID[3]

[1]*Institute of Chemistry, University of the Punjab, Quaid-e-Azam Campus Lahore-54590,* [2]*University of Sargodha u* [3]*Institute of Mycology and Plant Pathology, University of the Punjab, Quaid-e-Azam Campus Lahore, Pakistan*

Антимикробна активност два флавоноида, генистеин-7-*O*-глукозида (**1**) и (–)-епи-катехина (**2**), изолованих из лишћа *Azadirachta indica* A. Juss тестирана је спрам пет врста гљива: *Alternaria alternata* (Fr.) Keissler, *Aspergillus fumigatus* Fresenius, *Aspergillus niger* van Tieghem, *Macrophomina phaseolina* (Tassi) Goid. и *Penicillium citrii*, и четири врсте бактерија: *Lactobacillus* sp., *Escherichia coli*, *Azospirillium lipoferum* и *Bacillus* sp. Коришћене су следеће концентрације сваког од флавоноида у подлози хранљивог агара: 100, 300, 500, 700, 900 и 1000 ppm. Оба флавоноида, у свим примењеним концентрацијама, су значајно инхибирала раст гљива и бактерија. Највећа концентрација (1000 ppm) једињења **1** и **2** смањила је раст различитих врста гљива за 83–99 %, односно 82–95 %. Једињење **1** је врло ефикасно смањило раст бактерија *Lactobacillus* sp. за 52–100 %, у зависности од конецентарције. Једињење **2** је било ефикасно спрам бактерија *A. lipoferum* и *Bacillus* sp., смањујући њихов раст за 94–100 %, односно 73–99 %.

(Примљено 6. априла, ревидирано 1. септембра 2010)

REFERENCES

1. A. C. S. Chagas, L. S. Vieira, A. R. Freitas, M. R. A. Araújo, J. A. Araújo-Filho, W. R. Araguão, A. M. C. Navarro, *Vet. Parasitol.* **15** (2008) 68
2. P. Manikandan, V. Letchoumy, P. Gopalakrishnan, S. Nagini, *Food Chem. Toxicol.* **46** (2008) 2332
3. A. K. Mukherjee, R. Doley, D. Saikia, *Toxicon.* **51** (2008) 1548
4. P. Thakurta, P. Bhowmik, S. Mukherjee, T. K. Hajra, A. Patra, P. K. Bag, *J. Ethnopharmacol.* **111** (2007) 607
5. N. S. Randhawa, B. S. Parmar, *Neem Research and Development*, Society of Pesticide Science, New Delhi, 1993, p. 63
6. G. Prakash, A. K. Srivastava, *Biochem. Eng. J.* **29** (2006) 62
7. B. A. Bohm, *Introduction to Flavonoids*, Gordon & Breach, Amsterdam, 1998
8. J. A. Joule, G. F. Smith, *Heterocyclic Chemistry*, Van Nostrand Reinhold Company, London, 1972
9. J. B. Harborne, C. A. Williams *Phytochemistry* **55** (2000) 481
10. D. Treutter, *Environ. Chem. Lett.* **4** (2006) 147
11. T. P. T. Cushnie, A. J. Lamb, *Int. J. Antimicrob. Agents* **26** (2005) 343
12. B. Sathiamoorthy, P. Gupta, M. Kumar, A. K. Chaturvedi, P. K. Shukla, R. Maurya, *Bioorg. Med. Chem. Lett.* **17** (2007) 239
13. F. Galeotti, E. Barile, P. Curir, M. Dolci, V. Lanzotti, *Phytochem. Lett.* **1** (2008) 44
14. R. Alarcón, R. C. Flores, S. Ocampos, A. Lucatti, L. F. Galleguillo, C. Tonn, V. Sosa, *Planta Med.* **74** (2008) 1463
15. R. K. Grover, J. D. Moore, *Phytopathology* **52** (1962) 876
16. Q. Kanwal, I. Hussain, H. L. Siddiqui, A. Javaid, *J. Serb. Chem. Soc.* **74** (2009) 1389

17. R. G. D. Steel, J. H. Torrie, *Principles and Procedures of Statistics*. McGraw Hill Book Co. Inc., New York, 1980
18. J. Wandji, Z. T. Fomum, F. Tillequin, E. Seguim, M. Kock, *Phytochemistry* **35** (1994) 245
19. S. El-Masry, M. E. Amer, M. S. Abdel-Kader, H. H. Zaatout, *Phytochemistry* **60** (2002) 783
20. S. F. Wang, T. J. Smith, E. L. Ghisalberti *J. Chem. Ecol.* **24** (1998) 2089
21. L. J. Porter, R. H. Newman, L. Y. Foo, H. Wong, *J. Chem. Soc. Perkin Trans. 1* (1982) 1217
22. A. A. Shahat, *Pharm. Biol.* **44** (2006) 445
23. Y. C. Wang, H. W. Hsu, W. L. Liao, *LWT – Food Sci. Technol*. **41** (2008) 1793
24. L. Zhou, D. Li, J. Wang, Y. Liu, J. Wu, *Nat. Prod. Res.* **21** (2007) 283
25. A. Mori, C. Nishino, N. Enoki, S. Tawata, *Phytochemistry* **26** (1987) 2231
26. H. Tsuchiya, M. Iinuma, *Phytomedicine* **7** (2000) 161
27. H. Haraguchi, K. Tanimoto, Y. Tamura, K. Mizutani, T. Kinoshita, *Phytochemistry* **48** (1998) 125
28. K. Das, B. Fakrudin, D. K. Arora, *Microbiol. Res.* **163** (2008) 215.

Journal of the Serbian Chemical Society
JSCS-info@shd.org.rs • www.shd.org.rs/JSCS
J. Serb. Chem. Soc. 76 (3) 385–393 (2011)
JSCS–4126
UDC 542.913+546.732'742'562'472:547.756:547.553
Original scientific paper

Synthesis and characterization of divalent metal complexes of the macrocyclic ligand derived from isatin and 1,2-diaminobenzene

DHARAM PAL SINGH[1]*, VIDHI GROVER[1], KRISHAN KUMAR[2] and KIRAN JAIN[3]

[1]*Department of Chemistry, National Institute of Technology, Kurukshetra-136 119,* [2]*Department of Applied Sciences and Humanities, Gurgaon College of Engineering, Bilaspur-Tauru Road, Gurgaon-122 413 and* [3]*Department of Chemistry, M.L.N. College, Yamuna Nagar, India*

(Received 7 June, revised 23 September 2010)

Abstract: A novel series of complexes of the type $[M(C_{28}H_{18}N_6)X_2]$, where M=Co(II), Ni(II), Cu(II) or Zn(II) and X = Cl^-, NO_3^- or CH_3COO^-, were synthesized by template condensation of isatin and 1,2-diaminobenzene in methanolic medium. The complexes were characterized with the help of various physico–chemical techniques, such as elemental analyses, molar conductance measurements, magnetic measurements, and NMR, infrared and far infrared spectral studies. The low value of molar conductance indicates them to be non-electrolytes. Based on various studies, a distorted octahedral geometry may be proposed for all the complexes. All the synthesized macrocyclic complexes were also tested for their *in vitro* antibacterial activity against some pathogenic bacterial strains. The *MIC* values shown by the complexes against these bacterial strains were compared with those of the standard antibiotics linezolid and cefaclor. Some of the complexes showed good antibacterial activities.

Keywords: macrocyclic ligands; infrared; magnetic measurements; divalent metal complexes; antibacterial.

INTRODUCTION

The chemistry of macrocyclic complexes has received much attention in recent years[1] due to their potential applications and importance in the area of coordination chemistry.[2,3] Thus, the study of macrocyclic complexes is becoming a growing class of research.[4] Macrocycles are best prepared by the aid of metal ions as templates to direct the condensation reaction towards ring closure.[5] Transition metal complexes of nitrogen donor ligands have been studied in detail on account of their stereochemistry and wide practical utility.[6] A number of nit-

* Corresponding author. E-mails: dpsinghchem@gmail.com; krishandhaka2005@gmail.com
doi: 10.2298/JSC100607034S

rogen donor macrocyclic derivatives have long been used in analytical, industrial and medical applications.[7] Nitrogen-containing macrocycles have a strong tendency to form stable complexes with transition metals.[8] Some macrocyclic complexes have been reported to exhibit potent antibacterial, antifungal and anti-HIV activities.[9–11] Macrocyclic nickel complexes find use in DNA recognition and oxidation[12] while macrocyclic copper complexes are employed in DNA binding and cleavage.[13] Schiff bases obtained by the condensation of aromatic amines with isatin are powerful anticonvulsant, antiviral, antibacterial and antifungal agents.[14,15] Cu(II) complexes with isatin Schiff base ligands are potential antitumour agents.[16] In a previous work, macrocyclic complexes derived from isatin and ethylenediamine were reported.[17] Based on the above-mentioned studies, in the present paper, macrocyclic complexes of Co(II), Ni(II), Cu(II) and Zn(II) derived from isatin and 1,2-diaminobenzene (*o*-phenylenediamine) are reported. The complexes were characterized by various physico-chemical techniques, such as IR and NMR spectroscopy, magnetic susceptibilities, elemental analyses, and conductance.

EXPERIMENTAL

Isolation of the complexes

All the chemicals used were of AnalR Grade. All the employed solvents were of high purity. Moisture was excluded from the glass apparatus using $CaCl_2$ tubes.

All the complexes were obtained by template synthesis since any attempt to isolate the free macrocyclic ligand was unsuccessful. To a hot, well-stirred methanolic solution (≈40 cm^3) of 1,2-diaminobenzene (10 mmol), divalent cobalt, nickel, copper or zinc salts (hydrated) (5 mmol) (Cl^-, NO_3^-, CH_3COO^-) dissolved in the minimum quantity of methanol were added. The resulting solution was refluxed for 0.5 h. Subsequently, isatin (10 mmol) dissolved in ≈20 cm^3 methanol was added to the refluxing mixture and refluxing was continued for 6–8 h. The mixture was concentrated to half its volume, cooled to room temperature and kept in a desiccator overnight. After overnight standing, dark coloured precipitates separate out, which were filtered, then washed with methanol, acetone, and ether and dried *in vacuo*. The obtained yields were 41–48 %.

The template condensation of isatin and 1,2-diaminobenzene in the presence of divalent metal salts, in the molar ratio 2:2:1 is shown in Scheme I.

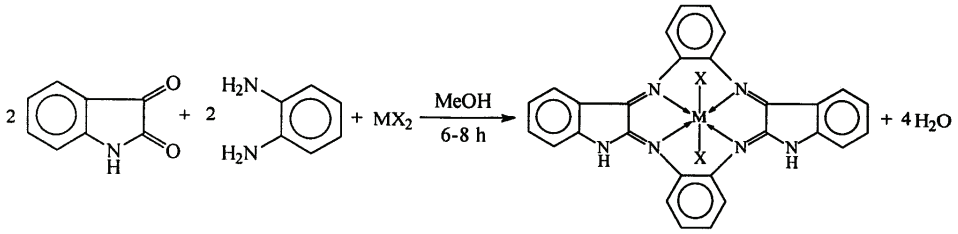

Scheme 1. Proposed structure of the synthesized complexes, where M = Co(II), Ni(II), Cu(II) or Zn(II) and X = Cl^-, NO_3^- or CH_3COO^-.

Analytical and physical measurements

The microanalyses of C, H and N were performed at the Sophisticated Analytical Instrument Facility (SAIF), CDRI, Lucknow. The melting points were determined using capillaries in an electrical M.P. apparatus. The metal contents were determined by standard EDTA methods. The electronic spectra (DMF) were recorded on a Cary 14 spectrophotometer. The magnetic susceptibility measurements were performed on a vibrating sample magnetometer at the SAIF, IIT Roorkee. The IR spectra were recorded on an FTIR spectrophotometer, Parkin Elmer, in the range 4000–200 cm^{-1} using Nujol Mull/KBr pellets. The NMR spectra were recorded on Bruker NMR spectrometer (300 MHz). The conductivity was measured on a digital conductivity meter (HPG System, G-3001).

Antibacterial activity

All synthesized macrocyclic complexes were tested for their *in vitro* antibacterial activity against some bacterial strains using the spot-on-lawn method on Muller Hinton Agar (MHA) medium.[18]

Five test pathogenic bacterial strains, *viz. Staphylococcus aureus*, *Bacillus pumilus*, *Bacillus megaterium* and *Staphylococcus epidermidis* (Gram-positive), *Pseudomonas aeruginosa* (Gram-negative) were considered for the determination of the minimum inhibitory concentration (*MIC*) value of selected complexes. The *MIC* is the lowest concentration of an antimicrobial agent that prevents viable growth of microorganisms after overnight incubation. The turbidity of all the bacterial cultures was adjusted to 0.5 McFarland by preparing bacterial suspension of 4–6 well-isolated colonies of the same morphological type selected from a soybean casein digest agar (SCDA) plate. In this method, the test concentrations of the synthesized complexes were made from 128 to 0.25 μg cm^{-3} (4 mg cm^{-3} of DMSO) in sterile tubes No. 1––10. SCDA medium was prepared and 100 μl of the sterile SCDA was poured into each sterile tube followed by the addition of 200 μl of the complex in tube 1. Two-fold serial dilutions were performed from tube 1–10 and the excess SCDA (100 μl) was discarded from the last tube No. 10. To each tube, 100 μl of standard inoculum was added. All the tubes were incubated for 24 h at 37 °C. Dilutions of standard antibiotics (linelozid and cefaclor) were prepared in the same manner for comparison. DMSO, the solvent, was used as a negative control.

RESULTS AND DISCUSSION

The complexes were soluble in DMF and DMSO but were insoluble in common organic solvents and water. All complexes were thermally stable up to 255 °C. Conductivity measurements in DMSO indicated them to be non-electrolyte (10 S cm^2 mol^{-1}).[19] The tests for the anions were positive only after decomposition of the complexes, indicating their presence inside the coordination sphere. The analytical data of the reported complexes are as follows:

$Co(C_{28}H_{18}N_6)Cl_2$ ***(1)***. Yield: 48.70 %; F.W.: 567.9; Anal. Calcd.: C, 59.16; H, 3.16; N, 14.79; Co, 10.37 %. Found: C, 59.09; H, 3.10; N, 14.71; Co, 10.21 %.

$Co(C_{28}H_{18}N_6)(CH_3COO)_2$ ***(2)***. Yield: 42.15 %: F.W.: 614.9; Anal. Calcd.: C, 62.45; H 3.90; 13.66; Co, 9.58 %. Found: C, 62.36; H, 3.81; N, 13.58; Co, 9.43 %.

$Ni(C_{28}H_{18}N_6)Cl_2$ ***(3)***. Yield: 43.12 %; F.W.: 567.7; Anal. Calcd.: C, 59.19; H, 3.17; N, 14.79; Ni, 10.34 %. Found: C, 59.11; H, 3.09; N, 14.66; Ni, 10.23 %.

Ni($C_{28}H_{18}N_6$)(NO_3)$_2$ ***(4)***. Yield: 43.89 %; F.W.: 620.7; Anal. Calcd.: C, 54.13; H, 2.93; %: N, 18.04; Ni, 9.46 %. Found: C, 54.02; H, 2.87; N, 17.98; Ni, 9.29.

Ni($C_{28}H_{18}N_6$)(CH_3COO)$_2$ ***(5)***. Yield: 41.50 %; F.W.: 614.7; Anal. Calcd.: C, 62.47; H, 3.90; N, 13.67; Ni, 9.55 %. Found: C, 62.35; H, 3.81; N, 13.59; Ni, 9.34 %.

Cu($C_{28}H_{18}N_6$)Cl_2 ***(6)***. Yield: 46.95 %; F.W.: 572.5; Anal. Calcd.: C, 58.69; H, 3.14; N, 14.67; Cu, 11.09 %. Found: C, 58.54; H, 3.07; N, 14.58; Cu, 10.89 %.

Cu($C_{28}H_{18}N_6$)(NO_3)$_2$ ***(7)***. Yield: 42.46 %; F.W.: 625.5; Anal. Calcd.: C, 53.72; H, 2.88; N, 17.91; Cu, 10.15 %. Found: C, 53.63; H, 2.82; N, 17.85; Cu, 9.92 %.

Cu($C_{28}H_{18}N_6$)(CH_3COO)$_2$ ***(8)***. Yield: 45.59 %; F.W.: 619.5; Anal. Calcd.: C, 61.99; H, 3.87; N, 13.56; Cu, 10.25 %. Found: C, 61.82; H, 3.80; N, 13.46; Cu, 10.12 %.

Zn($C_{28}H_{18}N_6$)(CH_3COO)$_2$ ***(9)***. Yield: 42.64 %; F.W.: 621.0; Anal. Calcd.: C, 61.84; H, 3.86; N, 13.53; Zn, 10.47 %. Found: C, 61.79; H, 3.76; N, 13.44; Zn, 10.27 %.

IR spectra

The presence of a single medium band in the region ≈3265–3350 cm^{-1} in all the complexes may be assigned to N–H stretching vibrations (Table I).[20] It was noted that a pair of bands corresponding to ν(NH_2) stretching vibrations appeared at 3210–3435 cm^{-1} in the IR spectrum of 1,2-diaminobenzene but was absent in the IR spectra of all the metal complexes. Furthermore, no strong absorption band was observed in the spectra of the complexes near 1700 cm^{-1}, indicating the absence of the >C=O group of isatin and thus confirming the condensation of the carbonyl group of isatin and the amino group of 1,2-diaminobenzene.[21,22] A strong absorption band in the region 1595–1625 cm^{-1} may be assigned to C=N stretching vibrations.[5,23] These results provide strong evidence for the formation of the macrocyclic frame.[24] The lower values of ν(C=N) may be explained based on a drift of the lone pair electron density of the azomethine nitrogen towards the central metal atom.[22,25] Another set of medium intensity bands in the region 1500–1585 cm^{-1} were attributed to ν(C=C) aromatic stretching vibrations of the phenyl groups and the bands around 845–875 cm^{-1} may be assigned to C–H out--of-plane bending vibrations of the phenyl groups. The C–N stretching vibrations may occur in the range 1015–1355 cm^{-1}.

The far IR spectra of the complexes showed bands in the region 422–435 cm^{-1} corresponding to ν(M–N) stretching vibrations,[26,27] which give insight into the coordination of the azomethine nitrogen to the central metal atom.[28] The bands present at 315–330 cm^{-1} in the chloro compounds were assigned to ν(M–Cl)

stretching vibrations.[3,26] The bands present at 210–245 cm^{-1} in all nitrate and acetate complexes may be assigned to ν(M–O) stretching vibrations (Table I).[26]

Table I. Infrared spectral data, ν / cm^{-1}, of the divalent Co, Ni, Cu and Zn complexes derived from isatin and 1,2-diaminobenzene

Cmpd.	Complex	N–H	C=N	C=C	C–N	M–N	M–Cl	M–O
1	$[Co(C_{28}H_{18}N_6)Cl_2]$	3270	1605	1500–1580	1230	425	320	–
2	$[Co(C_{28}H_{18}N_6)(CH_3COO)_2]$	3265	1599	1502–1580	1245	422	–	238
3	$[Ni\ (C_{28}H_{18}N_6)Cl_2]$	3320	1623	1500–1585	1268	455	330	–
4	$[Ni(C_{28}H_{18}N_6)(NO3)_2]$	3345	1625	1502–1584	1136	456	–	210
5	$[Ni(C_{28}H_{18}N_6)(CH_3COO)_2]$	3318	1598	1502–1575	1015	460	–	245
6	$[Cu(C_{28}H_{18}N_6)Cl_2]$	3299	1595	1510–1570	1333	453	311	–
7	$[Cu(C_{28}H_{18}N_6)(NO_3)_2]$	3289	1625	1502–1580	1299	428	–	220
8	$[Cu(C_{28}H_{18}N_6)(CH_3COO)_2]$	3336	1610	1502–1575	1355	432	–	235
9	$[Zn(C_{28}H_{18}N_6)(CH_3COO)_2]$	3350	1622	1502–1575	1256	445	–	228

NMR Spectra

The ^{1}H-NMR spectrum of the zinc(II) complex showed a broad signal at 10.8 ppm, which may be assigned to the NH protons of the isatin moiety.[29,30] The multiplets observed in the region 6.65–7.88 ppm may be assigned to the aromatic ring protons of isatin and the *o*-phenylene moiety.[31]

Magnetic measurements and electronic spectra

Cobalt complexes. The magnetic moments of the cobalt(II) complexes were measured at room temperature and were found in the range 4.92–4.96 μ_B, which is consistent with three unpaired electrons. The solution spectra of the cobalt(II) complexes exhibited absorptions in the regions 8185–9100cm^{-1} (ν_1), ≈12650–15750 cm^{-1}(ν_2) and 18,720–20,250 cm^{-1}(ν_3). The spectra resemble to those reported for distorted octahedral cobalt(II) complexes.[32] The various bands may be assigned to $^4T_{1g} \rightarrow {}^4T_{2g}$(F), ($\nu_1$); $^4T_{1g} \rightarrow {}^4A_{2g}$(F) ($\nu_2$) and $^4T_{1g} \rightarrow {}^4T_{1g}$(P) ($\nu_3$). The assignment of the first spin-allowed band seems plausible since the first band appears at approximately half the energy of the visible band.[33]

Nickel complexes. The magnetic moments of nickel(II) complexes were measured at room temperature and were found in the range 2.96–2.99 μ_B, consistent with two unpaired electrons in the nickel(II) ion. The solution spectra of the Ni(II) complexes exhibit a well discernable band with a shoulder on the low energy side. Two other bands, generally observed in the region 16650–17020 cm^{-1} (ν_2), and 27800–28260 cm^{-1} (ν_3), were assigned to $^3A_{2g} \rightarrow {}^3T_{1g}$(F), and $^3A_{2g} \rightarrow {}^3T_{1g}$(P), respectively. The first two bands, resulting from the splitting of the ν_1 band, were in the range 9700–10280 and 11750–12280 cm^{-1} and may be assigned to $^3B_{1g} \rightarrow {}^3E_g$ and $^3B_{1g} \rightarrow {}^3B_{2g}$.[33] The intense higher energy band at 34480 cm^{-1} may be due to a π–π* transition of the (C=N) group. The various

bands do not follow any regular pattern and seem to be anion independent. The spectra suggest a distorted octahedral nature for these complexes.

Copper complexes. The magnetic moments of copper complexes were found in the range 1.76–1.82 μ_B, corresponding to one unpaired electron in the copper(II) ion. The absorption spectra of the copper complexes exhibited bands in the region 17700–19630 cm^{-1} with a shoulder on the low energy side at 14550––16320 cm^{-1}, which showed that these complexes were distorted octahedral.[32,33] Assuming tetragonal distortion in the molecule, the d-orbital energy level sequence for these complexes may be represented as: $x^2–y^2 > z^2 > xy > xz > yz$ and the shoulder may be assigned to: $z^2 \rightarrow x^2–y^2$ ($^2B_{1g} \rightarrow {}^2B_{2g}$) and the broad band contains both the $xy \rightarrow x^2–y^2$ ($^2B_{1g} \rightarrow {}^2E_g$) and $xz, yz \rightarrow x^2–y^2$ ($^2B_{1g} \rightarrow {}^2A_{2g}$) transitions.[34] The band separation of the spectra of the complexes was of the order of 2500 cm^{-1}, which is consistent with the proposed geometry of these complexes.[34] Therefore, it may be concluded that all the complexes of copper(II) have a distorted octahedral geometry.

Biological results

All the synthesized macrocyclic metal complexes were tested for their *in vitro* antibacterial activities against five test bacterial strains, *viz. S. aureus*, *B. pumilus*, *B. megaterium*, *P. aeruginosa* and *S. epidermidis*. It has been suggested that chelation/coordination reduces the polarity of the metal ion mainly because of the partial sharing of its positive charge with donor groups within the whole chelate ring system.[35] Thus, the process of chelation increases the lipophilic nature of the central metal atom, which, in turn, favours its permeation through the lipoid layer of the bacterial membrane, thereby allowing the metal complex to cross the membrane more effectively, thus increasing the activity of the complexes. In addition to this, many other factors, such as solubility, dipole moment and conductivity, are influenced by the metal ion, which may be possible reasons for the antibacterial activities of these metal complexes.[36] It was also observed that some moieties, such as an azomethine linkage or a heteroaromatic nucleus, introduced into such compounds exhibit extensive biological activities that may be responsible for the increase in the hydrophobic character and liposolubility of the molecules in crossing the cell membrane of the microorganism, thereby enhancing the biological utilization ratio and activity of such complexes.[37]

All the complexes of the tested series possessed good antibacterial activities against all the tested bacterial strains. The *MIC* (minimum inhibitory concentration) shown by the metal complexes against these bacterial strains was compared with the *MIC* values shown by the standard antibiotics linezolid and cefaclor (Table II). In the whole series, complex **7** showed the highest activity, with *MIC* of 2 μg cm^{-3} against the bacterial strains *P. aeruginosa* and *S. epidermidis*. Complex **7** also showed a *MIC* of 8 μg cm^{-3} against the bacterial strain *B. pumilus*,

which was equal to the *MIC* shown by the standard antibiotic cefaclor against the same bacterial strain. Complex **5** showed an *MIC* of 8 μg cm^{-3} against the bacterial strain *P. aeruginosa*, which was equal to the *MIC* values shown by the standard antibiotics cefaclor and linezolid against the same bacterial strain. Complexes **6** and **8** showed an *MIC* of 8 μg cm^{-3} against the bacterial strain *B. megaterium*, which was equal to the *MIC* shown by the standard antibiotic cefaclor against the same bacterial strain. Similarly, complex **9** also showed an *MIC* of 8 μg cm^{-3} against the bacterial strain *B. pumilus*, which was equal to *MIC* shown by standard antibiotic cefaclor against the same bacterial strain (Table II).

Table II Minimum inhibitory concentration (*MIC* / μg cm^{-3}) of the complexes determined using the macro dilution method

Cmpd.	Complex	*MIC* / μg cm^{-3}				
		S. aureus	*B. pumilus*	*B. megaterium*	*P. aeruginosa*	*S. epidermidis*
1	$[Co(C_{28}H_{18}N_6)Cl_2]$	64	128	>128	32	64
2	$[Co(C_{28}H_{18}N_6)(CH_3COO)_2]$	64	32	64	32	16
3	$[Ni(C_{28}H_{18}N_6)Cl_2]$	128	64	32	16	32
4	$[Ni(C_{28}H_{18}N_6)(NO_3)_2]$	8	16	32	64	16
5	$[Ni(C_{28}H_{18}N_6)(CH_3COO)_2]$	32	64	16	8	32
6	$[Cu(C_{28}H_{18}N_6)Cl_2]$	16	32	8	16	16
7	$[Cu(C_{28}H_{18}N_6)(NO_3)_2]$	32	8	16	2	2
8	$[Cu(C_{28}H_{18}N_6)(CH_3COO)_2]$	64	32	8	6	32
9	$[Zn(C_{28}H_{18}N_6)(CH_3COO)_2]$	16	8	32	4	16
Linezolid		4	4	4	8	8
Cefaclor		2	8	8	8	2

Some complexes, *i.e.*, **7**–**9**, showing *MIC* values of 2, 6 and 4 μg cm^{-3}, respectively, were found to be even better than the standard antibiotics against some bacterial strains (Table II). The *MIC* values of complex **2** were found to be in the range 16–64 μg cm^{-3} and complex **4** registered *MIC* values in the range 8–––64 μg/cm^{-3} (Table II).

ABBREVIATIONS

MIC – Minimum inhibitory concentration
MTCC – Microbial type culture collection
MHA – Muller Hinton agar
CFU – Colony forming unit
DMF – *N*,*N*-Dimethylformamide
DMSO – Dimethyl sulphoxide
NMR – Nuclear Magnetic Resonance
IR – Infrared
SCDA – Soybean casein digest agar
EDTA – Ethylenediaminetetraacetic acid

DNA – Deoxyribonucleic acid
HIV – Human immunodeficiency virus.

CONCLUSIONS

Based on elemental analyses, conductivity and magnetic measurements, and electronic, IR and NMR spectral studies, the structure as shown in Scheme I may be proposed for all of the synthesized complexes.

However, not all the synthesized macrocyclic metal complexes showed good antibacterial activities against all the bacterial strains, but some of the complexes of copper and zinc, *viz*., **7**–**9** that showed *MIC* values of 2, 6 and 4 μg cm^{-3}, respectively, were even better than the standard antibiotics linezolid and cefaclor against some bacterial strains.

Acknowledgement. D. S. thanks to the authorities of the National Institute of Technology, Kurukshetra for providing the necessary research facilities.

И З В О Д

СИНТЕЗА И КАРАКТЕРИЗАЦИЈА НЕКИХ МЕТАЛ(II) КОМПЛЕКСА СА МАКРОЦИКЛИЧНИМ ТИПОМ ЛИГАНДА КОЈИ ЈЕ ДОБИВЕН У РЕАКЦИЈИ ИЗАТИНА СА 1,2-ДИАМИНОБЕНЗЕНОМ

DHARAM PAL SINGH[1], VIDHI GROVER[1], KRISHAN KUMAR[2] и KIRAN JAIN[3]

[1]*Department of Chemistry, National Institute of Technology, Kurukshetra-136 119,* [2]*Department of Applied Sciences and Humanities, Gurgaon College of Engineering, Bilaspur-Tauru Road, Gurgaon-122 413 и* [3]*Department of Chemistry, M.L.N. College, Yamuna Nagar, India*

Темплатном кондензационом синтезом, полазећи из изатина и 1,2-диаминобензена, синтетизована је серија новик комплекса опште формуле $[M(C_{28}H_{18}N_6)X_2]$, где је M = Co(II), Ni(II), Cu(II), Zn(II); X = Cl^-, NO_3^-, CH_3COO^-. За карактеризацију ових комплекса употребљене су различите физичкохемијске методе, као што се елементална микроанализа, кондуктометријска и магнетна мерења, нуклеарна магнетно-резонанциона, инфрацрвена и далека инфрацрвена спектроскопска мерења. Ниске вредности за моларну проводљивост указују да су изоловани комплекси неелектролити, а на бази спектроскопских мерења закључено је да ови комплекси имају дисторговану октаедарску геомтерију. Сви изоловани макроциклични комплекси су тестирани *in vitro* на антибактеријску активност за неколико патогених бактеријских линија. Добивене MIC вредности ових комплекса су поређене са одговарајућим вредностима за стандардне антибиотике линезолид и цефаклор. Нађено је да неки испитивани комплекси имају завидну антибактеријску активност.

(Примљено 7. јуна, ревидирано 23. септембра 2010)

REFERENCES

1. a) A. Chaudhary, N. Bansal, N. Fahmi, R. V. Singh, *Indian J. Chem*. **43A** (2000) 320; b) *Macrocyclic Chemistry: Current Trends and Future Perspectives*, K. Gloe, Ed., Dordrecht, Springer, 2005.
2. S. Chandra, S. D. Sharma, *Transition Met. Chem.* **27** (2002) 732
3. S. Chandra, R. Kumar, *Transition Met. Chem.* **29** (2004) 269
4. S. Chandra, R. Gupta, N. Gupta, S. S. Bawa, *Transition Met. Chem.* **31** (2006) 147

5. A. K. Singh, R. Singh, P. Saxena, *Transition Met. Chem.* **29** (2004) 867
6. D. K. Dey, D. Bandhopadhya, K. Nandi, S. N. Paddan, G. Mukhopadhay, G. B. Kauffman, *Synth. React. Inorg. Met.–Org. Chem.* **22** (1992) 1111
7. W. Ma, Y. Tian, S. Zhang, J. Wu, *Transition Met. Chem.* **31** (2006) 97
8. R. N. Prasad, S. Gupta, *J. Serb. Chem. Soc*. **67** (2002) 523
9. M. B. Ferrari, C. Pelizzi, G. Pelosi, M. C. Rodriguez, *Polyhedron* **21** (2002) 2593
10. D. P. Singh, R. Kumar, P. Tyagi, *Transition Met. Chem.* **31** (2006) 970
11. A. Chaudhary, R. Swaroop, R. Singh, Bol. Soc. *Chile Quim*. **47** (2002) 203
12. J. G. Muller, X. Chen, A. C. Dadig, S. E. Rokita, C. J. Burrows, *Pure Appl. Chem*. **65** (1993) 545
13. J. Liu, T. B. Lu, H. Deng, L. N. Ji, L. H. Qu, H. Zhou, *Transition Met. Chem*. **28** (2003) 116
14. B. Contabrana, A. Baamonde, F. Andras-Irellas, H. Hidalgo, *Gen. Pharm*. **21** (1990) 89
15. W. Zhang, Y. Zhao, H. Qigang, *Shengzhi Biyun* **9** (1989) 16 (in Chinese)
16. G. Cerchiaro, A. M. Ferreira, *J. Brazil. Chem. Soc*. **17** (2006) 1473
17. D. P. Singh, V. Grover, K. Jain, R. Kumar, Russ. *J. Coord. Chem*. **34** (2008) 233
18. D. P. Singh, R. Kumar, J. Singh, *Eur. J. Med. Chem*. **44** (2009) 1731
19. W. J. Geary, *Coord. Chem. Rev*. **7** (1971) 81
20. J. S. Casas, E. E. Castellano, M. S. G. Tasende, *Inorg. Chim. Acta* **304** (2000) 283
21. S. S. Nivasan, P. Athappan, *Transition Met. Chem*. **26** (2001) 588
22. Q. Zeng, J. Sun, S. Gou, K. Zhou, J. Fang, H. Chen, *Transition Met. Chem.* **23** (1998) 371
23. L. K. Gupta, S. Chandra, *Transition Met. Chem*. **31** (2006) 368
24. A. K. Mohamed, K. S. Islam, S. S. Hasan, M. Shakir, *Transition Met. Chem*. **24** (1999) 198
25. C. Lodeiro, R. Bastida, E. Bertolo, A. Macias, R. Rodriguez, *Transition Met. Chem*. **28** (2003) 388
26. M. Shakir, K. S. Islam, A. K. Mohamed, *Transition Met. Chem.* **24** (1999) 577
27. F. M. A. M. Aqra, *Transition Met. Chem*. **24** (1999) 337
28. V. B. Rana, D. P. Singh, P. Singh, M. P. Teotia, *Transition Met. Chem*. **7** (1982) 174
29. G. A. Bain, D. X. West, J. Krejci, J. Valdes-s-Martinez, S. Hernandez-ortega. R.A. Toscano, *Polyhedron* **16** (1997) 855
30. E. Labisbal, A. Sousa, A. Castineiras, *Polyhedron* **19** (2000) 1255
31. M. S. Niasari, A. Amiri, *Transition Met. Chem*. **31** (2006) 157
32. a) V. B. Rana, D. P. Singh, P. Singh, M. P. Teotia, *Transition Met. Chem*. **6** (1981) 36; b) V. B. Rana, D. P. Singh, P. Singh, M. P. Teotia, *Polyhedron* **1** (1982) 377
33. A. B. P. Lever, *Inorganic Electronic Spectroscopy*, Amsterdam, Elsevier, 1968
34. A. B. P. Lever, E. Mantovani, *Inorg. Chem.* **10** (1971) 817
35. N. Raman, S.R. Johnson, A. Sakthivel, *J. Coord. Chem.* **62** (2009) 691
36. Z. H. Chohan, M. U. Hassan, K. M. Khan, C. T. Supuran, *J. Enz. Inhib. Med. Chem*. **20** (2005) 183
37. K. Singh, D. P. Singh, M. S. Barwa, P. Tyagi, Y. Mirza, *J. Enz. Inhib. Med. Chem*. **21** (2006) 749.

Journal of the Serbian Chemical Society
JSCS-info@shd.org.rs • www.shd.org.rs/JSCS
J. Serb. Chem. Soc. *76* (3) 395–406 (2011)
JSCS–4127
UDC 547.7:547.517:532.74:537.872
Original scientific paper

Density functional theory (DFT) calculations of conformational energies and interconversion pathways in 1,2,7-thiadiazepane

MINA HAGHDADI[1]* and NAHID FAROKHI[2]

[1]*Department of Chemistry, Islamic Azad University, Babol Branch and* [2]*Department of Chemistry, Islamic Azad University, Rasht Branch, Iran*

(Received 12 August, revised 7 September 2010)

Abstract: The molecular structure and conformational analysis of 1,2,7-thiadiazapane conformers were investigated by density functional theory (DFT) calculations at the B3LYP/cc-pVDZ level of theory. Four twist-chair (**TC**), six twist-boat (**TB**), two boat (**B**), two chair (**C**) and four twist (**T**) conformers were identified as minima and transition states for 1,2,7-thiadiazepane. The **TC1** conformer is the most stable conformer and the twist-chair conformers are predicted to be lower in energy than their corresponding boat and chair conformations. DFT predicts a small barrier to pseudo-rotation and a remarkable activation barrier for the conformational interconversion of the twist-chair conformers to their corresponding boat conformers. The simplest conformational process and the one with the lowest barrier is the degenerate interconversion of the twist-chair 3 (**TC3**) conformation with itself *via* the C_S symmetric chair (**C2**) transition state. The calculated strain energy barrier for this process is 2.41 kJ mol^{-1}. The highest conformational interconversion barrier is between **TC2** and twist-boat 3 (**TB3**) forms, which was found to be 75.62 kJ mol^{-1}.

Keywords: conformational analysis; 1,2,7-thiadiazepane; DFT calculation.

INTRODUCTION

The chemistry and biological activities of seven-membered heterocyclic compounds has continued to command significant attention in recent years.[1] Cycloheptane and its hetero derivatives (heterocycloheptanes), which are found in Alzheimer drugs, anticancer agents, antimalarials,[2,3] and natural products,[4–8] are important compounds in many areas of science. These compounds can be both fused and non-fused heterocycles, with an emphasis on N, S, and O as the heteroatom in the seven-membered ring components. Many synthetic methods were reported for these compounds in recent decades.[9]

* Corresponding author. E-mail: mhaghdadi2@yahoo.co.uk
doi: 10.2298/JSC100812040H

There are many reports concerning the synthesis and pharmacological activities of cyclic sulfonamide compounds (as heterocycloheptane derivatives).[10–13] These compounds inhibit the HIV protease by affecting its binding to protein.[14–16] Contrary to the abundance of information on the synthesis and pharmacological activities of 7-membered heterocyclic compounds, there is relatively little information available about the conformational properties of these compounds. It is difficult to study experimentally the stereodynamics of compounds containing a seven-membered ring since the conformations are often structurally similar and show complex conformational and pseudo-rotational equilibria with low barriers among the chair (**C**), twist chair (**TC**), boat (**B**), and twist-boat (**TB**) conformations and transition states.

As a continuation of our interest in the conformations of medium ring sized heterocycles,[17–20] this study was undertaken in order to investigate the conformational analysis of 1,2,7-thiadiazepane (Scheme 1) by computational methods to determine their preferred conformers. The effects of changes in bond length, bond angle and torsion angle of these compounds were also of interest. Therefore, the density functional theory (DFT) method was applied in this work to calculate the molecular structures, energy differences and conformational interconversion pathways of 1,2,7-thiadiazepane conformers at the B3LYP/cc-pVDZ//B3LYP/cc-pVDZ level (full optimization).

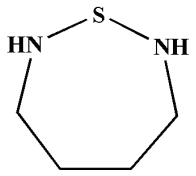

Scheme 1. Schematic representation of 1,2,7-thiadiazepane.

COMPUTATIONAL DETAILS

In the present study, the density functional theory method was used to optimize the conformations of 1,2,7-thiadiazepane. The Becke three-parameter exact exchange functional (B3)[21] combined with the gradient-corrected correlation functional of Lee–Yang–Parr (LYP)[22] of DFT methods, implementing the cc-pVDZ basis set was employed to optimize the molecules.

The nature of the optimized geometries at the B3LYP level was checked with frequency calculations. The vibrational frequencies were calculated at the cc-pVDZ level for all minimum energies and transition states, which were confirmed to have zero and one imaginary frequency, respectively. All calculations were performed using the Gaussian 2003W computational package.[23]

RESULTS AND DISCUSSION

The results of the density functional theory (B3LYP/cc-pVDZ//B3LYP/cc-pVDZ) calculations showed that twenty two geometries, of which eleven were energy minima, were important in the description of the conformational pro-

perties of 1,2,7-thiadiazepane (**1**). There are eleven transition states which are required to describe the dynamic conformational properties of compound **1**. Corrected zero point (*ZPE*°) and total electronic (*Eel*) energies ($E° = E_{el} + ZPE°$) for conformations of compound **1** are given in Table I. The energy surfaces for the interconversion of the energy-minimum conformers were obtained by changing different torsional angles, as shown in Figs. 1 and 2. The energy minima and transition state geometries are shown in Schemes 2 and 3, respectively.

TABLE I. Calculated total, zero-point vibrational energies and relative energies between the most stable minimum stereoisomers and transition states

B3LYP/cc-pVDZ///	B3LYP/cc-pVDZ, Hartree	*ZPE*°, Hartree	E_{rel} / kJ mol^{-1}
TC1	–666.133904	0.147023	0
TC3	–666.1325829	0.147161	3.83
C2	–666.1316392	0.147009	5.91
C4	–666.1313194	0.146932	6.53
TC2	–666.130937	0.146846	7.33
TC4	–666.1306823	0.146799	7.88
TC5	–666.1315934	0.147977	8.54
C1	–666.1285964	0.146740	13.2
C3	–666.1264443	0.146967	19.44
TB1	–666.1268317	0.147617	20.11
TB3	–666.1244648	0.147199	25.24
B3	–666.1248174	0.147561	25.25
TB4	–666.1241074	0.147335	26.53
TB5	–666.1239418	0.147215	26.65
TB2	–666.122806	0.147186	29.56
B2	–666.1222725	0.147020	30.53
TB6	–666.1205977	0.147129	35.21
B1	–666.118878	0.147375	40.36
T4	–666.1167305	0.146650	44.12
T2	–666.1165628	0.147106	45.75
T3	–666.1075709	0.147107	69.36
T1	–666.1027653	0.144662	75.624

Molecular structures of 1,2,7-thiadiazepane conformers

Conformational studies of 1,2,7-thiadiazepane revealed some minima and transition states with similar energies and geometries among the twist-chair, chair, boat, twist-boat and twist conformations and transition states. The S and N atoms occupy positions which avoid transannular hydrogen–hydrogen steric and the lone pair–lone pair interactions. The geometrical parameters of 1,2,7-thiadiazepane conformers were calculated and are presented in Tables II and III. Five twist-chair (**TC**), six twist-boat (**TB**), three boat (**B**), four chair (**C**) and four twist (**T**) conformers were identified as minima and transition states for compound **1** (Schemes 2 and 3). The possible minima forms are: **TC1**–**TC5** for the twist-chair

structure, **C1**–**C4** for the chair structure, **B1**–**B3** for the boat structure, **TB1**–**TB6** for the twist-boat structure and **T1**–**T4** for twist structure. The **TC1** conformer is the most stable, with the highest dihedral angles of φ_4 and φ_7 (Table II) of the minimum conformers. In the **TC5** conformer, the dihedral angles of φ_2 and φ_6 (which geometrically correspond to φ_4 and φ_7 of **TC1**) were increased in comparison with the others. The lowest value of the dihedral angle of φ_7 was observed in the **TB2** conformer and φ_1 was decreased in the **TB6** structure. While the dihedral angle of φ_5 in the **TB1** conformer and φ_4 in the **B3** conformer were decreased, these dihedral angles have the highest values in the **TC3** and **TC1** conformers, respectively. The **TC2** conformer has the highest value of dihedral angle of φ_3 which is decreased in the **TB1** conformer.

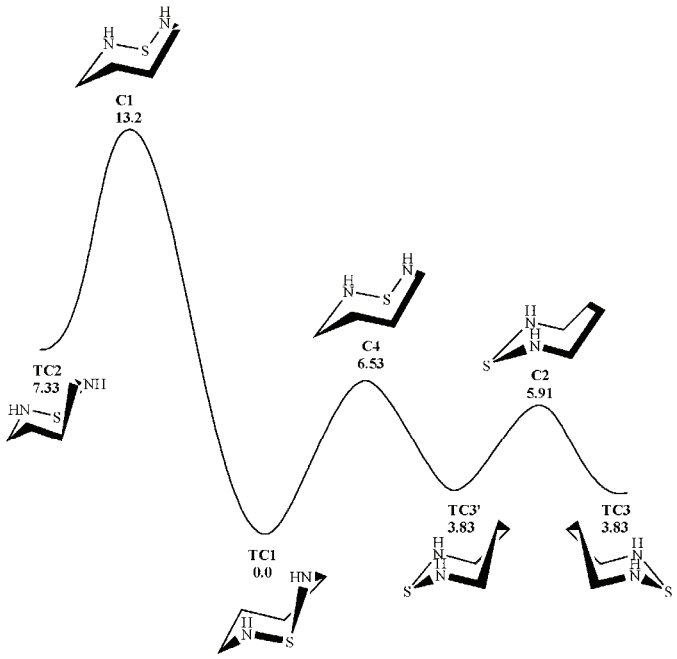

Fig. 1. Calculated B3LYP/cc-pVDZ// B3LYP/cc-pVDZ strain energy (kJ mol^{-1}) profiles for the conformational interconversion of the twist-chair family of 1,2,7-thiadiazepane.

Comparison between the calculated bond angles indicated that θ_1 (110.90°) in the **TC4**, θ_6 (117.54°) in the **TC2**, θ_7 (122.71°) in the **TC1,** θ_5 (117.89°) and θ_3 (117.93°) in the **TC3** and θ_2 (119.64°) in the **TB3** conformers were wider than the corresponding bond angles of the other conformers (stereo-electronic effects). B3LYP/cc-pVDZ calculations predicted that the bond length of N_1–S was the shortest and the bond length of N_2–S was the longest in the **TB5** conformer, while in the **TB2** conformer, the bond distance of N_1–S was the longest and N_2–S was the shortest.

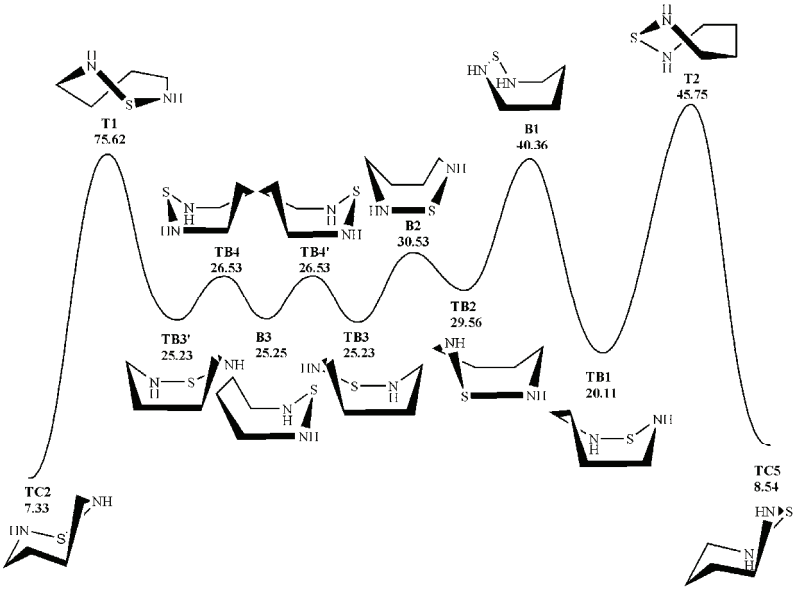

Fig. 2. Calculated B3LYP/cc-pVDZ// B3LYP/cc-pVDZ strain energy (kJ mol^{-1}) profiles for the conformational interconversion of the twist-boat geometries of 1,2,7-thiadiazepane.

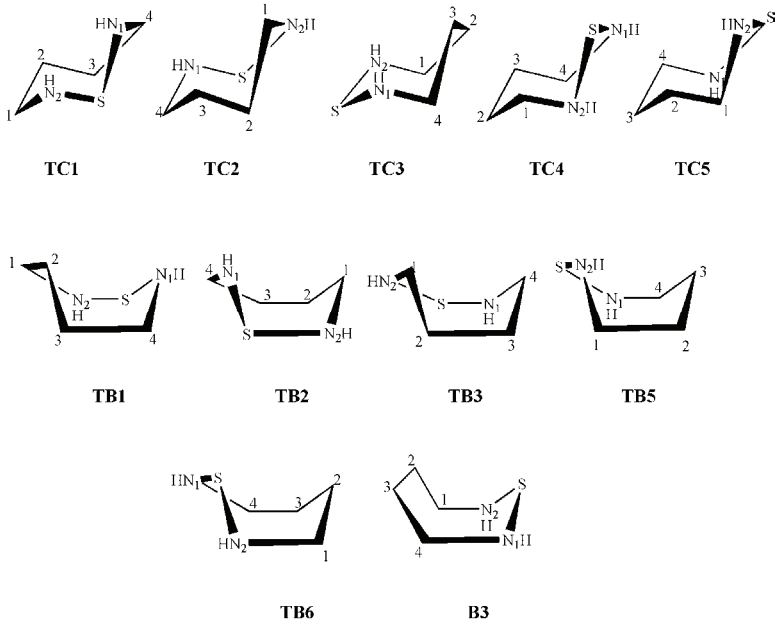

Scheme 2. The various minimum conformations of 1,2,7-thiadiazepane.

The bond lengths tend to depend more on the type of bond and the dihedral angles depend more on the conformation of the molecule.

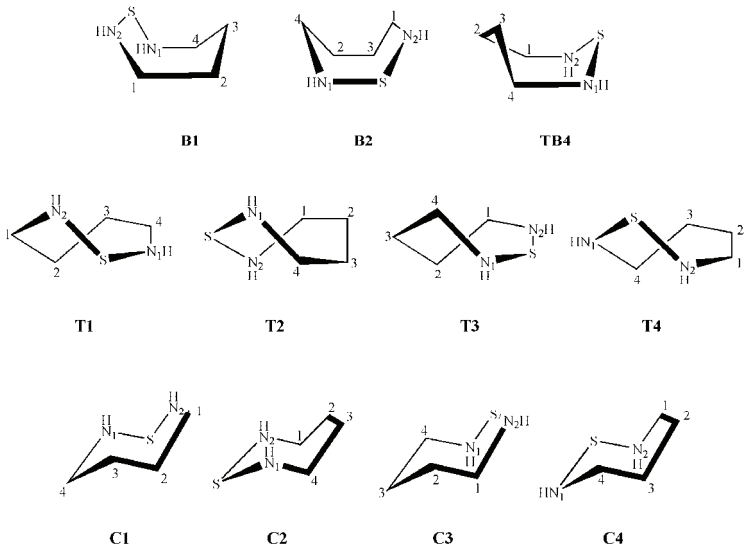

Scheme 3. The transition state conformations of 1,2,7-thiadiazepane.

Conformational analysis

The results of the DFT calculations showed that there are eleven minima (twist-chair, **TC1**, **TC2**, **TC3**, **TC4** and **TC5**; twist-boat, **TB1**, **TB2**, **TB3**, **TB4** and **TB5**; boat, **B1**) and eleven transition states (chair, **C1**, **C2**, **C3** and **C4**; twist, **T1**, **T2**, **T3** and **T4**; twist-boat, **TB6**; boat, **B2** and **B3**) in the 1,2,7-thiadiazepane conformations (Schemes 2 and 3). The conformational interconversion pathways and structure optimization of **1** are shown in Figs. 1 and 2 and Tables II and III. The most stable conformation of **1** is the unsymmetrical **TC1** form, which by changing the twist of $S–N_1C_4C_3$ the **TC2** conformer was formed (7.33 kJ mol^{-1}) (Fig. 1). The structure of the transition state was obtained from the QST3 subroutine using the optimized geometries of the **TC1** and **TC2** conformations. The calculated energy barrier for interconversion of these two conformers occurs *via* the unsymmetrical chair (**C1**) as the transition state. The second energy minimum conformation of **1** is twist-chair 3 (**TC3**), which is higher in energy than **TC1** by 3.83 kJ mol^{-1}. The degenerate interconversion of **TC3** with its mirror image occurs *via* the C_s symmetric chair 2 (**C2**), as the transition state. Moreover, the **TC3** conformation could transform *via* chair 4 (**C4**) to **TC1**. The strain energy barrier for this process is 6.53 kJ mol^{-1}.

The twist-chair 4 (**TC4**) is another energy-minimum structure, which was found to be less stable than the **TC1** conformer by 7.88 kJ mol^{-1} and more stable than twist-chair 5 (**TC5**), which has the opposite twist in the C–N–S–N angle in the ring (see Scheme 2). The transition state linking **TC5** and **TC4** is the unsymmetrical chair 3 (**C3**) with the calculated strain energy barrier for this process being 19.44 kJ mol^{-1} (Fig. 3).

TABLE II. Calculated geometrical parameters for the minimum conformers of 1,2,7-thiadiazepane (**1**)

Bond	TC1	TC2	TC3	TC4	TC5	TB1	TB2	TB3	TB5	TB6	B3
					r / Å						
N_1–S (r_1)	1.709	1.717	1.728	1.737	1.736	1.734	1.780	1.754	1.703	1.700	1.722
S–N_2 (r_2)	1.730	1.733	1.719	1.715	1.736	1.734	1.708	1.704	1.798	1.752	1.722
N_2–C_1 (r_3)	1.464	1.478	1.464	1.465	1.466	1.463	1.489	1.481	1.467	1.472	1.477
C_1-C_2 (r_4)	1.541	1.532	1.547	1.537	1.541	1.564	1.535	1.531	2.628	1.538	1.533
C_2–C_3 (r_5)	1.541	1.544	1.546	1.543	1.538	1.539	1.546	1.557	1.537	1.539	1.564
C_3–C_4 (r_6)	1.536	1.537	1.544	1.532	1.541	1.564	1.533	1.534	1.536	1.532	1.533
C_4–N_1 (r_7)	1.473	1.465	1.468	1.478	1.466	1.463	1.470	1.471	1.471	1.487	1.477
					θ / °						
N_1–S–N_2 (θ_1)	108.89	110.86	109.54	110.90	108.58	107.77	107.05	108.02	107.63	107.79	108.57
S–N_2–C_1 (θ_2)	117.95	121.84	116.92	116.40	118.76	118.13	118.86	120.45	113.92	115.67	117.58
N_2–C_1–C_2 (θ_3)	117.56	116.06	117.93	117.53	114.05	116.65	115.00	113.75	117.19	116.89	113.91
C_1–C_2–C_3 (θ_4)	114.82	115.01	118.33	116.64	117.85	114.55	116.99	116.61	116.29	116.49	117.89
C_2–C_3–C_4 (θ_5)	116.49	116.62	118.61	114.89	117.85	114.55	117.08	117.75	116.36	114.67	117.89
C_3–C_4–N_1 (θ_6)	116.89	117.54	115.01	116.00	114.05	116.65	115.79	114.79	115.45	113.11	113.91
C_4–N_1–S (θ_7)	112.71	116.38	117.58	121.47	118.76	118.13	114.55	114.47	120.52	119.28	117.58
					φ / °						
N_1–S–N_2–C_1 (φ_1)	66.69	43.16	66.51	–76.06	38.85	–45.06	–71.74	65.45	–15.00	–15.00	–53.52
S–N_2–C_1–C_2 (φ_2)	–56.91	22.68	–82.92	66.19	–84.86	61.88	11.16	7.13	75.43	–62.31	–29.03
N_2–C_1–C_2–C_3 (φ_3)	68.95	–81.10	36.51	–58.15	71.78	20.68	65.88	–69.85	–29.43	46.58	71.40
C_1–C_2–C_3–C_4 (φ_4)	–88.94	80.84	39.44	79.99	–54.32	–80.25	–35.00	20.35	–61.64	50.30	–0.01
C_2–C_3–C_4–N_1 (φ_5)	52.66	–58.71	–85.53	–82.62	71.78	20.69	–59.51	68.93	50.30	–69.04	–71.40
C_3–C_4–N_1–S (φ_6)	22.68	65.55	71.50	25.52	–84.86	61.87	60.21	–50.37	40.88	–16.42	29.05
C_4–N_1–S–N_2 (φ_7)	–70.66	–75.84	–50.95	41.10	38.84	–45.07	23.35	–35.00	–64.19	71.14	53.50

TABLE III. Calculated geometrical parameters for the transition states conformers of 1,2,7-thiadiazepane (**1**)

Bond	C1	C2	C3	C4	T1	T2	T3	T4	B1	B2	TB4
					r / Å						
N_1–S (r_1)	1.755	1.721	1.695	1.727	1.678	1.733	1.705	1.697	1.727	1.746	1.720
S–N_2 (r_2)	1.696	1.721	1.810	1.717	1.728	1.733	1.751	1.742	1.718	1.708	1.739
N_2–C_1 (r_3)	1.485	1.466	1.467	1.462	1.482	1.461	1.489	1.474	1.470	1.489	1.475
C_1–C_2 (r_4)	1.536	1.540	1.545	1.563	1.572	1.559	1.535	1.530	1.550	1.532	1.534
C_2–C_3 (r_5)	1.544	1.561	1.536	1.539	1.536	1.566	1.537	1.551	1.537	1.549	1.566
C_3–C_4 (r_6)	1.534	1.540	1.533	1.544	1.540	1.559	1.558	1.566	1.533	1.539	1.532
C_4–N_1 (r_7)	1.467	1.466	1.465	1.464	1.459	1.461	1.460	1.474	1.475	1.472	1.480
					θ / °						
N_1–S–N_2 (θ_1)	102.64	109.01	109.67	109.12	103.75	106.32	112.33	107.25	107.96	107.92	109.85
S–N_2–C_1 (θ_2)	120.09	117.31	116.84	119.14	126.07	115.02	125.60	115.67	116.52	119.04	115.70
N_2–C_1–C_2 (θ_3)	117.35	116.48	118.26	119.41	120.48	118.01	120.30	111.90	117.24	112.19	113.69
C_1–C_2–C_3 (θ_4)	117.01	119.90	116.94	118.68	122.56	122.68	117.65	117.43	116.36	115.37	116.72
C_2–C_3–C_4 (θ_5)	116.91	119.90	115.99	116.34	115.99	122.68	115.42	122.61	116.36	118.34	116.23
C_3–C_4–N_1 (θ_6)	111.24	116.48	114.67	116.50	112.12	118.00	115.24	120.79	115.37	118.64	113.36
C_4–N_1–S (θ_7)	113.89	117.31	120.97	117.97	117.06	115.02	119.35	122.36	120.23	116.31	118.52
					φ / °						
N_1–S–N_2–C_1 (φ_1)	–62.27	–58.00	–2.22	75.27	–29.33	–46.22	0.81	–43.10	5.00	–68.29	–42.52
S–N_2–C_1–C_2 (φ_2)	–2.22	82.09	64.45	–63.90	–19.99	83.38	8.23	–40.44	72.11	–3.93	–42.30
N_2–C_1–C_2–C_3 (φ_3)	70.52	–65.46	–86.83	–2.22	–4.54	–24.70	–69.12	90.91	–36.21	76.52	74.24
C_1–C_2–C_3–C_4 (φ_4)	–81.45	0.00	63.55	68.15	71.07	–19.17	72.50	–36.34	–53.19	–37.00	13.16
C_2–C_3–C_4–N_1 (φ_5)	61.77	65.46	–61.78	–84.26	–49.01	–24.70	9.11	–12.39	55.71	–52.54	–74.79
C_3–C_4–N_1–S (φ_6)	–73.71	–82.09	83.95	62.50	–45.00	83.38	–78.69	–22.08	32.54	43.73	25.88
C_4–N_1–S–N_2 (φ_7)	91.41	58.00	–64.50	–55.34	88.74	–46.22	56.66	75.75	–66.74	37.17	54.06

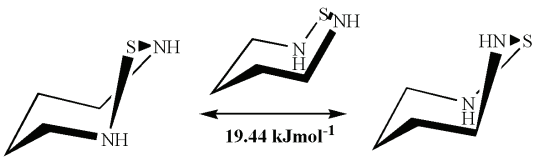

TC4 **TC5**

Fig. 3. The strain energy barrier for the conformational interconversion of **TC4** and **TC5**.

The results of calculations showed that there are a number of twist-boat conformations, which are energy minima in the pseudorotation pathways and are also higher in energy than the twist-chair conformers. The most stable conformer in the twist-boat family is twist boat 1 (**TB1**), which is 20.11 kJ mol^{-1} higher in energy than **TC1** (the most stable conformer of the twist-chair family) (Table I).

The **TB1** conformer can be related to the twist-boat 2 (**TB2**) geometry *via* the unsymmetrical boat conformer (**B1**), requiring an energy of 40.36 kJ mol^{-1} (Fig. 2) Moreover, by changing the C–C–N–S twist in the **TB2** conformer, it could be converted to twist-boat 3 (**TB3**) *via* the unsymmetrical boat form (**B2**). The calculated strain energy barrier for this process is 30.53 kJ mol^{-1}. The degenerate interconversion of **TB3** with its mirror image could occur *via* the unsymmetrical twist-boat 4 (**TB4**) as the transition state, as well as the C_s symmetric boat 3 (**B3**) geometry as a local minimum. Moreover, the twist-boat 5 (**TB5**), as another minimum conformation, could be converted to twist-boat 6 (**TB6**) *via* **B1** as the transition state.

The results of the B3LYP/cc-pVDZ calculations for the conformational interconversion pathways showed that the twist-chair families can be related to the boat families *via* twist conformers as the transition states. The **TC1** geometry could be converted to **B3** *via* twist 1 (**T1**) as the transition state, for which the strain energy barrier is 75.62 kJ mol^{-1}. The **TB2** conformer, from the twist boat family, could be converted to twist chair conformations *via* two conformational processes. The simplest conformational process is the interconversion of the **TB1** and **TC5**, *via* the C_{2v} symmetric twist 2 (**T2**) as the transition state, which requires 45.75 kJ mol^{-1} (Fig. 2). The second (high-energy) process involves the conformational interconversion of the **TB1** and **TC3** forms that occurs *via* the unsymmetrical twist 3 (**T3)** as the transition state (Fig. 4). The strain energy barrier for this process is 69.36 kJ mol^{-1}. On the other hand, the **TC2** conformation could transform *via* twist geometry 4 (**T4**) to the **B3** geometry with an energy barrier to interconversion of 44.12 kJ mol^{-1} (Fig. 5).

As can be seen from the results of DFT in Table I and Figs. 1 and 2, the twist-chair conformer (**TC1**) is lower in energy than the boat and twist-boat conformers, and the chair transition states (**C1**, **C2**, **C3** and **C4**) are lower in energy than the boat and twist–boat conformers. Based on the energetic results, it could

be concluded that, among the various conformations of compound **1**, the twist-chair and chair conformers are the most important forms, as they could be significantly populated at room temperature.

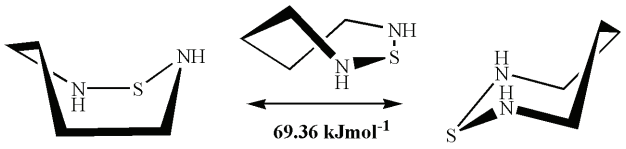

TB1 **TC3**

Fig. 4. The strain energy barrier for the conformational interconversion of **TB1** and **TC3**.

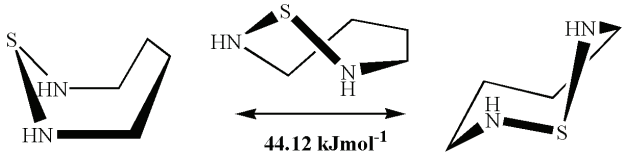

TB3 **TC2**

Fig. 5. The strain energy barrier for the conformational interconversion of **B3** and **TC2**.

CONCLUSIONS

The stability of 1,2,7-thiadiazepane conformers were studied by DFT calculations. Four chair, five twist-chair, three boat, six twist-boat and four twist conformers were identified as minima and transition states for 1,2,7-thiadiazepane. Among the various conformations of compound **1**, the unsymmetrical **TC1** form was found to be the most stable geometry, the **TC3** form, as the second lowest energy minimum, has the simplest conformational process, with the lowest energy barrier, namely the degenerate interconversion of **TC3** with itself *via* the C_S symmetric chair (**C2**) transition state. The results of the calculations showed that the twist-chair and chair conformers are more stable than the twist-boat conformers, as the minimum energy conformation of twist-boat family is 20.11 kJ mol^{-1} less stable than the lowest energy form (**TC1**) of **1**. Therefore the twist-chair conformations are the most important because they are expected to be significantly populated at room temperature.

Acknowledgments. The authors wish to acknowledge Louise S. Price, University College London, UK, for reading the manuscript and providing valuable suggestions.

ИЗВОД

РАЧУНАЊЕ ЕНЕРГИЈЕ КОНФОРМЕРА 1,2,7-ТИАДИАЗЕПАНА И ПУТЕВА ЗА ЊИХОВУ ИНТЕРКОНВЕРЗИЈУ DFT МЕТОДОМ

MINA HAGHDADI и NAHID FAROKHI

Department of Chemistry, Islamic Azad University, Iran

Помоћу DFT израчунавања истраживана је молекулска структура и конформације 1,2,7--тијадиазепана, на нивоу теорије B3LYP/cc-pVDZ. Идентификоване су четири конформације облика увијене столице (*twist chair*, **TC**), шест облика увијене лађе (*twist boat*, **TB**), две облика лађе (*boat*, **B**), две облика столице (*chair*, **C**) и четири увијене (*twist*, **T**) као енергетски минимуми или прелазна стања 1,2,7-тијадиазепана. Конформер **TC1** је најстабилнији, док је за конформере **TB** предвиђено да имају нижу енергију од **B** и **C** конформација. DFT предвиђа малу баријеру за псеудоротацију али знатну активациону баријеру за интерконверзију **TC** конформера у **B** конформере. Најједноставнији процес, онај с најнижом баријером, јесте дегенерисана интерконверзија конформера **TC3** у самог себе преко C_S-симетричног прелазног стања облика **C2**. Израчуната енергетска баријера за овај процесс је 2,41 kJ mol^{-1}. Највиша баријера је за интерконверзију **TC2** у **TB3** форму, и нађена је да износи 75,62 kJ mol^{-1}.

(Примљено 12. августа, ревидирано 7. септембра 2010)

REFERENCES

1. J. A. Smith, P. P. Molesworth, J. H. Ryan, *Prog. Heterocycl. Chem*. **21** (2009) 491
2. H.-X. Jin, Q. Zhang, H.-S. Kim, Y. Wataya, H.-H. Liu, Y. Wu, *Tetrahedron* **62** (2006) 7699
3. K. J. McCullough, M. Nojima, *Curr. Org. Chem*. **5** (2001) 601
4. J. G. Rodriguez, A. Perales, *J. Nat. Prod*. **58** (1995) 564
5. A. F. Barrero, M. M. Herrador, J. M. Molina, J. F. Quilez, M. Quiros, *J. Nat. Prod*. **57** (1994) 873
6. J. J. Piwinski, J. K. Wong, T. M. Chan, M. J. Green, A. K. Ganguly, *J. Org. Chem*. **55** (1990) 3341
7. A. Romo de Vivar, G. Delgado, M. Soriano-Garcia, R. A. Toscano, E. Huerta, R. G. Reza-Garduno, *J. Nat. Prod*. **50** (1987) 284
8. K. C. Nicolaou, F. P. J. T. Rutjes, E. A. Theodorakis, J. Tiebes, M. Sato, E. Untersteller, *J. Am. Chem. Soc*. **117** (1995) 1173
9. a) O. V. Denisko, *Comprehensive Heterocyclic Chemistry III*, Elsevier, Oxford, 2008, p. 489; b) G. I. Yranzo, E. L. Moyano *Comprehensive Heterocyclic Chemistry III*, Elsevier, Oxford, 2008, p. 399; c) A. Kiselyov, A. Khvat *Comprehensive Heterocyclic Chemistry III*, Elsevier, Oxford, 2008, p. 387; d) R. Kumar, S. Perumal, M. Balasubramanian *Comprehensive Heterocyclic Chemistry III*, Elsevier, Oxford, 2008, p. 433; e) T. Tsuchiya, *Comprehensive Heterocyclic Chemistry II*, Elsevier, Oxford, 1996, p. 299; f) J. T. Sharp, *Comprehensive Heterocyclic Chemistry*, Elsevier, Oxford, 1984, p. 593
10. J. Hultn, H. O. Andersson, W. Schaal, H. U. Danielson, B. Classon, I. Kvarnstrm, A. Karln, T. Unge, B. Samuelsson, A. Hallberg, *J. Med. Chem*. **42** (1999) 4054
11. D. Giannotti, J. G. Viti, P. Sbraci, V. Pestellini, G. Volterra, F. Borsini, A. Lecci, A. Meli, P. Dapporto, P. Paolio, *J. Med. Chem*. **34** (1991) 1356
12. N. Lebegue, S. Gallet, N. Flouquet, P. Carato, B. Pfeiffer, P. Renard, S. Léonce, A. Pierre, P. Chavatte, P. Berthelot, *J. Med. Chem*. **48** (2005) 7363

13. W. Schaal, A. Karlsson, G. Ahlsèn, J. Lindberg, H. O. Andersson, U. H. Danielson, B. Classon, T. Unge, B. Samuelsson, J. Hultèn, A. Hallberg, A. Karlèn, *J. Med. Chem.* **44** (2001) 155
14. R. F. Kaltenbach, D. A. Nugiel, P. Y. S. Lam, R. M. Klabe, S. P. Seitz, *J. Med. Chem.* **41** (1998) 5113
15. K. Bäckbro, S. Löwgren, K. Österlund, J. Atepo, T. Unge, *J. Med. Chem.* **40** (1997) 898
16. J. Hultn, N. M. Bonham, U. Nillroth, T. Hansson, G. Zuccarello, A. Bouzide, J. Qvist, B. Classon, U. H. Danielson, A. Karln, I. Kvarnstrm, B. Samuelsson, A. Hallberg, *J. Med. Chem.* **40** (1997) 885
17. M. Haghdadi, M. Hamzehlouiyan, *Chin. J. Chem.* **26** (2008) 1
18. M. Haghdadi, *Asian J. Chem.* **20** (2008) 3331
19. I. Yavari, M. Haghdadi, R. Amiry, *Phosphorus, Sulfur Silicon Relat. Elem.* **181** (2006) 1693
20. I. Yavari, M. Haghdadi, R. Amiry, *Phosphorus, Sulfur Silicon Relat. Elem.* **181** (2006) 2163
21. A. D. Beke, *Phys. Rev. A* **38** (1998) 3098
22. C. Lee, Y. Wang, R. G. Parr, *Phys. Rev. B* **37** (1988) 785
23. *Gaussian 98, Revision A. 6*, Gaussian. Inc., Pittsburgh, PA, 2003.

Journal of the Serbian Chemical Society
JSCS-info@shd.org.rs • www.shd.org.rs/JSCS
J. Serb. Chem. Soc. *76* (3) 407–416 (2011)
JSCS–4128
UDC 621.357+549.21:667.622
Original scientific paper

Diamond deposition on thin cylindrical substrates

GORDANA S. RISTIĆ[1*#], ŽARKO D. BOGDANOV[1], MILAN S. TRTICA[1#] and ŠĆEPAN S. MILJANIĆ[1,2]

[1]*VINČA Institute of Nuclear Sciences, P.O. Box 522, 11001 Belgrade and* [2]*Faculty of Physical Chemistry, University of Belgrade, P.O. Box 137, 11001 Belgrade, Serbia*

(Received 20 April, revised 28 September 2010)

Abstract: Diamond coatings were deposited onto different cylindrical substrates (Cu, SiC, W and Mo) by the hot filament chemical vapor deposition (CVD) method. Continuous, adhered and well-faceted crystalline coatings of diamond were obtained on Cu-wire using a special pretreatment with a mixture of diamond and metal powders as well as carefully controlled deposition at lower power. Diamond deposition on SiC-fiber gave continuous and uniform coatings when only the filament power was properly selected. Uniform, homogeneous, euchedral diamond coatings on W- and Mo-wires, attained at a higher filament power, confirmed once more the convenience of refractory metals as substrates for diamond deposition by the CVD technique. Characterization of the obtained coatings was realized using scanning electron microscopy (SEM). The obtained results are compared with the literature data. Differences are discussed with regard to the chemical nature of the substrates as well as their thermophysical characteristics.

Keywords: diamond coating; CVD; cylindrical substrates; Cu; SiC; W; Mo.

INTRODUCTION

The ease with which diamond film can follow any substrate shape and simultaneously maintain the characteristics of the hardest precious solid make it an attractive engineering material. The chemical vapor deposition (CVD) technique enables the synthesis of a diamond coating on various 3-D objects made of different materials in a rather simple and inexpensive way. Among the various CVD techniques, the hot filament CVD method stands on first place for its versatility and scalability, as well as its low cost and ease of realization. The activating agent of this method – the hot filament itself – can be quickly and easily adjusted

* Corresponding author. E-mail: eristic@vinca.rs
# Serbian Chemical Society member.
doi: 10.2298/JSC100420030R

to a particular task by a proper choice of filament power and the manner of the filament-to-substrate mounting.

Different substrate materials in many different shapes are used in diamond CVD. The requirements for these come from various engineering and scientific areas. In technological applications generally, a strong adhesion between the substrate and the coating is required, as it determines the strength of a substrate–coating system. Sometimes, the substrate should provide only a mechanical support for the growing coating (*e.g.*, for self-standing structures). A cylindrical substrate shape, both in micro and macro dimensions, with either sharp or rounded edge is required in numerous applications, such as special burrs (dental, tool-drill), various probes (thermal, X-ray), cross-field amplifiers, flow nozzles, wire dies, fiber-components for reinforcing composites (metal, ceramic, polymer).

Diamond coatings deposited on thin cylindrical substrates made of different materials, copper, silicon carbide, tungsten, molybdenum are presented in this work. Cu is a soft metal, inert to deposition working conditions, commonly used in growing self-standing elements;[1–4] the latter ones of a cylindrical form, especially with a closed end, could be very useful as storage vials, sample vessels, special test tubes. SiC fiber is a high-tech product, characterized with high strength and high heat resistance as well as low thermal expansion and low electrical conductivity. Diamond-coated SiC fibers can be used for reinforcing different composite materials, *e.g.*, those which are concerned with rigidity, low density and high temperature conditions (up to 1200 °C).[5] The refractory metal W, a strong and hard material, when coated with diamond is used in many demanding technological applications, such as tools,[6] high-temperature probes,[7] and wear-resistant parts.[8] Mo, another refractory metal of lower density and better ductility, as well as lower price, can substitute W in some applications.[9]

EXPERIMENTAL

The deposition experiments were performed in a hot filament CVD reactor coupled to a vacuum apparatus equipped with a pump, a gas flowmeter and pressure gauges.[10] The activating filament was formed as a large-diameter coil and the substrates were mounted through the coil centre, in order to obtain homogeneous and uniform diamond coatings on the thin cylindrical substrates, as well as to avoid complexity and expensiveness of the experimental apparatus (*e.g.*, use of several filaments arranged symmetrically around the substrate, or the possibility of substrate rotation aside the filament). A disadvantage of the coaxial mounting, *i.e.*, impossibility of substrate temperature measurement, either by an optical pyrometer or by a thermocouple, was overcome by performing several preliminary deposition experiments, with purpose of which was to determine the optimal power of the activating filament. The tantalum filament (0.5 mm diameter) coil of 2–3 turns (8 mm diameter) was heated by an electric current from the ac mains through variable transformers. The filament power was controlled manually and kept constant at about 150 or 240 W, depending on the substrate type. It was also possible to modify the effects of the applied power by changing the position of the substrate.

Wire substrates with a typical length of 50 mm were coaxially mounted in a special cartridge/holder into the tantalum coil. By pulling the cartridge into/out of the holder, the substrate mounting could be adjusted. First, the copper wire (0.20 mm diameter) of electrolytic purity was manually abraded with emery paper (P 500) perpendicular to the length axis. As the deposition result was unsatisfactory, the other Cu substrates were manually abraded with a mixture of powders* (Mo:W:diamond = 20:50:30). The SiC fiber (SCS-6, Speciality Materials, Lowell, USA) with a diameter 0.142 mm was used as obtained without any pretreatment. Refractory metal wires (W, Mo) of several diameters were used in deposition experiments. The thicker ones (0.5 mm diameter) were manually abraded with emery paper (P 320), perpendicularly to the length axis. The thin Mo wire (0.1 mm diameter) and W wire (0.025 mm diameter) were not pretreated, but used as received.

Other experimental conditions were as follows: working gas mixture methane (0.5 %) in hydrogen, total gas pressure 30 mbar, gas flow rate 50 cm^3 min^{-1}, deposition duration 9 or 16 h. Before the deposition, the Ta filament was conditioned by heating in the mixture of methane (5 %) in hydrogen for about 45 min.

Characterization of the obtained diamond coatings was performed by scanning electron microscopy (Jeol JSM 35, accelerating voltage 25 kV)

RESULTS AND DISCUSSION

For the achievement of good quality diamond coatings, of all four investigated materials, Cu required the most attention and effort. Diamond deposition on Cu was a peculiar challenge in that copper does not react with the working atmosphere to form carbide (which would assist the growth and adhesion of a diamond coating) and because the thermal expansion coefficients of Cu and diamond are very different (which causes thermal stress in the coating, subsequent cracking and coating delamination upon cooling from deposition to room temperature). In diamond deposition experiments on the thin, cylindrical substrate, *i.e.*, on the Cu filament, another disadvantage of Cu became evident – the melting temperature of Cu, which is very close to the working temperature of diamond deposition. This inherent characteristic of Cu was not so noticeable in the experiments with planar, thick (2.5 mm) substrates mounted laterally with respect to the activating filament.[10] A small diameter (0.20 mm) of the substrate was chosen in the present experiments in order to achieve a thicker diamond coating, inside which bonding forces could equalize and possibly surpass the thermal stress after termination of the deposition.

An insufficient power of the activating tantalum filament, 125 W, gave negligible diamond nuclei on the thin non-diamond layer during 9 h deposition, whereas with a sufficient filament power of 150 W during 9 h deposition resulted in continuous coatings. The coatings obtained on two Cu substrates at the same filament power (150 W) for the same duration (9 h) but pretreated differently are shown in Figs. 1a–1d. The diamond fiber morphology with characteristic nodules, Fig. 1a, and a crack in the coating, Fig. 1b, are shown as distinctive represen-

* Particle sizes, diamond: 0.310 μm; Mo and W: 5 μm, predominantly.

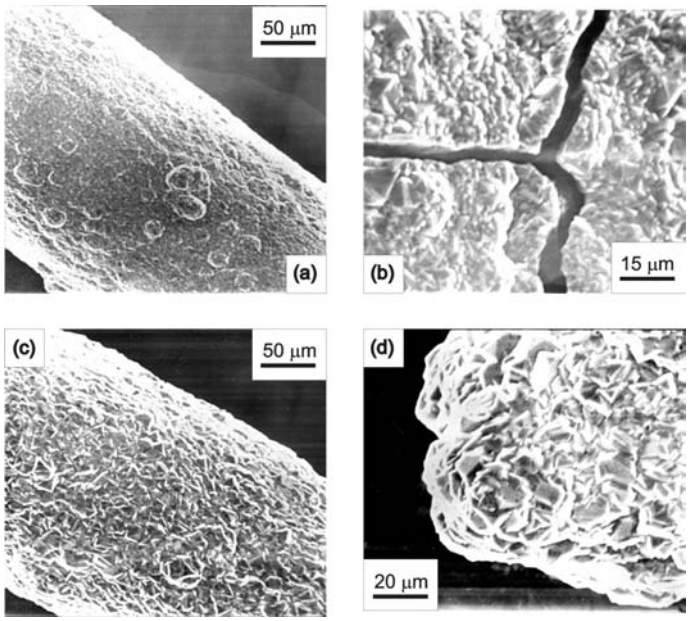

Fig. 1. Diamond fiber with a Cu core: diamond nodular morphology on an abraded substrate (a); crack in the coating grown on the abraded, unseeded substrate(b); diamond morphology on the abraded and seeded substrate (c); detail of the nodular end of the fiber shown in Fig. 1c (d).

sentatives of deposition on a Cu substrate abraded only with emery paper. This nodular morphology was previously observed in diamond coatings obtained by the hfCVD method on a thin Cu wire (50 μm) manually abraded,[1] with the addition of diamond grit (1–3 μm).[2–4] The samples obtained after abrading with a mixture of powders (Mo, W and diamond) are presented in Figs. 1c and 1d; the characteristic nodular morphology, composed of faceted diamond crystallites in Fig. 1c, and a detail of the fiber nodular end in Fig. 1d. Such a pretreatment procedure was aimed at improving the deposition of diamond on Cu. Rapid formation of the carbide layer and the extremely high diamond nucleation density on molybdenum,[11] as well as our positive experience,[10] were the reasons for choosing Mo as a component in the seeding mixture. Including W in the seeding mixture could positively affect the adhesion of the diamond deposit, as tungsten carbide has the lowest thermal expansion coefficient of all refractory metal carbides.[12] Diamond crystallites constitute an important component (sometimes the only one) of seeding powders, as they meet all the requirements (topochemical, geometrical) for diamond nucleation and growth. A gradual increase of the power to 150 W until a 9-h deposition period resulted in the diamond coatings seen in Figs. 1c and 1d: the particles of the seeding mixture helped the diamond crystallite habit of the coating to be restored, although nodules in the layer seemed to be unavoidable. One of the possible causes of this nodular morphology might be

the active participation of the Cu substrate in the diamond coating deposition, due to the similarity of the temperatures of Cu melting and diamond deposition. Hence, in such an experimental set-up, deposition onto a shorter substrate or pulling the substrate out of the active helix by some 1–2 mm is suggested, as the hottest temperature zone is just at the centre of the tantalum helix.

A similar pretreatment procedure of a flat Cu substrate, *i.e.*, abrading/seeding with diamond powder, annealing, melting the surface, and successive diamond film growth by the hfCVD method,[13] corroborated the necessity of providing the Cu surface with reactive germs, and the importance of the careful control of the activating filament power. The micro-sized diamond used for manual abrasion of the substrate surface, as well as a powder mixture of micro-sized refractory metal (Ti) and nano-sized diamond used for ultrasonication, enhanced very well the nucleation density and diamond film growth, respectively.[14]

Diamond coatings on the SiC fiber grown at a filament power of 150 W after deposition for 16 h are shown in Figs. 2a–2d. A top-view of the diamond-coated fiber is shown in Fig. 2a. The characteristic morphology can be seen in Fig. 2b. A native fracture of the same sample, presenting an about 20 μm thick diamond coating, is given in Fig. 2c. A detailed view of the fracture is presented in Fig. 2d. Diamond deposition on the SiC fiber developed well with an activating filament power up to 150 W. The SiC fiber[15] (diameter 142 μm) consists of a car-

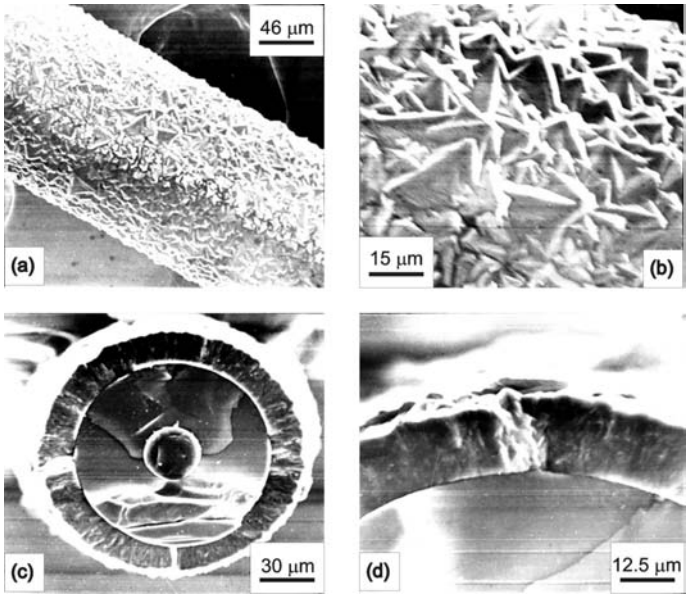

Fig. 2. Diamond fiber with a SiC core: top view of the diamond coated SiC fiber (a); detail of the morphology (b); native fracture showing an about 20 μm thick diamond coating (c); detail of the native fracture of the same sample (d).

bon core (33 μm) coated with β-SiC and a thin (about 3 μm) pyrocarbon overcoat. During the deposition experiment, the pyrocarbon layer was etched by atomic hydrogen and deposition of diamond occurred readily on the bare silicon carbide. No cracks or gaps can be seen in micrographs, evidencing diamond coating on the SiC fiber, Figs. 2a–2d. Adhesion of the diamond coating–SiC fiber system is very good because thermal expansion coefficients of diamond and SiC are quite similar.[12] Diamond-coated SiC fibers incorporated into a metal matrix composite (Ti–6Al–4V) should transfer their stiffness to the composite and enable weight savings compared to the existing reinforcement fibers.[5]

Diamond deposition on W and Mo wire substrates was performed with a filament activating power of about 240 W. The micrographs of diamond-coated W substrates of different diameters, obtained during 9 h deposition are presented in Figs. 3a–3d. Continuous and uniform coatings composed of euchedral crystallites obtained on the thick (0.5 mm) and thin (0.025 mm) wire substrates can be seen in Figs. 3a and 3c. During the course of the deposition, a common chemical compound with carbon from the working atmosphere, *i.e.*, carbide was formed, which is very favorable for diamond nucleation and growth. Due to the rather low difference in the thermal expansion coefficients of tungsten carbide and diamond,[12] the thermal stress was low, which also contributes to a good coating–substrate adhesion. In order to gain an inside view of the diamond fiber

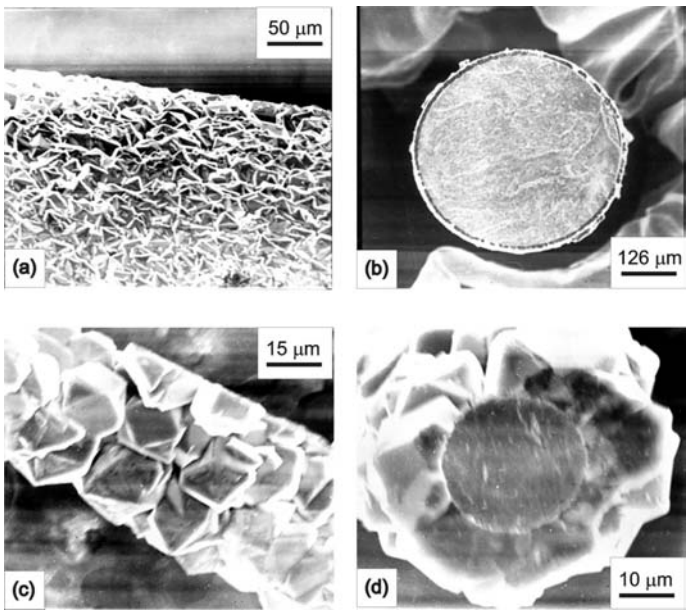

Fig. 3. Diamond fiber with a W core: morphology of the continuous and homogeneous coating on the thick (0.5 mm) W core (a); cross section of the same sample (b); top view of the thin W-cored (0.025 mm) diamond fiber (c); native fracture of the same sample (d).

structure, transversal sections were made. Both cross sections of the thick W-cored diamond fiber, in Fig. 3b, and the native fracture of the thin W-cored diamond fiber, in Fig. 3d, appear neat without cracking and chipping, thus proving the usability of tungsten in various technological applications: thermocouple probe,[7] flow controller micronozzle,[8] X-ray microdosimeter,[16] *etc*.

Diamond coatings on the Mo wire substrates of diameters 0.5 mm and 0.1 mm, grown during 9 h deposition, are given in Figs. 4a–4d. The morphology of the continuous coating on the 0.5 mm diameter Mo wire is presented in Fig. 4a, and the cross section of the same sample can be seen in Fig. 4b. The top view of the coating deposited on the 0.1 mm diameter Mo substrate is shown in Fig. 4c. The native fracture of the same sample, seen in Fig. 4d, displays a stratified appearance: the diamond layer (at the top), an interlayer (carbide) and the initial material, molybdenum, in the fiber core. A coating fragment next to the fiber fracture indicates the condition of the fiber, *i.e.*, the existence of stress in the shown specimen. As was previously observed,[10] diamond deposition on Mo can be realized without any surface pretreatment, *i.e.*, without the introduction or removal of existing defects, without seeding or application of some physical/ /chemical agent. The coatings obtained on the cylindrical substrates are counterparts of the ones obtained on planar substrates in terms of morphology, structure and characteristics. The coatings are continuous and homogeneous, Figs. 4a and

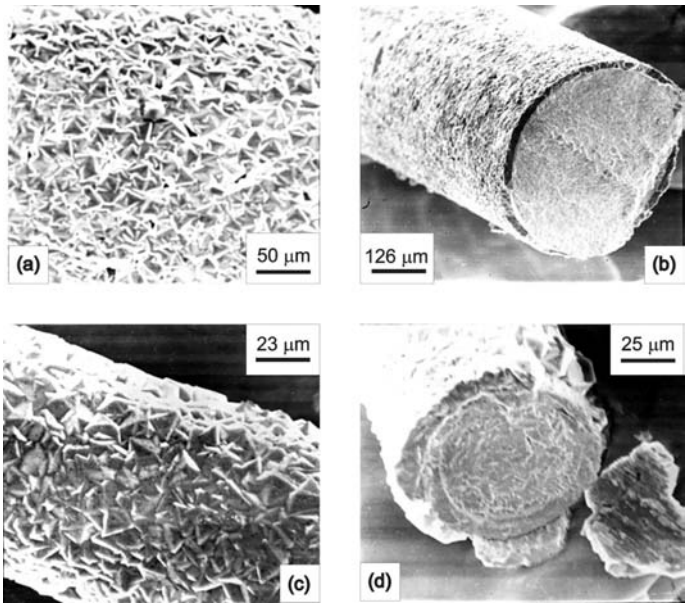

Fig. 4. Diamond fiber with a Mo core: morphology on the thick (0.5 mm) wire substrate (a); cross section of the same sample (b); top view of the coating deposited on the thin (0.1 mm) wire substrate (c); native fracture of the same sample showing a stratified fiber structure (d).

4c. In the native fracture of the thin fiber sample, Fig. 4d, the course of the deposition process can be easily seen: first the formation of a carbide layer and then subsequently diamond growth. Strong bonding forces between the substrate and the grown carbide layer as well as ones within the polycrystalline diamond layer can be assumed, since no gaps were visible. On the contrary, a gap between the layers of carbide and diamond could be discerned. The compact coating splinter observed when fracturing the sample, Fig. 4d, indicates the existence of the thermal stress in the coating and evidences a sporadic detachment of the coating from the substrate. It is possible to obtain a stress-free cylindrical diamond coating grown on Mo by making it thick compared to the substrate and then to make it free-standing, *i.e.*, to remove the substrate (by dissolution in hot acids). Subsequently, it can be brazed onto another part for further application.[9]

CONCLUSIONS

Diamond coatings on thin cylindrical substrates, required in numerous specific applications, were achieved on several different materials. It is found that the substrates exert a considerable influence on the deposited coatings. Chemical reactivity of the substrate material is the main prerequisite to begin diamond deposition without any surface pretreatment. In cases when the substrate material (W, Mo) reacts with the working deposition atmosphere, a common chemical compound, carbide, is formed, that enables a gradual, continuous transition from one crystal lattice to the other. Good adhesion and durability of the substrate––coating interface exist whenever strong chemical bonds are formed, which can prevail over debonding forces. In the case when the substrate material (Cu) does not react with the working atmosphere, bonding between the substrate and the coating was weak and, consequently, adhesion was poor.

The thermophysical characteristics of the substrate material are very important as diamond deposition occurs at high temperatures. The thermal expansion coefficients of the substrate (*i.e.*, of its grown carbide) and the coating should be as similar as possible in order to minimize the thermal stress that occurs upon cooling from working to room temperature. Thus, in the series of examined materials, the thermal stress decreases in the order Cu, Mo, SiC and W.

In deposition on the thin copper wire, low power deposition as well as the special pretreatment of the substrate surface, reactive seeds added to the surface, proved it is possible to obtain continuous, adhered and well faceted diamond coating on a chemically inert substrate.

Acknowledgements. This work was financially supported by the Ministry of science and technological development of the Republic of Serbia, under projects No. 142065 and 142067.

ИЗВОД

ДЕПОЗИЦИЈА ДИЈАМАНТА НА ТАНКИМ ЦИЛИНДРИЧНИМ СУПСТРАТИМА

ГОРДАНА С. РИСТИЋ[1], ЖАРКО Д. БОГДАНОВ[1], МИЛАН С. ТРТИЦА[1] и ШЋЕПАН С. МИЉАНИЋ[1,2]

[1]ВИНЧА Институт за нуклеарне науке, п.пр. 522, 11001 Београд и [2]Факултет за физичку хемију, Универзитет у Београду, п.пр. 137, 11001 Београд

Дијамантске превлаке депоноване су методом усијаног влакна ХДП на различитим цилиндричним супстратима (Cu, SiC, W и Mo). Добијене су непрекидне, приањајуће и лепо фасетиране дијамантске превлаке на Cu- жици, коришћењем специјалне предобраде смешом прахова рефракторних метала и дијаманта, уз брижљиву контролу депозиције при мањој снази, тј. нижем степену усијања влакна. Депозиција дијаманта на SiC влакну дала је непрекидне и уједначене превлаке већ само погодним избором снаге активирајућег влакна. Уједначене, равномерне и еухедралне дијамантске превлаке на W и на Mo жици, добијене при већој снази усијаног влакна, потврдиле су погодност рефракторних метала као супстрата за депозицију дијаманта ХДП техником. Карактеризација добијених превлака урађена је скенирајућом електронском микроскопијом (SEM). Добијени резултати су упоређени са подацима из литературе. Разлике су продискутоване с обзиром на хемијску природу супстрата и његове термофизичке карактеристике.

(Примљено 20. априла, ревидирано 28. септембра 2010)

REFERENCES

1. P. W. May, C. A. Rego, R. M. Thomas, M. N. R. Ashfold, K. N. Rosser, P. G. Partridge, N. M. Everitt, in *Proceedings of the 3rd Int. Symp. Diamond Mater.*, J. P. Dismukes, K. V. Ravi, Eds., Honolulu, HI, USA, 1993, Electrochem. Soc., Pennington, N.J., 1993, p. 1036
2. P. W. May, C. A. Rego, R. M. Thomas, M. N. R. Ashfold, K. N. Rosser, P. G. Partridge, N. M. Everitt, *J. Mater. Sci. Lett.* **13** (1994) 247
3. P. W. May, C. A. Rego, R. M. Thomas, M. N. R. Ashfold, K. N. Rosser, N. M. Everitt, *Diam. Relat. Mater.* **3** (1994) 810
4. P. W. May, C. A. Rego, M. N. R. Ashfold, K. N. Rosser, N. M. Everitt, P. G. Partridge, Q. S. Chia, G. Lu, in *Advances in New Diamond Science and Technology*, S. Saito, N. Fujimori, O. Fukunaga, M. Kamo, K. Kobashi, M. Yoshikawa, Eds., MYU, Tokyo, Japan, 1994, p. 211
5. E. D. Nicholson, J. E. Field, P. G. Partridge, M. N. R. Ashfold, *Mater. Res. Symp. Proc.* **383** (1996) 101
6. V. I. Gorokhovsky, *Surf. Coat. Technol.* **194** (2005) 300
7. N. P. Smith, M. N. R. Ashfold, D. J. Smith, T. R. A. Pearce, *Diam. Relat. Mater.* **8** (1999) 956
8. S. Silva, M. C. Salvadori, K. Kawakita, M. T. Pereira, W. Rossi, M. Cattani, *Diam. Relat. Mater.* **11** (2002) 237
9. V. J. Trava-Airoldi, J. R. Moro, E. J. Corat, E. C. Goulart, A. P. Silva, N. F. Leite, *Surf. Coat. Technol.* **108–109** (1998) 437
10. G. S. Ristić, Ž. D. Bogdanov, S. Zec, N. Romčević, Z. Dohčević-Mitrović, Š. S. Miljanić, *Mater. Chem. Phys.* **80** (2003) 529
11. P. O. Joffreau, R. Haubner, B. Lux, *Int. J. Ref. Hard Mater.* **7** (1988) 186
12. H. Liu, D. S. Dandy, *Diamond Chemical Vapor Deposition: Nucleation and Early Growth Stages*, Noyes Publications, Park Ridge, NJ, USA, 1995

13. M. Ece, B. Oral, J. Patscheider, *Diam. Relat. Mater.* **5** (1996) 211
14. J. G. Buijnsters, L. Vazquez, J. J. der Meulen, *Diam. Relat. Mater.* **18** (2009) 1239
15. Specialty Materials, Inc., http://www.specmaterials.com (accessed in March 2010)
16. C. Manfredotti, G. Apostolo, F. Fizzotti, A. Lo Giudice, M. Morando, R. Pignolo, P. Polesello, M. Truccato, E. Vittone, U. Nastasi, *Diam. Relat. Mater.* **7** (1998) 523.

Journal of the Serbian Chemical Society
JSCS-info@shd.org.rs • www.shd.org.rs/JSCS
J. Serb. Chem. Soc. *76* (3) 417–423 (2011)
JSCS–4129
UDC 66–911.4+66–987:536.63:547–039.7
Short communication

SHORT COMMUNICATION

Prediction of high pressure liquid heat capacities of organic compounds by a group contribution method

JOVAN D. JOVANOVIĆ[1], ANĐELA B. KNEŽEVIĆ-STEVANOVIĆ[2] and DUŠAN K. GROZDANIĆ[1]*

[1]*Chemical Engineering Department, Faculty of Technology and Metallurgy, University of Belgrade, Karnegijeva 4, 11000 Belgrade, Serbia and* [2]*Metro Vancouver, 4330 Kingsway, Burnaby, British Columbia, V5H 4G8, Canada*

(Received 1 May, revised 1 September 2010)

Abstract: A new method for estimating high pressure liquid heat capacities based on molecular structure and group contribution is proposed. A common set of structural groups was employed. The method was developed using 67 sets of 43 organic compounds with 3449 experimental heat capacity data. A small number of measured compounds, data points per compound and other comparable methods were observed. This is a simple first-order approximation with acceptable accuracy of 2.55 %.

Keywords: high pressure heat capacity; prediction; group contribution; liquid; pure compound.

INTRODUCTION

Heat capacity is a basic thermodynamic property, like a heat of vaporization.[1] It is used in chemical engineering calculations to obtain the differences in thermodynamic functions between two different temperatures. The heat capacity of liquids is often necessary information for chemical engineering calculation and design.[2,3] Experimental liquid heat capacity data are available for many substances,[4–7] but mostly at the saturation line, at atmospheric or low pressures. In addition, for only a small number of compounds do the extant data cover the temperature interval from melting point up to the critical temperature. A wide pressure interval of experimental data is even harder to find and data sets with both intervals are very rare.[8] Under such circumstances, prediction methods are an obvious choice for providing liquid heat capacities for compounds for which there is a

* Corresponding author. E-mail: dule@tmf.bg.ac.rs
doi: 2298/JSC100511031J

complete lack of data or for which data are available only over limited temperature and/or pressure intervals.

Many methods for predicting liquid heat capacity data based only on temperature dependence[9–39] have been proposed. In this article, a new method is proposed with both temperature and pressure dependences.

METHOD DEVELOPMENT

Group contribution methods are among the simplest and easiest methods that apply techniques developed and tested for the estimation of various thermophysical properties. The aim of this article was to develop a simple group contribution estimation method using a consistent set of molecular groups that would cover a wide variety of organic compounds. We used the first order approximation (part of the Lydersen groups) because of insufficiency of experimental data and therefore inability to obtain reliable contributions for interactions between the groups and structurally dependent contributions. On the other hand, higher order contributions lead to significantly more complex estimation methods. After consideration and examination of many functional forms, as well as temperature and pressure influences, the following expression was developed:

$$c_{\mathrm{pl}} = T^{0.5}\sum \Delta c + A + BT + CpT \tag{1}$$

The linear least squares method was used to calculate the group contributions Δc, and the adjustable parameters A, B, and C in Eq. (1). The minimized objective function has the following form:

$$F = \sum_{i=1}^{N}\left(c_{\mathrm{pl,exp},i} - c_{\mathrm{pl,cal},i}\right)^2 \rightarrow \min \tag{2}$$

Finally, the proposed equation for liquid heat capacity estimation at pressures up to 300 MPa and at temperatures up to 0.9 T_{r} is as follows:

$$c_{\mathrm{pl}} = T^{0.5}\sum \Delta c + 136.38 + 0.45419\,T - 0.00029936\,pT \tag{3}$$

Overall percent errors were calculated as follows:

$$P_{\mathrm{av}} = \frac{\sum_{i=1}^{N} n_i AAPE_i}{\sum_{i=1}^{N} n_i} \tag{4}$$

$$AAPE = 100\sum_{i=1}^{n}\frac{\left|c_{\mathrm{pl,exp},i} - c_{\mathrm{pl,cal},i}\right|}{c_{\mathrm{pl,exp},i}} \tag{5}$$

The literature experimental data used for the development of the method, covering 3449 data points in 67 data sets for 43 organic compounds, are given in Supplementary material.

RESULTS AND DISCUSSION

An extensive evaluation of the proposed method was conducted by comparing the estimated heat capacities with raw experimental data from the literature. The calculated group contribution values are presented in Table I. The proposed method is linear and an extrapolation can be made, however it fails in the vicinity

of the critical point where the heat capacity rises quickly and becomes indefinite at the critical point. For improvement and further development of the proposed method, more experimental data (more compounds and broad temperature and pressure intervals, particularly near critical temperature) are required.

Table I. Group contributions

Group	Δc
CH_3–	–5.6218
–CH_2–	1.7236
>CH–	8.7826
>C<	15.817
–CH_2– (aromatic)	–1.2858
>CH– (aromatic)	5.7056
F–	–6.3816
Cl–	–6.1657
CN–	–5.7647
Br–	–6.6308
OH–	–3.0054
NH_2–	–7.2171
Cyclic correction	–16.325

The results of the prediction for the liquid heat capacities are presented in Table I-S (Supplementary material). In the absence of any predictive method for high pressures, the results of the proposed method are presented with the results of the method developed by Kolská [24] for moderate pressures. The table includes a list of chemical compounds (literature references are given in column "Ref.", Table I-S), number of experimental points per set n (the second number in the fourth column is the number of data used in correlation – at pressures up to 300 MPa and at temperatures up to 0.9 T_r), temperature ranges (minimal T_{min} and maximal T_{max} temperature per set), critical temperatures T_c, pressure ranges (minimal p_{min} and maximal p_{max} pressure per set), and the average percent errors per set for both methods. As can be seen from Table I-S, the proposed method with an overall accuracy of 2.55 % has very wide applications.

Training and verification sets are not necessary in this case, since the new model is a group contribution model. The regression procedure of group contribution models should include as many experimental values as possible to cover the widest application and give safe extrapolations.[11]

CONCLUSIONS

A group contribution method for estimating high pressure liquid heat capacity, where the group identification was defined by Lydersen, has been proposed. This method provides satisfactory correlation accuracy over broad temperature and pressure ranges. The average percent error obtained for all investigated com-

pounds is around 2.5 %. For further method development, additional experimental data are necessary.

SUPPLEMENTARY MATERIAL

The literature experimental data used for the development of the method, covering 3449 data points in 67 data sets for 43 organic compounds, are available electronically at http:// //www.shd.org.rs/JSCS/, or from the corresponding author on request.

Acknowledgements. This work was supported by a grant from the Research Fund of the Republic of Serbia (Project No. 172063), Belgrade and the Faculty of Technology and Metallurgy, University of Belgrade.

NOMENCLATURE

c_{pl}	Liquid heat capacity, J mol^{-1} K^{-1}
$c_{pl,exp}$	Experimental liquid heat capacity, J mol^{-1} K^{-1}
$c_{pl,cal}$	Calculated liquid heat capacity, J mol^{-1} K^{-1}
T	Temperature, K
p	Pressure, MPa
A,B,C	Adjustable method parameters
Δc	Group contribution
$AAPE$	Average percent error, %
P_{av}	Overall percent error, %
n	Number of experimental data points
N	Number of compounds
T_{max}	Maximal temperature value per set, K
T_{min}	Minimal temperature value per set, K
p_{max}	Maximal pressure value per set, MPa
p_{min}	Minimal pressure value per set, MPa
T_c	Critical temperature, K
T_r	Reduced temperature T/T_c

ИЗВОД

ПРЕДСКАЗИВАЊЕ ТОПЛОТНОГ КАПАЦИТЕТА ОРГАНСКИХ ТЕЧНОСТИ НА ВИСОКОМ ПРИТИСКУ ПОМОЋУ МЕТОДЕ ДОПРИНОСА ГРУПА

ЈОВАН Д. ЈОВАНОВИЋ[1], АЊЕЛА Б. КНЕЖЕВИЋ-СТЕВАНОВИЋ[2] и ДУШАН К. ГРОЗДАНИЋ[1]

[1]*Технолошко-металуршки факултет, Универзитет у Београду, Карнегијева 4, 11000 Београд и*
[2]*Metro Vancouver, 4330 Kingsway, Burnaby, British Columbia, V5H 4G8, Canada*

Предложен је нови метод за предсказивање вредности изобарског топлотног капацитета течности на високом притиску на основу молекулске структуре супстанце и вредности доприноса група у молекулу. Метод је развијен коришћењем 67 сетова експерименталних података за 43 различите органске супстанце са укупно 3449 података. Постојање експерименталних података за мали број различитих супстанци узроковао је ограничен број доприноса група. Предложени модел даје прихватљиво средње процентуално одступање од 2,55 %. У литератури није пронађен ни један метод за предсказивање вредности изобарског топлотног капацитета органских течности на високом притиску.

(Примљено 11. маја, ревидирано 1. септембра 2010)

REFERENCES

1. J. D. Jovanović, D. K. Grozdanić, *Korean J. Chem. Eng.* **25** (2008) 1499
2. O. Kwon, S. Ryou, W. Sung, *Korean J. Chem. Eng.* **18** (2001) 88
3. K.-S. Kim, J.-W. Lee, J.-S. Kim, H. Lee, *Korean J. Chem. Eng.* **20** (2003) 762
4. M. Palczewska-Tulińska, *Solid and Liquid Heat Capacity Data Collection: C_1–C_{33} Compounds*, Dechema, Frankfurt am Main, Germany, 1997
5. N. B. Vargaftik, Y. K. Vinogradov, *Handbook of Physical Properties of Liquids and Gases, Pure Substances and Mixtures*, Beggel House, New York, USA, 1996
6. M. Zábranský, V. Růžička, V. Majer, E. S. Domalski, *Heat Capacity of Liquids, Critical Review and Recommended Values*, Monograph No. 6, Vols. I and II, American Chemical Society, Washington D.C., USA, 1996
7. M. Zábranský, V. Růžička, E. S. Domalski, *J. Phys. Chem. Ref. Data* **30** (2002) 1199
8. J. D. Jovanović, A. B. Knežević-Stevanović, D. K. Grozdanić, *J. Taiwan Inst. Chem. Eng.* **40** (2008) 105
9. A. G. Ahmedov, M. F. Efendiev, B. M. Mirzoev, *Izv. Vyss. Uchebn. Zaved., Neft i Gaz* **30** (1987) 62 (in Russian)
10. A.-J. Briard, M. Bouroukba, D. Petitjean, M. Dirand, *J. Chem. Eng. Data* **48** (2003) 1508
11. R. Ceriani, R. Gani, A. J. A. Meirelles, *Fluid Phase Equilib.* **283** (2009) 49
12. J. S. Chickos, D. G. Hesse, J. F. Liebman, *Struct. Chem.* **4** (1993) 261
13. M. Chorążewski, P. Góralski, M. Tkaczyk, *J. Chem. Eng. Data* **50** (2005) 619
14. C. F. Chueh, A. C. Swanson, *Chem. Eng. Prog.* **69** (1973) 83
15. C. F. Chueh, A. C. Swanson, *Can. J. Chem. Eng.* **51** (1973) 596
16. S. Ernst, M. Chorążewski, M. Tkaczyk, P. Góralski, *Fluid Phase Equilib.* **174** (2000) 33
17. R. Fuchs, *J. Chem. Thermodyn.* **11** (1979) 959
18. R. Fuchs, *Can. J. Chem.* **58** (1980) 2305
19. R. L. Gardas, J. A. P. Coutinho, *Ind. Eng. Chem. Res* **47** (2008) 5751
20. P. Góralski, M. Tkaczyk, M. Chorążewski, *J. Chem. Eng. Data* **48** (2003) 492
21. A. A. Ivanova, V. A. Palyulin, A. N. Zefirov, N. S. Zefirov, *Russ. J. Org. Chem.* **40** (2004) 644
22. Y. Jin, B. Wunderlich, *J. Chem. Eng. Data* **35** (1990) 101
23. A. I. Johnson, C.-J. Huang, *Can. J. Technol.* **33** (1955) 421
24. Z. Kolská, J. Kukal, M. Zábranský, V. Růžička Jr. *Ind. Eng. Chem. Res.* **47** (2008) 2075
25. M. Luria, S. W. Benson, *J. Chem. Eng. Data* **22** (1977) 90
26. J. J. Marano, G. D. Holder, *Ind. Eng. Chem. Res.* **36** (1997) 2399
27. F. A. Missenard, *Comp. Rend.* **260** (1965) 5521
28. R. A. Mustafaev, *Izv. Vyss. Uchebn. Zaved., Neft i Gaz* **12** (1968) 75 (in Russian)
29. R. A. Mustafaev, S. I. Tagiev, T. D. Alieva, T. A. Stepanova, V. G. Krivcov, *Izv. Vyss. Uchebn. Zaved., Neft i Gaz* **30** (1987) 55 (in Russian)
30. V. Pachaiyappan, S. H. Ibrahim, N. R. Kuloor, *Chem. Eng.* **74** (1967) 241
31. J. C. Phillips, M. M. Mattamal, *J. Chem. Eng. Data* **21** (1976) 228
32. V. Růžička Jr., E. S. Domalski, *J. Phys. Chem. Ref. Data* **22** (1993) 597
33. V. Růžička Jr., E. S. Domalski, *J. Phys. Chem. Ref. Data* **22** (1993) 619
34. R. Shaw, *J. Chem. Eng. Data* **14** (1969) 461
35. I. Shehatta, *Thermochim. Acta* **213** (1993) 1
36. M. J. van Bommel, H. A. J. Oonk, J. C. van Miltenburg, *J. Chem. Eng. Data* **49** (2004) 1036

37. J. C. van Miltenburg, G. J. K. van der Berg, *J. Chem. Eng. Data* **49** (2004) 735
38. M. Zábranský, V. Růžička Jr., *J. Phys. Chem. Ref. Data* **33** (2004) 1071
39. M. Zábranský, V. Růžička Jr., *J. Phys. Chem. Ref. Data* **34** (2005) 39
40. R. Hykrda, J. Y. Coxam, V. Majer, *Int. J. Thermophys.* **25** (2004) 1677
41. H. Wirbser, G. Brauning, J. Gurtner, G. Ernst, *J. Chem. Thermodyn.* **24** (1992) 761
42. G. Ernst, J. Gurtner, H. Wirbser, *J. Chem. Thermodyn.* **29** (1997) 1113
43. H. Wirbser, G. Brauning, G. Ernst, *J. Chem. Thermodyn.* **24** (1992) 783
44. S. K. Garg, T. S. Banipal, J. C. Ahluwalia, *J. Chem. Thermodyn.* **25** (1993) 57
45. Z. I. Zaripov, S. A. Burtsev, A. V. Gavrilov, G. K. Mukhamedzyanov, *High Temp.* **42** (2004) 314
46. Ya. M. Naziev, M. M. Bashirov, Yu. A. Badalov, *Inzh.-Fiz. Zh.* **51** (1986) 789
47. M. Fulem, K. Ruzicka, V. Ruzicka, *Thermochim. Acta* **382** (2002) 119
48. Ya. M. Naziev, M. M. Bashirov, *Teplofiz. Visok. Temp.* **26** (1988) 58
49. Ya. M. Naziev, M. M. Bashirov, Yu. A. Badalov, *Inzh.-Fiz. Zh.* **51** (1986) 998
50. M. K. Johnson, H. Sato, A. G. Williamson, P. T. Eubank, *J. Chem. Eng. Data* **35** (1990) 101
51. Ya. M. Naziev, M. M. Bashirov, M. A. Talybov, *Zh. Prik. Khim.* **65** (1992) 2490
52. S. O. Guseinov, A. A. Mirzaliev, Sh. G. Shakhmuradov, *Izv. Vyssh. Uchebn. Zaved., Neft i Gaz* **31** (1988) 13 (in Russian)
53. I. Czarnota, *J. Chem. Thermodyn.* **20** (1988) 457
54. I. Czarnota, *J. Chem. Thermodyn.* **30** (1998) 291
55. I. Drehner, *J. Chem. Thermodyn.* **11** (1979) 993
56. I. Czarnota, *Bull. Acad. Pol. Sci. Ser. Sci. Chim.* **28** (1980) 651
57. M. Oguni, K. Watanabe, T. Matsuo, H. Suga, S. Seki, *Bull. Chem. Soc. Japan* **55** (1982) 77
58. T. S. Akhundov, C.I. Sultanov, *Izv. Vyssh. Uchebn. Zaved., Neft i Gaz* **17** (1974) 72 (in Russian)
59. I. Czarnota, *J. Chem. Thermodynamics* **23** (1991) 25
60. T. S. Akhundov, F. G. Abdullaev, R. T. Akhundov, A. A. Guseinov, N. M. Morduhaev, *Izv. Vyssh. Uchebn. Zaved., Neft i Gaz* **29** (1986) 56 (in Russian)
61. L. I. Safir, A. A. Gerasimov, B. A. Grigor'ev, *Izv. Vyssh. Uchebn. Zaved., Neft i Gaz* **18** (1975) 61 (in Russian)
62. T. Banipal, S. Garg, C. Ahluwalia, *J. Chem. Thermodyn.* **23** (1991) 923
63. I. Czarnota, *J. Chem. Thermodyn.* **25** (1993) 639
64. M. A. Kuznecov, V. E. Harin, A. A. Gerasimov, B. A. Grigor'ev, *Izv. Vyssh. Uchebn. Zaved., Neft i Gaz* **31** (1988) 49 (in Russian)
65. S. O. Guseinov, A. A. Mirzaliev, *Izv. Vyssh. Uchebn. Zaved., Neft i Gaz* **28** (1985) 58 (in Russian)
66. T. S. Akhundov, C. I. Sultanov, *Izv. Vyssh. Uchebn. Zaved., Neft i Gaz* **18** (1975) 74 (in Russian)
67. T. S. Akhundov, F. G. Abdullaev, R. T. Akhundov, A. A. Guseinov, *Izv. Vyssh. Uchebn. Zaved., Neft i Gaz* **29** (1986) 78 (in Russian)
68. S. O. Guseinov, A. A. Mirzaliev, *Izv. Vyssh. Uchebn. Zaved., Neft i Gaz* **27** (1984) 41 (in Russian)
69. D. Bessieres, H. Saint-Guirons, J.-L. Daridon, J.-Y. Coxam, *Meas. Sci. Technol.* **11** (2000) N69

70. A. A. Gerasimov, B. A. Grigor'ev, *Izv. Vyssh. Uchebn. Zaved., Neft i Gaz* **21** (1978) 46 (in Russian)
71. Z. I. Zaripov, S. A .Burtsev, A. V. Gavrilov, G. K. Mukhamedzyanov, *Theor. Found. Chem. Eng*. **36** (2002) 400
72. I. Czarnota, *J. Chem. Thermodyn.* **25** (1993) 355
73. V. E. Harin, B. A. Grigoriev, A. A. Gerasimov, J. L. Rastorguev, *Izv. Vyss. Uchebn. Zaved., Neft i Gaz* **28** (1985) 54 (in Russian)
74. T. S. Akhundov, R. A. Eksaev, *Izv. Vyssh. Uchebn. Zaved. Neft i Gaz* **16** (1973) 68 (in Russian)
75. S. N. Nefedov, L. P. Filippov, *Izv. Vyssh. Uchebn. Zaved., Neft i Gaz* **23** (1980) 51 (in Russian)
76. V. M. Shulga, F. G. Eldarov, Y. A. Atanov, A. A. Kuyumchev, *Int. J. Thermophys.* **7** (1986) 1147
77. L. Sun, J. Venart, R. Prasad, *Int. J. Thermophys.* **23** (2002) 1487
78. D. Bessieres, H. Saint-Guirons, J.-L. Daridon, *J. Therm. Anal. Cal*. **62** (2000) 621.

J. Serb. Chem. Soc. 76 (3) S19–S22 (2011)

Journal of the Serbian Chemical Society
JSCS@tmf.bg.ac.rs • www.shd.org.rs/JSCS

Supplementary material

SUPPLEMENTARY MATERIAL TO

Prediction of high pressure liquid heat capacities of organic compounds by a group contribution method

JOVAN D. JOVANOVIĆ[1], ANĐELA B. KNEŽEVIĆ-STEVANOVIĆ[2] and DUŠAN K. GROZDANIĆ[1]*

[1]*Chemical Engineering Department, Faculty of Technology and Metallurgy, University of Belgrade, Karnegijeva 4, 11000 Belgrade, Serbia and* [2]*Metro Vancouver, 4330 Kingsway, Burnaby, British Columbia, V5H 4G8, Canada*

J. Serb. Chem. Soc. 76 (3) (2011) 417–423

*Corresponding author. E-mail: dule@tmf.bg.ac.rs

TABLE I-S. The literature experimental data used for correlation and prediction results

Compound	Ref.	n	T_{min} K	T_{max} K	T_c K	p_{min} MPa	p_{max} MPa	Kolská %	New %
1,1,1,2,3,3,3-Heptafluoropropane	40	62	223.150	283.150	375.900	1.100	20.000	10.20	2.27
1,1,1,2,3,3,3-Heptafluoropropane	41	46/30	273.150	333.150	375.900	0.600	15.000	8.08	2.15
1,1,1,2-Tetrafluoroethane	42	59/32	273.000	333.000	374.100	0.500	30.000	5.20	5.73
1,1,1,2-Tetrafluoroethane	41	52	223.150	283.150	374.100	0.750	18.200	4.18	4.85
1,1,2-Trichlorotrifluoroethane	43	77/49	288.150	423.150	487.300	0.600	30.000	4.83	2.79
1,2-Dimethybenzene	44	36	318.150	373.150	630.300	0.100	10.000	0.91	0.78
1,3-Dimethybenzene	44	36	318.150	373.150	617.000	0.100	10.000	2.96	1.51
1,4-Dimethybenzene	44	36	318.150	373.150	616.200	0.100	10.000	2.61	1.46
1-Bromobutane	45	21	298.000	348.000	569.400	0.098	147.000	9.18	6.61
1-Bromoheptane	45	21	298.000	348.000	647.400[a]	0.098	147.000	13.10	3.42
1-Bromohexane	45	21	298.000	348.000	623.900[a]	0.098	147.000	11.60	1.49
1-Butanol	46	58/52	321.050	472.950	562.000	0.100	50.000	5.32	5.96
1-Decanol	47	94	325.700	570.700	687.300	2.000	30.000	15.12	4.52
1-Decanol	48	79	304.050	522.950	687.300	0.100	50.000	6.46	2.84
1-Heptanol	47	94/91	325.700	560.700	632.600	2.000	30.000	15.04	4.17
1-Heptanol	48	77	303.350	522.150	632.600	0.100	50.000	8.08	2.51
1-Hexanol	47	110/103	325.700	540.700	610.300	1.500	30.000	12.31	3.66
1-Nonanol	49	78	303.100	522.450	670.700	0.100	50.000	7.09	2.47
1-Octanol	47	92	325.700	570.700	652.500	2.000	30.000	14.79	4.13
1-Octanol	49	77	303.200	523.150	652.500	0.100	50.000	7.66	2.46
2,2,4-Trimethylpentane	50	18/14	360.000	480.000	543.800	2.000	10.000	7.56	4.61
2-Methyl-1-propanol	51	65/53	300.650	471.150	547.700	0.100	50.000	10.07	6.08
2-Methylaniline	52	57	303.150	523.150	717.000	0.100	25.000	29.08	1.45
2-Methylbutane	53	35/18	288.800	299.100	460.400	0.100	280.300	15.41	5.62
2-Methylpentane	54	20/10	298.300	299.500	497.700	0.100	257.000	8.43	0.42
2-Propanol	55	27/14	323.150	423.150	508.300	4.760	30.000	8.87	6.56
3-Methyl-1-butanol	51	64/58	302.050	496.850	577.200	0.100	50.000	10.26	4.64
3-Methylaniline	52	57	303.150	523.150	709.100	0.100	25.000	29.21	1.75

TABLE I-S. Continued

Compound	Ref.	n	T_{min} K	T_{max} K	T_c K	p_{min} MPa	p_{max} MPa	Kolská %	New %
3-Methylpentane	56	8/3	298.950	299.250	504.600	0.101	227.778	15.00	5.08
3-Methylpentane	57	137	110.310	291.060	504.600	0.100	108.000	5.40	2.34
Benzene	58	86/48	302.550	505.150	562.100	5.000	25.000	4.09	2.18
Benzene	59	8	298.300	298.600	562.100	0.100	68.100	2.84	4.01
Benzene	46	50	322.050	489.350	562.100	0.100	50.000	2.85	1.65
Chlorobenzene	60	240/175	301.260	568.240	632.300	0.500	15.000	1.45	1.49
Cyclohexane	61	128/82	295.420	493.700	553.800	0.500	50.000	3.58	3.71
Decane	62	72	318.150	373.150	617.600	0.100	10.000	2.10	0.51
Decane	63	12	298.800	299.200	617.600	0.100	254.500	4.58	4.25
Decane	64	69/62	292.650	548.420	617.600	0.101	60.000	4.93	0.53
Ethyl cyanide	65	64/59	303.150	503.150	564.400	0.100	25.000	25.69	1.00
Ethylbenzene	66	72/57	301.560	554.060	617.200	8.000	25.000	3.99	1.53
Ethylbenzene	44	36	318.150	373.150	617.200	0.100	10.000	0.75	2.93
Ethylbenzene	50	33	350.000	550.000	617.200	2.000	20.000	2.55	1.16
Ethylcyclohexane	50	21/18	380.000	540.000	609.100	2.000	10.000	11.10	1.54
Fluorobenzene	67	146/86	301.760	501.290	560.100	0.500	15.000	2.37	1.71
Fluorotrichloromethane	43	52/44	288.150	423.150	471.200	0.600	30.000	8.24	3.92
Heptane	68	52/44	303.150	483.150	540.100	0.100	25.000	5.03	1.35
Heptane	64	47/37	292.490	485.080	540.100	5.000	60.000	6.65	1.27
Hexadecane	62	60	318.150	373.150	720.600	0.100	10.000	1.52	0.41
Hexane	69	73	313.150	373.150	507.900	0.100	100.000	5.32	0.73
Hexane	70	65/52	293.390	453.240	507.900	0.500	60.000	5.46	1.04
Hexane	68	42/32	303.150	443.150	507.900	5.000	25.000	4.01	1.67
Hexane	65	44/32	313.150	443.150	507.900	5.000	25.000	4.40	1.70
Hexane	49	57/44	308.350	447.150	507.900	0.100	50.000	1.78	3.27
Hexane	71	18	298.120	348.170	507.900	0.098	147.000	10.73	5.30
Methyl cyanide	68	63/53	303.150	483.150	548.000	0.100	25.000	6.57	3.54
Nonane	62	72	318.150	373.150	594.600	0.100	10.000	2.30	0.89

TABLE I-S. Continued

Compound	Ref.	*n*	T_{min} K	T_{max} K	T_c K	p_{min} MPa	p_{max} MPa	Kolská %	New %
Nonane	64	41/32	323.820	524.370	594.600	5.000	60.000	7.51	0.85
Octane	62	60	318.150	373.150	568.800	0.100	10.000	2.39	0.63
Octane	72	18/13	298.100	299.100	568.800	0.100	294.300	10.38	6.34
Octane	64	34/25	323.920	494.380	568.800	5.000	60.000	8.16	1.16
Pentane	73	24/18	293.450	412.760	469.800	10.000	60.000	5.65	0.92
Propyl cyanide	65	65	303.150	523.150	582.300	0.100	25.000	25.33	2.56
Toluene	74	193/128	302.870	531.860	591.700	0.500	25.000	2.54	2.50
Toluene	75	60/48	300.000	520.000	591.700	5.000	30.000	4.00	2.49
Toluene	76	80/40	255.500	401.500	591.700	3.500	291.100	2.43	7.00
Toluene	77	24	297.460	423.920	591.700	0.100	100.000	4.64	4.77
Tridecane	78	77	313.150	373.150	676.200	0.100	100.000	2.41	0.58
Overall	–	4072/3449	–	–	–	–	–	7.52	2.55

[a]Predicted values

Journal of the Serbian Chemical Society
JSCS-info@shd.org.rs • www.shd.org.rs/JSCS
J. Serb. Chem. Soc. 76 (3) 425–438 (2011)
JSCS–4130
UDC 632.125.000.57:631.461:547.536
Original scientific paper

Investigation of the bioremediation potential of aerobic zymogenous microorganisms in soil for crude oil biodegradation

TATJANA ŠOLEVIĆ[1*#], MILAN NOVAKOVIĆ[2], MILA ILIĆ[1#], MALIŠA ANTIĆ[1,3#], MIROSLAV M. VRVIĆ[1,2#] and BRANIMIR JOVANČIĆEVIĆ[1,2#]

[1]Department of Chemistry, Institute of Chemistry, Technology and Metallurgy, University of Belgrade, Njegoševa 12, P.O. Box 473, 11001 Belgrade, [2]Faculty of Chemistry, University of Belgrade, Studentski trg 12–16, P.O. Box 158, 11001 Belgrade and [3]Faculty of Agriculture, University of Belgrade, Nemanjina 6, 11081 Belgrade, Serbia

(Received 31 May, revised 27 September 2010)

Abstract: The bioremediation potential of the aerobic zymogenous microorganisms in soil (Danube alluvium, Pančevo, Serbia) for crude oil biodegradation was investigated. A mixture of paraffinic types of oils was used as the substrate. The laboratory experiment of the simulated oil biodegradation lasted 15, 30, 45, 60 and 75 days. In parallel, an experiment with a control sample was conducted. Extracts were isolated from the samples with chloroform in a separation funnel. From these extracts, the hydrocarbons were isolated by column chromatography and analyzed by gas chromatography–mass spectrometry (GC–MS). *n*-Alkanes, isoprenoids, phenanthrene and its derivatives with one and two methyl groups were quantitatively analyzed. The ability and efficiency of zymogenous microorganisms in soil for crude oil bioremediation was assessed by comparison between the composition of samples which were exposed to the microorganisms and the control sample. The investigated microorganisms showed the highest bioremediation potential in the biodegradation of *n*-alkanes and isoprenoids. A considerably high bioremediation potential was confirmed in the biodegradation of phenanthrene and methyl phenanthrenes. Low bioremediation potential of these microorganisms was proven in the case of polycyclic alkanes of the sterane and triterpane types and dimethyl phenanthrenes.

Keywords: bioremediation; soil zymogenous microorganisms; crude oil; hydrocarbons.

INTRODUCTION

Bioremediation is a process in which naturally occurring microorganisms, through their normal life functions, degrade or detoxify substances hazardous to

* Corresponding author. E-mail: tsolevic@chem.bg.ac.rs
# Serbian Chemical Society member.
doi: 10.2298/JSC100531033S

human health and/or the environment.[1] As a natural cleaning process, bioremediation has been proven to be efficient in the removal of chlorinated solvents,[2] polyaromatic hydrocarbons,[3] pesticides,[4] and even some heavy metals.[5]

Bioremediation of the environment polluted by crude oil relies on the fact that indigenous microbial population can biodegrade most of the hydrocarbons present in oils, mineralizing them into carbon dioxide and water.[6] Compared to physico-chemical methods, bioremediation offers an effective technology for the treatment of oil pollution because the majority of molecules in the crude oil and refined products are biodegradable and oil-degrading microorganisms are ubiquitous.[7] However, some compounds present in oils can not be biodegraded, or the process is incomplete,[8] which restricts the usage of the microbial degradation as a bioremediation technique in oil pollution clean-up.

The aim of the research described in this paper was to investigate the bioremediation potential in crude oil biodegradation of zymogenous microorganisms which were isolated from soil in the vicinity of the wastewater canal (Oil Refinery Pančevo, Serbia). The water in the canal originates mainly from industrial effluents from the oil refinery and a nitrogen plant and is significantly polluted with petroleum hydrocarbons.[9]

The possibility of using zymogenous microorganisms from the wastewater canal for bioremediation purposes has already been investigated in detail.[10,11] Based on an experiment of simulated biodegradation under laboratory conditions, it was proven that the dominant microorganisms from the surface water of the wastewater canal have degradable effects on petroleum hydrocarbons.[10] However, the biodegradation was restrained to the *n*-alkanes and isoprenoids, while polycyclic alkanes of sterane and triterpane type remained unchanged both in their abundance and distribution. The investigations performed under the laboratory conditions confirmed certain bioremediation potential of zymogenous microorganisms isolated from the waste water canal sludge for the degradation of oil.[11] Nevertheless, these microbial cultures showed lower potential for oil degradation than those isolated from the waters of the canal.

The present research represents a continuation of our investigations on the bioremediation potential of zymogenous microorganisms from the area of the wastewater canal. Considering the fact that some components of the crude oil can be sorbed on soil particles and remain in the environment for a long time,[12] potentially influencing the quality of ground- and surface waters, these results are expected to help in the prediction of possibilities of bioremediation as a natural attenuation process of petroleum pollutants over the whole wastewater canal area.

EXPERIMENTAL

In this study, a series of laboratory experiments was conducted aimed at evaluating the bioremediation potential of zymogenous microorganisms in soil for crude oil biodegradation. The soil samples were taken in the vicinity of the waste water channel polluted primarily by

oil pollutants, located in the south industrial zone of the city of Pančevo (Danube alluvium, Serbia), where the oil refinery is situated. This area was described in detail by Kaisarevic *et al*., 2009.[13] Considering the fact that the efficiency of bioremediation depends not only on the characteristics of the microbial community present, but also on the crude oil composition and the environmental conditions,[7] all experiments were conducted under conditions similar to those existing in the area from which the soil samples were taken.

In the consortium of zymogenous microorganisms isolated from the soil samples the most numerous were bacteria from the genus *Bacillus* and actynomycetes, and species from the fungal genus *Penicillium.*

In order to isolate these organisms under the aerobic conditions, 1 g of soil was first seeded in 100 cm^3 sterile mineral medium, at 25 °C. The medium was prepared by dissolving 1.5 g NH_4Cl; 0.55 g KH_2PO_4; 0.25 g Na_2HPO_4; 0.25 g $MgSO_4$ $7H_2O$ and 5 cm^3 of a TSS (Trace Salts Solution) mixture in 1 dm^3 of distilled water. The TSS mixture was composed of: 500 mg dm^{-3} $Na_2EDTA{\cdot}2H_2O$; 200 mg dm^{-3} $FeSO_4$ $7H_2O$; 30 mg dm^{-3} H_3BO_3; 20 mg dm^{-3} $CoCl_2$ $6H_2O$; 10 mg dm^{-3} $ZnSO_4$ $7H_2O$; 3 mg dm^{-3} $MnSO_4$ H_2O; 3 mg dm^{-3} Na_2MoO_4 $2H_2O$; 2 mg dm^{-3} $NiSO_4$ $7H_2O$; 1 mg dm^{-3} $CuCl_2$ $2H_2O$ and 1 cm^3 NaOH, c = 10 mol dm^{-3}.[14]

Aimed at assessing the biodegradation effect of the microorganisms on crude oil, the solution of the mineral medium with microorganisms was added with the crude oil in quantity of *ca*. 100 μL in 100 cm^3, to achieve a concentration similar to that existing at the location of the wastewater canal.[10] For the present study, a mixture of paraffinic type of oils was used, carefully selected to be very similar to the oil pollutant previously identified in the wastewater canal area. A control sample included the sterile mineral medium without microorganisms and added mixture of oils.

The experiments of the simulated biodegradation were stopped after 15, 30, 45, 60, and 75 days by sterilization at 120 °C for 25 min, while the control experiment was stopped after 75 days. Organic substance from in total 6 samples was extracted with chloroform (HPLC, J.T., USA) by shaking in a separation funnel. From these extracts, the hydrocarbons (saturated and aromatic) were isolated by column chromatography: the extracts were saponified with a 5 % solution of KOH in methanol, and neutralized (after standing overnight) with 10 % hydrochloric acid. The products were dissolved in a mixture of dichloromethane (containing 1 % methanol) and hexane (1:40), and separated by column chromatography on alumina and silica gel. The hydrocarbon fractions were eluted with hexane followed by dichloromethane. A detailed description of the analytical procedure was discussed in previous papers.[15,16]

Hydrocarbons were analyzed by the gas chromatography–mass spectrometry (GC–MS) techniques. An Agilent 7890N gas chromatograph fitted with a HP5-MS capillary column (temperature range: 80 °C for 0 min; then 2 °C min^{-1} to 300 °C and held for 20 min) with helium as the carrier gas (flow rate 1 cm^3 min^{-1}) was used. The GC was coupled to a Hewlett--Packard 5972 MSD operated at 70 eV in the 45–550 scan range. Preliminary analyzes of the investigated samples were conducted in the full scan mode. Detailed analyses of the target compounds were conducted in the single ion monitoring mode (SIM), comprising the following ion chromatograms: *m*/*z* 57 (*n*-alkanes and isoprenoids), 217 (steranes), 191 (triterpanes), 178 (phenanthrene), 192 (methyl-phenanthrenes) and 206 (dimethyl-phenanthrenes). The most relevant peaks were identified according to organic geochemical literature data (*e.g*., Peters *et al*.[8]), or based on the total mass spectra, using mass spectra databases (NIST/EPA/NIH mass spectral library NIST2000, Wiley/NBS registry of mass spectral data, 7th ed., electronic versions). *n*-Alkanes and the isoprenoids pristane and phytane were quantified against squalane (supplied by Supelco) as an internal standard. Phenanthrene, methyl-phenanthrenes and dime-

thyl-phenanthrenes were quantified against phenanthrene-*d*10 (supplied by Supelco) as an external standard.

RESULTS AND DISCUSSION

The bioremediation potential of zymogenous microorganisms isolated from soil was investigated under controlled laboratory conditions using a mixture of paraffinic types of oils as a substrate. The ability and efficiency of these microorganisms in crude oil bioremediation was assessed by comparison between the composition of samples which were exposed to the microorganisms and a control sample which was prepared and treated in the same way, but containing no microorganisms. This study was focused on the transformations in the contents and distributions of the target compounds in the fraction of hydrocarbons.

The total ion current (TIC) chromatogram of the hydrocarbon fraction from the control experiment and TIC chromatograms of the hydrocarbon fractions of the samples after 15 and 75 days of the biodegradation experiment are shown in Fig. 1 (TIC chromatograms of the hydrocarbon fractions isolated from the extracts of the control sample and from the samples during the biodegradation ex-

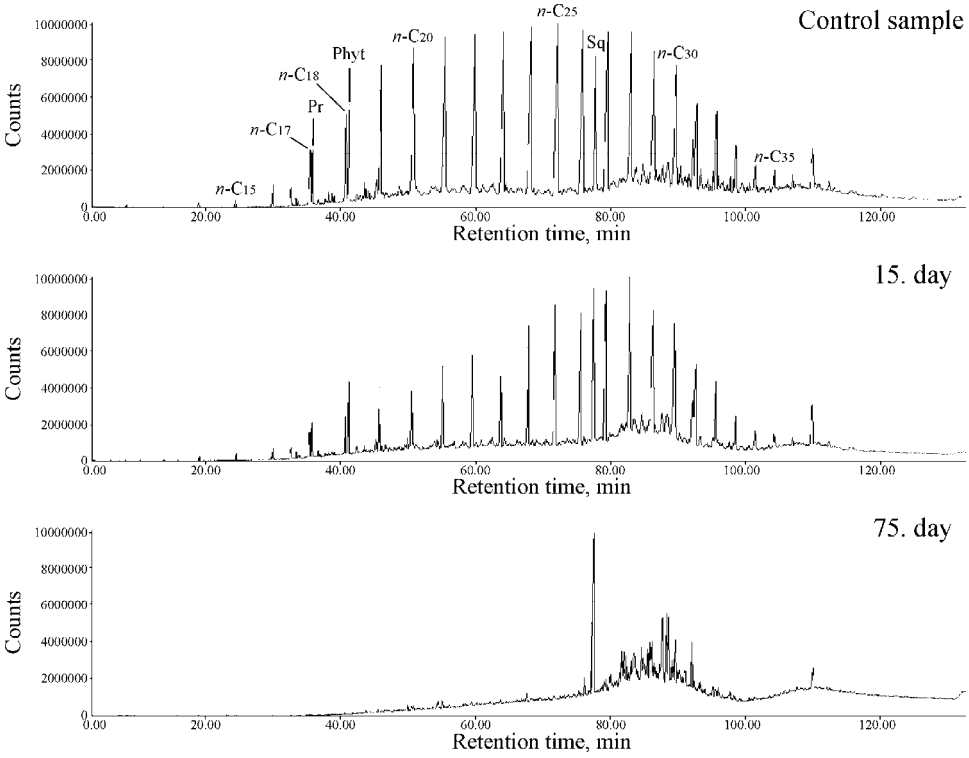

Fig. 1. TIC Chromatograms of the hydrocarbon fractions isolated from the extracts of the control sample and from the samples during the biodegradation experiment after 15 and 75 days (Pr = pristane; Phyt = phytane; Sq = squalane).

periment after 15, 30, 45, 60 and 75 days are shown in the Fig. 1-S in the Supplementary material). The dominant compounds in the hydrocarbon fraction of the control sample were *n*-alkanes and the isoprenoids pristane and phytane. These preliminary analyzes based on the TIC chromatograms showed a gradual decrease in the amount of *n*-alkanes and isoprenoids during 45 days. After 60 days of the experiment, *n*-alkanes and isoprenoids could not be observed in the TIC chromatograms indicating their possible complete degradation. At the end of the experiment, the TIC chromatograms were dominated by sterane biomarkers as the most abundant compounds in the fraction of hydrocarbons (Fig. 1).

n-Alkanes and isoprenoids

Detailed qualitative (Figs. 2 and 2-S in Supplementary material) and quantitative analyses (Fig. 3) of the *n*-alkanes and isoprenoids in the investigated samples enabled the calculation of the most characteristic biodegradation parameters (Table I) and provided a better insight into the dynamics of the biodegradation process.

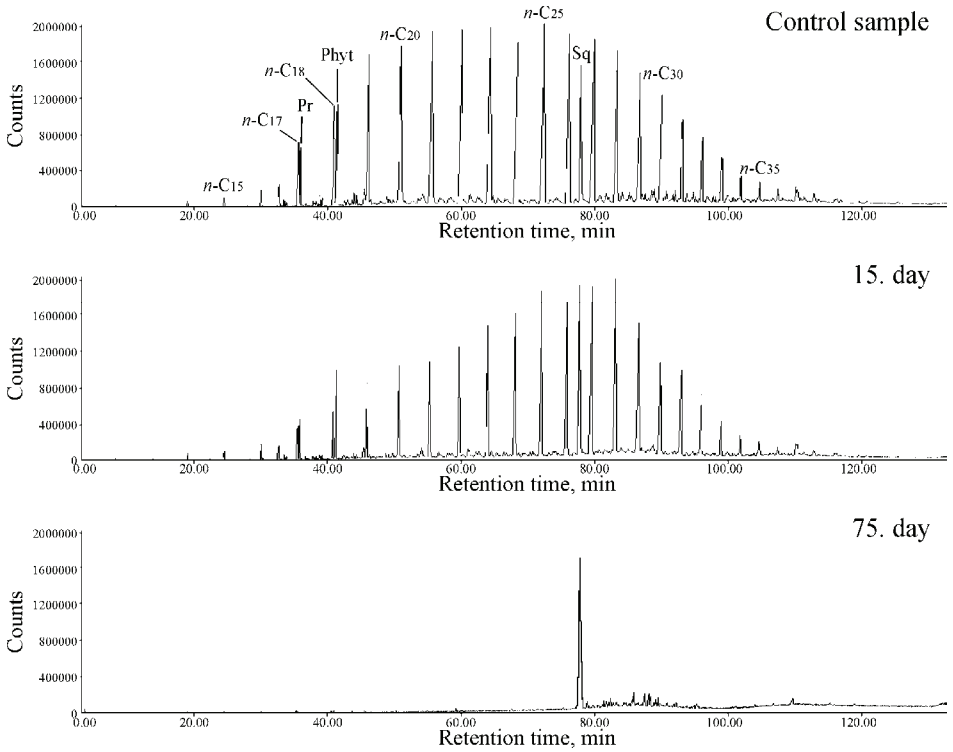

Fig. 2. GC–MS ion fragmentograms of the *n*-alkanes and isoprenoids (*m*/*z* 57) in the hydrocarbon fractions isolated from the extracts of the control sample and from the samples during biodegradation experiment after 15 and 75 days. (Pr = pristane; Phyt = phytane; Sq = squalane).

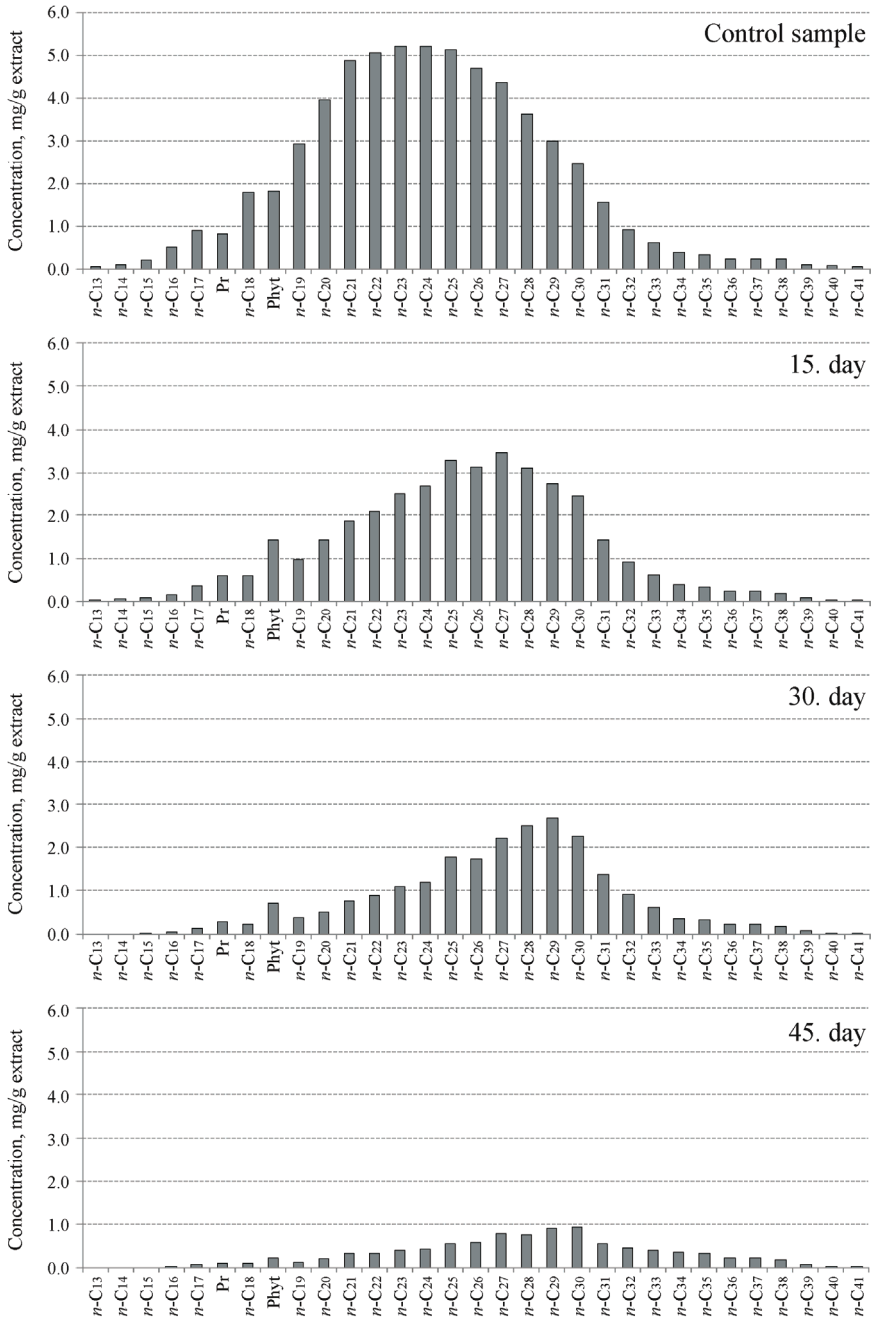

Fig. 3. Quantitative analysis of the *n*-alkanes and the isoprenoids pristane (Pr) and phytane (Phyt) in the hydrocarbon fractions isolated from the extracts of the control sample and from the samples during the biodegradation experiment after 15, 30 and 45 days.

TABLE I. Biodegradation parameters calculated from the quantitative analysis of *n*-alkanes and isoprenoids pristane and phytane in the control sample and in the samples during the biodegradation experiment (Pr – pristane; Phyt – phytane)

Duration of experiment, days	*n*-Alkanes range	Pr/*n*-C_{17}	Phyt/*n*-C_{18}	Concentration of *n*-alkanes mg per g of the extract	Loss of *n*-alkanes % of the control sample
Control sample	C_{13}–C_{41}	0.90	1.02	61.41	–
15	C_{13}–C_{41}	1.62	2.43	37.50	38.94
30	C_{13}–C_{41}	2.15	3.17	23.81	61.23
45	C_{16}–C_{41}	1.36	2.37	9.76	84.11
60	C_{26}–C_{41}	ND[a]	ND[a]	1.00	> 98.37
75	ND[b]	ND[a]	ND[a]	ND[b]	100

[a]Parameter was not calculated due to the degradation of the *n*-alkanes and isoprenoids; [b]parameter was not calculated due to the degradation of the *n*-alkanes

The ion chromatogram of the *n*-alkanes and isoprenoids in the hydrocarbon fraction of the control sample is characterized by the presence of *n*-alkanes in the C_{13}–C_{41} range with the uniform distribution of the even and odd homologues (Figs. 2 and 2-S in Supplementary material). The alkanes *n*-C_{17} and *n*-C_{18} and the closely eluting isoprenoids pristane and phytane are present in similar concentrations, as indicated by the values of the corresponding parameters Pr/*n*-C_{17} = = 0.90 and Phyt/*n*-C_{18} = 1.02 (Fig. 3; Table I).

Comparing the ion chromatogram of the alkanes in the hydrocarbon fraction of the sample after 15 days of the experiment with the control sample (Fig. 2), it can be easily concluded that *n*-alkanes lower than C_{30} were the most affected by the microorganisms. This observation was additionally confirmed by the quantitative analysis of these compounds (Fig. 3). The analysis of isoprenoids pristane and phytane indicated some decrease in their concentrations (Fig. 3). However, higher values of Pr/*n*-C_{17} and Phyt/*n*-C_{18} ratios (1.62 and 2.43 respectively; Table I) comparing to the values of these parameters in the control sample, confirmed a lower susceptibility of isoprenoids compared to *n*-alkanes during the first 15 days of the biodegradation process. According to these results, it can be concluded that during the first 15 days of the biodegradation processes by the microorganisms used in this experiment, a loss of 38.94 % of the *n*-alkanes occurred (Table I). Additionally, it can be concluded that this loss was mainly due to a decrease in the concentrations of *n*-alkanes in the C_{13}–C_{30} range (Figs. 2, 2-S in Supplementary material, and 3).

After 30 days of the experiment, a gradual decrease in the concentration of *n*-alkanes was observed (Fig. 3; Table I). The biodegradation was extended to the homologues up to C_{32}, resulting in loss of 61.23 % of the *n*-alkanes compared to the control sample (Fig. 3; Table I). A further increase in the Pr/*n*-C_{17} and Phyt/ /*n*-C_{18} ratios (2.15 and 3.17, respectively, Table I) compared to the sample after 15 days of the experiment, indicated that the isoprenoids were biodegraded at a

lower rate than the *n*-alkanes even if more than 60 % of the *n*-alkanes had been removed.

During the next 15 days, a steady biodegradation of *n*-alkanes continued. As a result, after 45 days of the experiment, *n*-alkanes lower than C_{16} had been completely removed. The concentration of the remaining *n*-alkanes (comprising homologues in the C_{16}–C_{41} range) was 84.11 % lower than in the control sample (Fig. 3; Table I). The relative decrease of the isoprenoid/*n*-alkane ratios (Pr/*n*-C_{17} = 1.36 and Phyt/*n*-C_{18} = 2.37, Table I) compared to the previous sample (Pr/*n*-C_{17} = 2.15 and Phyt/*n*-C_{18} = 3.17, Table I) indicates that during this phase of the experiment, a significant biodegradation of the isoprenoids occurred. Accordingly, it can be concluded that under the conditions used in this experiment, significant biodegradation of isoprenoids occurred after more than 80 % of the *n*-alkanes had been removed.

After 60 days of the experiment, an almost complete degradation of the *n*-alkanes and isoprenoids was observed (Fig. 3). Although *n*-alkanes in the C_{26}–C_{41} range were identified (Fig. 3), most of them could not be quantified. Their total concentration was lower than 98.37 % of the amount of *n*-alkanes in the control sample (Table I).

Finally, by the end of the experiment, after 75 days of exposure to the zymogenous microorganisms isolated from soil, the *n*-alkanes and isoprenoids were completely degraded.

Steranes and triterpanes

Polycyclic alkanes of the sterane and terpane types in crude oils in the subsurface are considered to be decomposed by microbial degradation after the degradation of acyclic hydrocarbons.[17] However, it was shown that crude oil biodegradation under aerobic conditions may follow completely different sequences than oil in reservoir rocks.[18] Additionally, an unusual biodegradation sequence of biomarker compounds was reported as a characteristic of biodegradation process during the bioremediation of refinery wastes.[19] Consequently, the hydrocarbon fractions of all samples exposed to microorganisms during the present experiment, as well as the corresponding control sample, were analyzed in detail for polycyclic alkanes of the sterane and terpane types. The corresponding ion chromatograms are shown in Figs. 4 and 3-S in Supplementary material.

In the control sample, biolipid and more stable geolipid isomers of the steranes and triterpanes types were identified with a distribution typical for crude oils (Figs. 4 and 3-S in Supplementary material). A detailed comparison of the abundances and distributions of these biomarkers in the control sample and in all samples during the biodegradation experiment showed no differences. Hence, it can be concluded that sterane and terpane biomarkers were not affected by biodegradation, and that the biodegradation of saturated hydrocarbons, under the

employed conditions, was restricted to the acyclic aliphatic compounds (*n*-alkanes and isoprenoids).

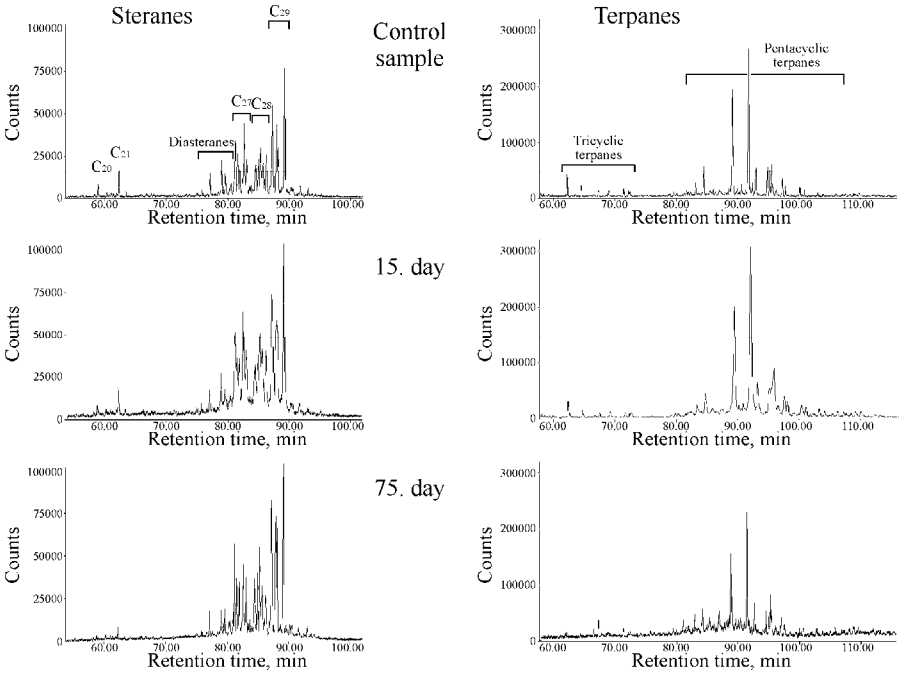

Fig. 4. GC–MS ion fragmentograms of steranes (*m*/*z* 217) and terpanes (*m*/*z* 191) in the hydrocarbon fractions isolated from the extracts of the control sample and from the samples during the biodegradation experiment after 15 and 75 days.

Aromatic hydrocarbons

Although the biodegradation of crude oil is often explained as a quasi-stepwise process in which various components are removed in a well-recognized sequence, it is well known that several compound classes are actually destroyed simultaneously but at different rates, reflecting differences in the rate of their catabolism under varying conditions.[8] Numerous studies showed that aromatic compounds can not only be degraded prior or concomitantly with sterane and terpane biomarkers in reservoir oils,[20] but also in the environmental conditions during oil spills.[21] Accordingly, aromatic compounds were carefully analyzed in all extracts during the present study.

Among aromatic hydrocarbons, the only compounds which could be identified and quantified in all samples investigated were phenanthrene and its derivatives with one and two methyl groups. The results of qualitative and quantitative analyses of these compounds are shown in Figs. 5, 4-S in Supplementary mate-

rial, and 6, respectively. Concentration changes of phenanthrene, methyl phenanthrenes and dimethyl phenanthrenes during the experiment are given in Table II.

The qualitative analyses of phenanthrene and its derivatives with one and two methyl groups showed that the hydrocarbon fraction of the control sample was characterized by the presence of these compounds in the distribution characteristic of mature crude oil (Figs. 5 and 4-S in Supplementary material).[8]

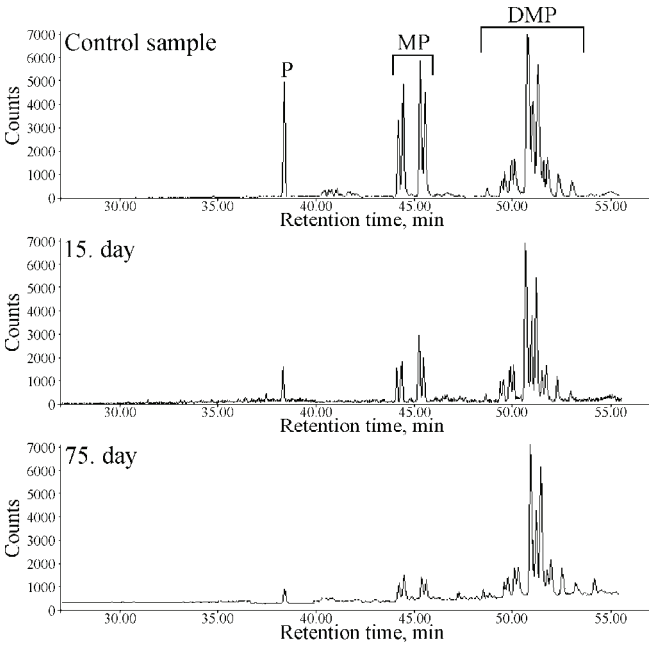

Fig. 5. Reconstructed GC–MS ion chromatograms of phenanthrene (P; *m*/*z* 178), methylphenanthrenes (MP; *m*/*z* 192) and dimethylphe-nanthrenes (DMP; *m*/*z* 206) in the hydrocarbon fractions isolated from the extracts of the control sample and from the samples during the biodegradation experiment after 15 and 75 days.

During the biodegradation experiment, the most distinct change in concentrations of these compounds was observed in the case of phenanthrene (Fig. 6; Table II). After only 15 days of the experiment, 61.90 % of phenanthrene had been degraded (Table II). However, during the rest of the experiment, the decrease in the concentration of phenanthrene was much less prominent. Compared to the control sample, after 30 days its loss was 75.13 %, and after 45 days it was 81.62 % (Table II). By the end of the experiment, 82.94 % of phenanthrene was degraded, leaving a residual concentration of 33.35 μg g^{-1} in the extract (Table II).

Methyl phenanthrenes underwent a significant decrease in the concentration during this experiment, but not as prominent as that of phenanthrene. After 15 days of the experiment, 48.49 % of methyl phenanthrenes had been degraded (Table II). During the rest of the experiment, a gradual loss of methyl phenanthrenes was observed (Fig. 6; Table II). Finally, at the end of the experiment, after 75 days of exposure to the zymogenous microorganisms isolated from soil, 74.74 % of the methyl phenanthrenes were degraded, leaving the residual con-

centration of 186.32 μg g^{-1} extract (Table II). Accordingly, it can be concluded that under the conditions used in this experiment, the zymogenous microorganisms exerted a considerably high bioremediation potential in the biodegradation of phenanthrene and methyl phenanthrenes. However, it must be emphasized that at the end of the experiment, the biodegradation of these compounds was not complete.

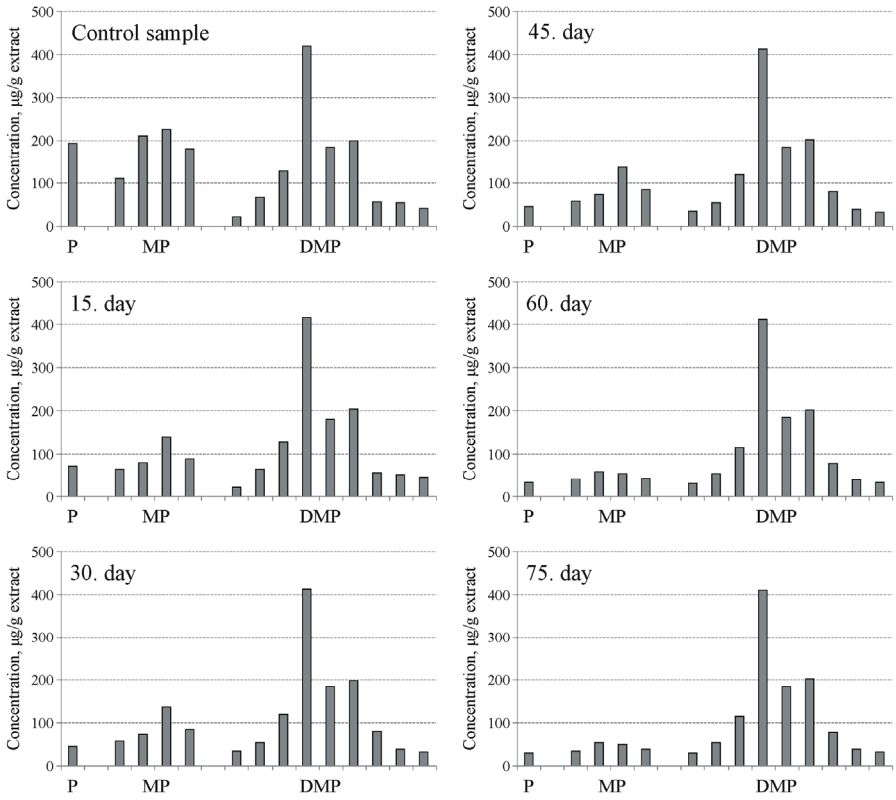

Fig. 6. Quantitative analysis of phenanthrene (P), methylphenanthrenes (MP) and dimethylphenanthrenes (DMP) in the hydrocarbon fractions isolated from the extracts of the control sample and from the samples during the biodegradation experiment after 15, 30, 45, 60 and 75 days.

During this biodegradation experiment no significant alteration in the concentration of dimethyl phenanthrenes was observed (Fig. 6). After 75 days, the concentration of these compounds was reduced by only 2.34 % (Table II), leaving them in almost unchanged amount compared to the control sample. Hence, it can be concluded that the zymogenous microorganisms isolated from soil have a low bioremediation potential for the degradation of dimethyl phenanthrenes under the conditions employed in this study.

TABLE II. Concentration changes of phenanthrene, methyl phenanthrenes and dimethyl phenanthrenes in the control sample and in the samples during the biodegradation experiment (P – phenanthrene; MP – methylphenanthrenes; DMP – dimethylphenanthrenes)

Duration of experiment	Concentration, μg per g of the extract			Loss, % of the control sample		
days	P	MP	DMP	P	MP	DMP
Control sample	195.50	737.67	1194.80	–	–	–
15	74.49	380.00	1193.68	61.90	48.49	0.09
30	48.62	363.82	1173.97	75.13	50.68	1.74
45	35.93	281.70	1170.22	81.62	61.81	2.06
60	34.08	204.39	1167.35	82.57	72.29	2.30
75	33.35	186.32	1166.82	82.94	74.74	2.34

CONCLUSIONS

In this study, the experiments were conducted with the aim of establishing the bioremediation potential of zymogenous microorganisms for crude oil biodegradation. The microorganisms were isolated from soil samples taken from within the oil refinery Pančevo (Danube alluvium, Serbia).

The investigated soil zymogenous microorganisms showed the highest bioremediation potential in biodegradation of *n*-alkanes and isoprenoids. During this experiment, a gradual decrease in the concentration of *n*-alkanes was observed. Significant biodegradation of isoprenoids occurred after more than 80 % of the *n*-alkanes had been removed. By the end of the experiment, after 75 days of exposure to the zymogenous microorganisms isolated from soil, the *n*-alkanes and isoprenoids had been completely degraded.

In the class of aromatic hydrocarbons, it was confirmed that the zymogenous microorganisms isolated from soil had a considerably high bioremediation potential in the biodegradation of phenanthrene and methyl phenanthrenes. However, the biodegradation of these compounds, under conditions used in this study, was not complete.

The low bioremediation potential of these microorganisms was proven in the case of polycyclic alkanes of the sterane and triterpane type and dimethyl phenanthrenes. After 75 days of the experiment, no significant alteration in the concentration of these compounds was observed.

The zymogenous microorganisms isolated from the soil in the vicinity of the wastewater canal showed somewhat a higher bioremediation potential for crude oil biodegradation than the microorganisms isolated from the water and from the sludge of this canal.[10,11] However, it must be stated that the biodegradation of crude oil by the soil aerobic zymogenous microorganisms at this location under natural conditions would be limited to the *n*-alkanes and isoprenoids. On the other hand, biodegradation of more complex polycyclic saturated and aromatic compounds, under the same conditions, would, most probably, not go to completion.

SUPPLEMENTARY MATERIAL

Complete data during the biodegradation experiments (Figs. 1-S–4-S) are available electronically at http://www.shd.org.rs/JSCS/, or from the corresponding author on request.

Acknowledgments. This work was supported by the Ministry of Science and Technological Development of the Republic of Serbia (Projects No.: 146008, 142018 and 20131).

И З В О Д

ИСПИТИВАЊЕ БИОРЕМЕДИЈАЦИОНОГ ПОТЕНЦИЈАЛА АЕРОБНИХ ЗИМОГЕНИХ МИКРООРГАНИЗАМА ИЗ ЗЕМЉИШТА У БИОДЕГРАДАЦИЈИ СИРОВЕ НАФТЕ

TATJANA ŠOLEVIĆ[1], MILAN NOVAKOVIĆ[2], MILA ILIĆ[1], MALIŠA ANTIĆ[1,3], MIROSLAV M. VRVIĆ[1,2] и BRANIMIR JOVANČIĆEVIĆ[1,2]

[1]Центар за хемију, Институт за хемију, технологију и металургију, Универзитет у Београду, Његошева 12, п. пр. 473, 11001 Београд, [2]Хемијски факултет, Универзитет у Београду,Студентски трг 12–16, п. пр. 158, 11001 Београд и [3]Пољопривредни факултет, Универзитет у Београду, Немањина 6, 11081 Београд

Испитиван је биоремедијациони потенцијал аеробних зимогених микроорганизама из земљишта у биодеградацији сирове нафте (алувијална раван реке Дунав, Панчево). Смеша сирових нафти парафинског типа коришћена је као супстрат. Лабораторијски експеримент симулиране биодеградације трајао је 15, 30, 45, 60 и 75 дана. Паралелно је рађен и експеримент са контролним узорком. Екстракти су изоловани из узорака хлороформом у левку за одвајање. Из ових екстраката, угљоводоници су изоловани хроматографијом на колони и анализирани гаснохроматографски–масеноспектрометријски (GC–MS). *n*-Алкани, изопреноиди, фенантрен и његови деривати са једном и две метил групе квантитативно су анализирани. Способност и ефикасност зимогених микроорганизама из земљишта у биодеградацији сирове нафте процењена је поређењем састава узорака који су били изложени микроорганизмима и контролног узорка. Испитивани микроорганизми показали су највиши биоремедијациони потенцијал у биодеградацији *n*-алкана и изопреноида. Висок биодеградациони потенцијал уочен је при биодеградацији фенантрена и метилфенантрена. Низак биоремедијациони потенцијал ових микроорганизма доказан је у случају полицикличних алкана типа стерана и терпана, као и диметилфенантрена.

(Примљено 31. маја, ревидирано 27. септембра 2010)

REFERENCES

1. M. Vidali, *Pure Appl. Chem.* **73** (2001) 1163
2. J. F. Ferguson, J. M. H. Pietari, *Environ. Pollut.* **107** (2000) 209
3. S. M. Bamforth, I. Singleton, *J. Chem. Technol. Biotechnol.* **80** (2005) 723
4. M. Gavrilescu, *Eng. Life Sci.* **5** (2005) 497
5. H. Seidel, C. Löser, A. Zehnsdorf, P. Hoffmann, R. Schmerold, *Environ. Sci. Technol.* **38** (2004) 1582
6. W. Fritsche, M. Hofrichter, ин *Biotechnology*, Vol. 11b, 2nd ed., H. J. Rehm, G. Reed, Eds.**,** Wiley-VCH, New York, USA, 2008, p. 144
7. J. D. Van Hamme, A. Singh, O. P. Ward, *Microbiol. Mol. Biol. Rev.* **67** (2003) 503
8. K. E. Peters, C. C. Walters, J. M. Moldowan, *The biomarker guide*, Cambridge University Press, Cambridge, UK, 2005
9. UNEP (1999) UNEP/UNCHS Balkans Task Force, *BTF Technical Mission Report for Group D: Complimentary Measures to Assess the Environmental Impacts of the Conflicts*

to the Danube, http://www.grid.unep.ch/btf/missions/august/danube.pdf (accessed 15 March 2010)
10. M. P. Antić, B. S. Jovančićević, M. M. Vrvić, J. Schwarzbauer, *Environ. Sci. Pollut. Res.* **13** (2006) 320
11. M. Ilić, M. Antić, V. Antić, J. Schwarzbauer, M. Vrvić, B. Jovančićević, *Environ. Chem. Lett.* **9** (2011) 133
12. D. J. Friend, *Remediation of petroleum-contaminated soils*, National Academy Press, Washington DC, USA, 1996
13. S. Kaisarevic, U. Lubcke-von Varel, D. Orcic, G. Streck, T. Schulze, K. Pogrmic, I. Teodorovic, W. Brack, R. Kovacevic, *Chemosphere* **77** (2009) 907
14. C. Löser, H. Seidel, A. Zehnsdorf, U. Stottmeister, *Appl. Microbiol. Biotechnol.* **49** (1998) 631
15. B. Jovančićević, P. Polić, M. Vrvić, G. Sheeder, T. Teschner, H. Wehner, *Environ. Chem. Lett.* **1** (2003) 73
16. B. S. Jovančićević, M. P. Antić, T. M. Šolević, M. M. Vrvić, A. Kronimus, J. Schwarzbauer, *Environ. Sci. Pollut. Res.* **12** (2005) 205
17. J. K. Volkman, R. Alexander, R. I. Kagi, G. W. Woodhouse, *Geochim. Cosmochim. Acta* **47** (1983) 785
18. Z. Wang, M. F. Fingas, L. Sigouin, E. H. Owens, in *Proceedings of the 2001 International Oil Spill Conference*, Tampa, FL, USA, 2001, p. 115
19. J. M. Moldowan, J. Dahl, M. A. McCaffrey, W. J. Smith, J. C. Petzer, *Energy Fuels* **9** (1995) 155
20. H. Huang, B. F. J. Bowler, T. B. P. Oldenburg, S. R. Larter, *Org. Geochem.* **35** (2004) 1619
21. Z. Wang, M. Fingas, *J. Chromatogr. A* **774** (1997) 51.

Journal of the Serbian Chemical Society
JSCS@tmf.bg.ac.rs • www.shd.org.rs/JSCS
J. Serb. Chem. Soc. 76 (3) S23–S27 (2011) *Supplementary material*

SUPPLEMENTARY MATERIAL TO

Investigation of the bioremediation potential of aerobic zymogenous microorganisms in soil for crude oil biodegradation

TATJANA ŠOLEVIĆ[1]*, MILAN NOVAKOVIĆ[2], MILA ILIĆ[1#], MALIŠA ANTIĆ[1,3#], MIROSLAV M. VRVIĆ[1,2#] and BRANIMIR JOVANČIĆEVIĆ[1,2#]

[1]Department of Chemistry, Institute of Chemistry, Technology and Metallurgy, University of Belgrade, Njegoševa 12, P.O. Box 473, 11001 Belgrade, [2]Faculty of Chemistry, University of Belgrade, Studentski trg 12–16, P.O. Box 158, 11001 Belgrade and [3]Faculty of Agriculture, University of Belgrade, Nemanjina 6, 11081 Belgrade, Serbia

J. Serb. Chem. Soc. 76 (3) (2011) 425–438

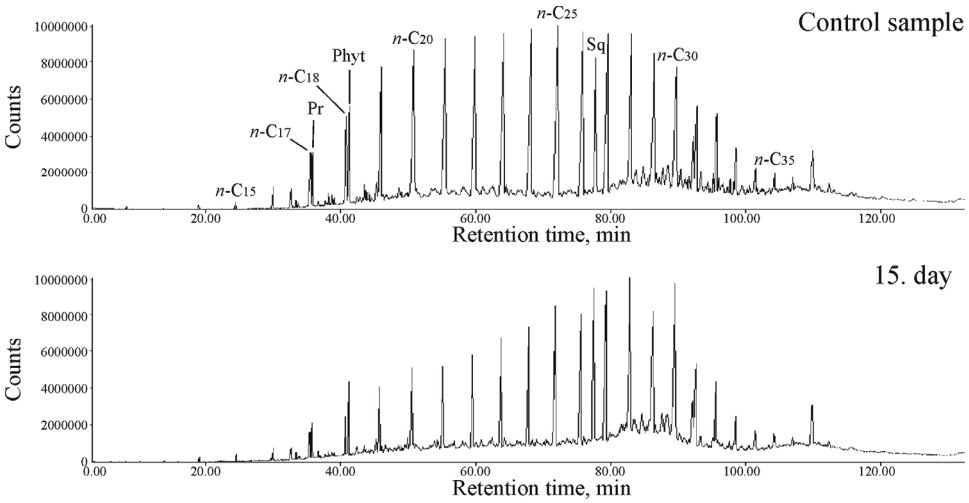

Fig. 1-S. TIC Chromatograms of the hydrocarbon fractions isolated from the extracts of the control sample and from the samples after the biodegradation of 15 days (Pr = pristane; Phyt = phytane; Sq = squalane).

* Corresponding author. E-mail: tsolevic@chem.bg.ac.rs
# Serbian Chemical Society member.

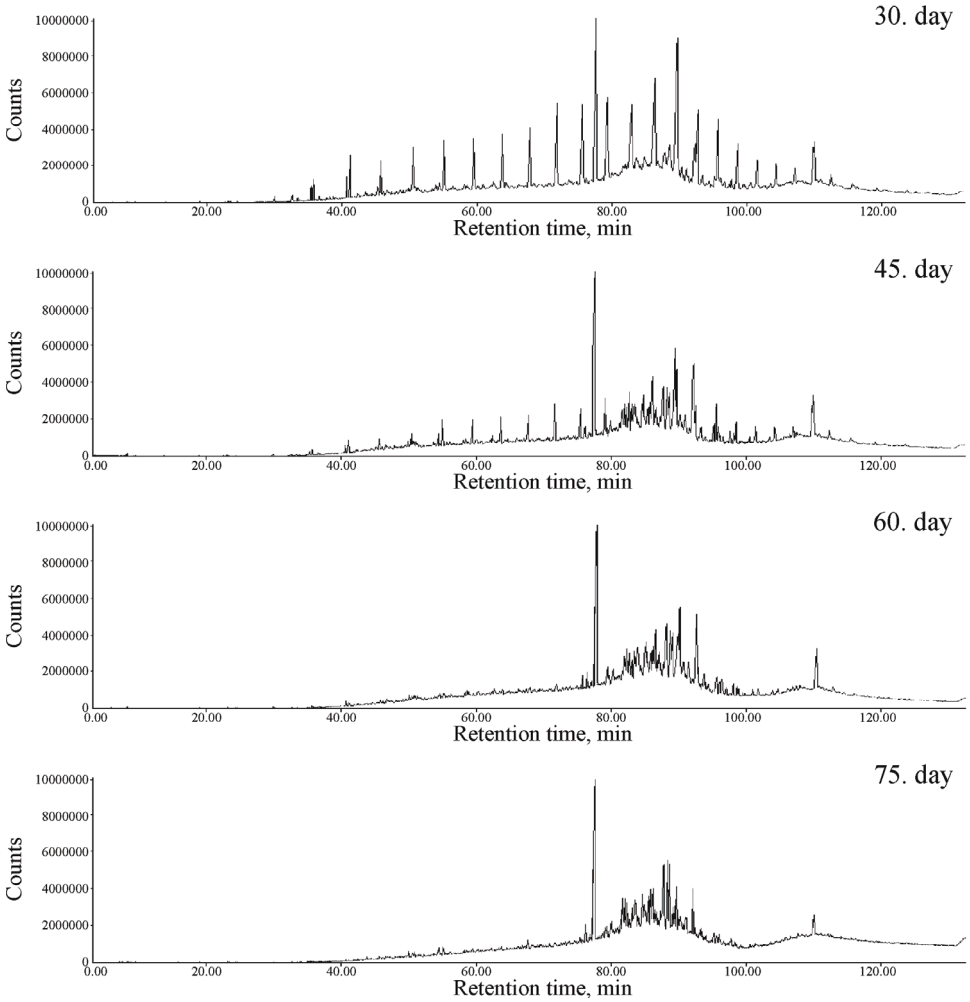

Fig. 1-S (continued). TIC Chromatograms of the hydrocarbon fractions isolated from the samples during the biodegradation experiment after 30, 45, 60 and 75 days (Pr = pristane; Phyt = phytane; Sq = squalane).

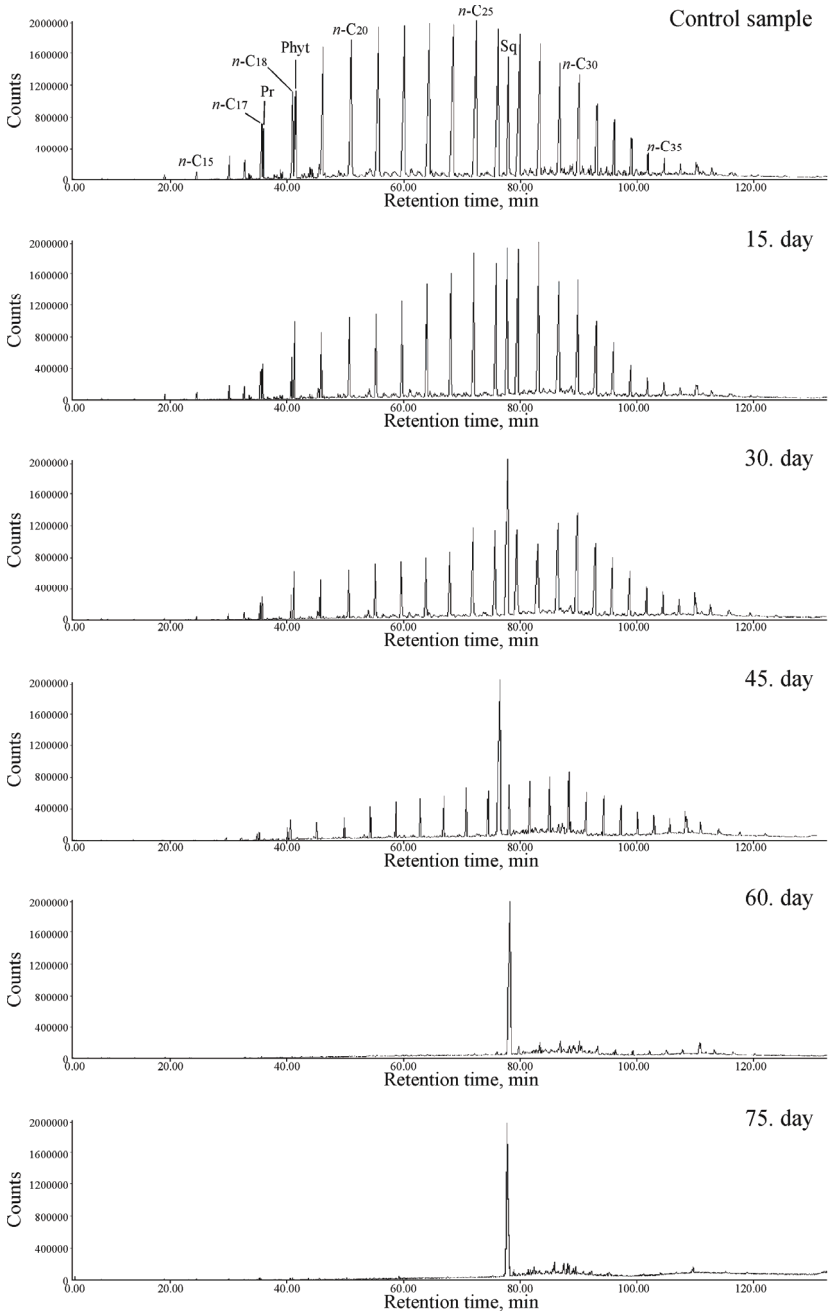

Fig. 2-S. GC–MS ion fragmentograms of the *n*-alkanes and isoprenoids (*m*/*z* 57) in the hydrocarbon fractions isolated from the extracts of the control sample and from the samples during biodegradation experiment after 15, 30, 45, 60 and 75 days. (Pr = pristane; Phyt = phytane; Sq = squalane).

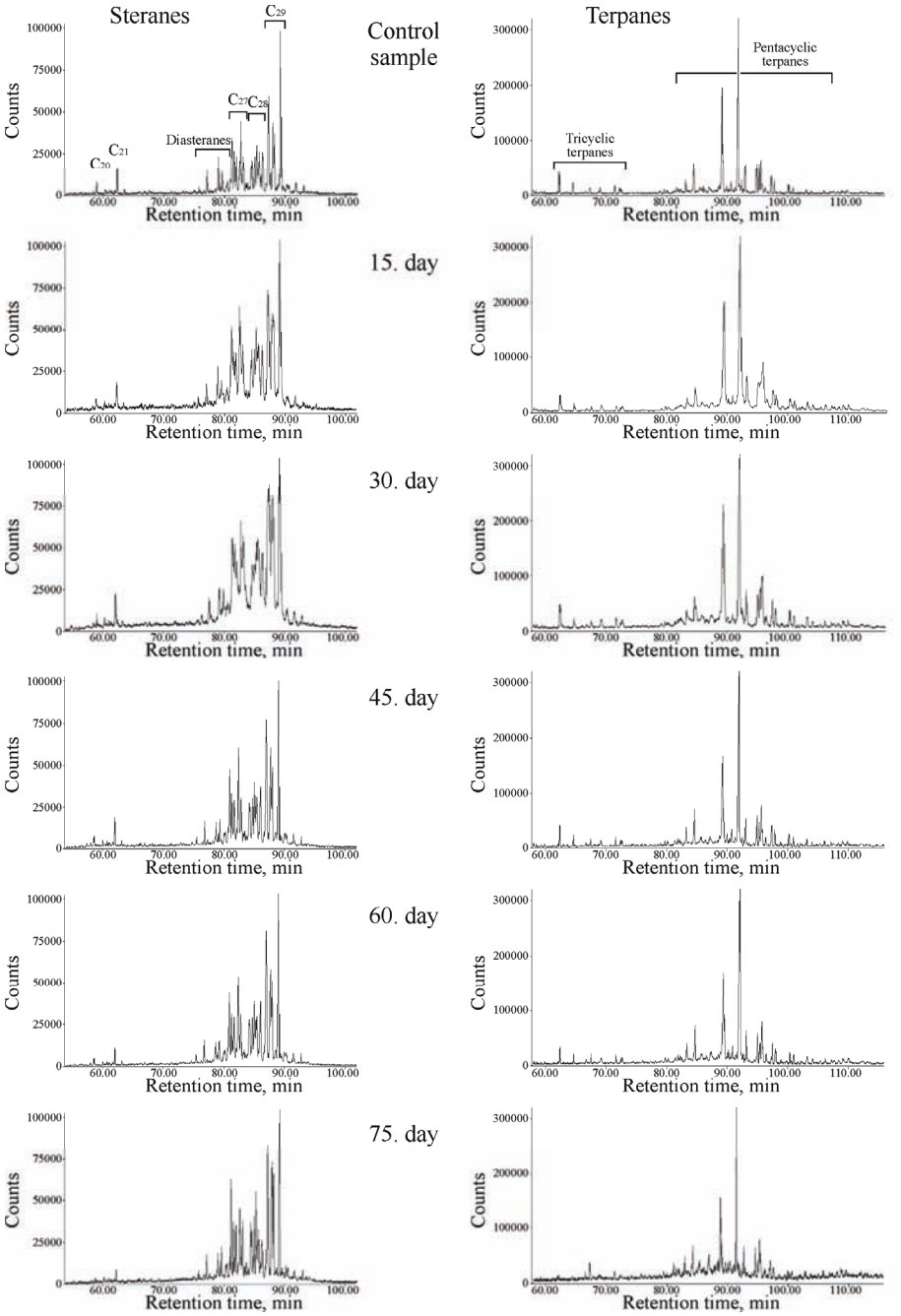

Fig. 3-S. GC–MS ion fragmentograms of steranes (*m*/*z* 217) and terpanes (*m*/*z* 191) in the hydrocarbon fractions isolated from the extracts of the control sample and from the samples during the biodegradation experiment after 15, 30, 45, 60 and 75 days.

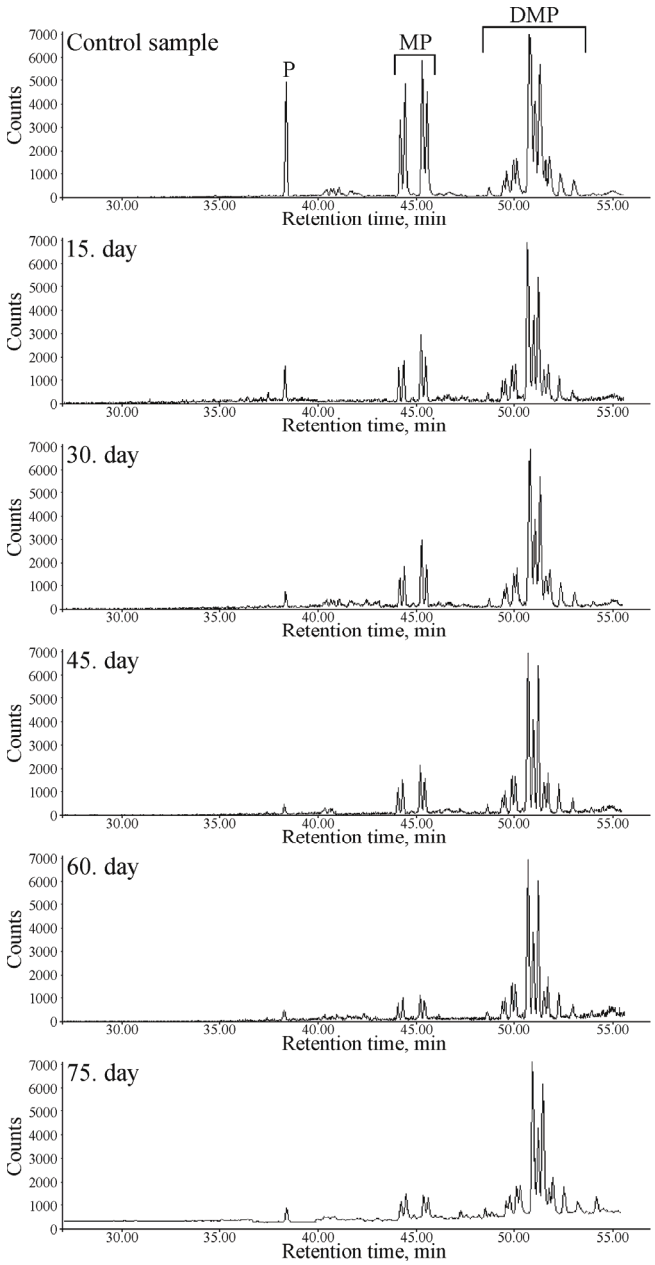

Fig. 4-S. Reconstructed GC–MS ion chromatograms of phenanthrene (P; *m*/*z* 178), methylphenanthrenes (MP; *m*/*z* 192) and dimethylphenanthrenes (DMP; *m*/*z* 206) in the hydrocarbon fractions isolated from the extracts of the control sample and from the samples during the biodegradation experiment after 15, 30, 45, 60 and 75 days.

Journal of the Serbian Chemical Society
JSCS-info@shd.org.rs • www.shd.org.rs/JSCS
J. Serb. Chem. Soc. 76 (3) 439–446 (2011)
JSCS–4131
UDC 675:628.3.03.034.2:628.315.23+
Botryosphaeria rhodina
Original scientific paper

Biotreatment of industrial tannery wastewater using *Botryosphaeria rhodina*

MARIA CLAUDIA HASEGAWA[1], ANELI M. BARBOSA[2] and KEIKO TAKASHIMA[1]*

[1]*Laboratório de Processos de Oxidação Avançados, Departamento de Química, CCE and* [2]*Laboratório de Bioquímica de Microrganismos, Departamento de Bioquímica e Biotecnologia, CCE, Universidade Estadual de Londrina,Caixa Postal 6001, CEP 86051-990, Londrina, PR, Brazil*

(Received 3 July, revised 8 October 2010)

Abstract: The treatment of a tannery wastewater was performed on the laboratory scale using the ascomyceteous fungus *Botryosphaeria rhodina* MAMB-05, a ligninolytic and a constitutive producer of laccases (EC: 1.10.3.2). The wastewater samples were collected in the retanning and dyeing steps and presented high values of chemical oxygen demand, *COD* (15,023±60.0 mg L^{-1}), fifth-day biochemical oxygen demand, BOD_5 (4374±0.1 mg L^{-1}), total solids (28500±2.0 mg L^{-1}), total organic carbon, *TOC* (4685 mg L^{-1}), and chloride ion concentration (2911±0.3 mg L^{-1}). The fungus was inoculated and after five days under agitation at 180 rpm at 28 °C, the *COD* was reduced by 91 %. The total organic carbon also decreased from 4685 to 375.0 mg L^{-1} and the turbidity from 331.0 to 6.5 NTU, indicating that the biological treatment was efficient as the fungus consumed almost all the organic compounds present in the wastewater. It was not necessary to add an additional carbon source for the treatment, indicating that the concentration of organic compounds presented in the tannery wastewater effluent were sufficient for microorganism growth, during which the *COD* and *TOC* were reduced by about 91 and 93 %, respectively.

Keywords: *Botryosphaeria rhodina* MAMB-05; wastewater treatment; tannery industry; *COD*.

INTRODUCTION

The tannery industry represents an important sector in the economy of many countries. On the other hand, depending on the leather process, it generates large quantities of wastewater with ammonium, sulfates, surfactants, acids, dyes, sulfonated oils and organic substances, including natural or synthetic tannins. These chemical substances are applied to transform the animal skin into products with

* Corresponding author. E-mail: keiko@uel.br
doi: 10.2298/JSC100603039H

great capacities for dyeing, as well as to increase the mechanical and hydrothermal resistance. Considering that the greater part of these organic compounds are resistant to conventional chemical and biological treatments, the wastes discharged into natural waters increase environmental pollution and the health risks. The treatment of this type of wastewater is very complex mainly because of the variety of chemical products added in different concentrations.[1–4]

The fact that environmental legislation is very strict in almost all countries that are leather producers, a great deal of effort has been made to develop treatments for and remediation of the contaminated environments. Several methods have been described in the scientific literature, such as direct recycling,[5] coagulation,[6] flocculation,[7] chemical precipitation,[5,8] ion-exchange,[9] adsorption,[10] biological treatment,[11–13] electrochemical treatment,[14,15] membrane separation,[16–18] thermal techniques[9,19] and others. Physical chemistry processes, such as coagulation/flocculation, adsorption and membrane separation, have been the most utilized for the removal of colored effluents. However, these treatments do not solve the problem because of the transfer of contaminants from one phase to another. However, in biological treatment, the microorganisms degrade the organic pollutants using them as a carbon source to produce metabolic energy to survive.

A study of some biotechnological processes showed that ascomycetes and basidiomycetes are efficient at degrading a large variety of dyes, phenolic and non-phenolic compounds, demonstrating a high potential for environmental bioremediation.[20] The fungus *Botryosphaeria rhodina* MAMB-05 is ligninolytic and a constitutive producer of laccases (EC: 1.10.3.2).[21, 22] These enzymes are multi-copper oxidases, in which the copper atoms participate in the active site and in catalytic reactions. Laccases are also involved in lignin degradation,[21,23] and in the decolorization of effluents.[24] Microorganisms that are laccase producers have potential to be used in bioremediation processes and biodegradation of xenobiotic compounds.[25] The technological importance of laccases is correlated with its catalytic capacity to oxidize a large number of phenolic and non-phenolic compounds, as well as some other aromatic and non-aromatic compounds when these are oxidized in the presence of mediators.[24,26,27]

This work describes the biological treatment of effluent from a tannery collected in the retanning and dyeing steps, employing the fungus *Botryosphaeria rhodina* MAMB-05, with the objective to decrease the *COD* and remove organic compounds.

EXPERIMENTAL

All the reagents used in this work were of analytical grade: citric acid ($C_6H_8O_7$) 99 %, zinc sulfate heptahydrate ($ZnSO_4 \cdot 7H_2O$) 99 %, ammonium iron(II) sulfate dodecahydrate ($Fe(NH_4)_2 \cdot 12H_2O$) 98 %, potassium bromide (KBr) 98 %, sodium chloride (NaCl) 98 %, sodium molybdate dihydrate ($Na_2MoO_4 \cdot 2H_2O$) 84 % and sodium bicarbonate ($NaHCO_3$) 98 %

were purchased from Synth; potassium dihydrogen phosphate (KH_2PO_4) 98 %, ammonium nitrate (NH_4NO_3) 98 %, calcium chloride dihydrate ($CaCl_2 \cdot 2H_2O$) 99 % were obtained from Nuclear; boric acid (H_3BO_3) 99 %; potassium chloride (KCl) 98 %; magnesium chloride ($MgCl_2$) 98 % from Merck; sodium citrate dihydrate ($Na_3C_6H_5O_7 \cdot 2H_2O$) 99 %; anhydrous D(+)-glucose ($C_6H_{12}O_6$) 99 % were purchased from Biotec; copper(II) sulfate pentahydrate ($CuSO_4 \cdot 5H_2O$) 98 % from Quimibras; magnesium sulfate heptahydrate ($MgSO_4 \cdot 7H_2O$) 98 % from Chemco; manganese(II) sulfate monohydrate ($MnSO_4 \cdot H_2O$) 98 %, from CAAL, agar from Biobras.

The crude effluent generated from the retanning step was collected in a leather company located in the north of the Paraná State, in the south of Brazil. The effluent was maintained at 4 °C in a cold room, and after being homogenized vigorously, was filtered to remove all suspended solids. Then, the filtrate was diluted with distilled water in two proportions (1:2 and 1:10) before inoculation with the fungus. The effluent characteristics without previous treatment are presented in Table I.

TABLE I. Characterization of the crude retanning and dyeing step effluent

Property	Value
pH	3.5±0.7
COD / mg L^{-1}	15,023±60.0
BOD_5 / mg L^{-1}	4,374±0.1
BOD_5/COD	0.29
TOC / mg L^{-1}	4,685
Total solids, mg L^{-1}	28,500±2.0
Fixed total solids, mg L^{-1}	17,983±2.0
Volatile total solids, mg L^{-1}	10,517±4.0
Chloride, mg L^{-1}	2,911±0.3
Turbidity, NTU	331±0.02
Chromium content, mg L^{-1}	198±0.5
Ammonium nitrogen content, mg L^{-1}	376±0.1

The inoculum was prepared by transferring the fungus *B. rhodina* MAMB-05 from the agar medium to Petri dishes containing 30 mL of solid VGA medium (minimum Vogel salts medium, 1 % (w/v) glucose and 2 % (w/v) agar) in a laminar film hood (Veco, model MM200600). These plates were incubated for 5 days at 28±2 °C in a BOD type incubator (Nova Ética 411D). The effluent was sterilized for 20 min in an autoclave (Fabbe Primar, model 103) and the pH was adjusted to 7.0. The treatment was developed in Erlenmeyer flasks (125 mL) containing 25 mL of effluent with or without the addition of minimum Vogel salts medium and 1 % (w/v) glucose. Four plugs (0.7 cm diameter) of solid VGA culture medium covered with *B. rhodina* hyphae were inoculated into each Erlenmeyer flask. All flasks were incubated at 28±2 °C on a rotary bench shaker (Cientec, model CT712) under agitation at 180 rpm for 5 days. All assay procedures were developed in triplicate and the results correspond to the average and standard deviation. After five days, the effluent treatments were centrifuged (Boeco, model U-32R) at 7000 rpm at –4 °C for 15 min. The supernatants were filtered through glass wool and used for analytical determinations. The fungal biomass produced by *B. rhodina* MAMB-05 was determined by gravimetric measurements (Fanem, model 315-SE) after drying at 70 °C to constant weight.

All the effluent analyses (*COD*, BOD_5, total solids, turbidity, ammonium nitrogen) before and after the biological treatment step were performed following the methods described by the standard methods for the examination of water and wastewater.[28] Total organic carbon (*TOC*) was analyzed by the combustion method in a Shimadzu model TOC 5000 A analyzer. Chlorides were determined by the Mohr method[29] and the turbidity was measured in a turbidimeter (Hach, model 2100P). The chromium concentration was determined by atomic absorption spectrometry (Shimadzu, model 6601F).

RESULTS AND DISCUSSION

Animal skin is transformed to leather through three operations: tanning, retanning and dyeing, and painting. The effluent of each step is mixed in a later step to produce a homogenized effluent, characterized as recalcitrant, which is highly pollutant. The physico-chemical characteristics of the retanning and dyeing effluent before the biological treatment are given in Table I. The effluent studied herein presented high values of *COD* (15023±60.0 mg L^{-1}), BOD_5 (4374±0.1 mg L^{-1}), total solids (28500±2.0 mg L^{-1}), *TOC* (4685 mg L^{-1}) and chloride ion concentration (2911±0.3 mg L^{-1}), due to the presence of chemical products such as dyes, synthetic and vegetable tannins, surfactants, chromium and aluminum salts, organic acids, proteins, *etc*. The *COD*, BOD_5, and *TOC* values of this retanning and dyeing effluent without any treatment were, at least, 100 fold higher than those described by Schrank *et al.*,[1,2] Preethi *et al.*,[4] Garrote *et al.*,[30] Dantas *et al.*[31] and Sauer *et al.*,[32] as shown in Table II.

TABLE II. Some tannery wastewater chemical treatments described in the scientific literature

Process	*COD* / mg L^{-1}		BOD_5 / mg L^{-1}		*TOC* / mg L^{-1}		pH	Reference
	Before	After	Before	After	Before	After		
H_2O_2/Fe^{2+} and H_2O_2/Fe^{2+}/UV	1803	180	106	n.d.	n.d.	n.d.	2.5	31
H_2O_2/Fe^{2+} (100 mg L^{-1}/100 mg L^{-1})	130	48	47	29	45	28	3.5	1,2
H_2O_2/UV (1020 mg L^{-1})	130	n.d.	47	15	45	19	3.0	
Electro-fenton	2810	1686	910	n.d	n.d.	n.d.	7.2	3
O_3	2365	2095	1010	660	820	720	11.0	1,2
O_3/UV	2365	1860	1010	645	820	710	11.0	
O_3/O_2	5000	4000	300	195	n.d.	n.d.	11.0	4
TiO_2/UV	2365	2295	1010	1010	820	740	11.0	1,2
$FeCl_3/Ca(OH)_2$	3192	445	506	n.d.	n.d.	n.d.	8.8	30
TiO_2/UV	801	626	349.1	26.9	n.d.	n.d.	8.7	32

The *COD*, BOD_5 and *TOC* values found in the scientific literature before and after different chemical treatments, converted to the same units (mg L^{-1}) for comparison, are given in Table II. Usually, the papers did not mention the process step from where the effluents were collected. Comparing these values, discrepancies can be observed among the literature values and those obtained in this study, which can be attributed to the effluent, collected after different steps du-

ring leather production. This information is important because, depending on the process step, the composition and volume percentages can vary considerably, as described by Cassano *et al*.[33] In this paper, the authors emphasized the high variation of *COD* values between the chromium tanning phase (from 400 to 800 mg L^{-1}) and the dyeing, fat liquoring and retanning steps (from 15000 to 75000 mg L^{-1}). Comparing the results presented in Table II before and after different chemical treatments, it is possible to observe that some treatments were more efficient than others and some had no efficiency. This also can be explained by the composition of the effluent in leather industries, which varies depending on the leather treatment step.[33]

Most of the biological treatments of tannery effluents described in the literature used bacteria,[34–36] and a few used fungi. Srivastava and Thakur[37] isolated fungal strains from tannery effluents, and optimized some parameters of the treatment process to remove chromium with a strain of *Aspergillus* sp, which removed 70 % of the chromium after 3 days in the bioreactor. To the best of our knowledge, this is the first report that describes the employment of the ascomycete fungus *B. rhodina* MAMB-05 to treat tannery effluent. Fungal biomass is a useful parameter to evaluate the toxicity of wastewater;[21,23] thus in this work, it was considered the mycelium biomass produced by *B. rhodina* MAMB-05 with and without addition of minimum Vogel salts medium and/or glucose as a carbon source, at an initial pH of 7.0 was considered at a 5-day cultivation at 28 °C with effluent dilutions 1:2 and 1:10, Table III.

TABLE III. Biomass produced by *Botryosphaeria rhodina* with and without addition of nutrients and carbon source using 7.0 as initial pH

Treatment	Dilution	Biomass content, mg L^{-1}	COD[a] / mg L^{-1}	COD RD reduct %	pH_{final}
Bot[b]	1:2	0.402±0.003	9126±91.0	39.3	6.6
Bot	1:10	0.621±0.002	5422±46.0	64.1	6.7
Bot+Glc [c]	1:2	0.585±0.010	22546±67.0	–	6.7
Bot+Glc	1:10	3.402±0.005	9705±81.0	39.6	6.8
Bot+Vogel[d]	1:2	0.953±0.006	3341± 60.0	77.8	6.8
Bot+Vogel	1:10	1.265±0.008	1305±144.0	91.3	6.7
Bot+Vogel+Glc	1:2	0.998±0.002	4300±60.0	71.4	6.8
Bot+Vogel+Glc	1:10	8.198±0.030	3123±133.0	79.2	6.9

[a]Initial *COD* was 15023±60.0 mg L^{-1}; [b]*Botryosphaeria rhodina* MAMB-05; [c]glucose (10.0 g L^{-1}); [d]Vogel minimal salts medium

B. rhodina MAMB-05 did not grow in the crude effluent and it was necessary to dilute it 1:2 and 1:10. As shown in Table III, the effluent pH had decreased from 7.0 to within the range 6.9 to 6.6 after 5 days, and it was dependent on the effluent dilution. When the effluent was diluted 1:2 without any addition, a *COD* reduction of 39 % was registered, whereby 0.40 mg L^{-1} of fungal bio-

mass was produced. However, the biomass increased to 0.62 mg L^{-1} when the effluent was diluted 1:10 and the *COD* reduction was 64 %. These results indicate that there were sufficient organic compounds in this tannery effluent to promote fungal growth after effluent dilution to decrease its toxicity.

When glucose 1 % (w/v) was added to the effluent in both the previously mentioned dilutions, the production of biomass increased to 0.58 mg L^{-1} and the *COD* did not decrease using the dilution 1:2. Moreover the biomass increased to 3.4 mg L^{-1} when the dilution was increased to 1:10 and the *COD* was the same as that obtained without glucose (39 %), using the dilution 1:2 (Table III). The addition of glucose was important for *B. rhodina* MAMB-05 growth, which can be explained by the high biomass production; it was observed that the effluent visually became more viscous. This increase in viscosity is due to *B. rhodina* MAMB-05 producing a β-(1→3);(1→6)-D-glucan named botryosphaeran,[38] that could explain the lower *COD* reduction.

The addition of minimum Vogel medium to the effluent at the same dilution confirmed that the fungus grew better when the effluent was diluted 1:10, producing 1.26 mg L^{-1} of biomass. Under these conditions, the *COD* reduction was the highest (91 %). The minimum Vogel salts medium contains microelements and the trace elements that are important for fungal growth in conjunction with the organic compounds present in the tannery effluent, which simultaneously aided in the effluent treatment. However, the simultaneous addition of Vogel salts and glucose confirmed that it is more important to increase the biomass production (8.1 mg L^{-1}), mainly when the effluent was diluted 1:10, once the *COD* had decreased to 79 %.

Consequently, some physico-chemical parameters of the effluent were determined using the dilution 1:10, because this presented the best biological treatment results in terms of *COD* reduction. Hence, after the treatment, the chromium concentration had decreased from 198.0 to 1.2 mg L^{-1}, the turbidity from 331.0 to 6.5 NTU and the *TOC* to 93 % (338 mg L^{-1}), indicating that the fungus was efficient in leather wastewater treatment.

CONCLUSIONS

The ascomycete *B. rhodina* MAMB-05 was able to grow and treat the tannery effluent more efficiently when it was diluted 1:10 and minimum Vogel salts medium added. No extra carbon source was necessary, indicating that the concentration of organic compounds present in the tannery wastewater effluent were sufficient for microorganism growth and to decrease the *COD* and *TOC* values by around 91 and 93 %, respectively.

Acknowledgments. The authors acknowledge CNPq-Brazil and Fundação Araucária do Paraná by the financial support. M. C. H. is also grateful to CAPES for a scholarship.

ИЗВОД

БИОТРЕТМАН ОТПАДНЕ ВОДЕ ИНДУСТРИЈСКЕ ШТАВИОНИЦЕ КОРИШЋЕЊЕМ *Botryosphaeria rhodina*

MARIA CLAUDIA HASEGAWA[1], ANELI M. BARBOSA[2] и KEIKO TAKASHIMA[1]

[1]*Laboratório de Processos de Oxidação Avançados, Departamento de Química, CCE и* [2]*Laboratório de Bioquímica de Microrganismos, Departamento de Bioquímica e Biotecnologia, CCE, Universidade Estadual de Londrina,Caixa Postal 6001, CEP 86051-990, Londrina, PR, Brazil*

Третман отпадних вода штавионице изведен је у лабораторијским условима помоћу аскомицетне гљивице *Botryosphaeria rhodina* MAMB-05, која је лигнолитична и конститутивни произвођач лаказа (EC: 1.10.3.2). Узорци отпадне воде су сакупљани у фазама задржавања и бојења, а садржавали су високе вредности *COD* (15023±60 mg L^{-1}), *BOD* (4374±0,1 mg L^{-1}), укупно чврсте материје (28500±2 mg L^{-1}), *TOC* (4685 mg L^{-1}), и хлоридних јонова (2911±0,3 mg L^{-1}). Гљивица је инокулисана и након пет дана, уз мешање на 180 o min^{-1} и 28 °C, *COD* је смањен за 91 %. Укупни органски угљеник је такође смањен од 4685 на 375 mg L^{-1}, а мутноћа од 331 на 6,5 NTU, што указује на то да је биолошки третман био ефикасан, јер је гљивица конзумирала готово сва органска једињења присутна у отпадној води. Није био потребан никакав додатни извор угљеника у третману, што значи да је концентрација органских једињења присутних у отпадној води штавионице била довољна за раст микроорганизма и за смањење *COD* и *TOC* концентрација за око 91, односно 93 %.

(Примљено 3. јула, ревидирано 8. октобра 2010)

REFERENCES

1. S. G. Schrank, H. J. José, R. F. P. M. Moreira, H. F. Schröder, *Chemosphere* **56** (2004) 411
2. S. G. Schrank, H. J. José, R. F. P. M. Moreira, H. F. Schröder, *Chemosphere* **60** (2005) 644
3. U. Kurt, O. Apaydin, M. T. Gonullu, *J. Hazard Mater. B* **143** (2007) 33
4. V. Preethi, K. S. P. Kalyani, C. Srinivasakannan, N. Balasubramaniam, K. Ilyappan, N. Vedaraman, *J. Hazard. Mater. B* **166** (2009) 150
5. Z. R. Guo, G. Zhang, J. Fang, X. Dou, *J. Cleaner Prod.* **14** (2006) 75
6. Z. Song, C. J. Williams, R. G. J. Edyvean, *Desalination* **164** (2004) 249
7. A. Mishra, A. Yadav, M. Agarwal, M. Bajpai, *React. Funct. Polym*. **59** (2004) 99
8. Z. Song, C. J. Williams, R. G. J. Edyvean, *Water Res*. **34** (1999) 2171
9. O. Lefebvre, R. Moletta, *Water Res*. **40** (2006) 3671
10. A. G. Espantaleón, J. A. Nieto, M. Fernández, A. Marsal, *Appl. Clay Sci.* **24** (2003) 105
11. B. V. L. Campos, R. Moraga, J. Yánez, C. A. Zaror, M. A. Mondaca, *Bull. Environ. Contam. Toxicol*. **75** (2005) 400
12. U. N. Rai, S. Dwivedi, R. D. Tripathi, O. P. Shukla, N. K. Singh, *Bull. Environ. Contam. Toxicol*. **75** (2005) 297
13. S. Srivastava, A. H. Ahmad, I. S. Thakur, *Bioresour. Technol.* **98** (2007)1128
14. A. G. Vlyssides, C. Israilides, *J. Environ. Pollut.* **97** (1997) 147
15. C. R. Costa, C. M. R. Botta, E. L. G. Espindola, P. Olivi, *J. Hazard. Mater*. **153** (2008) 616
16. A. Cassano, E. Drioli, R. Molinari, *Desalination* **113** (1997) 251
17. W. G. Scholz, P. Rouge, A. Bódalo, U. Leitz, *Environ. Sci. Technol.* **39** (2005) 8505

18. M. A. S. Rodrigues, F. D. R. Amado, J. L. N. Xavier, K. F. Streit, A. M. Bernardes, J. Z. Ferreira, *J. Cleaner Prod*. **16** (2008) 605
19. A. Bódalo, J. L. Gómez, E. Gómez, A. M. Hidalgo, A. Alemán, *Waste Manage. Res.* **25** (2007) 467
20. 20. J. S. Knapp, P. S. Newby, L. P. Reece, *Enzyme Microb. Technol.* **17** (1995) 664
21. A. M. Barbosa, R. F. H. Dekker, G. E. St. Hardy, *Lett. Appl. Microbiol*. **23** (1996) 93
22. R. F. H. Dekker, A. M. Barbosa, *Enzyme Microb. Technol.* **28** (2001) 81
23. R. F. H. Dekker, A. M. Barbosa, K. Sargent, *Enzyme Microb. Technol.* **30** (2002) 374
24. B. Viswanath, M. S. Chandra, K. P. Kumar, H. Pallavi, B. R. Reddy, in *Dynamic Biochemistry, Process Biotechnology and Molecular Biology 2*, Global Science Books, Edinburgh, UK, 2008, p. 1.
25. L. Gianfreda, F. Xu, J. M. Bollag, *Bioremediation J.* **3** (1999) 1
26. G. Hublik, F. Schinner, *Enzyme Microb. Technol.* **27** (2000) 330
27. C. Mougin, C. Jolivalt, P. Briozzo, C. Madzak, *Environ. Chem. Lett*. **1** (2003) 145
28. APHA, AWWA, WEF. *Standard methods for the examination of water and wastewater*, 21st ed., A. D. Eaton, L. Clesceri, E. W. Rice, A. E. Greenberg, Eds., American Public Health Association, Washington DC, 2005
29. J. Mendham, R. C. Denney, J. D. Barnes, M. J. K. Thomas, *Vogel: Análise Química Quantitativa* 6th ed., LTC, Rio de Janeiro, 2002
30. J. I. Garrote, M. Bao, P. Castro, M. J. Bao, *Water Res.* **29** (1995) 2605
31. T. L. P. Dantas, H. J. José, F. P. M. Moreira, *Acta Scient. Technol*. **25** (2003) 91
32. T. P. Sauer, L. Casaril, A. L. B. Oberziner, H. J. José, R. F. P. M. Moreira, *J. Hazard. Mater. B* **135** (2006) 274
33. A. Cassano, R. Molinari, M. Romano, E. Drioli, *J. Membrane Sci*. **181** (2001) 111
34. S. Shah, I. S. Thakur, *Curr. Microbiol*. **47** (2003) 65
35. S. Leta, F. Assefa, G. Dalhammar, *World J. Microb. Biotechnol*. **21**(2005) 545
36. O. P. Shukla, U. N. Rai, *Bull. Environ. Contam. Toxicol.* **77** (2006) 96
37. S. Srivastava, I. S. Thakur, *Bioresour. Technol*. **97** (2006) 1167
38. A. M. Barbosa, R. M. Stelutti, R. F. H. Dekker, M. S. Cardoso, M. L. C. Silva, *Carbohydr. Res.* **338** (2003) 1692.

Journal of the Serbian Chemical Society
JSCS-info@shd.org.rs • www.shd.org.rs/JSCS
J. Serb. Chem. Soc. 76 (3) 447–458 (2011) UDC 54–72+66.071.9+547.52:628.516+628.52
JSCS–4132 *Original scientific paper*

The octanol–air partition coefficient, K_{OA}, as a predictor of gas–particle partitioning of polycyclic aromatic hydrocarbons and polychlorinated biphenyls at industrial and urban sites

JELENA RADONIĆ*, MIRJANA VOJINOVIĆ MILORADOV#, MAJA TURK SEKULIĆ, JELENA KIURSKI, MAJA DJOGO and DUŠAN MILOVANOVIĆ

Faculty of Technical Sciences, University of Novi Sad, Trg Dositeja Obradovica 6, 21000 Novi Sad, Serbia

(Received 16 June, revised 15 October 2010)

Abstract: The main objectives of the research were to estimate the relationship between the gas–particle partition coefficient, K_p, and the octanol–air partition coefficient, K_{OA}, of polycyclic aromatic hydrocarbons, PAHs, and polychlorinated biphenyls, PCBs, at industrial and urban sites in the Vojvodina region, to compare the obtained slopes and intercepts of the log K_p *vs.* log K_{OA} relations with the results of regression analyses reported in previous studies and to assess the consistency between the particle-bound fractions predicted by the K_{OA} absorption model and the results obtained within field measurements. Fairly good log K_P – log K_{OA} correlations, with an average value of the correlation coefficients of 0.70, indicate that the partition coefficient K_{OA} can be used as a prediction parameter of the gas–particle partitioning processes for both classes of compounds. The results of modelling the atmospheric distribution of PAHs using the K_{OA} absorption model showed inconsistencies between the measured and predicted values of the particle-bound fraction, ϕ, of 1–2 orders of magnitude, while significantly higher discrepancies for PAHs in the Nap–Ace range were found. A similar variability of the measured/modelled ϕ values was obtained using the Junge–Pankow adsorption model, indicating the presence of particles enriched with PAHs. The conducted research showed that the K_{OA}-based approach was less suitable for predicting the gas–particle partitioning of PCBs in urban and industrial sites, compared to the Junge-Pankow model.

Keywords: gas–particle partitioning; polycyclic aromatic hydrocarbons; polychlorinated biphenyls; octanol–air partition coefficient.

* Corresponding author. E-mail: jelenaradonic@uns.ac.rs
# Serbian Chemical Society member.
doi: 10.2298/JSC100616037R

INTRODUCTION

Polycyclic aromatic hydrocarbons (PAHs) are formed during the processes of incomplete combustion of organic matter exposed to a temperature of 700 °C. The most frequent sources of PAHs include motor vehicles, re-suspended soils, oil- or gas-fired residential heaters, residential fireplaces, refineries, power plants and the food industry.[1–3] PAHs are primarily emitted into the atmosphere and are mostly sorbed to particulate matter. However, PAHs are also present in the gaseous phase. PAHs having two or three rings (naphthalene, acenaphthene, anthracene, fluorene and phenanthrene) are present in the air, predominantly in the vapour phase. PAHs that have four rings (fluoranthene, pyrene, benz(*a*)anthracene, chrysene) exist both in the vapour and in the particulate phases, and PAHs having five or more rings (benz(*a*)pyrene, benzo(*g*,*h*,*i*)perylene) are found predominantly in the particulate phase.[4] Due to their well-known carcinogenic, teratogenic and mutagenic properties, the Agency for toxic substances and disease registry has included 17 PAHs, with log K_{OA} (octanol–air partition coefficient) values in the range 5.13–11.01 in the list of toxic pollutants.

Polychlorinated biphenyls (PCBs) are dominantly synthetic organochlorines, widely manufactured in the mid 1900s for industrial use and commercially available until the late 1970s.[5] The term PCBs refers to 209 congeners. The number and location of the chlorines in each congener (especially dioxin-like) govern both the environmental fate and toxicity. PCBs are extremely hydrophobic (log K_{OW} – octanol–water partition coefficient values from 4.34–7.12) and highly resistant to chemical reactions and biological degradation, which leads to their persistence, once they are emitted into the environment. The exposure to PCBs is reported to be a cause of cancer and impairment of the immune, reproductive, nervous and endocrine systems. Due to their health risk to the humans and to the environment, the usage of PCB is banned in numerous countries, according to the Stockholm Convention.

Their atmospheric distribution directly determines the fate, long-range transport (LRT) and transformation processes of semi-volatile organic compounds (SVOC), including PAHs, PCBs, polychlorinated dibenzo-dioxins and furans and organochlorine pesticides, in the atmosphere. Recent investigations have been focused on estimating, modelling and predicting the atmospheric partitioning of SVOC into the particle and vapour phases.[1,6–12]

Several approaches for describing gas–particle partitioning of semi-volatile organic compounds have been proposed in the literature. The first model was developed by Junge and Pankow and it assumes that physical adsorption onto the aerosol surface is the main mechanism that governs the atmospheric distribution.[13,14] The Junge–Pankow relation uses the sub-cooled liquid vapour pressure as the predictor of the particle bound fraction of SVOC. Another frequently used approach is the opposing Harner–Bidleman model, which assumes that absorp-

tion into the aerosol organic matter dominates the partition process.[15] The absorption model proposes the octanol–air partitioning coefficient, K_{OA}, and the organic fraction of the aerosol, f_{OM}, as prediction parameters for the gas–particle partition coefficient.

The objectives of the study were to estimate the relationship between the gas–particle partition coefficient and octanol–air partition coefficient of PAHs and PCBs at industrial and urban sites in the Vojvodina region, and to compare the obtained slopes and intercepts of the log K_p *vs*. log K_{OA} relation to the results of regression analyses reported in the literature. An assessment of the consistency between the particle-bound fraction, ϕ, predicted by the K_{OA} absorption model and the ϕ obtained from field measurements was also one of the goals.

EXPERIMENTAL

Collection of air samples

The air sampling campaign was conducted during the APOPSBAL FP5 project, in the early summer period (median temperature was 19 °C), at six selected urban and industrial localities in the Vojvodina region of Serbia. The sampling spots were located in Novi Sad and Pančevo, as cities with significant industrial activities. Three samples were collected in the industrial zone within the Oil Refinery of Novi Sad (locality N1), three samples were taken in the residential zone of Novi Sad in the proximity and downwind to the oil refinery (locality N2) and three air samples were collected from the third, heavy traffic contaminated, urban sampling spot, in the city centre of Novi Sad (locality N3). Two sampling spots in Pančevo were located in the industrial area – the Oil Refinery of Pančevo (locality P1) and the Chemical Industry of Pančevo (P2). The city centre of Pančevo was chosen as the third, urban locality (P3). Four samples of ambient air were taken from the localities P1 and P3 and three air samples from the sampling spot P2.

Three high volume ambient air samplers were used (one GV2360 Thermoandersen TSP sampler and two samplers that were made of stainless steel boxes equipped with an 8×10 inch filter holder and a 9 cm-diameter polyurethane foam filter holder, 30 cm long). The average total air sampled was 1600 m^3/24 h for the GV2360 Thermoandersen TSP sampler and 900 m^3/24 h for the other two samplers. One glass fibre filter (Whatmann, fraction d_{ae} < 50 μm) and two polyurethane foam filters (Gumotex Břeclav, density: 0.03 g m^{-3}) were used for each sampling period. Prior to the sampling campaign, the glass fibre filters were heated at 450 °C for 5 h and the polyurethane foam filters were Soxhlet extracted with 1:1 acetone/hexane (Merck SupraSolv) using a Foss Tecator Soxtec 1045 HT-2 apparatus for 4 h at 120 °C. The glass fibre and polyurethane foam filters were wrapped in aluminium foil and then placed in a zipped plastic bag. Common usage of both types of sampling medium enabled the simultaneous collection of the suspended particles and gaseous phase of pollutants. All the samples were taken over a period of 24 h.

Analysis of samples

The samples were analyzed using GC–ECD (HP 5890) supplied with a Quadrex fused silica column 5 % Ph for PCBs, while 16 US EPA polycyclic aromatic hydrocarbons were determined in samples using a GC–MS instrument (HP 6890 – HP 5972) supplied with a J & W Scientific fused silica column DB-5MS. Analytical details and Quality Assurance / Quality Control measures were published earlier.[12,16] All analytical procedures were performed in the

laboratories of the Research Centre for Environmental Chemistry and Ecotoxicology (RECETOX), Masaryk University, Brno, Czech Republic.

The statistical analysis was performed using Statistica 8.0 (StatSoft, Inc. USA).

RESULTS AND DISCUSSION

The selected localities, the cities of Novi Sad and Pančevo, located in the Pannonian Plain of the Autonomous Province of Vojvodina in Serbia, were defined as hotspots by UNEP, as the most jeopardized cities during the conflict period in 1999.

The cities of Novi Sad and Pančevo have similar characteristics: developed industrial activity, the River Danube runs through both cities and both have oil refineries in the industrial zones that were heavily damaged by explosions and fires. The city of Pančevo has the Petrochemical Industry, which was partly destroyed during the 1999 war conflict.

Gas–particle partitioning

Semi-volatile organic compounds (SVOCs) are present in the gas phase and attached to particles. The experimental value of the particle-bound fraction, ϕ / %, of each compound (PAHs and PCBs) was determined using the following equation:

$$\phi = \frac{c_{\mathrm{P}}}{c_{\mathrm{G}} + c_{\mathrm{P}}} = \frac{K_{\mathrm{P}} TSP}{1 + K_{\mathrm{P}} TSP} \tag{1}$$

where c_{P} is the concentration of the compound on particles in ng μg^{-1} of particles, c_{G} is the concentration of the compound in the gas phase in ng m^{-3} of air, K_{P} is the gas–particle partition coefficient in m^3 μg^{-1} and *TSP* is the concentration of the total suspended particles in the ambient air in µg aerosol m^{-3} of air. The results are presented in Table I.

The lowest variability of the ϕ values was observed among the group of PAHs of high molecular mass, starting with chrysene. Benzo(*b*)fluoranthene, benzo*(k)*fluoranthene, benzo(*a*)pyrene, indeno(1,2,3-*cd*)pyrene, dibenz(*a*,*h*)anthracene and benzo(*ghi*)perylene were close to 100 % particle-bound.[12] The exception was the locality P1 (Oil Refinery of Pančevo), where the PAHs with a high molecular mass were 50 % and less particle-bound. The unforeseen atmospheric distribution obtained for the sampling spot at the Oil Refinery in Pančevo did not indicate, *a priori*, the low concentration of the total suspended particles in the ambient air. The high concentration levels of polycyclic aromatic hydrocarbons in the gaseous phase or sorbed to fine nano-particles, which could not be collected by glass fibre filters, were probably responsible for gas–particle partitioning of the higher PAHs at the locality P1.

In the atmosphere of the selected sampling points, the PCBs were generally found in the gaseous phase. In the group of compounds with a log K_{OA} value

between 5–8,[17] the median ϕ values of the PCBs corresponded to the median ϕ values of the PAHs. The exception was the locality P3 (city centre of Pančevo), where the fractions of the PCB congeners 52 and 101 sorbed to particles (7.04 and 10.63 %, respectively) were significantly higher than those of the PAHs. For the compounds with log K_{OA} values higher than 8, elevated ϕ values were detected for the PAHs, in comparison to the PCBs. The results for the fraction ϕ obtained in the present study were significantly lower than the previously published values. While in earlier studies of urban, rural and adjacent coastal areas, the PCBs were associated with the atmospheric particles even up to 47 %,[8,18–20] the present analyses showed that the values of the fraction ϕ lay within the interval 0–22.5 % (Table I).

Table I. Median particle-bound fractions, ϕ / %, of PAHs and PCBs at all sampling sites (Nap – naphthalene, Acy – acenaphthylene, Ace – acenaphthene, Flo – fluorene, Phe – phenanthrene, Ant – anthracene, Flu – fluoranthene, Pyr – pyrene, B(*a*)A – benzo(*a*)anthracene, Chr – chrysene, B(*b*)F – benzo(*b*)fluoranthene, B(*k*)F – benzo(*k*)fluoranthene, B(*a*)P – benzo(*a*)pyrene, I(123*cd*)P – indeno(1,2,3*cd*)pyrene, D(*ah*)A – dibenzo(*a,h*)anthracene, B(*ghi*)P – – benzo(*ghi*)perylene)

PAHs	N1	N2	N3	P1	P2	P3
Nap	2.315	5.890	3.365	0.939	1.754	1.576
Acy	10.714	10.870	1.724	2.778	0.000	0.000
Ace	2.804	5.660	5.714	8.771	10.811	4.952
Flo	0.993	1.818	1.439	0.062	0.390	0.829
Phe	0.395	0.631	0.789	0.153	0.094	0.435
Ant	1.245	1.237	2.264	0.000	0.304	0.639
Flu	4.762	3.807	2.921	1.150	0.852	3.430
Pyr	5.665	6.480	3.173	1.072	1.995	4.802
B(*a*)A	41.176	66.138	43.529	27.390	53.846	33.561
Chr	33.065	30.369	35.357	8.563	28.205	33.996
B(*b*)F	97.388	98.022	94.211	36.614	93.500	91.905
B(*k*)F	96.685	96.284	95.149	42.006	95.050	92.922
B(*a*)P	100.000	100.000	100.000	23.333	100.000	100.000
I(123*cd*)P	100.000	100.000	100.000	48.589	100.000	100.000
D(*ah*)A	100.000	100.000	100.000	100.000	100.000	100.000
B(*ghi*)P	100.000	100.000	100.000	49.560	100.000	100.000
PCB 28	0.00	0.00	0.00	0.00	1.54	0.00
PCB 52	5.45	0.72	1.66	0.54	1.31	7.04
PCB 101	0.00	0.00	0.00	1.00	1.64	10.63
PCB 118	0.00	0.00	0.00	0.00	0.00	0.00
PCB 153	2.63	2.33	0.00	1.29	1.45	7.74
PCB 138	5.00	2.00	0.00	1.54	1.59	5.72
PCB 180	12.50	7.69	0.00	3.89	2.78	22.50

Correlation log K_P vs. *log* K_{OA}

Assuming that the absorption into an organic film that coats the particles is the main mechanism of the gas–particle partitioning of SVOCs, the following

equation can be used for the prediction of the atmospheric distribution at 298 K:[15,21]

$$\log K_P = \log \frac{c_P}{TSPc_G} = m_{K_{OA}} \log K_{OA} + b_{K_{OA}} \quad (2)$$

For the state of equilibrium, the slope of the log K_P – log K_{OA} correlation is expected to have a value of +1. The intercept of Eq. (2) depends on the organic fraction of the aerosol, which determines the absorption capacity of the aerosol.[22]

The K_{OA} values used in Eq. (2) were cited or calculated using the equation:[17]

$$K_{OA} = \frac{K_{OW} RT}{H} \quad (3)$$

where K_{OW} is the octanol–water partition coefficient,[17] T is the absolute temperature and H represents the constant in the Henry Law.[17]

The plots obtained as the result of linear regression analysis of the log K_P *vs.* log K_{OA} values for the PAHs at the six localities are shown in Supplementary Material, Fig. 1-S.

All the results were statistically significant, with the critical p-value less than 0.05. The slopes of Eq. (2) ranged from 0.43 to 0.56, with an overall average of 0.51, while the intercepts varied from −7.09 to −7.59 (average: −7.33). The values of the correlation coefficient (R^2) ranged between 0.60 and 0.78, with an average value of 0.70.

The resulting regression for PAHs is:

$$\log K_P = 0.51 \log K_{OA} - 7.33 \quad (4)$$

The regression plots of log K_P – log K_{OA} for the PCBs are given in Supplementary material, Fig. 2-S.

For the statistically significant cases ($p < 0.05$), the slopes of the log K_P *vs.* log K_{OA} correlations ranged from 0.16 to 0.37 (average: 0.24). In addition, the intercepts of the plots were in the range from –5.25 to –7.52, with an average value of –6.12 (R^2 = 0.59–0.86, average: 0.70). The results of the linear regression analysis of the log K_P *vs.* log K_{OA} plots indicated statistical insignificance for the localities: N3, P2 and P3 ($p > 0.05$). This might be due to the low concentration levels of PCBs in the particulate phase and the small number of individual congeners which were present in the particulate phase above the detection limit.

The resulting regression of the log K_P – log K_{OA} correlation for PCBs is presented by Eq. (5):

$$\log K_P = 0.24 \log K_{OA} - 6.12 \quad (5)$$

The correlations obtained from the log K_P – log K_{OA} plots in the present and earlier investigations are presented in Table II.

Table II. Correlations obtained from the log K_P *vs*. log K_{OA} plots in the present study and previously reported studies

Equation	Category of sampling site	Reference
PAHs		
$\log K_P = 0.51 \log K_{OA} - 7.33$, $R^2 = 0.70$	Urban and industrial	Present study
$\log K_P = 0.79 \log K_{OA} - 10.01$, $R^2 = 0.97$	From urban to rural	21
$\log K_P = 0.829 \log K_{OA} - 10.263$, $R^2 = 0.999$	Urban	15
$\log K_P = 0.83 \log K_{OA} - 9.89$, $R^2 = 0.87$	Heavy traffic urban	10
PCBs		
$\log K_P = 0.24 \log K_{OA} - 6.12$, $R^2 = 0.70$	Urban and industrial	Present study
$\log K_P = 0.55 \log K_{OA} - 8.20$, $R^2 = 0.79$	From urban to rural	21
$\log K_P = 0.654 \log K_{OA} - 9.183$, $R^2 = 0.876$	Urban	15
$\log K_P = 0.735 \log K_{OA} - 9.947$, $R^2 = 0.918$	Urban	23
$\log K_P = 0.54 \log K_{OA} - 8.23$, $R^2 = 0.82$	Urban	22
$\log K_P = 0.57 \log K_{OA} - 7$, $R^2 = 0.67–0.93$	Industrial	7

The quite good correlations between log K_P and log K_{OA}, with an average value of the correlation coefficients of 0.70, indicate that the partition coefficient K_{OA} can be used as a prediction parameter of the gas–particle partitioning processes for both classes of compounds. The steeper slopes and higher intercepts of the linear regression analyses for the PAHs and PCBs obtained in previous studies at urban, rural, industrial and heavy traffic contaminated zones[7,10,15,21–23] indicate to states closer to equilibrium, contrary to the present results (Table II). In addition to non-equilibrium in the atmospheric heterogeneous solid–gas system, the presence of several other phenomena, *e.g*., variability among the activity coefficients in the organic matter, γ_{OM}, and in the surrogate of organic matter, octanol, γ_{oct} and adsorption of chemicals onto the surface of the particles, could result in the slopes differing from the theoretical value of +1.[10,24]

The K_{OA} *absorption model*

Assuming that the entire organic matter of the aerosol is available to absorb gaseous compounds, the K_{OA} absorption model, given by Eq. (6), can be used to predict the values of partition coefficient K_P, knowing the coefficient K_{OA} and the organic fraction of the aerosol, f_{OM}:[15]

$$\log K_P = \log K_{OA} + \log f_{OM} - 11.91 \quad (6)$$

The values of the particle-bound fraction, ϕ, can be calculated using the partition coefficient, K_P, and the concentration of suspended particles in the ambient air, *TSP*, by applying Eq. (7):

$$\phi = \frac{K_P TSP}{1 + K_P TSP} \quad (7)$$

The modelled and measured particle-bound fractions were compared in order to estimate the validity of the K_{OA} absorption model. The fraction of the organic matter in the atmospheric particles was assumed to be f_{OM} = 20 %, which is the value expected for urban aerosols.[15]

The ratios between the measured ϕ values and the ϕ predicted using the K_{OA} model (log $\phi_{measured}/\phi_{predicted}$) for PAHs are presented in Fig. 1. The experimental results for the PAHs of higher molecular mass (B(*b*)F, B(*k*)F, B(*a*)P, I(123*cd*)P, D(*ah*)A and B(*ghi*)P) were in line with the modelled fractions. The gap between the estimated and measured ϕ values was less than one order of magnitude for the medium molecular mass PAHs: phenanthrene, fluoranthene, pyrene and benz(*a*)anthracene. Chrysene was barely over predicted. An underestimation in the range of one to two orders of magnitude was observed for the low molecular mass PAHs (fluorene and anthracene), with a higher disagreement for acenaphthylene and acenaphthene (two orders of magnitude), and for naphthalene (even three orders of magnitude). The highest variability of the ϕ value was registered for anthracene, which indicated to different emission sources at the measuring points.

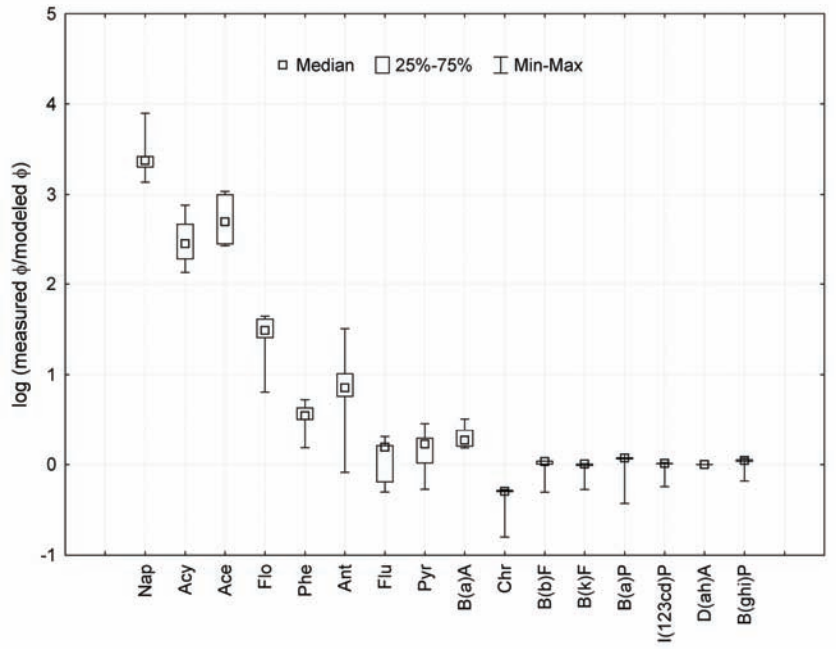

Fig. 1. Ratios of the modelled (K_{OA} absorption model) and measured particle-bound fraction (logarithmic) for PAHs.

Previously reported results on the atmospheric distribution of PAHs distinguished an inconsistency between the measured and predicted ϕ values of 1–2

orders of magnitude,[15,25] while a significantly higher discrepancy for PAHs in the range Nap–Ace was obtained in the present study. The differences could be explained by the presence of a non-exchangeable, inert fraction of the PAH compounds in the aerosols and a slow re-equilibrium process between the PAH molecules in the gaseous phase and freshly emitted PM in the urban and industrial environments. A similar variability of the measured/modelled ϕ values was obtained using the Junge–Pankow adsorption model,[12] once again indicating to the existence of particles enriched with PAHs, whereby the main mechanism which governed the gas–particle partitioning of the PAHs remains unknown.

The median values and variability of the measured/modelled ϕ values for the PCB congeners are presented in Fig. 2.

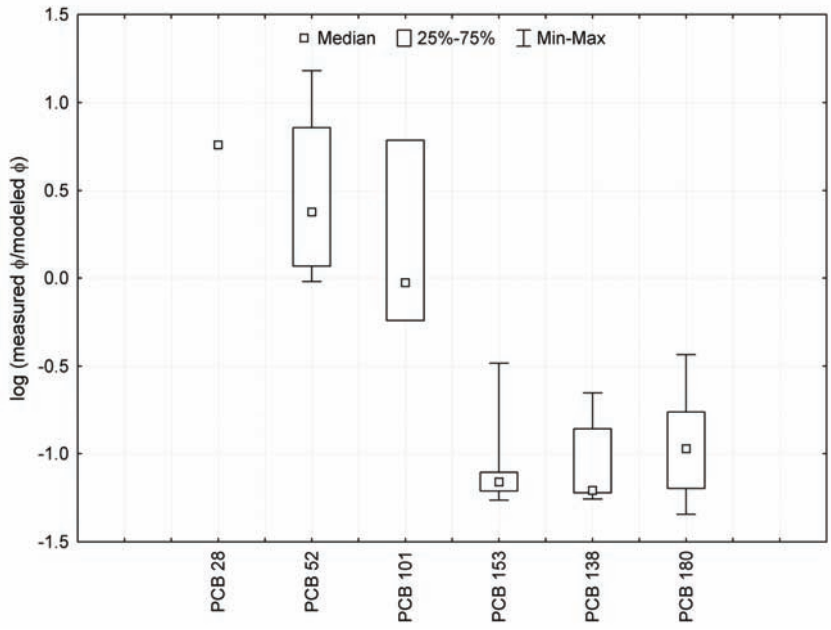

Fig. 2. Ratios of the modelled (K_{OA} absorption model) and measured particle-bound fraction (logarithmic) for PCBs.

The median values of the measured and modelled particle-bound fraction of the PCB congener 101 were in line. The congeners PCB 28 and 52 were underestimated by less than one order of magnitude, while the heavier PCB congeners (PCB 138, PCB 153 and PCB 180) were over predicted (by up to one order of magnitude).

These results are in good agreement with the results of previously published studies on the modelling of the atmospheric distribution of PCB congeners.[9] The investigation showed that the K_{OA}-based approach was less suitable for the gas–

–particle partitioning of PCBs in urban and industrial sites, compared to the Junge–Pankow model.[12] The same observation was obtained in previously reported studies of urban[22] and rural[9] localities, while the results of Harner and Bidleman at urban sampling sites lead to the opposite conclusion.[15]

CONCLUSIONS

The present research was conducted in two industrial cities, Novi Sad and Pančevo, in the Province of Vojvodina, Serbia, with similar geoecological and industrial characteristics, defined as the hotspots in Serbia by UNEP.

The particle-bound fractions of the PAHs at the urban and industrial localities ranged from less than 1 to 100 %, which is in agreement with previously reported values. The PCB congeners (28, 52, 101, 118, 138, 153, and 180) were generally found in a gaseous phase in the atmosphere of the sampling sites. The results for the fraction ϕ were significantly lower than previously published values. While the studies in different countries (Korea, Turkey, and Greece) in urban, rural and adjacent coastal areas indicated that PCBs were sorbed on particles even up to 47 %, the present analysis showed that the values of the fraction φ lay within the interval 0–22.5 %.

The quite good log K_P – log K_{OA} correlations, with an average value of the correlation coefficient of 0.70 for PAHs and PCBs, indicated that the partition coefficient K_{OA} could be used as a prediction parameter of the gas–particle partitioning processes for both classes of compounds. The obtained lower values for the slopes could indicate to a slow re-equilibrium between PAHs and PCBs in a gaseous phase and freshly emitted particulate matter in the urban and industrial environment, variability among the γ_{OM} and γ_{oct}, and adsorption of chemicals onto the surface of the particles.

Previously reported studies on the modelling of the atmospheric distribution of PAHs using the K_{OA} absorption model indicated inconsistency between the measured and predicted ϕ values by 1–2 orders of magnitude, while the present study showed a significantly higher discrepancy for PAHs in the range Nap–Ace. The results of this could be explained by the presence of a non-exchangeable, inert fraction of PAH compounds in the suspended particles. A similar variability of the measured/modelled ϕ values was obtained using the Junge–Pankow adsorption model, indicating to the presence of PAHs enriched particles. The research showed that the K_{OA}-based approach was less suitable for gas–particle partitioning of PCBs in urban and industrial sites, compared to the Junge–Pankow model.

The analysis of the residues of PAHs and PCBs in the ambient air was performed for the first time in the Vojvodina region, in order to obtain non-existing data for gas–particle partitioning processes at industrial and urban sites in this part of the western Balkan Region.

SUPPLEMENTARY MATERIAL

The plots of linear regression analysis of the log K_P *vs.* log K_{OA} values for the PAHs at the six localities and the regression plots of log K_P – log K_{OA} for the PCBs are available electronically from http://www.shd.org.rs/JSCS/, or from the corresponding author on request.

Acknowledgments. A part of this research was financially supported by 5FP EU (ICFP501A2PR02 – APOPSBAL), the Ministry of Science and Technological Development of the Republic of Serbia (21014) and the Provincial Secretariat for Science and Technological Development (114-451-00603). Special thanks go to Dr Jana Klánová, Dr Ivan Holoubek and the Research Centre for Environmental Chemistry and Ecotoxicology (RECETOX), Masaryk University, Brno, Czech Republic.

И З В О Д

КОЕФИЦИЈЕНТ РАСПОДЕЛЕ K_{OA} КАО ПРЕДИКТОР АТМОСФЕРСКЕ ДИСТРИБУЦИЈЕ ПОЛИЦИКЛИЧНИХ АРОМАТИЧНИХ УГЉОВОДОНИКА И ПОЛИХЛОРОВАНИХ БИФЕНИЛА НА ИНДУСТРИЈСКИМ И УРБАНИМ ЛОКАЛИТЕТИМА

ЈЕЛЕНА РАДОНИЋ, МИРЈАНА ВОЈИНОВИЋ МИЛОРАДОВ, МАЈА ТУРК СЕКУЛИЋ, ЈЕЛЕНА КИУРСКИ, МАЈА ЂОГО и ДУШАН МИЛОВАНОВИЋ

Факултет техничких наука, Универзитет у Новом Саду, Трг Доситеја Обрадовића 6, 21000 Нови Сад

Рад приказује зависност коефицијената расподеле PAH и PCB између гасовите и чврсте суспендоване фазе у атмосфери индустријских и урбаних локалитета региона Војводине од коефицијената K_{OA}, поређење добијених нагиба и одсечака корелације log K_P – log K_{OA} са резултатима регресионе анализе из претходних истраживања и одступање удела PAH и PCB у суспендованим атмосферским честицама од вредности процењених коришћењем апсорпционог K_{OA} модела атмосферске дистрибуције. Задовољавајућа корелација log K_P – log K_{OA}, са просечном вредношћу коефицијента корелације 0,7, указује да се коефицијент K_{OA} може користити за предвиђање партиције између гасовите и чврсте суспендоване фазе у атмосфери, за обе класе једињења. Претходним истраживањима предикције атмосферске дистрибуције PAH употребом апсорпционог K_{OA} модела добијена су одступања измерених од моделованих вредности φ за 1–2 реда величине, док мерења спроведена у оквиру истраживања указују на значајно већу неусаглашеност за нафтален, аценафтилен и аценафтен. Слични резултати одступања измерених и моделованих φ вредности добијени су и применом адсорпционог Junge–Pankow модела, што недвосмислено указује на присуство атмосферских честица са високим садржајем PAH на одабраним мерним местима. Истраживање је показало да се боља процена партиције PCB на урбаним и индустријским локалитетима добија коришћењем Junge–Pankow модела, у односу на апсорпциони модел базиран на коефицијенту расподеле октанол–ваздух.

(Примљено 16. јуна, ревидирано 15. октобра 2010)

REFERENCES

1. E. Galarneau, T. F. Bidleman, P. Blanchard, *Atmos. Environ.* **40** (2006) 182
2. C. Vasilakos, N. Levi, T. Maggos, J. Hatzianestis, J. Michopoulos, C. Helmis, *J. Hazard. Mater.* **140** (2007) 45
3. K. Ravindra, R. Sokhi, R. Van Grieken, *Atmos. Environ.* 42 (2008) 2895
4. World Health Organization, *Health risks of persistent organic pollutants from long-range transboundary air pollution*, http://www.euro.who.int/Document/e78963.pdf (accessed 2003)

5. I. Holoubek, in *PCBs: recent advances in environmental toxicology and health effects*, L. W. Robertson, L. G. Hansen, Eds., The University Press of Kentucky, Lexington, KY, USA, 2001, pp. 17–25
6. Y. Su, Y. D. Lei, F. Wania, M. Shoeib, T. Harner, *Environ. Sci. Technol.* **40** (2006) 3558
7. S. S. Cindoruk, F. Esen, Y. Tasdemir, *Atmos. Res.* **85** (2007) 338
8. S. S. Cindoruk, Y. Tasdemir, *Environ. Pollut.* **148** (2007) 325
9. M. Mandalakis, E. G. Stephanou, *Environ. Pollut.* **147** (2007) 211
10. Y. Tasdemir, F. Esen, *Atmos. Res.* **84** (2007) 1
11. M. T. Sekulic, J. Radonic, M. Djogo, in *Environmental, Health and Humanity Issues in the Down Danubian Region: Multidisciplinary Approaches*, D. Mihailović, M. V. Miloradov, Eds., World Scientific Pub Co Inc, Singapore, 2008, pp. 284–295
12. J. Radonic, M. T. Sekulic, M. V. Miloradov, P. Cupr, J. Klanova, *Environ. Sci. Pollut. Res.* **16** (2009) 65
13. C. Junge, in *Fate of pollutants in the air and water environments*, I. H. Suffet, Ed., Wiley, New York, USA, 1977, pp. 7–26
14. J. F. Pankow, *Atmos. Environ.* **21** (1987) 2275
15. T. Harner, T. F. Bidleman, *Environ. Sci. Technol.* **32** (1998) 1494
16. M. Turk, J. Jaksic, M. V. Miloradov, J. Klanova, *Environ. Chem. Lett.* **5** (2007) 109
17. D. Mackay, W. Y. Shiu, K. C. Ma, S. C. Lee, *Handbook of Physical-Chemical Properties and Environmental Fate for Organic Chemicals*, 2nd ed., CRC Press Taylor & Francis Group, Boca Raton, FL, USA, 2006
18. H. Kaupp, M. S. McLachlan, *Chemosphere* **38** (1999) 3411
19. M. Mandalakis, M. Tsapakis, A. Tsoga, E. G. Stephanou, *Atmos. Environ.* **36** (2002) 4023
20. H. G. Yeo, M. Choi, M. Y. Chun, Y. Sunwoo, *Atmos. Environ.* **37** (2003) 3561
21. A. Finizio, D. Mackay, T. Bidleman, T. Harner, *Atmos. Environ.* **31** (1997) 2289
22. R. Lohmann, T. Harner, G. O. Thomas, K. C. Jones, *Environ. Sci. Technol.* **34** (2000) 4943
23. R. L. Falconer, T. Harner, *Atmos. Environ.* **34** (2000) 4043
24. K. U. Goss, R. P. Schwarzenbach, *Environ. Sci. Technol.* **32** (1998) 2025
25. P. Fernandez, J. O. Grimalt, R. M. Vilanova, *Environ. Sci. Technol.* **36** (2002) 1162.

Journal of the Serbian Chemical Society
JSCS@tmf.bg.ac.rs • www.shd.org.rs/JSCS
J. Serb. Chem. Soc. 76 (3) S29–S31 (2011)

Supplementary material

SUPPLEMENTARY MATERIAL TO

The octanol–air partition coefficient, K_{OA}, as a predictor of gas–particle partitioning of polycyclic aromatic hydrocarbons and polychlorinated biphenyls at industrial and urban sites

JELENA RADONIĆ*, MIRJANA VOJINOVIĆ MILORADOV#, MAJA TURK SEKULIĆ, JELENA KIURSKI, MAJA DJOGO and DUŠAN MILOVANOVIĆ

Faculty of Technical Sciences, University of Novi Sad, Trg Dositeja Obradovica 6, 21000 Novi Sad, Serbia

J. Serb. Chem. Soc. 76 (3) (2011) 447–458

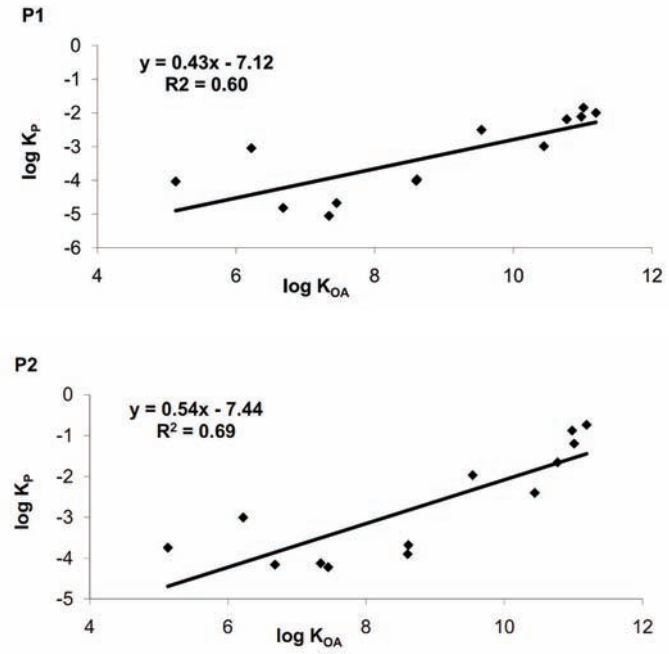

Fig. 1-S. Logarithmic correlations of K_P *vs.* K_{OA} for PAHs at six sampling locations.

* Corresponding author. E-mail: jelenaradonic@uns.ac.rs
# Serbian Chemical Society member.
doi: 10.2298/JSC100616037R

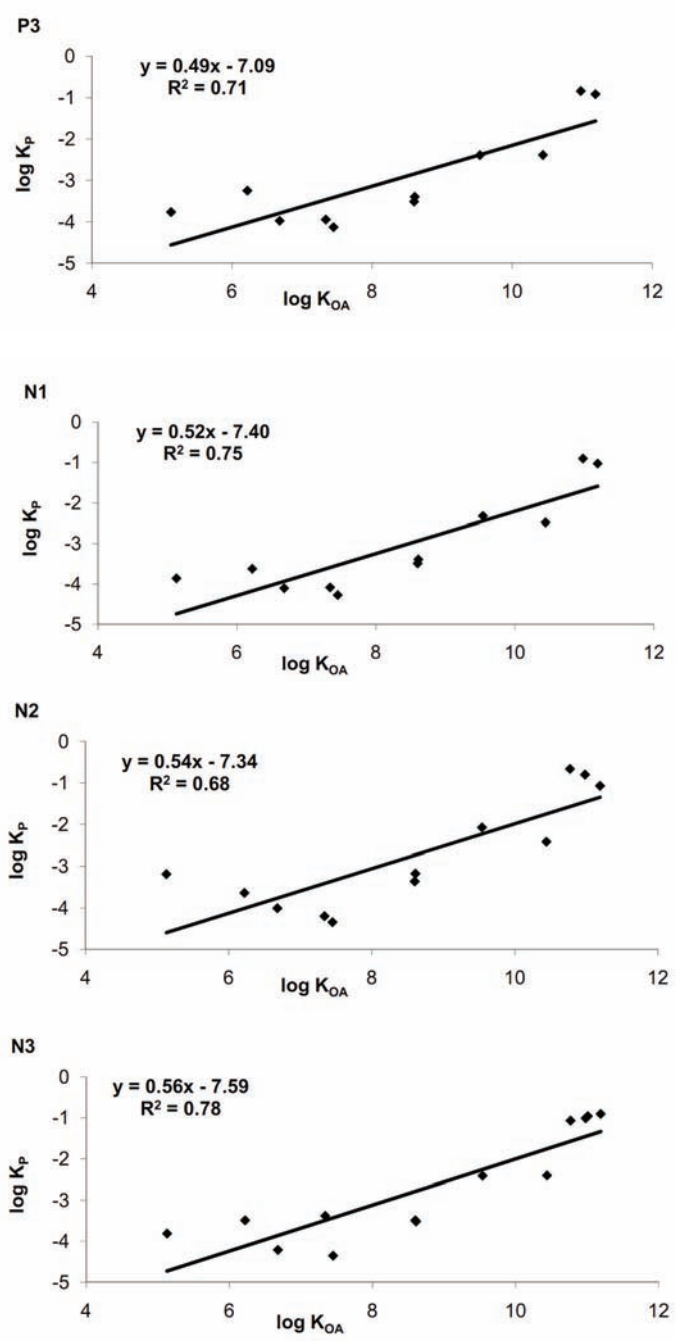

Fig. 1-S. Continued.

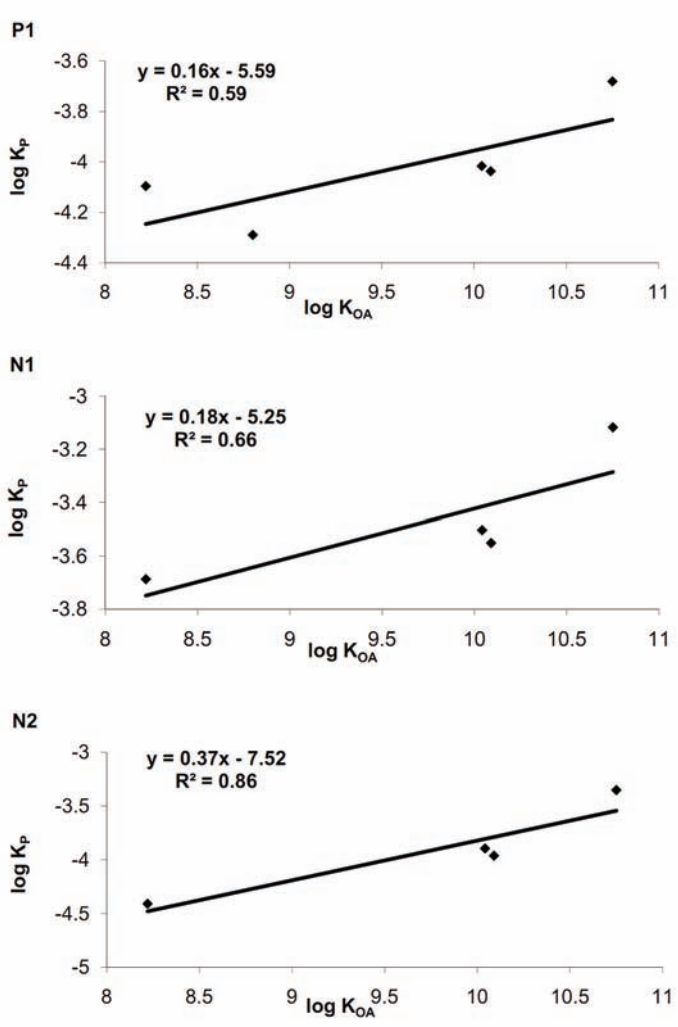

Fig. 2-S. Logarithmic correlation of K_P *vs.* K_{OA} for PCBs at three sampling locations.

Journal of the Serbian Chemical Society
JSCS-info@shd.org.rs • www.shd.org.rs/JSCS
J. Serb. Chem. Soc. 76 (3) 459–478 (2011)
JSCS–4133
UDC 332.12:338.45+628.3.03.034.2+628.336+311.213.3(497.13)
Original scientific paper

Wastewater canal Vojlovica, industrial complex Pančevo, Serbia – preliminary ecotoxicological assessment of contaminated sediment

IVANA PLANOJEVIĆ[1]*, IVANA TEODOROVIĆ[1], KATERINA BARTOVA[2], ALEKSANDRA TUBIĆ[3#], TAMARA JURCA[4], WILLI KOPF[5], JIRI MACHAT[2], LUDEK BLAHA[2] and RADMILA KOVAČEVIĆ[1]

[1]University of Novi Sad, Faculty of Sciences, Department of Biology and Ecology, Laboratory for Ecotoxicology (LECOTOX), Trg D. Obradovica 2, 21000 Novi Sad, Serbia, [2]Research Centre for Toxic Compounds in the Environment – RECETOX, Masaryk University, Faculty of Science, Brno, Czech Republic, [3]University of Novi Sad, Faculty of Sciences, Department of Chemistry, Novi Sad, [4]University of Novi Sad, Faculty of Sciences, Department of Biology and Ecology, Laboratory for Hydrobiology, Novi Sad, Serbia and [5]Bavarian Environment Agency, Munich Office, Germany

(Received 5 May, revised 2 September 2010)

Abstract: Effluents collected from the industrial complex of Pančevo, Serbia (oil refinery, petrochemical plant, and fertilizer factory), are discharged into a wastewater canal entering the Danube River. In this study, which was focused on sediment assessment, a complex triad approach consisting of chemical analysis, sediment toxicity tests and macrozoobenthos community analysis was applied. In toxicity tests on sediment elutriates, the following responses were registered – stimulatory effect in algal bioassay, no effect in acute test with *Daphnia magna*, and low to moderate toxicity in the conventional *Vibrio fischeri* test. Moderate to high toxicities were recorded in solid phase tests on *Myriophyllum aquaticum* and *V. fischeri*. High content of Hg, certain PAHs and non-characterised sediment contaminants accumulated over years contribute not only to the registered toxicity, but also to the complete absence of macrozoobenthos. The obtained results proved that regularly measured conventional and priority pollutants are hardly ever the only toxic contaminants present in sediments. Toxicity tests, in particular the contact test, might guide towards a better selection of parameters to be regularly or occasionally monitored. In addition, complete sediment toxicity tests proved to be an appropriate method for assessing the bioavailability of the chemically detected contaminants. The analysis of the macrozoobenthos composition and structure as inevitable part of se-

* Corresponding author. E-mail: ivana.planojevic@dbe.uns.ac.rs
# Serbian Chemical Society member.
doi: 10.2298/JSC100505036P

diment risk assessment procedures integrates the effects of multiple stressors and gives a realistic insight into not only sediment contamination by toxic pollutants, but also the sediment status in general.

Keywords: sediment; wastewater canal; toxicity tests; test battery.

INTRODUCTION

Water authorities and regulatory bodies have underestimated sediments as integral components of aquatic ecosystems in the past, due to practical problems as well as to the complex nature of sediments. The European Union Water Framework Directive (WFD), aimed at achieving good ecological and good surface water chemical status, is also focused on the water column and considers contaminants from point and diffuse sources, but underestimates the role of sediments as long-term secondary sources of contaminants and, therefore, a possible cause for deterioration of ecological status.[1] Chapman indicated the need for addressing sediments and sediment quality in addition to water quality since: a) various toxic contaminants found in only trace amounts in the water column accumulate in sediments to elevated levels; b) sediments serve as both a reservoir and a source of contaminants to the water column; c) sediments integrate contaminant concentrations over time whereas water column contaminant concentrations are much more variable; d) sediment contaminants in addition to water column contaminants affect benthic and other sediment-associated organisms; e) sediments are an integral part of the aquatic environment, providing habitat, feeding and rearing areas for many aquatic biota.[2]

To evaluate aquatic sediments with respect to their adverse effects on biota and ecosystems as a whole, neither biotests nor chemical analytical techniques alone are sufficient. For instance, sediment chemistry can provide information on contamination, but even with strong evidence of anthropogenic impacts on the benthic community at many sediment sites, the degree of toxicity (or even its presence or absence) cannot be predicted by contaminant concentrations alone.[3] On the other hand, sediment bioassays can yield data with respect to toxic effects in selected test organisms and test systems; however, the selected tests are conducted under laboratory conditions and usually cannot be applied under *in situ* conditions due to varying environmental conditions.[4]

Thus, integrated approaches are required in order to gain insight into the ecological state of sediments. With the sediment quality triad (SQT), Chapman suggested such an integrated approach, which simultaneously investigates sediment chemistry and sediment toxicity, as well as alternations in the field, for example, modifications of benthic community structure.[5]

Chemical data, including sediment quality guidelines (SQGs), have been used for a number of years by regulatory agencies in different countries to assess and manage contaminated sediments.[6,7] Complex evaluation of sediment quality,

based on multiple lines of evidence, including biological effect-based assessment (*in situ* and *ex situ* BEBA) has already found its place in environmental risk assessment of many European countries, such as Belgium, the Netherlands and Germany.[8] In Serbia, the official surface water quality monitoring programmes have relied for years mostly on physico–chemical water quality parameters and to some extent on biomonitoring data (saprobic indices based on plankton communities). Ambient standards, now already rather outdated, are only set for water column, while sediment quality criteria have not been established so far.[9] In addition, WET (whole effluent testing), ambient water, and sediment toxicity evaluation have never been included into official monitoring programmes.[10]

Official monitoring programmes and independent studies performed recently identified several hot spots of severe freshwater pollution and soil and sediment contamination that are attributed to historic pollution, outdated environmental policy, regulations and management practice, heavy pollution caused by insufficient waste water treatment as well as major accidental spills (as the result of the NATO campaign in 1999 or the Baya Mare cyanide accident in 2000, for instance).[11–16] The largest individual hot-spot is the industrial complex near the city of Pančevo – effluents are discharged into the wastewater canal Vojlovica, which enters the Danube River.[9]

The wastewater canal Vojlovica was built in 1962 to collect the wastewater discharges from the industrial complex located at the southern end of the city of Pančevo, the so-called “South zone industrial complex” (SZIC), 20 km to the northeast of Belgrade. The SZIC complex includes a petrochemical factory (HIP Petrohemija), an oil Refinery (NIS Rafinerija, Pančevo) and chemical fertilizers factory (HIP Azotara). The canal is about 2 km long, around 76 m wide and directly connected to the Danube River (Fig. 1). The canal is artificial with no natural flows. For a long time, the environmental conditions of the area surrounding

Fig. 1. Map of the study area – wastewater canal Vojlovica entering the Danube River.

the canal have been strongly affected by the presence of the industrial complex, and the 1999 NATO bombing events exacerbated the already existing vulnerable system.[17]

Since August 1999, several surveys have been performed to evaluate the impact of the Pančevo canal on the Danube River, but they were all realised using chemical analysis of the water column and sediments only, providing no data on ecotoxicity. Hitherto, the resident macrozoobenthos community has never been surveyed. First sediment investigations conducted jointly by the UNEP (The United Nations Environment Programme) and the UNCHS (The United Nations Centre for Human Settlements) in 1999 and 2001 showed long-term pollution from the industrial complex, consisting, in particular, of mercury and petroleum hydrocarbons components, as well as free phase dichloroethane (DCE) and a high concentration of mineral oil. The main conclusion was that the water in the canal was not significantly polluted, while the sediments were classified as hazardous wastes (class H-11) due to their high content of mineral oil, mercury, PAHs, DCE and BTEX (benzene, toluene, ethylbenzene and xylene – volatile aromatic compounds typically found in petroleum products). UNOPS (The United Nations Office for Project Services) performed another study of the Pančevo canal in 2002, but again based on chemical analyses only. It was found that the pollutants were strongly bound to sediment particles, while sediment pore-water was not significantly affected.[11] The last of the series of official assessments, which eventually resulted in a feasibility study for remediation of the wastewater canal, was performed in 2005/6 by D'Appolonia S.p.A Genoa, Italy, appointed by the Italian Ministry of the environment and territory (IMET).[18] The results of the chemical analysis were in agreement with the previously reported ones, but no ecological impact assessments have been conducted nor any concrete actions undertaken so far, either in terms of dredging or *in situ* remediation.

According to Wenning and Ingersoll, a sediment ecological risk assessment (ERA) should include lines of evidence derived from several different investigations: nature and extent of contamination; expected or acceptable indices of benthic diversity and abundance in the absence of contamination; estimates of the potential for bioavailability, bioaccumulation and adverse effects posed by chemicals and mixtures of chemicals (the potential for chronic and acute effects) on aquatic organisms; stability (fate and transport) of the sediments and contaminants; and estimates of the potential risks posed by contamination to aquatic biota and associated resources.[19]

Therefore, the purpose of this study was to apply the sediment quality triad, which integrates chemical, ecotoxicological and macrozoobenthos community analysis, to evaluate not only the quality or level of contamination of the Vojlovica canal sediment but also to provide a more realistic assessment of ecological impact that long-term simultaneous contamination by diverse toxic pollutants

might pose on the macrozoobenthos and aquatic ecosystems as a whole. The application of several different toxicity tests, using different test species covering all three trophic levels (primary producers – algae *Pseudokirchneriella subcapitata*, aquatic macrophyte *Myriophyllum aquaticum*, consumers – represented by the zooplankton *Daphnia magna* and decomposers – the bacteria *Vibrio fischeri*), test set-ups (solid phase and elutriate) and end-points (primary production, growth, mortality and bioluminescence) was intended to lead to the selection of the most appropriate tests for risk assessment of sediments contaminated by oil and petrochemical industry effluents.

EXPERIMENTAL

Sample collection

Grab sediment samples (surface sediments layer of 5 cm) were taken by a Van Veen sampler for macrozoobenthos community analyses, transported in plastic bags and stored in the laboratory at +4 °C. For comparative purposes, the same types of samples were also taken from the navigation canal flowing parallel to wastewater canal but not receiving any direct discharge of industrial wastewaters. The sediment samples were washed out and sieved through a system of sieves of various mesh size. The identification of macroinvertebrate taxa was performed using standard taxonomical keys.[20]

The sediment samples for chemical analyses and toxicity tests were taken by an Eijkelkamp corer (surface sediments of 40 cm depth) at three sampling sites along the wastewater canal Vojlovica:

V1 sampling site – downstream from the fertilizer factory outlet;

V2 sampling site – downstream from the petrochemical plant and oil refinery outlets;

V3 sampling site – near the confluence of the wastewater canal and the Danube River.

The collected sediment samples were stored at +4 °C in glass jars during transport to the laboratory and then stored at –20 °C. Sediment samples for chemical analyses and toxicity tests on elutriates were freeze-dried and sieved (0.072 mm), while bulk sediment samples were used for solid phase toxicity tests.

Chemical analyses

The total organic carbon (*TOC*) was determined using a high temperature LiquiTOC II analyzer (Elementar Analysensysteme). The heavy metal contents (Cd, Cr, Cu, Hg, Pb, Ni and Zn) in the sediment samples were evaluated based on the aqua regia leaching process according to the ISO 11466 protocol,[21] modified with respect to the employed analytical instrumentation (3 g of dry sediment sample was leached overnight by 7 ml of HNO_3 and 21 ml of HCl and then heated under reflux for 2 h; after cooling, the mixture was filled up in the volumetric flask and diluted before inductively coupled plasma mass spectrometry (ICP–MS) measurement on Agilent 7500ce instrument, Agilent Technologies, Japan. Mercury was determined by the thermo-oxidation method using an AMA-254 analyzer (Altec).

Sediment samples for 16 standard PAHs, and total PCB (standard mixture of 7 PCB congeners: PCB28, PCB52, PCB101, PCB153, PCB180 and PCB 209) analyses were prepared according to the standard methods,[22] and extracted in a Soxhlet apparatus with carbon tetrachloride (100 ml) for 6 h. Those extracts were passed over dry aluminium oxide. Samples were mixed with methanol (5 g wet sediment per ml of methanol) and extracted with a dichloromethane–hexane mixture (1:1) on a magnetic stirrer for 1 h. Elemental sulphur was removed

by adding Cu powder. The samples were fractionated over silica gel according to the EPA 3630C procedure.[23] The extracts were analyzed by GC–MS and GC–μECD (HP 5890GC Series II with a 5971 MSD) in the splitless mode. The practical quantisation limit (*PQL*) and method detection limit (*MDL*) for all compounds were 5 and 2 ng g^{-1}, respectively. Recovery for the applied method for PAH analyses was determined for phenanthrene and chrysene using soil samples spiked at the 20 μg kg^{-1} level. Recovery values (mean of 3 measurements) were 64 % for phenanthrene and 78 % for chrysene.

Toxicity tests

Sediment elutriates were prepared according to ISO 14735.[24] Lyophilised sediment samples were mixed with distilled water in a 1:10 ratio, put in closed flasks and shaken for 24 h on an automatic shaker with 5–10 rpm. After the sediment particles had settled, supernatant was used for the following toxicity tests: green algae *P. subcapitata*, invertebrate *D. magna*, and the test with the luminescent bacteria *V. fischeri*. Solid phase toxicity tests were performed with *V. fischeri* and with the aquatic plant *M. aquaticum.*

The algae were cultured under sterile conditions at a temperature of 23±2 °C, constant aeration and illumination of 60–120 μE m^{-2} s^{-1} in Zehnder–Bristol (modified Bold) (ZBB) medium. Three days before the test, sterile ZBB medium was inoculated with algae preculture with a cell density of 5×10^3–1×10^4 cells ml^{-1} in order for the algae to reach the exponential phase at the beginning of the test (approximately 1×10^6 cells ml^{-1}). The test was performed using a modified ISO protocol,[25] in microtitre plates in the following v/v concentrations of elutriate: 1.5, 3, 12.5, 25 and 75 %, in five replicates in three repetitions. The microtitre plates were placed on an automatic shaker in order to keep the algae cells in suspension and to prevent their sedimentation. The temperature and light regimes were the same as for the culturing. After 72 h, the algal optical density was measured at 680 nm using a spectrophotometer BioTek, PowerWave at the start and the end of the test. The results were transformed into number of algal cells using calibration curves and the specific growth rate was calculated for every elutriate concentration. Inhibition of the growth rate was determined in comparison to the control.

D. magna was cultured in standard synthetic water according to the United States Environment Protection Agency (USEPA) method in 10 l aquariums with constant aeration, a temperature of 25±2°C and illumination of 10–20 μE m^{-2} s^{-1} with photoperiod 16 h light/8 h dark.[26] The daphnids were fed daily with algae *P. subcapitata*. The procedure described in ISO 6341 was applied in the toxicity test,[27] *i.e.*, 24 h-old daphnids (neonates) were placed in 50 ml test vessels with 30 ml of test medium. The test was performed with 5 neonates in each vessel, 4 vessels per dilution. The test conditions were the same as for the culturing regarding the temperature and light regime, but the neonates were not fed during the test. Elutriates were tested in the following v/v concentrations: 3.12, 6.25, 12.5, 25 and 50 %. Immobilisation of the neonates was observed after 24 and 48 h and the results were compared to the control.

Toxicity tests on elutriates with freeze-dried *V. fischeri* bacteria, obtained from Macherey-Nagel, Germany, was conducted according to ISO 11348 (1998).[28] The luminescent bacteria were reconstituted in cold 2 % NaCl solution, equilibrated at 0 °C for 30 min, transferred to test tubes and equilibrated for an additional 15 min at 15 °C. In the test with *V. fischeri*, the following v/v concentrations of elutriates were tested: 5, 10, 20, 40 and 80%. In all test treatments, NaCl was added in order to obtain 2 % NaCl in the elutriates. Bioluminescence was measured in time 0 and 30 min using Lumino m90a illuminometer at a working temperature of 15 °C. The decrease in luminescence in each treatment was compared to the control treat-

ment and the percent inhibition was calculated using linear regression. The test was conducted in duplicate in two repetitions.

A sediment suspension for the solid phase test with *V. fischeri*, which was performed according to the method described by the Environment Canada, was made by mixing 7 g of fresh sediment with 35 ml of 2 %NaCl solution.[29] This working suspension was diluted to the defined geometrical range of the test concentrations 30.78–985 mg l^{-1}, with mixing on a vortex between the dilution steps to prevent settlement of the sediment particles. The test was realised in duplicate in two repetitions for a duration of 15 min at 15 °C. The bioluminescence was measured only at the end. For each test concentration, the bioluminescence was compared to the control and the percent inhibition was calculated. In both tests with *V. fischeri*, 2 % NaCl was used as the control.

M. aquaticum was cultured in a modified Steinberg medium,[30] at a constant temperature (24±0.5 ºC) with a 24-h photoperiod. The toxicity test was performed according to Feiler *et al.*,[31] *i.e.*, three whorls were placed in one glass vessel containing 80 g of bulk sediment, three vessels per sediment sample. Artificial sediment, as specified in the OECD Guideline 218, was used as the control,[32] in six replicates, and three whorls in each replicate. In order to minimize evaporation during the test, all vessels were covered with a glass lid and a few ml of Steinberg medium was added to each vessel daily. The plants were incubated for 10 days under constant temperature (24±0.5 °C), and constant light (neutral white 60–75 µE m^{-2} s^{-1}). The weight of each whorl was measured at the start and the end of test and compared to the control. The toxicity of the samples was quantified as % inhibition in comparison to the control.

RESULTS AND DISCUSSION

Chemical analyses

The first step in the complex assessment of the site was to analyse sediments for expected toxic pollutants. Taking into consideration the type of industrial effluents discharged into the canal, as well as the results of previously conducted studies,[11,17,18] the sediment samples were analysed for TOC, heavy metals, PAHs and PCBs.

TABLE I. Concentration of heavy metals (mg per kg of dry weight) in the sediment samples

Sampling site	Cd	Cr	Cu	Hg	Pb	Ni	Zn
V1	1.26	33.4	42.4	32.2	23.5	31.7	146
V2	1.41	38.1	43.8	9.62	26.3	31.8	170
V3	1.17	21.8	37.4	6.31	19.2	25.7	111
ICPDR JDS Danube sediment quality target values	1.2	100	60	0.8	100	50	200
Dutch target value	0.8	100	36	0.3	85	35	140
Rhine target value	1	100	50	0.5	100	50	200

For this artificial waterbody entering the Danube River, ICPDR JDS (Joint Danube Survey of International Commission for the Protection of the River Danube) – sediment quality target values were taken as reference concentrations,[33] while for comparative purposes, Dutch[34] and Rhine[35] target values are also shown. The measured concentrations of Hg (6.31–32.2 mg kg^{-1} dw) were consi-

derably higher than all three reference concentrations and Cd (1.17–1.41 mg kg^{-1} dw) was slightly higher than the reference concentrations for the Danube and Rhine target values, while the content of other metals did not exceed the target values (Table I). The Dutch target values, the most stringent of the three reference values, could be used for comparison only with certain reservation as they are set for sediments normalised to 10 % *TOC* and 25 % clay, while the *TOC* values in the Vojlovica wastewater canal (Table II) ranged from 6.8–7.5 %. Nevertheless, it is obvious that the contents of Cd, Cu, Hg and Zn exceeded the Dutch target values, while the Ni concentration was only slightly below. The two remaining metals, Cr and Pb, were the only two with measured concentrations well below the Dutch target values. However, only in the case of Hg was the Dutch intervention value (10 mg kg^{-1} dw) exceeded in sample V1, while the content in sample V2 was only slightly below.

TABLE II. Content of total organic carbon (*TOC*) in the sediment samples

Sampling site	*TOC* / %
V1	6.78
V2	6.85
V3	7.49

When compared to the USEPA recommendations for sediment quality,[36] which set consensus-based threshold effect concentration (*TEC*) values, below which harmful effects are unlikely to be observed, and consensus-based probable effect concentration (*PEC*) values, above which harmful effects are likely to be observed, only the content of mercury in all three samples exceeds both the *TEC* and *PEC* values (0.18 and 1.06 mg per kg of dry weight (dw), respectively). The chromium and lead contents in all three samples were below the *TEC* values (43.3 and 35.8 mg per kg of dw, respectively). The Canadian sediment quality guidelines,[37] which set values for interim sediment quality guidelines (*ISQG*) and a probable effect level (*PEL*) were also used to evaluate the quality of the Vojlovica sediments. Again, mercury stands out, with the measured concentrations in all three samples being above the *ISQG* and *PEL* values (0.17 and 0.49 mg kg^{-1} dw, respectively), while the measured concentrations of Pb (19.2–26.3 mg kg^{-1} dw) in all three samples were below both the *ISQG* (35.0 mg kg^{-1} dw) and *PEL* (91.3 mg kg^{-1} dw) values. The measured concentrations of Cu (37.4–43.8 mg kg^{-1} dw) and Cd (1.17–1.41 mg kg^{-1} dw) in all samples were above the *ISQG* (35.7 and 0.6 mg kg^{-1} dw, respectively), but below the *PEL* values (197 and 3.5 mg kg^{-1} dw, respectively). The chromium concentration in sample V2 (38.1 mg kg^{-1} dw) and the zinc concentrations in samples V1 and V2 (146 and 170 mg kg^{-1} dw, respectively) were just above the *ISQG* values (37.3 mg kg^{-1} dw for Cr and 123 mg kg^{-1} dw for Zn).

The highest concentrations of total 16 PAHs (35.02 mg kg^{-1}) with a high content of compounds of lower molecular weights was measured in sample V1 (Table III). If compared to the USEPA recommendations,[36] the content of total PAHs in all samples exceeded the *TEC* value (1.61 mg kg^{-1} dw), while only in sample V1 did it exceeds the *PEC* value (22.8 mg kg^{-1} dw). The USEPA also sets *TEC* and *PEC* values for individual PAHs. Values exceeding both the respective *TEC* and *PEC* were recorded for anthracene, fluorine, and naphthalene in sample V1; benzo(*a*)anthracene in sample V2 and pyrene in samples V1 and V2.

TABLE III. Concentration of PAHs (mg kg^{-1} dw) and total PCBs (μg kg^{-1} dw) in the sediment samples

Compound	V1	V2	V3
Naphthalene	5.81	0.21	1.18
Acenaphthylene	4.25	0.96	1.20
Acenaphthene	2.58	0.51	0.64
Fluorene	4.01	0.64	0.70
Phenanthrene	11.06	3.72	2.85
Anthracene	1.17	0.37	0.28
Fluoranthene	0.82	0.36	0.28
Pyrene	3.04	2.41	1.24
Benzo(*a*)anthracene	0.73	1.21	0.49
Chrysene	1.02	1.21	0.49
Benzo(*b*)fluoranthene	0.08	0.12	0.06
Benzo(*k*)fluoranthene	0.08	0.12	0.06
Benzo(*a*)pyrene	0.15	0.25	0.08
Dibenzo(*a,h*)anthracene	0.08	0.03	0.02
Benzo(*g,h,i*)perylene	0.06	0.09	0.04
Endeno(1,2,3-*cd*)pyrene	0.08	0.03	0.02
Total PAH, mg kg^{-1} dw[b]	35.02	12.25	9.61
Sum PAH[a], mg kg^{-1} dw	20.90	7.54	3.68
Total PCBs, μg kg^{-1} dw	116.12	164.57	83.2

[a]Summed PAH: naphthalene, phenanthrene, anthracene, fluoranthene, chrysene, benzo(*a*)fluoranthene, benzo(*k*)fluoranthene, benzo(*a*)pyrene, benzo(*g,h,i*)perylene; [b]dry weight

Dutch sediment quality values are set for Sum PAH (see explanation below Table III); the target value being 1 mg kg^{-1}, while the intervention value is 40 mg kg^{-1}. Obviously, the Sum PAH values in all samples exceeded the target value but remained below the intervention value.

The Canadian sediment quality guidelines are set for several individual PAH compounds.[37] The contents of naphthalene, acenaphthylene, acenaphthene, fluorene, phenanthrene, anthracene and pyrene along the whole canal exceeded both the theoretically and empirically probable effect values.

The content of PCBs was far below the Dutch target and intervention values, as well as the Canadian PEL (277 μg kg^{-1} dw) and the USEPA PEC (676 μg kg^{-1} dw) values.

From the presented results, it could be conservatively concluded that among the heavy metals, mercury could be identified as one of the possible key toxic pollutants that might cause or contribute to the severe impairment of the overall ecological conditions in the wastewater canal. The PCBs can be seen as a minor problem, while the high content of certain PAH compounds could be identified as other potential stressors. However, standard chemical analyses say very little about the bioaccessibility and bioavailability of toxic pollutants. Therefore, the second step of the triad approach consisted of toxicity tests of bulk sediments and elutriates – using various test species and test designs to estimate if the obviously present toxic pollutants in potentially toxic concentrations could be identified as the key toxic pollutants that might pose risks to the aquatic ecosystem as a whole.

Toxicity tests

The results of algae growth inhibition tests performed on three elutriates are shown in Fig. 2. Obviously, the tests did not result in typical dose-response curves, on the contrary, statistically significant (one-way ANOVA, $p \leq 0.05$) stimulatory effects in comparison to the control were observed in treatments with higher proportions of elutriate.

Statistically significant growth stimulation in comparison to the control was observed in treatments with ≥12.5 % elutriate (v/v) in the cases of samples V1 and V2 and in the treatment with 75 % elutriate (v/v) in the case of sample V3. Statistically significant growth inhibition in comparison to the control was registered only in the treatments with the lowest elutriate content (1.5 % v/v), *i.e.*, in samples V2 and V3. These findings are not surprising, as different authors have reported many times before similar outcomes of algal toxicity tests of environmental samples. These results can be explained by higher nutrient contents in treatments with higher proportions of elutriates in comparison to the control, indicating, on the other hand, that the aqueous phase does not contain bioavailable toxic pollutants in toxic concentration for the selected species.[38–41]

No negative effects on immobilisation were observed in the 24 and 48 h acute toxicity tests on sediment elutriates. Since *D. magna* is one of the most sensitive test species to heavy metals,[42] the fact that no negative effects were observed suggested, in agreement with the results of the algal test, that the metals present in the bulk sediment, particularly Hg which is, according to chemical analysis, present in concentrations that might cause toxic stress, are not readily bioavailable. Contrary to this, it was reported by Akkanen and Kukkukonen that *D. magna* is relatively insensitive to organic pollutants, PAHs in the first place, due to their ability to biotransform these groups of contaminants.[43] Therefore it should not be a surprising finding that the present PAH compounds did not have any effect on daphnids in the acute test. Moreover, the negative results of this acute test also suggest that other contaminants were present neither in lethal concentrations nor in a bioavailable form.

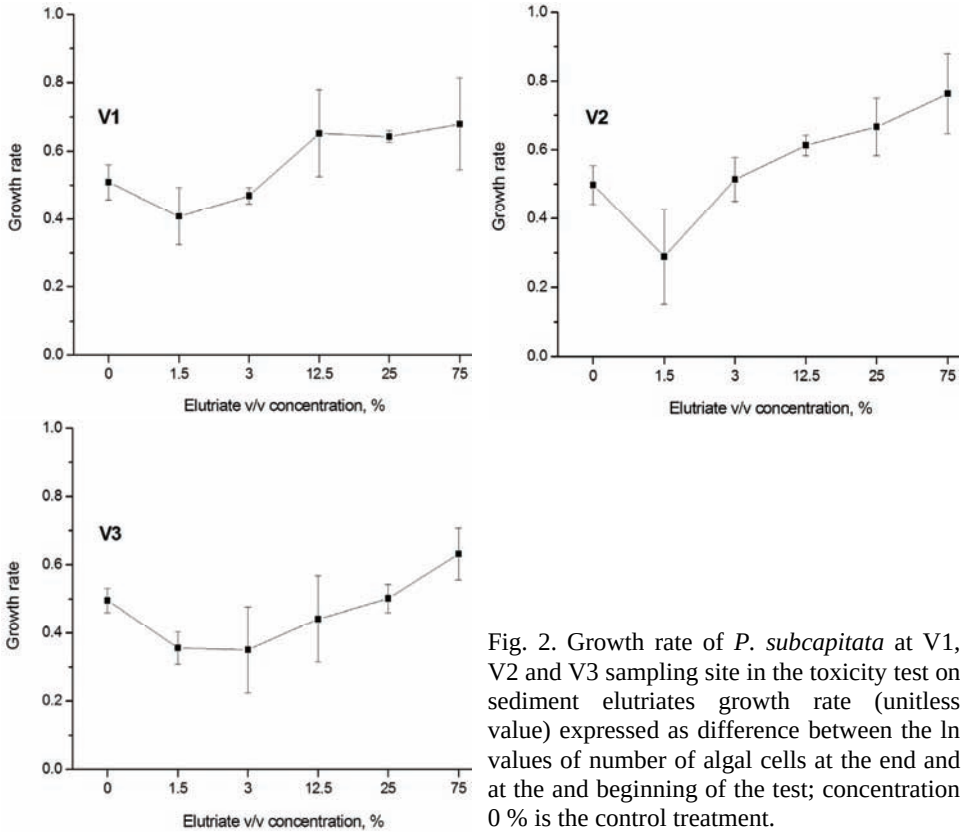

Fig. 2. Growth rate of *P. subcapitata* at V1, V2 and V3 sampling site in the toxicity test on sediment elutriates growth rate (unitless value) expressed as difference between the ln values of number of algal cells at the end and at the and beginning of the test; concentration 0 % is the control treatment.

The results of toxicity tests on sediment elutriate with the bioluminescent bacteria are shown in Fig. 3.

The sample V1 was identified as the most toxic with respect to the selected test species and set-up, EC_{50} 58.73 % and EC_{10} 4.32 %. For samples V2 and V3, only EC_{10} could be estimated at 23.21 and 24.70 %, respectively. Since bacterial species, including *V. fischeri*, were proved rather tolerant to metals,[44–46] it is more likely that the high content of total PAHs and the concentrations of several individual PAH compounds could be identified as potential causes of the observed toxic effect. Sensitivity of *V. fischeri* to certain PAH compounds has been proven earlier.[47–49] However, the testing of samples V2 and V3, which resulted in the hormesis effect in treatments with low elutriate contents, contradicts this hypothesis, as sample V2, that was non-toxic to *V. fischeri* was also characterised by high contents of several PAH compounds as well as total PCBs. Therefore, it could be hypothesised that other, non-characterised contaminants might be the possible cause of the observed toxicity of sample V1 to *V. fischeri*. Stimulatory effect in *V. fischeri* toxicity test in presence of sub-lethal concentrations of toxicant has already been observed and reported.[45,50,51]

Sediment solid phase toxicity tests with *V. fischeri* (Table IV) identified sample V2 as the most toxic (EC_{50} 17.03 mg l^{-1}), while for samples V1 and V3, 50 % inhibition was calculated at considerably higher levels (158.60and 342.11 mg l^{-1}, respectively).

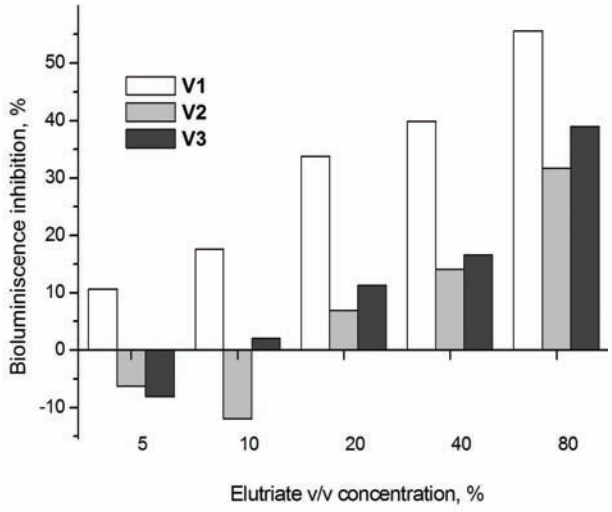

Fig. 3. Inhibition of bioluminescence in the test on sediment elutriates with *V. fischeri*.

TABLE IV. Results of solid phase toxicity tests with *V. fischeri*

Parameter	V1	V2	V3
EC_{50} / mg l^{-1}	158.60	17.03	342.11

According to chemical analysis, sample V2 was rich in several PAH compounds and heavy metals other than Hg. Again, the high content of Hg in sample V1 seems not to cause substantial effects on *V. fischeri*, which was expected due to low sensitivity of the selected species to metals. Thus, metals in sample V2 could not be regarded as the key pollutant group responsible for the high toxicity of sample V2 to *V. fischeri*. Again, it could be speculated that other, not measured contaminants could contribute to the toxicity of sample V2.

The results from sediment solid phase toxicity tests on *M. aquaticum* (Table V) are in agreement with the results from the conventional *V. fischeri* test; sample V1 was characterised as the most toxic – growth inhibition reached 70.35.% in comparison to the control, while with the other two samples, V2 and V3, growth inhibition did not even reach 50 %.

TABLE V. Growth inhibition of *M. aquaticum* in the sediment solid phase test

Parameter	V1	V2	V3
Growth inhibition, %	70.35	33.33	33.90

M. aquaticum is commonly used as test species in toxicity test on pesticides,[52,53] studies on the bioaccumulation of heavy metals,[54] and recently in sediment toxicity tests.[5,55] Stesevic *et al*. found *M. aquaticum* to be highly sensitive to metal burden in sediments of Lake Skadar, which could also explain the growth inhibition in samples rich in metals, observed in the present study.[55]

Analyses of the macrozoobenthos community

Analyses of the macrozoobenthos community were performed on sediment samples in the final tier of the sediment quality triad. The complete absence of a macrozoobenthos community was observed in all three samples taken from the wastewater canal. However, analyses of the macrozoobenthos community of the navigation canal, which flows parallel to the wastewater canal, indicated that the natural conditions are favourable for typical lowland slow-flowing rivers and canals, as it is represented by 4 groups Gastropods (1 species – *Viviparus sp*.), Decapoda (1 species – *Astacus* sp), Diptera (Chironomidae) and the dominant Oligochaeta (represented by three typical species tolerant to muddy substrates, low oxygen concentrations and high organic load – *Branchiura sowerbyi, Limnodrilus hoffmeisteri and L. claparedeanus*). These rather alarming findings on the complete absence of a macrozoobenthos community are not unique, but they are still exceptional in the Vojvodina region. They were reported several years ago for only a few other hot spots along the Danube–Tisa–Danube irrigation network, mainly due to severe organic load resulting in a constant oxygen deficit and the presence of hydrogen sulphide.[56,57] However, the absence of benthic invertebrates in the wastewater canal could not be attributed to similar reasons, as the characterisation of the sediments showed a medium content of organic matter (*TOC* ranging slightly from 6.8 to 7.5 %), which implies that toxic pollution might be seen as the cause, or at least the confounding factor, of the absence of macrozoobenthos. The absence of macroinvertebrates from all samples supports the hypothesis that apart from the measured expected pollutants, the whole sediment toxicity must be also attributed to other, not regularly monitored contaminants, as the overall conditions in the wastewater canal are equally unfavourable to macrozoobenthos despite the fact that the content of the monitored pollutants varies considerably between the different samples, being almost negligible in sample V3.

Integrative assessment of the level of contamination of the Vojlovica canal sediments

For an integrative assessment of the site of the present study, a complex triad approach, which uses multiple lines of evidence of ecosystem disturbances caused by constant contamination, was applied. The results of chemical analyses, restricted to the expected contaminants commonly measured in sediments under the

direct pressure of effluents originating from the oil industry, did not, and could not, reveal anything new in comparison to previously conducted studies. Instead, the present results simply confirmed the already existing findings regarding the high content of Hg and PAH compounds in the canal sediments. The authors of the cited studies, however, did not have the possibility to compare their findings with any regionally relevant sediment standards, since those for the Danube River have been suggested only recently. In addition, they refrained from comparing their results with biologically derived standards, such as the Canadian or USEPA. In direct comparison, as shown in Table I, it is obvious that the contents of all the measured metals (except Hg) were still below the Danube River target values. In addition, a comparison of the present findings with other sediment standards, such as the Canadian or USEPA, which are based more on the probable effects of sediment-bound contaminants to aquatic biota, also support the conclusion that among metals Hg really stands out as the potential key toxic pollutant, while contamination with standard PAH compounds, as expected, proved to be rather severe, as it exceeded all biologically derived standards used for comparison, indicating that this group of compounds most probably could cause toxic effects to aquatic biota.

The sampling sites were selected to enable discrimination of the impact of two industrial facilities, which discharge different types of effluents. The content of Hg, as expected, was the highest in sample V1 showing that the long-term discharge of effluents from the vinyl chloride plant has resulted in the accumulation of high quantities of Hg in relatively stable sediments; the concentrations of Hg further downstream (V2 and V3) are considerably lower. However, the highest concentrations of all other metals were recorded in V2. As far as other compounds are concerned, contrary to expectations, the highest value of total PAHs was recorded in sample V1, while V2 was characterised by the highest measured concentrations of PCBs and several individual PAH compounds (Table III). Thus, no clear contamination gradient was observed along the canal, apart from the fact that the V3 sampling site is characterised by the lowest concentrations of the majority of the investigated contaminants. This can be explained by the position of the sampling site in relation to the Danube River; in comparison to the other sampling sites, it is more affected by changes in the Danube water level, which washes out the most downstream sediments.

Toxicity tests followed the chemical analyses with the idea of testing the whole sediment toxicity, which would aid the assessment of the bioaccessibility and bioavailability of all the contaminants present, analysed or non-analysed. Another objective of the toxicity testing was to attempt to establish links between the content of the measured contaminants and their possible effect on biotic systems and the ecosystem in general in the search for an answer to whether the measured contaminants are really the key toxic pollutants. Sample V3 proved to

be the least toxic to all selected test species, regardless of the test set-up and sediment phase tested. This was to have been expected, due to the lowest content of contaminants recorded, as just explained above. However, the toxicity testing of samples V1 and V2 resulted with rather inconsistent outcomes. Sample V1 was the most toxic of the 3 samples tested using *V. fischeri* in the aqueous phase, while sample V2 was most toxic to *V. fischeri* in the solid phase.

The differences in the test results with aqueous and solid phase can be explained by different properties of the test phases – in tests on the aqueous phase, only soluble the fraction of the contaminants present in the samples contributed to the overall toxicity, while in the direct contact test, the effects of contaminant bound to the sediment particles are taken into account as well. However, taking into consideration all the differences between the test set-ups and relative sensitivity of the chosen species towards respective environmental contaminants, it could be speculated that the measured contaminants are not the only toxic pollutants present in the Vojlovica canal sediments that contribute to the observed sediment toxicity. This speculation is supported by recently published results on an assessment of Vojlovica sediment performed by Effect Directed Analyses (EDA) using micro-EROD and cell proliferation tests in different fractions obtained from the same samples tested in the study.[58] Chemical analysis of the most active fractions revealed high concentrations of methylated PAHs and other alkyl-substituted PAHs. Only minor portions of biologically derived TCDD-EQs could be attributed to the monitored PAHs with known relative potencies (*REP*s). Therefore, it is hypothesised that a major part of the activity was due to non-monitored alkylated and heterocyclic PAHs. The results of the cell cytotoxicity/proliferation assay on rat hepatoma H4IIE cell line also suggested the presence of uncharacterised sediment pollutants with pronounced potency to disturb cell growth. All these speculations are supported by the results of macrozoobenthos community analysis. Its complete absence along the whole canal, even from sample V3 characterised by the lowest content of the measured pollutants as well as the lowest toxicity to all selected species, indicate not only extreme contamination of the canal sediment, but also unfavourable overall conditions in the canal.

Selection of the appropriate tests for sediments contaminated with oil refinery and petrochemical effluents

In the tests on elutriates, inhibition was observed only in the toxicity test on *V. fischeri*. Since no toxic or inhibitory effects were observed in the algal and crustacean tests, *V. fischeri* proved to be the most sensitive species in the selected test battery. Davoren *et al.*, in their assessment of contaminated estuarine sediments, found *V. fischeri* as the most sensitive species in comparison to algal tests and even to the survival test with *Artemia salina*.[40]

As test species, algae are predominately sensitive to herbicides and to some extent to heavy metals,[59] while their relative tolerance towards organic contaminants apart from pesticides is well documented.[60] On the other hand, both solid phase tests were sensitive enough to detect the toxic effects of the investigated sediments, proving that contact tests have by far a greater potential in risk assessment of contaminated sediments than aqueous phase tests. It has been proven repeatedly, including this study, that sediment-bound contaminants are neither readily bioavailable nor, consequently, easily extractable by overlying water. Therefore, a more realistic estimate of the whole sediment toxicity, as a part of a complex sediment risk assessment procedure, could be obtained using sediment contact tests. The *V. fischeri* solid phase test has already shown some of advantages, but care should be taken with the interpretation of the results obtained by its application, as it has been well documented that the species is highly sensitive to hydrogen sulphide, which is often present in contaminated sediments.[61,62]

Aquatic organisms of the three trophic levels (producers, consumers, reducers) have been used for a long time for ecotoxicological assessments of water quality. Algae, daphnia, and luminescent bacteria are often used as test organisms in biotest systems that have become established standards. However, the results of the present study, as well as comparative studies, have shown that algae are not sufficiently sensitive to a large number of contaminants and thus cannot be the exclusive indicator organism of any toxic effects on autotrophic life. Moreover, the EU Water Framework Directive (EU-WFD) sets equally, side-by-side, macrozoobenthos, fish, phytoplankton, and macrophytes as indicators of the status of waters.[63] Nevertheless, biotest systems relying on higher plants have rarely been used in assessments of aquatic sediments to date. Against this background, the aquatic duckweed test was developed and standardised,[30] and the sediment contact test was developed with *M. aquaticum*.[31] Compared to tests with algae, some of its advantages is that it is more representative of higher plants, since target organism and test organism are closer related in terms of evolutionary history. The results of this study, as well as of the study of Feiler *et al.*, demonstrated that the application of biotests with higher plants in analyses of contaminated sediments yields valuable results that may contribute to a concept for the integrative risk assessment of contaminated sediment much more efficiently than algal tests.[64]

CONCLUSIONS

In this study, we applied a complex triad approach was applied in an assessment of sediments of an industrial wastewater canal. According to the obtained results, the selected study site justified its well-known status as a contamination hot spot. The high contents of not only Hg and certain PAHs but also of non-characterised sediment contaminants accumulated over years of severe pollution by partly treated or untreated effluents contribute not only to the observed toxi-

city to some of the selected species (namely, *M. aquaticum* and *V. fischeri*), but also to the complete absence of macrozoobenthos, which indicates extremely unfavourable overall conditions in the canal and can be regarded as a serious signal for immediate remediation action.

Sediment risk assessment cannot be imagined without chemical analysis, but obviously, regularly measured conventional and priority pollutants are hardly ever the only toxic contaminants present in sediments. Toxicity tests, particularly contact tests, along with targeted bioanalyses might guide, more precisely and efficiently, towards a better selection of parameters to be regularly or occasionally monitored. In addition, if put in reverse order, whole sediment toxicity tests proved to be an appropriate method for assessing bioavailability of chemically detected contaminants.

Finally, macrozoobenthos community analysis, as an unavoidable part of sediment risk assessment procedures, integrates the effects of multiple stressors and gives realistic insight not only into sediment contamination by toxic pollutants, but also into the sediment status in general, is necessary and valuable not only in sediment ERA, but also for an accurate evaluation of the ecological status of every waterbody as well.

Acknowledgments. We thank Ms. Dubravka Bugarski Alimpić for English revision of the manuscript. The paper was presented at the 2nd REP LECOTOX Workshop "Trends in Ecological Risk Assessment", Novi Sad, September 21st to 23rd, 2009, within the frame of the REP LECOTOX project (INCO – CT – 2006 – 043559 –REP – LECOTOX UNSFS). The research was supported by the Ministry for Science and Technological Development of the Republic of Serbia, Project No. 143058, CETOCOEN Project and the Bayerisches Landesamt für Umwelt, Munich, Germany.

ИЗВОД

ПРЕЛИМИНАРНА ЕКОТОКСИКОЛОШКА ПРОЦЕНА КОНТАМИНИРАНОГ СЕДИМЕНТА – КАНАЛ ОТПАДНИХ ВОДА ВОЈЛОВИЦА, ИНДУСТРИЈСКИ КОМПЛЕКС ПАНЧЕВО, СРБИЈА

ИВАНА ПЛАНОЈЕВИЋ[1], ИВАНА ТЕОДОРОВИЋ[1], KATERINA BARTOVA[2], АЛЕКСАНДРА ТУБИЋ[3], ТАМАРА ЈУРЦА[4], WILLI KORF[5], JIRI MACHAT[2], LUDEK BLAHA[2] и РАДМИЛА КОВАЧЕВИЋ[1]

[1]Универзитет у Новом Саду Природно-математички факултет, Департман за биологију и екологију, Лабораторија за екотоксикологију (LECOTOX), Трг Доситеја Обрадовића 2, 21000 Нови Сад, [2]Research Centre for Toxic Compounds in the Environment - RECETOX, Masaryk University, Faculty of Science, Brno, Czech Republic, [3]Универзитет у Новом Саду, Природно-математички факултет, Департман за хемију, Нови Сад, [4]Универзитет у Новом Саду Природно-математички факултет, Департман за биологију и екологију, Лабораторија за хидробиологију и [5]Bavarian Environment Agency, Office Munich, Germany

У нашем истраживању које се фокусира на процену седимента, примењен је тријажни приступ који се састоји од: хемијских анализа, тестова токсичности на узорцима седимента и анализе бентосне фауне на узорцима седимента из канала отпадних вода Војловица. У тестовима тоскичности на елуатима седимента забележени су следећи одговори: стимулација раста у алгалном тесту, изостанак токсичносг ефекта у тесту са *Daphnia magna* и слаба до умерена токсичност у конвенционалном тесту са *Vibrio fischeri.* Умерена до изражена токсичност је

забележена у тесту чврсте фазе седимента са тест врстама *Myriophyllum aquaticum* и *Vibrio fischeri.* Високе концентрације живе, појединих PAH једињења, али такође и контаминаната који нису анализирани, акумулирани у седименту дуги низ година, доприносе не само забележеној токсичности него и потпуном одсуству бентосне фауне. Наши резултати потврђују да редовно праћени и мерени конвенционални и приоритетни полутанти у већини случајева не представљају једине токсичне контаминанте присутне у седименту. Тестови токсичности, нарочито контактни тестови, могу дате смернице за бољи одабир параметара за редовно или повремено праћење. Такође, тестови токсичности чврсте фазе седимента су се показали као одговарајући метод за процену биодоступности анализираних контаминаната. Анализа састава и структуре бентосне фауне, као саставног дела процене ризика седимента, интегрише ефекте мултиплих стресора и даје реалну слику не само о контаминираности седимента токсичним полутатнима, него и о статусу седимента уопште.

(Примљено 5. маја, ревидирано 2. септембра 2010)

REFERENCES

1. U. Forstner, *J. Soils Sediments* **2** (2002) 54
2. P. M. Chapman, *Environ. Toxicol. Chem*. **8** (1989) 589
3. S. E. Apitz, J. W. Davis, K. Finkelstein, D. W. Hohreiter, R. Hoke, R. H. Jensen, J. Jersak, V. J. Kirtay, E. Mack, V. S. Magar, D. Moore, D. Reible, R. G. Stahl Jr., *Integr. Environ. Assess. Manag.* **1** (2005) 2
4. G. A. Burton Jr., *Environ. Toxicol. Chem*. **10** (1991) 1585
5. P. M. Chapman, *Environ. Toxicol. Chem*. **5** (1986) 957
6. M. P. Babut, W. Ahlf, G. E. Batley, M. Camusso, E. de Deckere, P. J. den Besten, in *Use of Sediment: Quality Guidelines and Related Tools for the Assessment of Contaminated Sediments*, R. J. Wenning, G. E. Batley, C. G. Ingersoll, D. W. Moore, Eds., Setac Press, Pensacola, FL, USA, 2005, p. 345
7. W. J. Berry, T. S. Bridges, S. J. Ells, T. H. Gries, D. S. Ireland, E. M. Maher, C. A. Menzie, L. M. Porebski, J. Stronkhorst, in *Use of Sediment: Quality Guidelines and Related Tools for the Assessment of Contaminated Sediments*, R. J. Wenning, G. E. Batley, C. G. Ingersoll, D. W. Moore, Eds., Setac Press, Pensacola, FL, USA, 2005, p. 383
8. P. J. den Besten, E. de Deckere, M. P. Babut, B. Power, T. A. DelValls, C. Zago, A. M. P. Oen, S. Heise, *J. Soils Sediments* **3** (2003) 144
9. I. Teodorovic, *Environ. Sci. Pollut. Res.* **16** (2009), Suppl. S-123
10. I. Teodorovic, M. Becelic, I. Planojevic, I. Ivancev-Tumbas, B. Dalmacija, *Environ. Monit. Assess.* **158** (2009) 381
11. *The United Nations Environment Programme, From Conflict to Sustainable Development, Assessment of Environmental Hot Spots, Serbia and Montene*gro, 2004, http://postconflict.unep.ch/publications/sam.pdf (accessed March, 2011)
12. I. Ivancev-Tumbas, B. Dalmacija, E. Maljevic, J. Trickovic, S. Roncevic, J. Agbaba, in *Proceedings of 2nd European Conference on Dredged Sludge Remediation*, (2004), CD Proceedings, Amsterdam, The Netherlands, 2004
13. I. Ivancev-Tumbas, E. Maljevic, Z. Tamas, E. Karlovic, B. Dalmacija, *Water Sci. Technol. Water Supply* **7** (2007) 155
14. S. Terzić, I. Senta, M. Ahel, M. Gros, M. Petrović., D. Barcel, J. Müller, T. Knepper, I. Martí, F. Ventura, P. Jovančić, D. Jabučar, *Sci. Total Environ.* **399** (2008) 66
15. S. Sakan, I. Gržetić, D. Đorđević, *Environ. Sci. Pollut. Res.* **14** (2007) 229
16. M. B. Radenkovic, S. A. Cupac, J. D: Joksic, D. J. Todorovic, *Environ. Sci. Pollut. Res.* **15** (2008) 61

17. The United Nations Environment Programme, United Nations Centre for Human Settlements, *The Kosovo Conflict: Consequences for the Environment and Human Settlements*, Final Report, 1999, http://postconflict.unep.ch/publications/finalreport.pdf
18. D'Appolonia, *Implementation of the Pančevo Action Programme (Phase II), Final Report, Volume IX, Clean Up of the Pančevo Canal*, 2006
19. R. J. Wenning, C. G. Ingersoll, in *Summary of the SETAC Pellston Workshop on Use of sediment quality guidelines and related tools for the assessment of contaminated sediments*, 2002, Fairmont, Montana, SETAC, Pensacola, FL, USA, 2002, http:// //www.setac.org/files/SQGSummary.pdf
20. R. O. Brinkhurst, B. G. Jamieson, *Aquatic Oligochaeta of the World*, Oliver & Boyd, Edinburg, UK, 1971, p. 860
21. *ISO 11466, Soil quality – Extraction of trace elements soluble in aqua regia*, 1995
22. *APHA-AWWA-WEF, Standard Methods for the Examination of Water and Waste Water*, 19th ed., American Public Health Association, Washington DC, USA, 1995
23. United States Environmental Protection Agency, *Method 3630X Silica Gel Cleanup, Revision 3, Test Methods for Evaluating Solid Waste, Physical/Chemical Methods (SW--486)*, USEPA Office of Solid Waste, 1996, http://www.epa.gov/epaoswer/hazwaste/test
24. *ISO 14735, Characterisation of waste – Preparation of waste samples for ecotoxicity tests*, 2005
25. *ISO 8692, Water Quality – freshwater algal growth inhibition test with* Desmodesmus subspicatus *and* Pseudokirchneriella subcapitata, 2004
26. United States Environment Protection Agency, *Methods for Measuring the Acute Toxicity of Effluents and Receiving Waters to Freshwater and Marine Organisms*, 4th ed., EPA/600/4-90/027F. USEPA, Environment Monitoring System laboratory, Cincinnati, OH, USA, 1993
27. *ISO 6341, Water quality – Determination of the inhibition of the mobility of* Daphnia magna Straus *(Cladocera, Crustacea) – Acute toxicity test*, 1996
28. *ISO 11348-3, Water Quality – Determination of the inhibitory effect of water samples on the light emission of Vibrio fischeri (Luminescent bacteria test)*, 1998
29. *Biological Test Method: Method for Determining the Toxicity of Sediment Using Luminescent Bacteria in Solid-Phase Test, Report EPS 1/RM/42, Method Development and Application Section*, Environment Canada, Ottawa, Canada, 2002
30. *ISO 20079, Water quality – Determination of the toxic effect of water constituents and waste water on duckweed (Lemna minor) - Duckweed growth inhibition test*, 2005
31. U. Feiler, I. Kirchesch, P. Heininger. *J. Soils Sediments* **4** (2004) 261
32. *OECD 218, Sediment–water Chironomid Toxicity Test Using Spiked Sediment*, OECD Guidelines for the testing of chemicals, 2004
33. International Commission for Protection of the Danube River, *Joint Danube Survey 2*, Final Scientific Report, ICPDR – International Commission for the Protection of the Danube River, 2009, http://www.icpdr.org
34. Ministry of Housing, Spatial Planning and Environment Directorate-General for Environmental Protection, *Circular on target values and intervention values for soil remediation*, Netherlands Government Gazette, 2000
35. International Commission for the Protection of the Rhine, *Sediment Management Plan Rhine, Summary Report 175e, ICPR*, 2005, http://www.iksr.org/uploads/media/ /Bericht_175e_02.pdf (accessed March 2011)
36. United States Environment Protection Agency, *A Guidance Manual to Support the Assessment of Contaminated Sediments in Freshwater Ecosystems. Volume III – Inter-*

pretation of the Results of Sediment Quality Investigations, EPA-905-B02-001-C, USEPA Great Lakes National Program Office, Chicago, IL, USA, 2002
37. Canadian Council of Ministers of the Environment, *Protocol for the derivation of Canadian Sediment quality guidelines for the protection of aquatic life, CCME EPC-98E*. Environment Canada, Guideline Division, Technical Secretariat of the CCME Task Group on Water Quality Guidelines, Ottawa, Canada, 1995
38. V. Aruoja, I. Kurvet, H. C. Dubourguier, A. Kahru, *Environ. Toxicol.* **19** (2004) 396
39. I. Blinova, *Environ. Toxicol.* **19** (2004) 425
40. M. Davoren, S. N. Shuilleabhain, J. O'Halloran, M. G. J. Hartl, D. Sheehan, N. M. O'Brien, F. N. A. M. van Pelt, C. Mothersill, *Ecotoxicol.* **14** (2005) 741
41. F. Wang, A. O. W. Leunga, S. C. Wua, M. S. Yanga, M. H. Wong, *Environ Pollut*, **157** (2009) 2082
42. USEPA website, *ECOTOX database*, http://cfpub.epa.gov/ecotox/ecotox_home.cfm
43. J. Akkanen, J. Kukkonen, *Aquat. Toxicol.* **64** (2003) 53
44. K. Choi, P. G. Meier, *Environ. Toxicol*. **16** (2001) 136
45. E. Fulladosa, J. C. Murat, I. Villaescusa, *Arch. Environ. Contam. Toxicol*. **49** (2005) 299
46. I. Teodorovic, I. Planojevic, P. Knezevic, S. Radak, I. Nemet, *Cent. Eur. J. Biol.* **4** (2009) 482
47. M. P. Eisman, S. Landon-Arnold, C. M. Swindoll, *Bull. Environ. Contam. Toxicol.* **47** (1991) 811
48. A. P. Loibner, O. H. J. Szolar, R. Braun, D. Hirmann, *Environ. Toxicol. Chem*. **23** (2004) 557
49. P. J. Van den Brink, B. J. Kater, *Ecotoxicology* **15** (2006) 451
50. C. Hoffman, N. Christofi, *Environ. Toxicol*. **16** (2001) 422
51. N. Christofi, C. Hoffmann, L. Tosh, *Ecotox. Environ. Safety* **52** (2002) 227
52. C. Turgut, A. Fomin, *Bull. Environ. Contam. Toxicol.* **69** (2002) 601
53. C. Turgut, *Environ. Sci. Pollut. Res.* **12** (2005) 342
54. M. Kamal, A. E. Ghaly, N. Mahmoud, R. Cote, *Environ. Int*. **29** (2004) 1029
55. D. Stesevic, U. Feiler, D. Sundic, S. Mijovic, L. Erdinger, T. B. Seiler, P. Heininger, H. Hollert, *J. Soils Sediments* **7** (2007) 342
56. I. Teodorović, S. Radulović, K. Nemeš, B. Miljanović, T. Bunjevački, *Zbornik radova PMF-a, serija za biologiju* (2002–03) 57 (in Serbian)
57. B. Miljanovic, *PhD Thesis*, Universtity of Novi Sad, Faculty of Sciences, Novi Sad, Serbia, 2006 (in Serbian)
58. S. Kaisarevic, U. Lubcke-von Varel, D. Orcic, G. Streck, T. Schulze, K. Pogrmic, I. Teodorovic, W. Brack, R. Kovacevic, *Chemosphere* **77** (2009) 907
59. G. A. Burton Jr., C. MacPherson, in *Handbook of Ecotoxicology*, D. J. Hoffman, B. A. Rattner, G. A. Burton Jr., J. Cairns Jr., Eds., CRC Press, Lewis Publishers, Boca Raton, FL, USA, 1995, p. 70
60. S. Santiago, R. L. Thomas, G. Larbaigt, D. Rossel, M. A. Echeverria, J. Tarradellas, J. L. Loizeau, L. McCarthy, C. I. Mayfield, C. Corvi, *Hydrobiologia* **252** (1993) 231
61. M. W. Jacobs, J. J. Delfino, G. Bitton, *Environ. Toxicol. Chem.* **11** (1992) 1137
62. M. Salizzato, B. Pavoni, A. V. Ghirardini, P. F. Ghetti, *Chemosphere* **36** (1998) 2949
63. *Directive 2000/60/EC of the European Parliament and of the Council of 23 October 2000, Establishing a framework for Community action in the field of water policy*, Official Journal of the European Communities, L 327/1–72
64. U. Feiler, E. Claus, D. Spira, P. Heininger, *Umweltwiss. Schadst. Forsch.* **21** (2009) 264.